

# Proteomic and Microscopic Analysis of Lipid Droplets and Associated Proteins in Hepatitis C Virus-infected Cells

Dissertation  
submitted to the  
Department of Chemistry  
Faculty of Mathematics, Informatics, and Natural Sciences  
University of Hamburg  
In fulfillment of the requirements  
for the degree of  
Doctor of Natural Sciences (Dr. rer. nat.)

by  
Kathrin Rösch

Hamburg, 2016



Reviewer of the dissertation:

Dr. rer. nat. Eva Herker

PD Dr. rer. nat. habil. Markus Perbandt

Oral defense:

October 28, 2016



This dissertation was conducted between November 2011 and August 2016 at the Heinrich-Pette-Institute, Leibniz-Institute for Experimental Virology, under the supervision of Dr. rer. nat. Eva Herker and PD Dr. rer. nat. habil. Markus Perbandt.



# Contents

|   |           |
|---|-----------|
| <b>Publications and presentations</b>   | <b>1</b>  |
| <b>Abbreviations</b>  | <b>3</b>  |
| <b>Zusammenfassung</b>  | <b>7</b>  |
| <b>Abstract</b>   | <b>9</b>  |
| <b>1. Introduction</b>  | <b>11</b> |
| 1.1. HCV classification and epidemiology . . . . .                              | 11        |
| 1.2. HCV transmission . . . . .   | 11        |
| 1.3. HCV infection and therapy . . . . .  | 12        |
| 1.4. The viral life cycle . . . . .   | 13        |
| 1.4.1. Viral entry . . . . .  | 13        |
| 1.4.2. The viral RNA genome and its translation . . . . .                       | 15        |
| 1.4.3. Structure and function of HCV proteins . . . . .                         | 17        |
| 1.4.4. Viral RNA replication . . . . .  | 19        |
| 1.4.5. Virion assembly and release . . . . .                                    | 19        |
| 1.5. HCV particles . . . . .  | 21        |
| 1.6. HCV cell culture systems . . . . .   | 22        |
| 1.7. Role of lipids in the viral life cycle . . . . .                           | 24        |
| 1.8. Structure and function of cellular LDs . . . . .                           | 25        |
| 1.8.1. Pathogens that target LDs . . . . .                                      | 27        |
| 1.8.2. Tracking LDs by super resolution microscopy . . . . .                    | 28        |
| 1.9. Annexins . . . . .   | 30        |
| 1.9.1. Annexin A3 . . . . .   | 31        |
| <b>2. Aim of the dissertation</b>   | <b>33</b> |
| <b>3. Results</b>   | <b>35</b> |
| 3.1. Quantitative LD proteome analysis of HCV-infected hepatoma cells . . . . . | 35        |
| 3.1.1. SILAC labeling of Huh7.5 cells . . . . .                                 | 35        |
| 3.1.2. Quantification of LD-associated proteins . . . . .                       | 35        |
| 3.1.3. Validation of LD-associated host proteins . . . . .                      | 41        |
| 3.1.4. ANXA3 is recruited to LDs in HCV-infected cells . . . . .                | 49        |
| 3.1.5. ANXA3 has no impact on viral RNA replication and translation . . . . .   | 56        |
| 3.1.6. ANXA3 influences late steps of viral replication . . . . .               | 58        |
| 3.1.7. ANXA3 has no effect on capsid assembly and envelopment . . . . .         | 59        |

|           |   |            |
|-----------|---|------------|
| 3.1.8.    | Density and specific infectivity of virions is affected by ANXA3 expression . . . . .                       | 62         |
| 3.1.9.    | ANXA3 is not part of the lipovirions . . . . .  | 65         |
| 3.1.10.   | ANXA3 contributes to HCV virion maturation by facilitating incorporation of ApoE . . . . .                  | 68         |
| 3.2.      | Visualization of viral proteins at LDs by super-resolution microscopy (dSTORM) . . . . .                    | 75         |
| 3.2.1.    | Generation and validation of Flag-E2 tagged viral strains . . . . .   | 75         |
| 3.2.2.    | Confocal microscopy of JFH1 <sup>E2-Flag</sup> / Jc1 <sup>E2-Flag</sup> -infected cells . . . . .           | 77         |
| 3.2.3.    | Visualization of LDs by dSTORM . . . . .  | 81         |
| 3.2.4.    | 2D and 3D dSTORM analysis of Jc1 <sup>Flag-E2</sup> - and JFH1 <sup>Flag-E2</sup> -infected cells . . . . . | 82         |
| 3.2.5.    | Analysis of 3D distribution of core/NS5A and Flag-E2 at LDs . . . . .                                       | 87         |
| 3.2.6.    | 3D reconstruction of viral proteins surrounding LDs . . . . .   | 88         |
| <b>4.</b> | <b>Discussion</b>   | <b>93</b>  |
| 4.1.      | LD proteome analysis of HCV-infected hepatoma cells . . . . .   | 93         |
| 4.1.1.    | Future aspects regarding the functional role of ANXA3 in the HCV life cycle . . . . .                       | 98         |
| 4.2.      | dSTORM analysis of viral protein expression at LDs . . . . .  | 100        |
| 4.2.1.    | Future perspectives regarding dSTORM analysis of HCV assembly . . . . .                                     | 102        |
| 4.3.      | Conclusion . . . . .  | 102        |
| <b>5.</b> | <b>Material</b>   | <b>103</b> |
| 5.1.      | Bacteria strains . . . . .  | 103        |
| 5.2.      | Eukaryotic cell lines . . . . .   | 103        |
| 5.3.      | Media . . . . .   | 103        |
| 5.3.1.    | Media for culturing bacteria . . . . .  | 103        |
| 5.3.2.    | Media for culturing eukaryotic cell lines . . . . .   | 104        |
| 5.3.3.    | Cell culture media ingredients . . . . .  | 104        |
| 5.4.      | Oligonucleotides . . . . .  | 105        |
| 5.4.1.    | DNA / Protein ladder . . . . .  | 108        |
| 5.4.2.    | PCR nucleotides . . . . .   | 108        |
| 5.5.      | Plasmids . . . . .  | 109        |
| 5.5.1.    | HCV plasmids . . . . .  | 109        |
| 5.5.2.    | Expression plasmids . . . . .   | 110        |
| 5.6.      | Enzymes . . . . .   | 111        |
| 5.6.1.    | Restriction endonucleases . . . . .   | 111        |
| 5.6.2.    | Other enzymes . . . . .   | 111        |
| 5.7.      | Inhibitors . . . . .  | 111        |
| 5.8.      | Antibodies . . . . .  | 112        |
| 5.9.      | Dyes . . . . .  | 114        |
| 5.10.     | Chemicals . . . . .   | 114        |
| 5.11.     | Kits . . . . .  | 116        |
| 5.12.     | Solvents and buffers . . . . .  | 117        |



---

|  |            |
|--|------------|
| 5.13. Consumables . . . . .  | 118        |
| 5.14. Equipment . . . . .  | 119        |
| 5.15. Software . . . . .   | 121        |
| <b>6. Methods</b>  | <b>123</b> |
| 6.1. Molecular Biological Methods . . . . .  | 123        |
| 6.1.1. Cultivation of bacteria . . . . .   | 123        |
| 6.1.2. Isolation of plasmid DNA . . . . .  | 123        |
| 6.1.3. Cloning . . . . .   | 123        |
| 6.1.4. Bacteria transformation . . . . .   | 127        |
| 6.1.5. DNA sequencing . . . . .  | 127        |
| 6.1.6. Glycerol stocks . . . . .   | 127        |
| 6.1.7. <i>In vitro</i> transcription of HCV RNA . . . . .                                    | 127        |
| 6.2. Cell Biological Methods . . . . .   | 128        |
| 6.2.1. Freeze and thaw of eukaryotic cells . . . . .   | 128        |
| 6.2.2. Cultivation of eukaryotic cells . . . . .   | 128        |
| 6.2.3. Knockout of ANXA3 using the CRISPR/Cas9 system . . . . .                              | 128        |
| 6.2.4. Transfection of eukaryotic cells . . . . .  | 128        |
| 6.2.5. Determination of viral titers (TCID <sub>50</sub> ) . . . . .                         | 129        |
| 6.2.6. HCV infection and viral spreading . . . . .   | 129        |
| 6.2.7. Subgenomic HCV replicon assays . . . . .  | 129        |
| 6.2.8. Luciferase HCV replicon assays . . . . .  | 129        |
| 6.2.9. MTT viability assay . . . . .   | 130        |
| 6.2.10. Flow cytometry . . . . .   | 130        |
| 6.2.11. Immunofluorescence staining and confocal microscopy . . . . .                        | 130        |
| 6.2.12. dSTORM and image analysis . . . . .  | 130        |
| 6.2.13. HCV neutralization assay . . . . .   | 131        |
| 6.2.14. LD isolation . . . . .   | 131        |
| 6.2.15. SILAC-labeling, HCV-infection, and LD isolation for mass spec-<br>trometry . . . . . | 131        |
| 6.3. Biochemical Methods . . . . .   | 132        |
| 6.3.1. Cell lysis . . . . .  | 132        |
| 6.3.2. SDS-PAGE and western blotting . . . . .   | 132        |
| 6.3.3. Membrane floatation assay . . . . .   | 132        |
| 6.3.4. Iodixanol gradient centrifugation . . . . .   | 133        |
| 6.3.5. 2D blue native /SDS-PAGE . . . . .  | 133        |
| 6.3.6. Proteinase K digestion protection assay . . . . .                                     | 133        |
| 6.3.7. MTP activity measurement . . . . .  | 133        |
| 6.3.8. Measurement of ApoE/ApoB secretion . . . . .  | 134        |
| 6.3.9. Quantification of HCV core and ApoE protein by ELISA . . . . .                        | 134        |
| 6.3.10. Co-immunoprecipitation . . . . .   | 134        |
| 6.3.11. Affinity purification of HCV particles . . . . .                                     | 134        |
| 6.3.12. Quantification of cPLA2 activity . . . . .   | 134        |
| 6.3.13. RNA isolation and quantitative RT-qPCR . . . . .                                     | 135        |

|   |            |
|---|------------|
| 6.3.14. Mass spectrometry . . . . .                       | 135        |
| 6.3.15. Data analysis . . . . .                           | 135        |
| 6.3.16. Bioinformatics and statistical analysis . . . . . | 136        |
| <b>Bibliography</b>                                       | <b>137</b> |
| <b>A. Toxicity of chemicals</b>                           | <b>155</b> |
| A.1. GHS Hazard statements . . . . .                      | 161        |
| A.1.1. Physical hazards: . . . . .                        | 161        |
| A.1.2. Health hazards: . . . . .                          | 162        |
| A.1.3. Environmental hazards: . . . . .                   | 162        |
| A.2. GHS precautionary statements . . . . .               | 163        |
| A.2.1. Prevention precautionary statements: . . . . .     | 163        |
| A.2.2. Response precautionary statements: . . . . .       | 164        |
| <b>B. Supplementary data</b>                              | <b>167</b> |
| <b>List of Figures</b>                                    | <b>177</b> |

# Publications and presentations

## Publications

Parts of the dissertation are published or accepted for publication in:

Kathrin Rösch, Marcel Kwiatkowski, Sarah Hofmann, Anja Schöbel, Cordula Grütner, Marcus Wurlitzer, Hartmut Schlüter, and Eva Herker, *Quantitative Lipid Droplet Proteome Analysis Identifies Annexin A3 as a Cofactor for HCV Particle Production*, Cell Reports 16, 3219 (2016).

Dennis Eggert, Kathrin Rösch, Rudolph Reimer, and Eva Herker, *Visualization and Analysis of Hepatitis C Virus Structural Proteins at Lipid Droplets by Super-Resolution Microscopy*, PlosOne 9, e102511 (2014).

## Presentations

The author presented parts of the dissertation at the following conferences:

- Kathrin Rösch, Marcel Kwiatkowski, Sarah Hofmann, Anja Schöbel, Cordula Grütner, Marcus Wurlitzer, Hartmut Schlüter, and Eva Herker, *Lipid Droplet Proteome Analysis Identifies Novel Regulators of Hepatitis C Virus Replication*, 13th Workshop 'Cell Biology of Viral Infections', Kloster Schöntal, Germany, October 2014, oral presentation
- Kathrin Rösch, Marcel Kwiatkowski, Sarah Hofmann, Anja Schöbel, Cordula Grütner, Marcus Wurlitzer, Hartmut Schlüter, and Eva Herker, *Annexin A3 is Recruited to Lipid Droplet in HCV-Infected Cells and Regulates HCV Replication*, 24th Annual Meeting of the Society of Virology, Bochum, Germany, March 2015, poster, *best poster price*
- Kathrin Rösch, Marcel Kwiatkowski, Sarah Hofmann, Anja Schöbel, Cordula Grütner, Marcus Wurlitzer, Hartmut Schlüter, and Eva Herker, *Annexin A3 is Recruited to Lipid Droplet in HCV-Infected Cells and Regulates HCV Replication*, 22nd International Symposium on Hepatitis C and related Viruses, Strasbourg, France, October 2015, oral presentation, *travel award*

- Kathrin Rösch, Marcel Kwiatkowski, Sarah Hofmann, Anja Schöbel, Cordula Grütner, Marcus Wurlitzer, Hartmut Schlüter, and Eva Herker,  
*Annexin A3 is Recruited to Lipid Droplet in HCV-Infected Cells and Regulates HCV Replication*,  
HPI Scientific Retreat, Hamburg, Germany, October 2015, oral presentation
- Kathrin Rösch, Marcel Kwiatkowski, Sarah Hofmann, Anja Schöbel, Cordula Grütner, Marcus Wurlitzer, Hartmut Schlüter, and Eva Herker,  
*Quantitative Lipid Droplet Proteome Analysis Identifies Annexin A3 as a Cofactor for HCV Particle Production*,  
26th Annual Meeting of the Society for Virology, Münster, Germany, April 2016, oral presentation

# Abbreviations

| Abbreviation    | Meaning   |
|-----------------|---|
| °C              | degree Celsius  |
| μF              | microfarad  |
| μg              | microgram   |
| μl              | microliter  |
| μm              | micromolar  |
| 3D              | three dimensional   |
| ACAT            | acyl-CoA:cholesterol acyltransferase  |
| ADRP            | adipose differentiation related protein   |
| ALT             | alanine aminotransferase  |
| ANXA            | annexin   |
| ARF4            | ADP-ribosylation factor 4   |
| ATP             | adenosine triphosphate  |
| BP              | biological process  |
| BSA             | bovine serum albumin  |
| BSD             | blasticidin S deaminase   |
| BSL             | bio safety level  |
| C14orf166       | UPF0586 protein C14orf166   |
| CC              | cellular compartment  |
| cLD             | cytosolic lipid droplets  |
| CLDN1           | claudin-1   |
| CLSM            | confocal laser scanning microscopy  |
| CO <sub>2</sub> | carbon dioxide  |
| Con1 SGR        | Con1 subgenomic replicon  |
| cPLA2           | cytosolic phospholipase A2  |
| D               | domain  |
| DAA             | direct acting antivirals  |
| DC-SIGN         | dendritic-cell-specific intracellular adhesion molecule 3-grabbing non-integrin |
| DGAT1           | diacylglycerol O-acyltransferase 1  |
| DMSO            | dimethyl sulfoxide  |
| DNA             | deoxyribonucleic acid   |
| DPP4            | dipeptidyl peptidase 4  |
| dSTORM          | direct stochastic optical reconstruction microscopy                             |
| DTT             | 1,4-Dithiothreitol  |
| ECMV            | Encephalomyocarditis virus  |
| eGFP            | enhanced green fluorescence protein   |
| EGFR            | epidermal growth factor receptor  |
| ER              | endoplasmic reticulum   |
| ESCRT           | endosomal-sorting complex required for transport                                |
| FC              | flow cytometry  |
| FCS             | fetal calf serum  |
| FDA             | Food and Drug Administration  |

## Abbreviations

---

|                   |   |
|-------------------|---|
| FFU               | focus forming units   |
| FLuc              | firefly luciferase  |
| fPALM             | fluorescence photoactivated localization microscopy                           |
| FSP27             | fat specific protein of 27 kDa  |
| fw                | forward   |
| g                 | gram  |
| GAPDH             | glyceraldehyde 3-phosphate dehydrogenase                                      |
| GLuc              | gaussia luciferase  |
| gRNA              | guide RNA   |
| h                 | hour  |
| HA                | hemagglutinin   |
| HCC               | hepatocellular carcinoma  |
| HCV               | Hepatitis C Virus   |
| HCV <sub>cc</sub> | cell culture-derived HCV  |
| HCV <sub>pp</sub> | HCV pseudoparticles   |
| HIV1              | human immunodeficiency virus 1  |
| HMM               | high molecular mass   |
| HRP               | horseradish peroxidase  |
| HSPG              | heparan sulphate proteoglycans  |
| IAV               | Influenza A virus   |
| IF                | immunofluorescence  |
| IMPDH             | inosine monophosphate dehydrogenase   |
| IP                | immunoprecipitation   |
| IRES              | internal ribosomal entry site   |
| JACoP             | Just Another colocalization Plugin  |
| JFH1              | Japanese Fulminant Hepatitis 1  |
| kb                | kilo-base pair  |
| kDa               | kilodalton  |
| KEGG              | Kyoto Encyclopedia of Genes and Genomes                                       |
| l                 | liter   |
| LB                | Luria Bertani   |
| LC-ESI-MS/MS      | liquid chromatography-electrospray ionization-tandem mass spectrometry        |
| LD                | lipid droplet   |
| LDL               | low density-lipoproteins  |
| LDLR              | low-density lipoprotein receptor  |
| LMAN2             | lectin mannose-binding 2  |
| LMM               | low molecular mass  |
| LSIGN             | liver/lymph node-specific intracellular adhesion molecule 3-grabbing integrin |
| LV                | Lentivirus  |
| LVP               | lipoviroparticles   |
| M                 | molar   |
| m/z               | mass to charge  |
| MCC               | Manders' colocalization coefficient   |
| MCS               | multiple cloning site   |
| MF                | molecular function  |
| mg                | milligram   |
| min               | minutes   |
| mKO2              | monomeric kusabria orange 2   |
| mM                | millimolar  |

---

|                 |  |
|-----------------|--|
| mm              | millimetre   |
| MnSOD           | manganese-dependent superoxide dismutase                     |
| MOI             | multiplicity of infection                                    |
| mRNA            | messenger RNA  |
| ms              | mouse  |
| MS              | mass spectrometry  |
| MTP             | microsomal triglyceride transport protein                    |
| MW              | membranous web   |
| NCR             | non-coding regions   |
| neo             | neomycin   |
| nm              | nanometer  |
| NPC1L1          | Niemann-Pick-C1-like cholesterol absorption receptor         |
| NS              | non-structural   |
| nt              | nucleotides  |
| NT              | non-targeting  |
| OCLN            | occludin   |
| ORF             | open reading frame   |
| PABPC1          | polyadenylate-binding protein 1                              |
| PCC             | Pearson's correlation coefficient                            |
| PCR             | polymerase chain reaction                                    |
| PEG-IFN         | pegylated interferon-alpha                                   |
| PFA             | paraformaldehyde   |
| PHH             | primary human hepatocytes                                    |
| PBS             | phosphate-buffered saline                                    |
| PI4P            | phosphatidylinositol-4-phosphate                             |
| PIC             | protease inhibitor cocktail                                  |
| PLIN            | perilipin  |
| PMSF            | phenylmethylsulfonyl fluoride                                |
| PPAR $\gamma$ 2 | peroxisome proliferator-activated receptor $\gamma$ 2        |
| PPB             | potassium phosphate buffer                                   |
| r               | pearson correlation coefficient                              |
| RAB32           | Ras-related protein RAB-32                                   |
| rb              | rabbit   |
| RdRp            | RNA-dependent RNA polymerase                                 |
| REAC            | reactome database  |
| rev             | reverse  |
| RFP             | red fluorescence protein                                     |
| RIG1            | retinoic acid inducible gene I                               |
| RLU             | relative light units   |
| RNA             | ribonucleic acid   |
| rpm             | revolutions per minute                                       |
| RT              | room temperature   |
| SDS             | dodecyl sulfate sodium salt                                  |
| SEM             | standard error of the mean                                   |
| SILAC           | stable isotope labeling by heavy amino acids in cell culture |
| SNP             | single nucleotide polymorphisms                              |
| SR-B1           | scavenger receptor class B type 1                            |
| STED            | stimulated emission depletion                                |
| SVR             | sustained virological response                               |

## Abbreviations

---

|                    |                                      |
|--------------------|--------------------------------------|
| TCID <sub>50</sub> | 50% tissue culture infective dose    |
| TfR1               | transferrin receptor 1               |
| TG                 | triacylglycerol                      |
| TIP47              | tail-interacting protein of 47       |
| TIRF               | total internal reflection microscopy |
| TMD                | transmembrane domain                 |
| V                  | volt                                 |
| VLDL               | very-low density-lipoproteins        |
| VP                 | viral protein                        |
| WB                 | western blotting                     |
| WT                 | wild type                            |



# Zusammenfassung

*Lipid droplets* (LDs) sind zytoplasmatische Organellen, welche als intrazelluläre Fettspeicher hauptsächlich der Energieversorgung der Zelle dienen. LDs bestehen aus einem hydrophoben Kern, der sich aus Triglyceriden und Cholesterolestern zusammensetzt und von einer einfachen Phospholipidschicht sowie LD-assoziierten Proteinen umgeben ist. LDs spielen im Lebenszyklus des Hepatitis C Virus (HCV) eine essentielle Rolle, da sie als virale Assemblierungsplattform fungieren. Ob und inwiefern HCV eine Änderung in LD-assoziierten Proteinen hervorruft, um die Assemblierung neuer HCV Partikel zu ermöglichen, ist bisher noch nicht genau verstanden.

In der vorliegenden Arbeit wurde eine quantitative LD Proteomanalyse von HCV infizierten Hepatomzellen durchgeführt, um neue Wirtsfaktoren der HCV Replikation zu identifizieren. Mittels dieses Ansatzes wurden Proteine identifiziert, die abhängig von der viralen Infektion signifikant an LDs angereichert oder reduziert waren. Eines der signifikant angereicherten Proteine war das Phospholipid-bindende Protein Annexin A3 (ANXA3). ANXA3 wurde durch die viralen Proteine Core und NS5A an LD-assoziierte Membranen rekrutiert. Der shRNA-vermittelte *knockdown* von ANXA3 führte zu einer starken Reduktion der viralen Replikation. Frühe Phasen der Infektion wurden nicht beeinträchtigt, was darauf hindeutet, dass ANXA3 an den späten Schritten während des Zusammenbaus oder der Reifung von HCV Partikeln beteiligt ist. In HCV-infizierten Zellen beeinflusst ANXA3 die Sekretion von Apolipoprotein (Apo) E, ebenso wie die Interaktion des viralen Hüllproteins E2 mit ApoE oder dem viralen Core Protein. ANXA3-*knockdown*-Zellen bildeten Viruspartikel mit geringerer Infektiosität, die gleichzeitig eine höhere Dichte aufwiesen. Interessanterweise scheint die Sekretion von Lipoproteinen in nicht infizierten Zellen unabhängig von ANXA3 zu sein, was darauf hindeutet, dass sich die Lipoproteinsekretion in HCV infizierten Zellen maßgeblich von der in nicht infizierten Zellen unterscheidet. Im Vergleich zu naiven Zellen zeigten Immunofluoreszenz-Analysen von HCV-infizierten Zellen eine Mislokalisierung von ApoE, die mit einer Fragmentierung des Golgi Apparates korrelierte. Beides wurde entscheidend durch ANXA3 beeinflusst, da die Reduktion der ANXA3 Expression die Golgi Fragmentierung in HCV infizierten Zellen größtenteils verhinderte und ApoE wieder innerhalb des intakten Golgi Apparats detektiert wurde. Das lässt den Schluss zu, dass ANXA3 direkt oder indirekt zum Transport von ApoE und der Reifung viraler Partikel während einer HCV Infektion beiträgt. Somit konnte ANXA3 als HCV Wirtsfaktor identifiziert werden, welcher maßgeblich an der Bildung infektiöser viraler Partikel beteiligt ist.

Darüber hinaus wurde die räumliche Verteilung von viralen Proteinen an LDs mittels *super-resolution* Fluoreszenzmikroskopie untersucht. Hierfür wurden Virus-Konstrukte hergestellt, die ein Flag-markiertes E2 Protein tragen. Mit diesen modifizierten Viren konnten *direct stochastic optical reconstruction microscopy* (dSTORM) Aufnahmen der viralen Proteine Core oder NS5A, welche mit Flag-E2 an LDs kolokalisieren, generiert werden. Mögliche virale Assemblierungsprozesse wurden anhand dieser Aufnahmen drei-

dimensional dargestellt.

Zusammenfassend wurde erstmals eine quantitative LD Proteomanalyse von HCV infizierten Hepatomzellen durchgeführt. Hierdurch konnten neue HCV Wirtsfaktoren identifiziert und charakterisiert werden. Zusätzlich konnten mögliche HCV Assemblierungsprozesse anhand einer *super-resolution* Mikroskopietechnik visualisiert werden. Somit leistet diese Dissertation einen wichtigen Beitrag zum besseren Verständnis des HCV Assemblierungsprozesses.

# Abstract

Lipid droplets (LDs) are dynamic cytoplasmic organelles mainly functioning as intracellular lipid reservoirs providing the cell with energy. They consist of a hydrophobic core of cholesterol esters and triglycerides, surrounded by a phospholipid monolayer and LD-associated proteins. LDs are essential for HCV replication, acting as viral assembly platforms. However, if and how HCV changes the LD proteome in order to create an environment suitable for viral assembly is still poorly understood.

In this thesis a quantitative LD proteome analysis of HCV-infected hepatoma cells was performed to identify proteins that act as host factors for HCV replication. Using this approach, several proteins significantly enriched in or depleted from LD fractions of HCV-infected cells were identified. One of the proteins highly enriched in LD-fractions of HCV-infected cells was the phospholipid-binding protein Annexin A3 (ANXA3). Experimental analysis showed that ANXA3 was recruited to LD-associated membranes by the viral proteins core and NS5A. Silencing of ANXA3 severely impaired viral replication. However, early events of the viral life cycle were not affected by ANXA3-knockdown, suggesting that ANXA3 acts on viral assembly or maturation. ANXA3 influenced the secretion of apolipoprotein (Apo) E as well as the interaction between the viral envelope protein E2 and ApoE or E2 and viral core protein in HCV-infected cells. Silencing of ANXA3 reduced lipoviroparticle (LVP) infectivity accompanied by an increase in LVP density. Interestingly, ANXA3 was not needed for ApoE secretion in naïve cells, indicating that lipoprotein secretion is different in HCV-infected cells. Immunofluorescence analysis revealed mislocalization of ApoE in HCV-infected cells that correlated partially with fragmentation of the Golgi apparatus, both of which were prevented by silencing of ANXA3. This indicates that ANXA3 contributes to an HCV-induced Golgi fragmentation and directly or indirectly to the secretion of ApoE and maturation of LVPs. Thus, ANXA3 was identified as a HCV host factor, regulating viral particle production.

Furthermore, the spatial distribution of viral proteins close to LD was analyzed by multicolor super resolution microscopy. Viral genomes were modified to express a Flag-tagged version of E2. Using these viral strains, three color direct stochastic optical reconstruction microscopy (dSTORM) analyses of core/NS5A and Flag-E2 at LDs were performed, allowing reconstruction and analysis of putative viral assembly events in 3D.

In summary, a quantitative LD proteome analysis of HCV-infected hepatoma cells was performed for the first time. Thereby, novel HCV host factors were identified and characterized. Moreover, putative viral assembly sites were visualized by super-resolution microscopy. Thus, this thesis provides new insights that contribute to a better understanding of the HCV assembly process.



# 1. Introduction

Worldwide, approximately 185 million people ( $\sim 3\%$  of the world population) are infected with the Hepatitis C Virus (HCV) which can lead to progressive liver damage as e.g. steatosis, cirrhosis and hepatocellular carcinoma (HCC) [Koh14]. Chronic HCV infection accounts for up to 0.5 million deaths per year and is one of the leading causes of liver transplantation and liver-related mortality worldwide [Wed15]. Until 2011, treatment of HCV infections was based on pegylated interferon-alpha (PEG-IFN) combined with ribavirin. However, during the last 5 years, remarkable advances in HCV treatment were achieved with the development of direct acting antivirals (DAAs). DAAs are very efficient and treatment leads to clearance of HCV in 90-100% of chronically infected patients [Wed15]. Despite these profound changes in controlling HCV, the infection rates will most likely continue to rise in many countries due to the extremely high costs of DAA-based therapies. Furthermore, HCV infections are largely asymptomatic and extensive HCV screening programs are quite rare in most endemic countries, thus 95% of HCV-infected individuals are not aware of their HCV infection [Cox15]. Moreover, no vaccine is available up to now.

## 1.1. HCV classification and epidemiology

HCV is classified as a member of the *Hepacivirus* genus within the *Flaviviridae* family. The *Flaviviridae* includes four genera: Flavivirus (e.g. Yellow Fever Virus, Dengue Virus, Zika Virus or Japanese Encephalitis Virus), Pestivirus (e.g. Bovine Diarrhea- or Swine Fever Virus), Pegivirus (e.g. GBV-A or GBV-C) and Hepacivirus (e.g. HCV, GBV-B and Non-Primate Hepacivirus) [Pfa14]. Since its discovery in 1989 and the identification of the first complete genome sequence, it became obvious that HCV variants show substantial genetic diversity from each other [Cho89, Sim05]. So far, based on sequence analysis of whole viral genomes, seven genotypes (1-7) that differ in their sequence by up to 30% and several subtypes were identified. Genotype 1 is the most prevalent (46.2% of all HCV infections) followed by HCV subtypes of genotype 3 (30.1% of all cases). Genotype 2, 4 and 6 are the infection-causing HCV genotypes in 22.8% of all cases. Genotype 5 appears to be quite rare with  $\sim 1\%$  of all HCV infections. Of note, only one case of a genotype 7 infection has been reported so far [Mes15]. HCV genotypes are present in a characteristic geographical distribution [Lav11]. Genotype 1 shows a wide geographical spread accompanied by a high prevalence worldwide. The majority of infections caused by genotype 3 and 6 occur in South East Asia. Genotype 2 is highly prevalent in West Africa, while infections caused by genotype 4 are predominantly found in Central Africa. Infections caused by genotype 5 are typically found in Central/Southern Africa (Figure 1.1).

## 1.2. HCV transmission

HCV is primarily transmitted by parental routes, especially through needle sharing among injection drug users. For example it was shown that 30.3% of injection drug users developed HCV-antibodies within the first two years of drug use [Vil97]. Treatment with HCV-contaminated

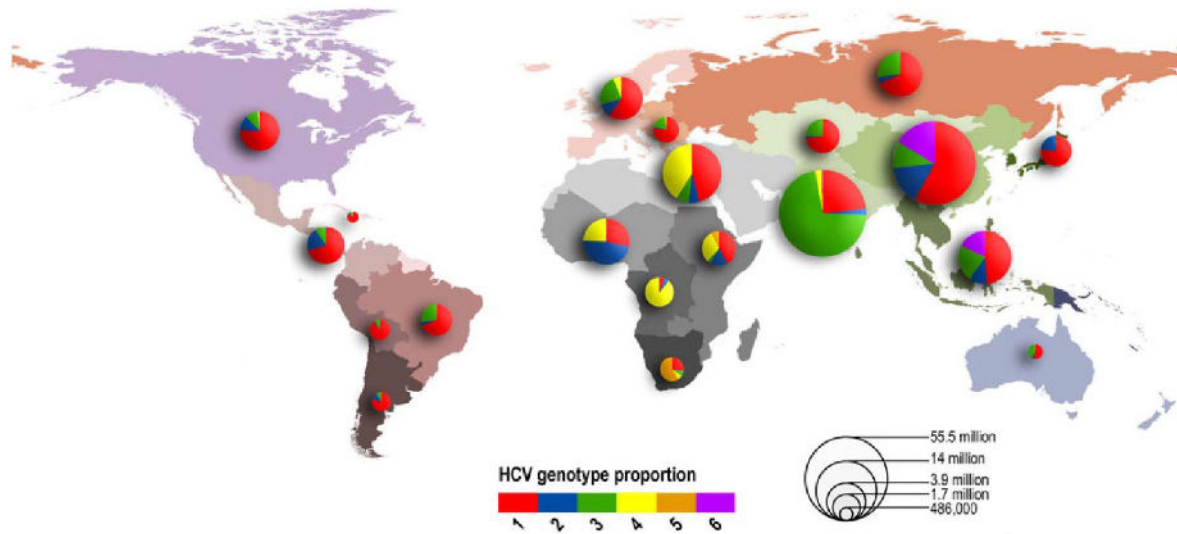


**Figure 1.1.: Global prevalence of HCV genotypes.** Shown are the most common HCV genotypes by country. The size of the pie charts reflects the number of reported cases. Modified from [Mes15].

blood products or medical treatment using contaminated instruments has also been a leading transmission route. However, due to improved safety standards, infections through blood products dropped in most countries. Also, transmission via sexual contact or transmission from mother to child during birth has been discussed, but seems to be an infrequent and inefficient event [Sy06].

### 1.3. HCV infection and therapy

HCV is very species restricted targeting only hepatocytes of humans or chimpanzees. Most of the acute HCV infections are asymptomatic or only lead to mild symptoms (e.g. fever or fatigue) soon after the infection. As such, HCV infections are likely to go unrecognized, which is beneficial for viral spread. Within the first 10-14 weeks of infection an increase in alanine aminotransferase (ALT) levels ( $< 10$  times over normal ALT levels) can be observed, indicating damage of the liver. One to three weeks after infection, viral RNA can be detected by polymerase chain reaction (PCR) and eight weeks after infection, HCV-specific antibodies can be measured. Approximately 20% of infected individuals spontaneously clear the virus. It has been shown that viral characteristics as well as host genetics account for viral control and clearance. A high viral load within the initial phase of infection correlates with a higher rate of spontaneous clearance [Liu12]. Also single nucleotide polymorphisms (SNPs) within the *Interleukin 28B* (*IL28B*) gene (encoding for interferon- $\lambda$ -3) are associated with the infection outcome. Individuals homozygous for this SNP (rs12979860) show an enhanced virological response to HCV therapy and natural clearance of the virus [Ge09]. However, clearance of HCV does not result in permanent immunity and up to 80% of acutely infected HCV patients progress to a chronic fate causing liver cirrhosis in 10-20% (within 10-20 years after infection). 1-4% of patients suffering from liver cirrhosis develop HCC [Paw04]. HCV standard therapies were based on PEG-IFN combined with ribavirin (a guanosine analog) leading to a sustained virological response (SVR) rate of  $\sim 80\%$  for genotype 2 and 3. However, genotype 1, which is responsible for most HCV infections,

shows lower SVR rates with 30-60%, often accompanied with significant adverse effects [Chu08]. Interferon-based therapies induce the activation of the immune system and therefore lead to an increased ability to clear HCV. For ribavirin several mechanisms of action are described so far. It has been reported as an HCV RNA polymerase inhibitor, cause of viral genome mutagenesis, inhibitor of inosine monophosphate dehydrogenase (IMPDH), modulator of T-cell activation and up-regulator of interferon-stimulated genes. However, the main antiviral mechanism of ribavirin is still unknown [Tho13]. Since 2011, multiple DAAs are available, acting not as broad as interferon but targeting the non-structural viral proteins directly and therefore disrupting viral replication. NS3/NS4A protease inhibitors (PI) sold as boceprevir and telaprevir, were the first generation DAAs, approved by the US Food and Drug Administration (FDA) in 2011. A combination of these PIs with the PEG-IFN standard therapy leads to remarkably increasing SVR rates (67-75%) of genotype 1 infected patients [Man13]. Since then, four classes of DAAs have been generated, defined by their target or their mechanism of action: NS3/NS4A protease- or NS5A-inhibitors, NS5B nucleoside polymerase inhibitors and NS5B non-nucleoside polymerase inhibitors [Kis13]. Introduction of these therapeutic molecules dramatically improved SVR rates up to 99% for all genotypes [Zha16].

## 1.4. The viral life cycle

### 1.4.1. Viral entry

Viral entry is thought to be a highly coordinated process involving several host entry factors in sequential steps. HCV particles circulating as lipovirions (LVPs) in the blood of HCV-infected patients are always associated with host lipoproteins, indicating that lipoprotein components as well as the viral glycoproteins contribute to viral entry. Circulating LVPs enter the liver through the sinusoidal blood. Sinusoids are populated by endothelial cells and Kupffer cells expressing liver / lymph node-specific intracellular adhesion molecule 3-grabbing integrin (LSIGN) and dendritic-cell-specific intracellular adhesion molecule 3-grabbing non-integrin (DC-SIGN). LSIGN and DC-SIGN show a high affinity for binding the viral glycoprotein E2, indicating that an interaction with E2 might contribute to capturing LVPs from blood and transferring them to hepatocytes [Loz03, Poh03]. Then, the attachment of LVPs on hepatocytes is initiated by a low-affinity interaction with the low-density lipoprotein receptor (LDLR) and heparan sulphate proteoglycans (HSPG). This interaction is most likely mediated by the apolipoprotein E (ApoE) and E2 [Jia12, Bar06]. After initial attachment, LVPs bind to the scavenger receptor class B type 1 (SR-B1), which is highly expressed on hepatocytes, and thereby might facilitate the hepatotropism of HCV. On hepatocytes, SR-B1 is normally involved in the binding of very-low density-lipoproteins (VLDLs) as well as oxidized forms of low density-lipoproteins (LDLs) or in supporting cholesterol uptake from these lipoproteins. During HCV entry, SR-B1 acts at three different steps: first through binding to HCV-associated lipoproteins, most likely ApoE, and therefore mediating primary attachment, second, due to the lipid transfer activity, SR-B1 promotes a conformational change within the LVP allowing exposure of the CD81 binding site of E2, and finally SR-B1 contributes to an enhanced entry via its interaction with E2 [DT12].

An additional entry factor involved in HCV post-attachment events is the tetraspanin CD81. Previous studies have shown, that treatment of HCV particles with soluble CD81 makes them sensitive to acid, suggesting that binding to CD81 primes LVPs for low pH-fusion within endosomes later on [Sha11]. Besides its priming function, CD81 is also important for defining the human tropism of HCV, as human CD81 and Occludin (OCLN) expressed in mice liver

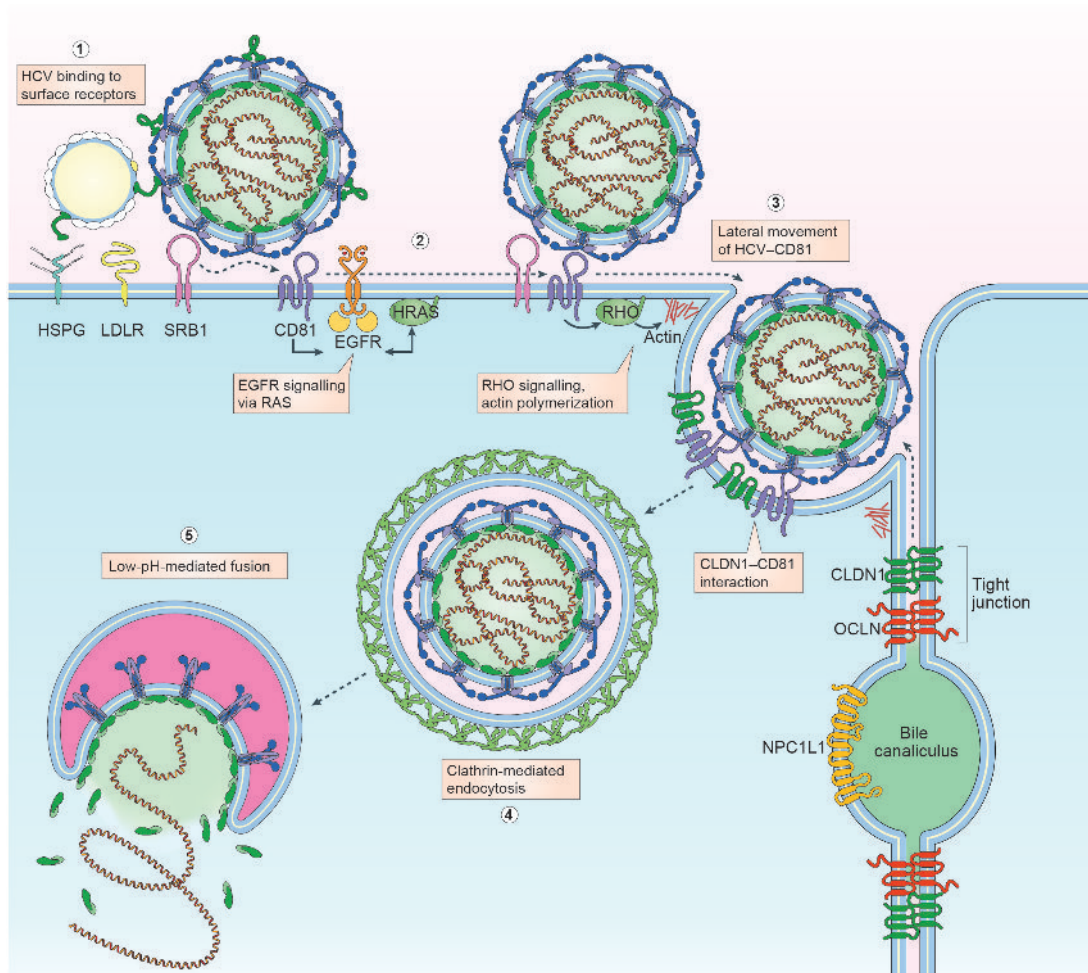


**Figure 1.2.: The HCV entry process.** HCV circulates as LVP through the sinusoidal blood. Interaction of lipoproteins associated to viral particles with LDLR and HSPG mediates the first attachment to the target cell (1), followed by an interaction of SRB1 with ApoE and E2, resulting in conformational changes in LVPs, which renders the LVP accessible for CD81 (2). Interaction of CD81 and E2 induces signaling pathways through EGFR, HRAS and RHO leading to lateral transport of the CD81-LVP complex to cell-cell contact sites (3). There, CD81 interacts with CLDN1 causing the internalization of LVPs bound to the CD81-CLDN1 complex via clathrin-mediated endocytosis (4), followed by fusion of the viral envelope with endosomal membranes and release of the viral genome into the cytoplasm (5). OCLN, Tfr1 and NPC1L1 also contribute to post-CD81binding events. However the mechanism is still unclear. Modified from [Lin13].



renders them susceptible for HCV entry [Dor13]. CD81 is ubiquitously expressed on the cell surface and directly binds to E2. This E2-CD81 complex interacts with HRas, epidermal growth factor receptor (EGFR) and RHO GTPases, which induces lateral membrane diffusion of E2-CD81 complex to sites of cell-cell contact. There, CD81 interacts with the tight junction protein Claudin-1 (CLDN1) thereby facilitating the internalization of LVPs [Har10]. The interaction of CD81 and CLDN1 is initiated by signaling pathways induced by EGFR and ephrin receptor 2a (EphA2) [Zon13, Lup11]. Furthermore, ectopic expression of CLDN1 in kidney-derived HEK 293T cells renders them permissive for HCV, emphasizing CLDN1 as a key player in HCV entry [Eva07]. Another tight junction protein involved in viral entry is OCLN. However, whether OCLN directly interacts with E2 or indirectly via the CD81/CLDN complex is still unknown. Furthermore, the transferrin receptor 1 (TfR1) has been identified as an entry factor acting after CD81-binding events. However, the mechanism of how TfR1 facilitates HCV internalization is still not known [Mar13]. Additionally, the Niemann-Pick-C1-like cholesterol absorption receptor (NPC1L1) has also been identified as an HCV entry factor acting before virion-cell membrane fusion occurs [Sai12]. Finally, the interaction of LVPs with the CD81/CLDN1 complex promotes CD81 and CLDN1 endocytosis via a clathrin- and dynamin-mediated process [Far12]. Following internalization, HCV-CD81-CLDN1 complexes are transported to early endosomes. The low pH environment inside endosomes induces fusion of the viral envelope with the endosomal membrane, resulting in the release of the viral genome into the cytoplasm (Figure 1.2).

### 1.4.2. The viral RNA genome and its translation

Following internalization, the viral positive-sense RNA genome of 9600 nucleotides (nt) is released into the cytoplasm. It contains a single large open reading frame (ORF) flanked by non-coding regions (NCR) at the 5'- and the 3'-end. The 3' NCR is composed of a highly variable region, a short polypyrimidine (poly (U/UC) tract and a highly conserved 98-nt RNA element, termed X-tail. The X-tail is able to bind an RNA element (termed 5B SL3.2) within the NS5B coding sequence, resulting in the formation of a kissing-loop interaction essential for viral RNA replication [Fri05]. The 5' NCR is one of the most highly conserved HCV regions, often used for genotype analysis. It contains a microRNA 122 (miR122) binding site as well as an internal ribosomal entry site (IRES) and is therefore essential for translation initiation of the uncapped viral RNA [Ray04]. It has been shown that cis-acting elements within the 5' NCR are also essential for viral RNA replication [Fri01, Kim02, Jop05]. As HCV harbors a positive sense RNA genome, the viral RNA serves as mRNA and is directly translated by binding of the 5' IRES to ribosomes. The IRES-mediated translation of the ORF results in a polyprotein of > 3000 amino acids which is co- and posttranslationally processed into 10 mature viral proteins (Figure 1.3 A). A cellular signal peptidase processes the immature core protein, which is further cleaved by a signal peptide peptidase into the mature core protein, whereas E1, E2 and p7 are cleaved directly by signal peptidases. Furthermore, the viral polyprotein encodes for two proteases: the NS2-3 autoprotease mediating the cleavage between NS2 and NS3 as well as the NS3/NS4A protease processing the remaining proteins NS3 to NS5B. Polyprotein processing leads to the generation of the three structural proteins (core, E1 and E2) and the seven non-structural proteins (p7, NS2-NS5B) (Figure 1.3 B).

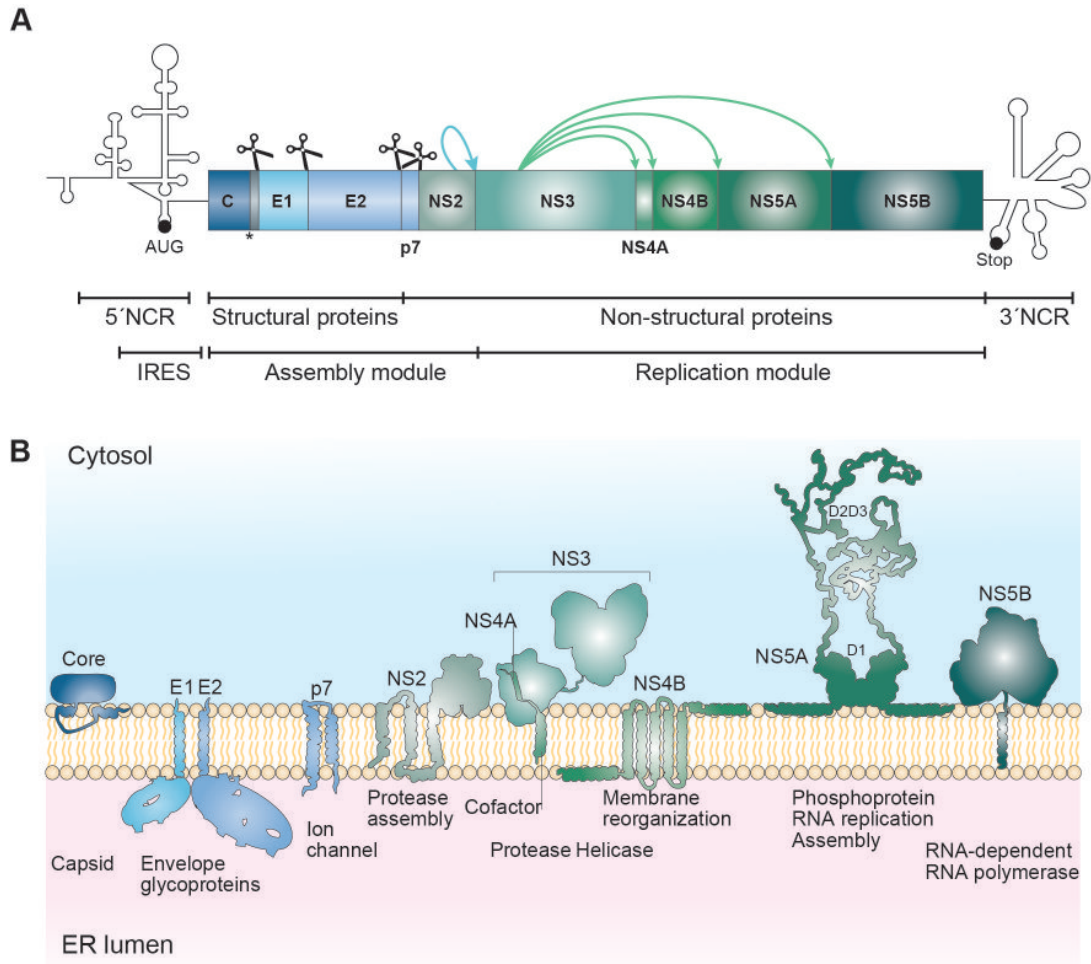


**Figure 1.3.: HCV genome organization and polyprotein processing.** HCV contains a 9.6 kb positive strand RNA genome flanked by non-coding regions (NCR). IRES-mediated translation converts the RNA genome into a single polyprotein. The polyprotein is processed by cellular signal peptidases and viral proteases into three mature structural and seven non-structural (NS) proteins. The 5' NCR contains the IRES as well as a start codon (AUG). Cellular signal peptidases are indicated by scissors. Cleavage of the C-terminal part of core is mediated by a cellular signal peptide peptidase indicated by an asterisk. Cleavage by viral proteases is indicated by arrows. The structural proteins as well as p7 and NS2 are involved in viral assembly and therefore summarized as assembly module. Non-structural proteins NS3-NS5B act mainly during viral replication and are merged as replication module. B) Major functions of mature HCV proteins and their association with membranes. Modified from [Bar13].

### 1.4.3. Structure and function of HCV proteins

Due to their function, mature HCV proteins can be classified into proteins involved in the assembly process (core-NS2) and proteins involved in viral RNA replication (NS3-NS5B). As the HCV genome only encodes for ten proteins, it is obvious that each single HCV protein must achieve multiple functions. A switch between different functions may be regulated by different interactions with viral or host proteins and / or changes in the structural conformation.

#### Core

The core protein fulfills many functions within the viral life cycle; however with respect to the virus, it mainly forms the capsid to protect the viral genome. During polyprotein processing, the immature core protein consists of 191 amino acids. Further processing removing the signal peptide for localization to the endoplasmic reticulum (ER) located in domain 3 (D3) by the signal peptide peptidase results in a 21 kDa mature core of 177 amino acids [Lus16]. This mature form consists of two domains: An N-terminal hydrophilic domain (D1, amino acids 1-117) mainly containing basic amino acid residues and the C-terminal domain 2 (D2, 118-177 amino acids). D1 has been linked to RNA-binding properties and nucleocapsid assembly. Furthermore, D1 can interact with different host proteins and thereby might influence the function of these cellular proteins. D2 is responsible for the association of core with lipid droplets (LDs). Another function of core lies in recruiting other HCV proteins, viral RNA and replication complexes to LD-associated membranes to initiate viral assembly [Miy07, Bou05]. Core has also been linked to HCV-mediated liver disease. Differences in the core sequence of genotype 1 and 3 HCV strains have been correlated with the tendency of genotype 3 to accumulate triglycerides in LDs and therefore to promote steatosis. Expression of HCV core in transgenic mice also facilitates the development of hepatic steatosis and the formation of hepatic nodules (one characteristic of HCC) [Mor97]. Core can interact with numerous cellular and viral proteins to facilitate its multifunctionality. Core expression influences DNA replication, cell cycle progression, lipid synthesis and transformation of cells. Furthermore, core interferes with the immune response, has pro- and anti-apoptotic properties and enhances cell proliferation [Per02, Kao16].

#### Glycoproteins E1 and E2

The envelope proteins E1 and E2 are type 1 transmembrane proteins; they are glycosylated and form a non-covalent complex. They have a molecular weight of 35 kDa (E1) and 70 kDa (E2) and consist of a large N-terminal ectodomain (E1 ~160 amino acids, E2 ~360 amino acids) and a short transmembrane domain (TMD, ~30 amino acids) at the C-terminus. During polyprotein processing, the ectodomains are located in the lumen of the endoplasmic reticulum (ER), where the TMD is integrated into the ER membrane. The two envelope proteins are essential for viral entry as they initiate attachment and internalization of viral particles into the host cell. Furthermore, E2 interacts with lipoproteins, which allows the formation of LVPs [Bar13].

#### p7

The p7 is a small (63 amino acids, 7 kDa) polypeptide composed of two TMDs connected by a short cytoplasmic loop. The N- and C-termini are orientated towards the ER lumen. p7 has no impact on viral RNA replication, but influences infectivity. It forms oligomers in order to fulfill ion channel activity, implicating that it might act as viroporin. p7 also influences the late steps of capsid assembly and initiation of budding events [Gen13, Bar13].

### **NS2**

NS2 is essential for the cleavage of the polyprotein at the NS2 / NS3 junction. It has a molecular weight of 21 kDa and consists of three TMDs at the N-terminal part, while the catalytic activity is located in the C-terminal part of NS2. The protease activity of NS2 can be strongly enhanced by the N-terminal part of NS3. Independently of its protease activity, NS2 also contributes to viral assembly by attracting envelope- and NS-proteins to viral assembly sites [Pop11].

### **NS3/4A complex**

The NS3 protein fulfills different functions in the viral life cycle. It contains a serine protease in the N-terminal third and a RNA helicase / NTPase located at the C-terminal part of the protein. NS4A acts as co-factor for NS3, enhancing the protease activity. They have a molecular weight of 69 kDa and 6 kDa, respectively. Furthermore, NS4A induces the ER-localization of NS3 via its N-terminal domain. The NS3/4A protease is essential for polyprotein processing downstream of NS3 and is also involved in downregulation of host defense mechanisms (e.g. proteolysis of mitochondrial antiviral signaling (MAVS) or TIR domain-containing adaptor inducing IFN $\beta$  (TRIF) leading to a disruption of antiviral signaling pathways) [Bar13].

### **NS4B**

The NS4B protein is able to induce the formation of the membranous web (MW), an alteration of ER-derived membranes where viral RNA replication takes place. It contains four TMDs, with the C- and N-termini located in the cytosol. However, a portion of the N-terminus can also be localized in the ER lumen, indicating that NS4B might act in the crosstalk between the cytosol and the ER lumen. NS4B has a molecular weight of 27 kDa [Bar13].

### **NS5A**

The NS5A protein is involved in viral RNA replication as well as viral assembly. NS5A contains a membrane anchor at the N-terminal region and three domains (D1: amino acids 36-213, D2: amino acids 250-342, D3: amino acids 356-447). D1 is essential for LD targeting of NS5A. D1 and D2 are also involved in RNA replication, whereas D3 participates in viral assembly and facilitates the interaction with core. NS5A is mainly localized in the cytoplasm and the perinuclear region. When expressed either alone or in the context of full viral genome, it co-localizes with core at LDs. NS5A also interacts with lipoproteins (e.g. ApoE and ApoA1). NS5A is a membrane-associated phosphoprotein that can be found in a phosphorylated (56 kDa) or hyper-phosphorylated form (58 kDa). Phosphorylated NS5A is involved in viral RNA replication and the hyper-phosphorylated variant acts on viral assembly, suggesting that the phosphorylation status might regulate the switch between replication and assembly functions [Shi02].

### **NS5B**

The NS5B protein belongs to the class of tail-anchored proteins, indicating that the C-terminal region forms a TMD targeting the functional protein domain on the cytosolic side of the ER. NS5B acts as RNA-dependent RNA polymerase (RdRp) in the synthesis of positive / negative strand HCV genomes [Bar13].

#### 1.4.4. Viral RNA replication

After viral RNA translation and polyprotein processing, the expression of NS3–NS5B induces extensive rearrangements of ER-derived membranes leading to an environment suitable for viral RNA replication. Such membrane alterations are physically different from the surrounding cytoplasm and essential for viral RNA replication. They are termed MW due to their complex structure of vesicles shielded by multiple membranes. Individual vesicles within the MW act as viral RNA replication sites. These vesicles are able to synthesize RNA *in vitro* and protect viral RNA from nuclease / protease or detergent treatment. The viral NS3–NS5B proteins generate the RNA replication machinery. However, NS5B acts as key enzyme synthesizing a positive-sense RNA genome through a negative-strand intermediate. The NS5B RdRp has no proof reading function, leading to high error rates ( $10^{-3}$  per site). Especially G:U/U:G mismatches are observed, which results in a high genetic variability of HCV isolates [Pow11]. Besides non-structural proteins, also numerous cellular factors contribute to viral RNA replication. For example, the cellular miR122, which interacts with the viral genome to promote viral RNA stabilization, translation and replication [Shi12, Jop05, Hen08].

#### 1.4.5. Virion assembly and release

Following RNA replication, HCV virions are generated at LD-associated membranes, bud into the ER lumen by components of the endosomal-sorting complex required for transport (ESCRT) pathway and likely transit through the secretory pathway. During this process, nascent viral particles mature and associate with lipoproteins, which give them their low-density properties. Afterwards, mature viral particles are released by exocytosis. Cytosolic LDs (cLD) are a key player in the viral assembly process as they act as viral assembly platforms. Mature core migrates to cLDs and recruits NS proteins as well as viral replication complexes to LD-associated membranes (Figure 1.4) [Miy07]. Trafficking of core to cLDs depends on host factors e.g. cytosolic phospholipase A2 (cPLA2) and diacylglycerol O-acyltransferase 1 (DGAT1) [Men12, Her10]. DGAT1 also recruits NS5A to cLDs [Cam13]. There, NS5A interacts with core initiating an interaction of viral RNA and core. This might recruit viral RNA to viral assembly sites and triggers nucleocapsid formation [Mas08]. After initiation of the assembly process, core has to be retrieved from cLD and migrates to ER budding sites where the viral budding into the ER lumen occurs. Core interacts with clathrin assembly protein complex 2 medium chain (AP2M1) resulting in the release of core from cLDs [Nev12]. Additionally, it might also be possible, that some fraction of core stays at ER membranes close by cLDs. Besides NS5A other NS proteins are facilitating HCV assembly as well. It has been shown, that NS2 interacts with NS3/4A, leading to the recruitment of core from cLDs into motile puncta, most likely representing transport vesicles containing virus particles [Cou11, Jir10]. NS2 also interacts with the E1/E2/p7 complex and NS3 in order to recruit E1/E2/p7 and NS3 to LD-associated assembly sites. Core and the E1/E2 complex cannot directly interact as the TMD of E1 and E2 lacks a cytosolic side (Figure 1.3, B). Therefore, NS2 might act as an adapter protein, connecting capsid formation and envelopment. This indicates that NS2 acts as a key player in viral assembly, coordinating the interaction of structural and non-structural proteins during viral particle formation. Several findings indicate that HCV- and VLDL-particles share a common route of secretion. First, mature viral particles are associated with VLDLs and acquire their low density during egress. Second, inhibition of the microsomal triglyceride transport protein (MTP), which promotes transfer of lipids within the ER lumen, blocks HCV particle production [Hua07]. And third, suppression of VLDL particle secretion also reduces HCV virion secretion [Sye10].

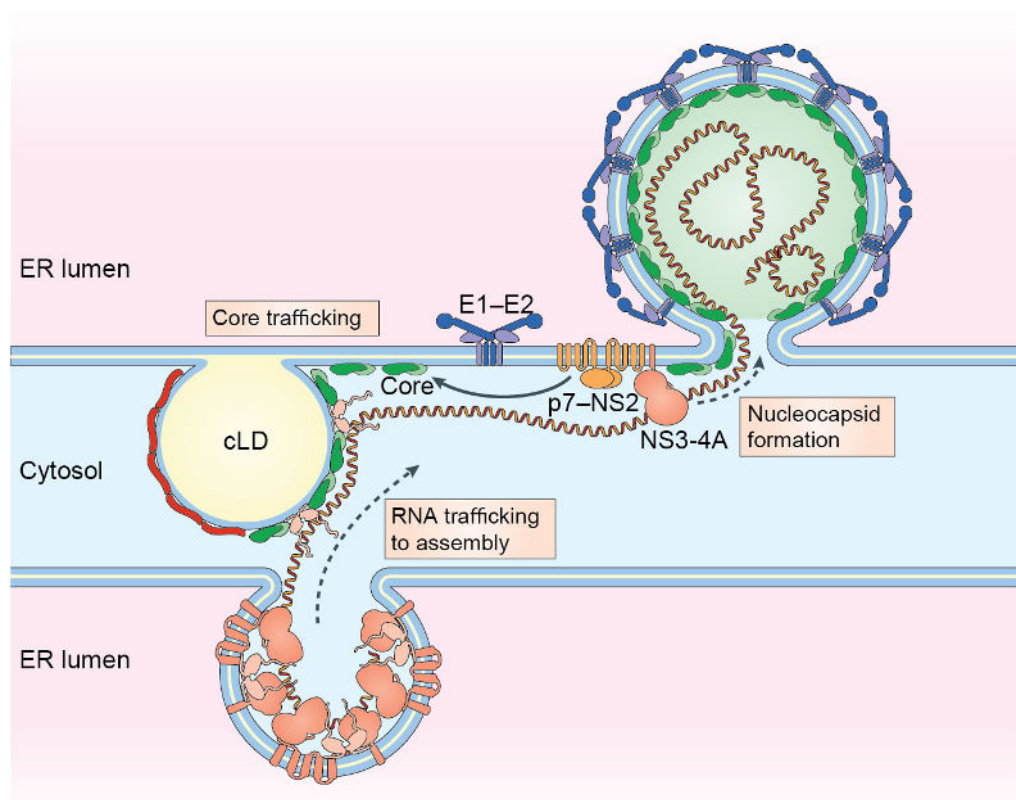


**Figure 1.4.: HCV assembly.** Core is recruited to cLDs by cPLA2 and DGAT1. DGAT1 also recruits NS5A to cLDs. Core and NS5A recruit viral replication complexes to LD surfaces to enable transfer of viral genomes for encapsidation by core. NS2 interacts with p7 and NS3/4A leading to the transfer of core to viral assembly sites and the formation of capsids containing viral RNA. NS2 also mediates trafficking of envelope proteins to viral budding sites. During budding into the ER lumen, capsids obtain a lipid envelope where viral glycoproteins are incorporated. Immature viral particles mature, transit through the secretory pathway and leave the cell by exocytosis. Modified from [Lin13].

## 1.5. HCV particles

HCV particles are 40-80 nm in diameter. The core protein forms a nucleocapsid containing the single-stranded RNA genome. The capsid is surrounded by a lipid bilayer where the glycoproteins E1 and E2 are embedded (Figure 1.5 A). HCV particles are termed LVPs due to their association with LDLs and VLDLs. LVPs are very heterogeneous in their size. Electron microscopy analysis demonstrated an electron dense core lacking any regular surface features (Figure 1.5 D).

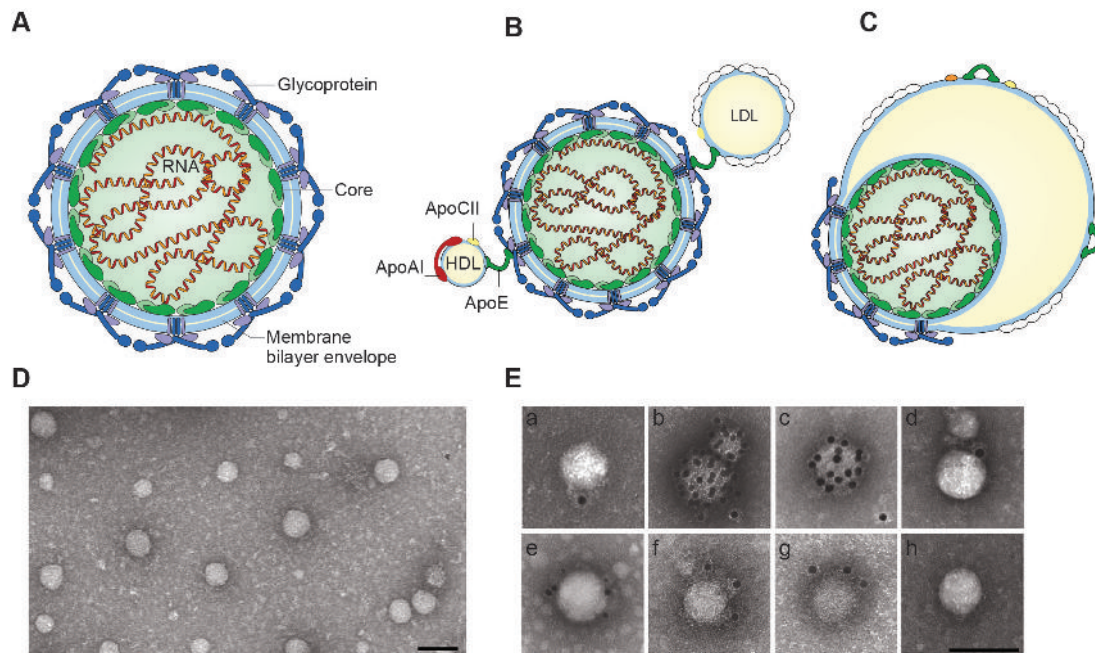


**Figure 1.5.: HCV; a lipovirion.** A) Model of an HCV particle. The core protein forms a capsid, protecting the single-stranded RNA genome inside. The capsid is enveloped by a membrane bilayer in which the envelope glycoproteins E1 and E2 are embedded. B) LVP formed by the two particle model, suggesting that HCV particles and serum-derived lipoproteins interact transiently. C) The hybrid LVP model demonstrating an HCV particle sharing the envelope with a LDL particle. D) Transmission electron microscopy (TEM) analysis of HCV particles purified from human hepatocyte cultures. E) TEM analysis of viral and host lipoproteins associated with HCV particles. 6xHis-2xStrepII tagged HCV particles were purified and immunolabeled for (a) viral glycoprotein E2, (b) Apo-E, (c) ApoA-I, (d) Apo-B100, (e) double stained for E2 (8 nm gold particles) and ApoE (18 nm gold particles), (f) StrepII tag, (g) 6xHis tag, (h) secondary antibody control. Scale bars 100 nm. A-C modified from [Lin13], D and E are modified from [Cat13b].

A key characteristic of HCV particles is their low buoyant density, which is essential for a high specific infectivity. Highly infectious cell culture-derived HCV particles (HCV<sub>CC</sub>) or HCV particles isolated from patient serum typically have a low buoyant density of 1.03-1.10 g/ml. This reflects a significant lower buoyant density as compared to other enveloped RNA viruses (e.g. Flaviviruses 1.20-1.23 g/ml, Pestiviruses 1.12-1.15 g/ml or Retroviruses 1.16-1.18 g/ml) [Lin13]. HCV particles are mainly associated with apolipoprotein E (ApoE), B100 (ApoB), C-I (ApoC-I) and A-I (ApoA-I). Apolipoproteins are proteins that interact with lipids to form a buoyant density lipid-protein complex. Thus, lipids associated by apolipoproteins to LVPs are responsible for LVP density. The formation of LVPs likely facilitates viral entry and shields viral particles from antibody neutralization (Figure 1.5 E) [Lus16, Cat13b]. Lipid profiling studies of HCV<sub>CC</sub>



particles revealed that their cholesterol and lipid levels are similar to LDLs and VLDLs. However, whether LVPs are formed by a transient interaction with separable lipoproteins or as a hybrid lipoviroparticle remains unknown (Figure 1.5 B, C) [Lin13].

### 1.6. HCV cell culture systems

HCV has a narrow host tropism restricted to chimpanzees and humans, which makes it difficult to establish an animal model system. Therefore, the establishment of a suitable cell culture model system was essential to study HCV. Since 1989, when the HCV genome was sequenced for the first time, many attempts were made to generate proper cell culture systems. First trials were based on transfection with cloned HCV RNA or inoculation of cultured cells with patient sera. However, HCV replication efficacy was low, limiting the benefit of these experimental approaches. In 1999 Lohmann *et al.* described the first system, which showed robust viral RNA replication in transfected cells. In these so-called replicon systems, the coding region of structural proteins was replaced by a selection marker (e.g. neomycin phosphotransferase, neo) combined with a second IRES (derived from the encephalomyocarditis virus (ECMV)), needed for NS3–NS5B translation. The RNA template used in this approach was isolated from liver tissue of a chronically-infected HCV patient (genotype 1b) [Loh99]. This system allows studying different aspects of viral RNA replication. However, due to the lack of structural proteins as well as p7 and NS2, viral entry and assembly / egress could not be analyzed. In 2003, HCV pseudoparticles (HCVpp) were generated allowing studying early steps of the viral life cycle, especially viral entry [Bar03]. This system utilizes the ability of retroviruses to incorporate heterologous glycoproteins (HCV E1/E2 complex) into their envelope. This system enabled the identification of CD81 and CLDN1 as HCV entry factors and also successfully identified neutralizing antibodies [Hsu03, Dre09]. In 2005, HCV research was dramatically improved by the identification of the first HCV strain that replicates and produces infectious viral particles in cell culture [Wak05]. This unique strain was isolated from a Japanese patient suffering from severe acute HCV infection (genotype 2a) and therefore termed Japanese Fulminant Hepatitis 1 (JFH1). In cell culture, JFH1 infects hepatoma cells resulting in viral RNA replication and production of infectious viral particles. JFH1 represented the first possibility to study the full viral life cycle *in vitro*. Importantly, JFH1 was also infectious for chimpanzees and in humanized mouse models [Lin06]. To date, several chimeric HCV strains have been generated, based on the replication module of the JFH1 clone in combination with the assembly module of other HCV genotypes, leading to an improvement of this system. For example the chimera Jc1, containing the assembly module (nt: 1–846) of a J6 strain (genotype 2a) and the replication module of JFH1 (nt: 847–3034), yields infectious titers 100–1000-fold higher than the parental strains. As a great advantage, HCV replicon- and HCVcc-systems allow the insertion of reporter sequenced (e.g. luciferase, fluorescence proteins or tags) (Figure 1.6) [Pie06, Loh14]. However, introducing insertions into NS5A severely impaired viral assembly and thereby limiting the benefit of such reporter stains [Sch07]. To avoid a defect in viral assembly, Webster *et al.*, established a Jc1 strain containing a reporter gene inserted between NS5A and NS5B. This reporter was flanked by duplicated NS5A / NS5B cleavage sites, which enables the release of the reporter from NS5A by the NS3/4A protease cleavage during polyprotein processing. Using this strategy, viral titers can be produced comparable to Jc1 wild type (WT) strains [Web13a].

As a hepatotropic virus, HCV replicates only in human hepatocytes and thereby limits cellular systems to study HCV *in vitro*. So far, the human hepatoma cell line Huh7 and their subclones are most permissive for HCV in cell culture. Huh7.5 cells are the most common cell



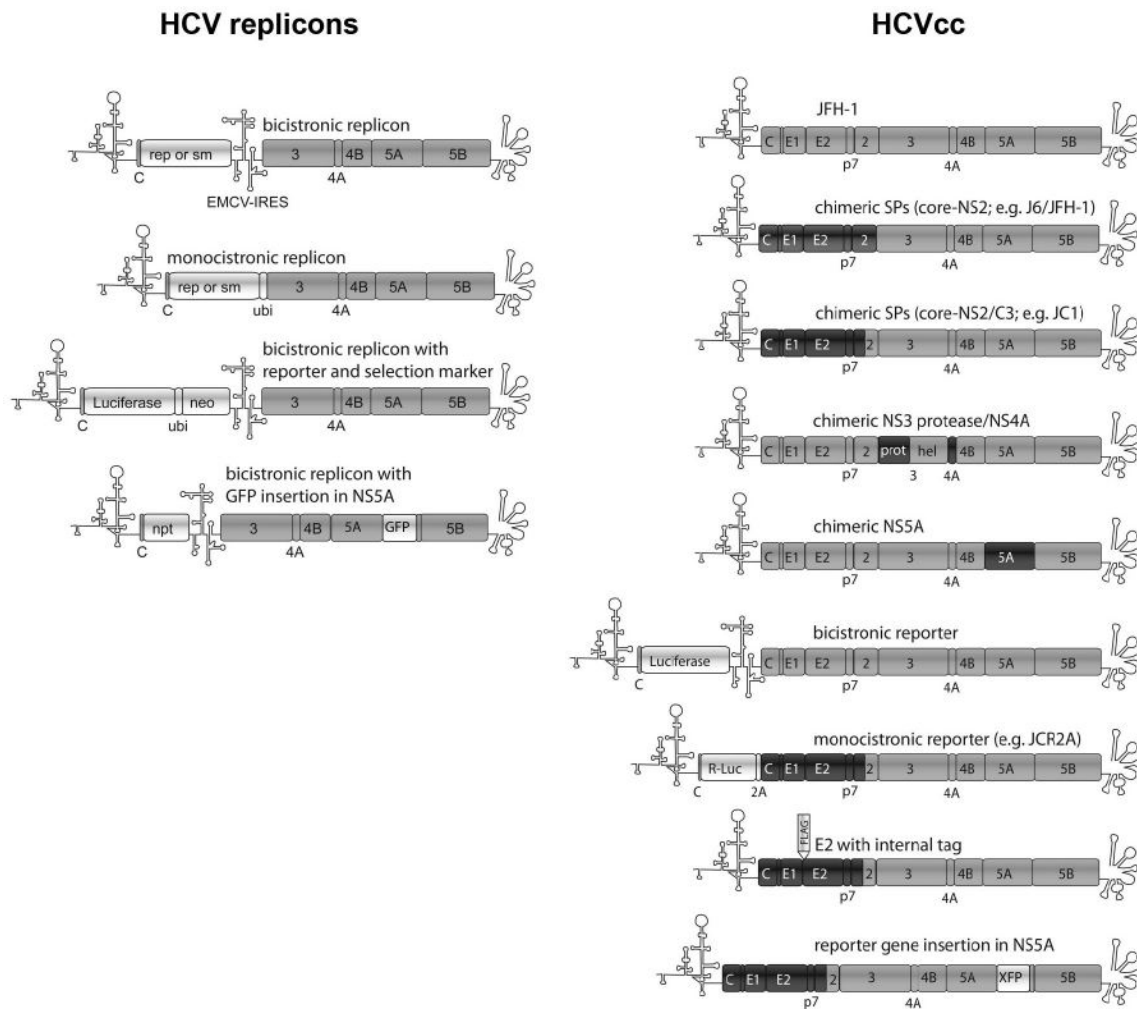


**Figure 1.6.: HCV cell culture systems.** Subgenomic mono- and bicistronic HCV replicons containing the coding region for NS3–NS5B, a reporter gene (rep. e.g. luciferase) and / or a selection marker (sm. e.g. neomycin). The EMCV-IRES as well as NCRs are indicated by their proposed secondary structure. HCVcc systems illustrate the JFH1 WT genome as well as several chimeras with / without a reporter sequence (shown in light gray). JFH1 sequences are shown in gray, sequences of a second genotype are shown in black. Modified from [Loh14].

line. Due to a mutation in the retinoic acid inducible gene I (RIG-I), these cells are deficient in a proper immune response and thereby highly susceptible for HCV. In Huh7.5 cells a robust HCV spreading infection and replication to high viral titers can be observed [Bli02, Sum05]. However, these cell lines are deficient in several characteristics of primary human hepatocytes (PHH) (e.g. lipid metabolism, polarity, innate immune response), which restricts their possible applications. PHHs serve as the gold standard to study HCV *in vitro*. However, several limitations (e.g. high costs, poor availability, donor variation, low HCV replication, dedifferentiation in cell culture) make this system quite challenging. Improvements were achieved by usage of human fetal hepatocytes which support significantly higher HCV replication over a long cell culture period, or by co-culturing of PHHs with fibroblasts, which resulted in a robust HCV replication for several weeks (Figure 1.7) [Laz07, Plo10]. However, due to ethical concerns, use of human fetal-derived material is restricted or even prohibited in many countries, e.g. in Germany.

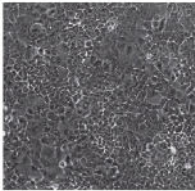
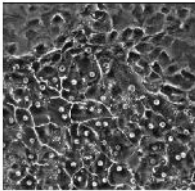
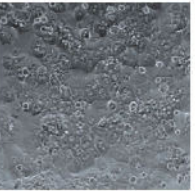
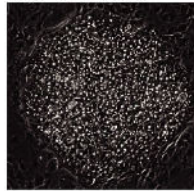
|                            | Huh7.5  | Fetal Hepatocytes   | Adult Hepatocytes  | Micropattern co-cultures  |
|----------------------------|---|---|--|---|
|                            |  |  |  |  |
| <b>Cell physiology</b>     | Hepatoma cell line  | PHH   | PHH  | PHH   |
| <b>Polarity</b>            | unpolarized   | polarized   | polarized  | polarized   |
| <b>HCV replication</b>     | high  | medium  | low  | low   |
| <b>HCV spread</b>          | high  | no  | no   | no  |
| <b>Infection frequency</b> | high  | low   | low  | low   |

Figure 1.7.: Cells used as HCV culture systems *in vitro*. Comparison of HCV permissive cells used as *in vitro* culture systems and their properties. Modified from [Cat15].

## 1.7. Role of lipids in the viral life cycle

The HCV life cycle is closely connected to the lipid metabolism of the host cell. Clinical studies show clear evidence that HCV interferes with the lipid metabolism. In HCV-infected patients, the viral infection is linked to steatosis, and an accumulation of core at LDs can be observed, clearly demonstrating that LDs are involved in viral replication *in vivo* [Lea06]. Furthermore, cell culture experiments demonstrated that HCV replication can be efficiently blocked by inhibition of sphingolipid biosynthesis [Sak05]. Inhibition of fatty acid synthesis negatively influences MW formation in HCV-infected cells and thereby leads to a decrease in viral replication [Lyn14]. Additionally, HCV induces the production of fatty acids in infected cells [Nas13]. HCV infection causes a distinct alteration of the cellular lipidome leading to disruption of normal metabolic functions and a shift from energy consumption towards energy conserving activities [Dia10]. Also, the local lipid composition seems to be an important factor for individual steps in the viral life cycle. HCV alters the cellular localization of the lipid kinase PI4KIII $\alpha$  and its product

phosphatidylinositol-4-phosphate (PI4P), leading to an intracellular increase of PI4P. PI4P modulates the lipid content of membranes and thereby facilitating MW formation needed for viral replication [Pau14]. In addition, expression of genotype 3a core changes the lipid composition of LDs as well as their size [LM14]. All these data clearly indicate that the HCV life cycle is closely linked to the lipid metabolism of the host cell.

## 1.8. Structure and function of cellular LDs

LDs are cytoplasmic organelles that are ubiquitously found in eukaryotic and also in prokaryotic cells. They consist of a central core of neutral lipids (triacylglycerol (TG), sterol- and retinylesters) enclosed by a phospholipid monolayer and LD-associated proteins including members of the perilipin family (PLINs), containing Perilipin1 (PLIN1), Perilipin2/adipose differentiation related protein (PLIN2/ADRP) and Perilipin3/tail-interacting protein of 47 kilodalton (PLIN3/TIP47) (Figure 1.8). PLIN proteins are crucial for LD-maintenance, -formation and -function. PLIN1 is mainly expressed in adipocytes and controls the TG-hydrolysis by restricting access of soluble lipases to stored lipids inside LDs [Bra00]. PLIN2, a ubiquitously expressed protein, promotes an accumulation of neutral lipids in LDs by limiting the interaction of neutral lipids with lipases [Lis07]. TIP47, mainly functions in LD biogenesis [Bul09]. LDs vary greatly in size (< 250 nm up to 100  $\mu\text{m}$  in diameter) depending on cellular signals, which can induce growing or shrinking of LDs. Mass spectrometry data revealed that 50-200 proteins are associated with LDs [Wil14a]. However, the protein composition can vary between LDs of different sizes or lipid composition within the same cell [Hsi12].

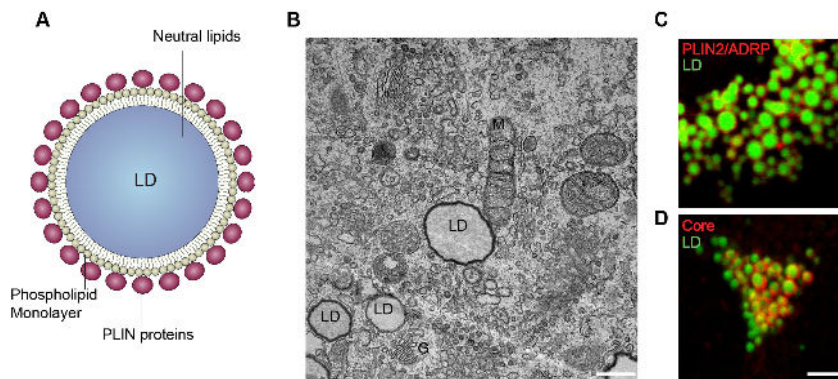


**Figure 1.8.: Morphology of LDs.** A) LD cores contain neutral lipids (e.g. TG and sterol esters), they are surrounded by a phospholipid monolayer and associated PLIN proteins. Modified from [Mar06]. B) LDs analyzed by electron microscopy in Huh7.5 cells. Shown are cytosolic LDs in close proximity to other cellular organelles like mitochondria (M) or Golgi (G). Scale bar 500 nm. Image kindly provided by Valerie Mordhorst. C) Immunofluorescence staining of LDs and PLIN2/ADRP. Huh7.5 cells were fixed and stained with an antibody detecting PLIN2/ADRP. LDs were labeled with the neutral lipid stain BODIPY and analyzed by confocal microscopy. D) Immunofluorescence staining of HCV-infected Huh7.5 cells. Cells were infected with an HCV Jc1 WT strain. At day 3 post infection, cells were fixed and stained with an HCV core-specific antibody. LDs were labeled with the neutral lipid stain BODIPY and analyzed by confocal microscopy. Scale bar 10  $\mu\text{m}$ .

LDs are formed *de novo* within the ER bilayer, where enzymes of the DGAT and acyl-CoA:cholesterol acyltransferase (ACAT) enzyme family are located. DGAT enzymes use acyl-CoA and diacylglycerol as substrate to generate TG [Kue08]. ACAT enzymes are responsible

## 1. Introduction

for production of sterol esters from cholesterol and acyl-CoA [Buh01]. The LD biogenesis can be separated into three distinct stages: 1) synthesis of neutral lipids within the ER bilayer. 2) Accumulation of neutral lipids leading to the formation of a lens between the leaflets of the ER bilayer. 3) Additional neutral lipids accumulate at the lens, leading to a deformation of the ER bilayer and budding of nascent LDs into the cytosol (Figure 1.9). LDs can grow by permeation, meaning neutral lipid transfer of smaller LDs to larger LDs most likely controlled by fat specific protein of 27 kDa (FSP27). Furthermore, large LDs can also be formed by fusion of several small LDs [Wil14a]. LDs are often located close to the ER and some of them are still connected via ER-LD bridges. Recently it has been shown that the Arf1/COPI machinery controls the formation of ER-LD bridges in order to facilitate the re-localization of TG synthesizing enzymes (e.g. DGAT2) from ER to LDs, which is crucial for LD growth [Wil14b].

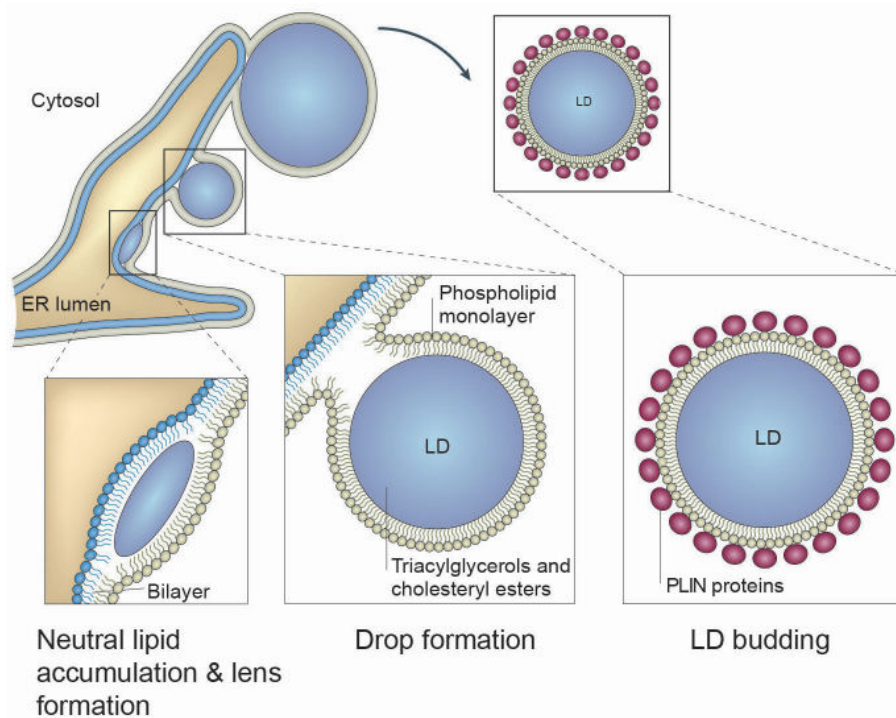


**Figure 1.9.: Formation of LDs.** LD formation starts with accumulation of neutral lipids between the leaflets of the ER bilayer. When the local neutral lipid concentration passes a threshold level, a lens of neutral lipids is formed. Additional neutral lipids lead to the deformation of the ER bilayer and budding of nascent LDs. Modified from [Mar06].

Beside the interaction with the ER, LDs are often found in close contact to other cellular organelles like peroxisomes, endosomes and mitochondria, indicating that LDs are actively involved in many cellular processes. Indeed, LDs accomplish multiple functions: they mainly act as lipid reservoirs, providing the cell with energy, lipids needed for membrane synthesis and signaling lipids, at any time [Wel15]. But they also fulfill protective functions by trapping large amounts of cholesterol or toxic lipids that could be otherwise harmful for the cell. For example, LDs are needed as buffers of *de novo* fatty acid synthesis to support ER homeostasis, autophagy and nutrient stress resistance [Vel16]. Furthermore LDs are involved in protein storage, e.g. histones during *Drosophila melanogaster* embryogenesis or HCV core during viral assembly [Far09]. LDs have also been linked to proteasomal/lysosomal degradation by temporarily storing hydrophobic

misfolded proteins (like ApoB, which would otherwise form aggregates within the cytosol) and providing a platform for degradation [Ohs06].

### 1.8.1. Pathogens that target LDs

LDs are also increasingly recognized as targets for diverse microbes, viruses and protozoan pathogens. It has been shown, that *Mycobacterium leprae* induce the recruitment and accumulation of LDs in bacteria-containing phagosomes of macrophages and Schwann cells. In macrophages LD recruitment depends on Toll-like receptor 2 (TLR2) signaling. This is in contrast to Schwann cells, where TLR6 signaling is involved, indicating a link between LD biology and innate immune response mechanisms. An accumulation of LDs contributes to an innate immune response that tolerates persistence of *Mycobacterium leprae* [Mat11b]. Another mycobacterium species, *Mycobacterium tuberculosis*, dysregulates the lipid metabolism of the host cell in order to create an environment permissive for long-term persistence. *Mycobacterium tuberculosis* infection leads to the differentiation of macrophages into lipid-rich foam cells. Foam cells accumulate LDs, which are needed as nutrient source for bacterial growth [Pey08]. LDs play also an important role in *Chlamydia trachomatis* infections. In infected epithelial cells LDs translocate to chlamydial replication centers; however the functional relevance is unclear so far. *Chlamydia trachomatis* encodes two proteins (Lda1 and Lda3) that target LDs when expressed individually. Furthermore, *Chlamydia trachomatis* changes the LD proteome leading to an enrichment of proteins involved in lipid metabolism, lipid biosynthesis and LD-specific functions clearly indicating that LD functions are modified and utilized by this bacteria [Sak15].

Dengue virus, a member of the *Flaviviridae* family, shares many characteristics with HCV such as its close connection to LDs. Dengue core protein localizes to LDs via an interaction with PLIN3/TIP47 [Car12]. It has been shown that LDs are involved in late steps of viral replication, providing a scaffold for nascent virion encapsidation. Blocking of LD formation by a fatty acid synthase inhibitor (C75) diminishes virion assembly and release, emphasizing an essential contribution of LDs during viral replication [Sam09]. LD-targeting is not limited to *Flaviviridae* as also Rotavirus, a member of the *Reoviridae*, associates with LDs. Early steps of Rotavirus replication occur in “viroplasms” representing cytoplasmic inclusion bodies. PLIN proteins co-localize with the major components of viroplasms at LDs. These interactions seem to be important for viroplasm formation and viral particle production, as drug-induced fragmentation of LDs significantly reduced viroplasms and virus production [Che10]. The outer capsid protein  $\mu 1$  of Orthoreoviruses (also a member of *Reoviridae* family) targets LDs and induces apoptosis. Interestingly, disruption of  $\mu 1$ /LD localization abolishes the induction of apoptosis. Thus localization of  $\mu 1$  to LDs might be a strategy to control apoptosis during viral replication [Cof06].

Several protozoan parasites are also able to trigger LD formation and induced LD modifications in the host cell. *Trypanosoma cruzi*, which causes the Chagas disease, induces an accumulation of LDs within macrophages through a TLR2-dependent mechanism. Inhibition of LD formation by C75 reduces intracellular parasite replication, suggesting a link between LD formation and *Trypanosoma cruzi* replication [Tol16]. An accumulation of LDs can also be observed in macrophages infected with *Leishmania major*. *Leishmania* lacks *de novo* mechanisms for cholesterol synthesis and has to hijack nutrients from the host cell; thereby LDs may act as energy source [Rab16]. So far, a number of other parasites has been described to modulate LD formation e.g. *Toxoplasma gondii*, *Plasmodium berghei*, *Plasmodium falciparum*, *Plasmodium yoelii*, *Leishmania amazonensis*, *Cryptosporidium parvum* and *Eimeria bovis* [Tol16].

### 1.8.2. Tracking LDs by super resolution microscopy

LDs are thought to represent HCV assembly sites and co-localization of viral proteins at LDs has been analyzed extensively by confocal laser scanning microscopy (CLSM). However, due to the small size ( $\sim 40\text{--}80\text{ nm}$ ) of HCV particles, they are observed as spots often twice their real size by conventional fluorescence microscopy, as CLSM shows a maximal resolution of  $200\text{ nm}$  laterally and  $500\text{ nm}$  axially [Col12]. To overcome this limitation, several super-resolution microscopy techniques were established, which can peer beyond the diffraction barrier ( $\sim 200\text{ nm}$ ). Especially, stimulated emission depletion (STED, resolution laterally  $30\text{--}50\text{ nm}$ , axially  $30\text{--}600\text{ nm}$ ), fluorescence photoactivated localization microscopy (fPALM, resolution laterally  $10\text{--}40\text{ nm}$ , axially  $\sim 10\text{--}50\text{ nm}$ ) or (direct) stochastic optical reconstruction microscopy (dSTORM, resolution laterally  $10\text{--}40\text{ nm}$ , axially  $\sim 10\text{--}50\text{ nm}$ ) are techniques reaching resolutions which should be suitable for imaging of viral particles or viral assembly sites (Figure 1.10) [Mag13].

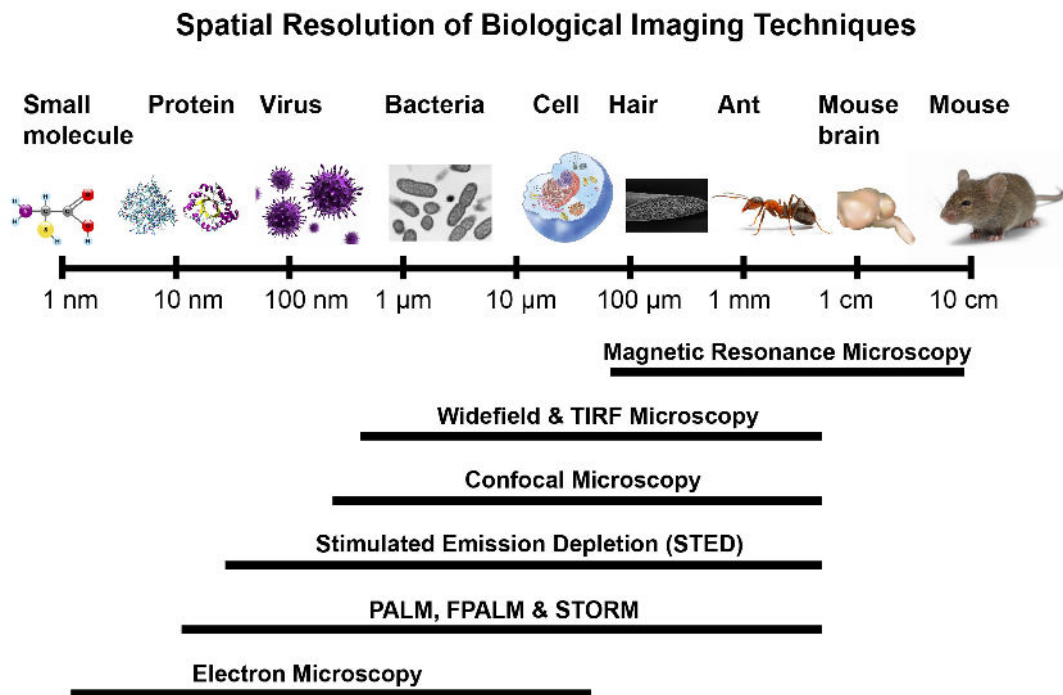


**Figure 1.10.:** Spatial resolution of several microscopy techniques. Shown are different microscopy techniques illustrating their range of spatial resolution.

STED microscopy was already used to visualize  $\beta$ -COP, a protein of the ADP ribosylation factor (Arf)/COPI machinery involved in vesicle trafficking, co-localizing with PLIN3/TIP47 at LDs (Figure 1.11) [Wil14b]. In STED, excited fluorophores at the periphery of the center of excitation were depleted by a donut-shaped depletion laser beam, resulting in an increased resolution beyond the diffraction limit. However, STED shows high photo bleaching and a limited axial resolution which make visualization of small viral particles or their assembly sites quite challenging [Mag13].

In dSTORM, high resolutions up to  $10\text{ nm}$  lateral and  $50\text{ nm}$  axial can be achieved. The improvement in resolution is based on reversible photo switching of fluorochromes. Therefore, most of the fluorochromes are transferred into a dark non-fluorescence state by buffers containing a reducing thiol compound (e.g. DTT) that quenches the fluorophore. Fluorescence signals of



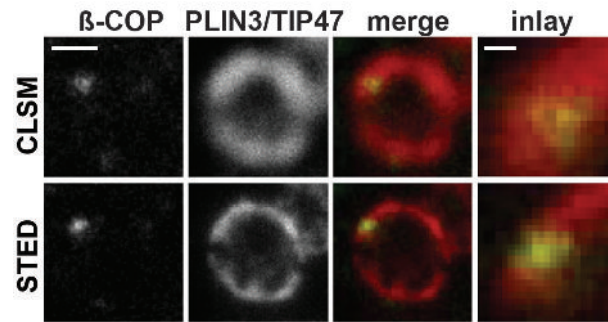


**Figure 1.11.:** Co-localization of the COPI machinery at LDs analyzed by STED. Co-localization of  $\beta$ -COP and PLIN3/TIP47 at LDs analyzed by CLSM and STED. Scale bar 500 nm (overview) or 100 nm (inlay) [Wil14b].

single molecules are then spontaneously recovered leading to “blinking” which can be used to determine the precise localization of each fluorophore. dSTORM images are then reconstructed by blotting the measured positions of each fluorescent molecule (Figure 1.12) [Hei10]. In virology, dSTORM has already successfully been used to perform multicolored analysis of herpes simplex virus type 1 particles or the visualization of human immunodeficiency virus (HIV1) assembly sites [Lai15, Mur13].

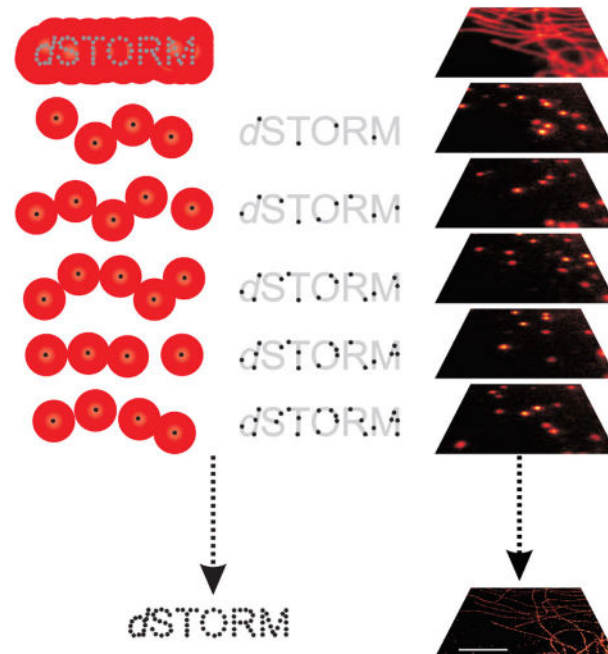


**Figure 1.12.:** Principle of dSTORM. In dSTORM only a subset of photoswitchable fluorophores are transferred from a dark state into a fluorescence state and the position of each fluorescent molecule is detected. dSTORM images are then reconstructed from thousands of these images. Scale bar 2  $\mu$ m. Modified from [vdL11].

## 1.9. Annexins

Annexins (ANXA) are  $\text{Ca}^{2+}$  and phospholipid-binding proteins. They are named after the Greek “annex” standing for “bring/hold together” which characterizes the common feature of all annexins: they bind to and potentially hold together cellular membranes and thereby act as bridging proteins. Annexins are characterized by two major criteria:  $\text{Ca}^{2+}$  dependent binding to negatively charged phospholipids and containing a conserved core domain. Annexins consists of two domains, a variable “head” domain at the N-terminus and the annexin core domain containing four conserved segments of 70 amino acids per segment. The core domain harbors the  $\text{Ca}^{2+}$  and lipid-binding sites. Chrystal structure analysis revealed a highly  $\alpha$ -helical fold of the annexin core domain leading to a slightly curved disc structure with principally two sides (Figure 1.13) [Ger02]. The convex side contains  $\text{Ca}^{2+}$  binding sites and therefore faces the membrane, when annexin binds to phospholipids. The concave side contains the N-terminal domain, opposing the membrane and mediating interaction with cytoplasmic interaction partners (e.g. ANXA2 interaction with the small dimeric S100 protein enables simultaneously binding of two membranes). Furthermore, the N-terminal domain partially interacts with the core domain. It has been shown that mutations in the N-terminal region of ANXA3 directly influence the  $\text{Ca}^{2+}$  dependent phospholipid-binding properties of the convex side of the molecule, indicating the importance of this domain.

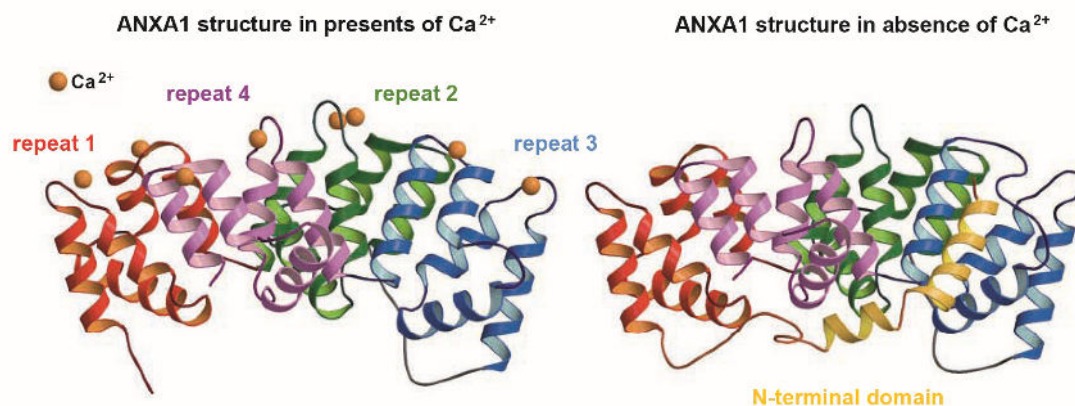


**Figure 1.13.: Crystal structure of ANXA1.** Ribbon diagrams of full length ANXA1 in the presence and absence of  $\text{Ca}^{2+}$ . The highly  $\alpha$ -helical folding of the core domain forms a disc (repeat 1 shown in red, repeat 2 in green, repeat 3 in blue, repeat 4 in purple). The N-terminal region is shown in yellow. Calcium ions are illustrated in orange. In the absence of  $\text{Ca}^{2+}$  ions, parts of the N-terminal domain integrate into the core domain.  $\text{Ca}^{2+}$  binding triggers exposure of the N-terminal region. Modified from [Ros03].

To date, more than 160 unique annexin proteins in more than 65 species (ranging from fungi to plants and higher vertebrates) have been identified. In humans there are 12 annexins (ANXA1–ANXA13, ANXA12 is unassigned) described so far [Ger02, Res04]. They are ranging in size from 15 kb (ANXA9) to 96 kb (ANXA10) and show a broad range in expression levels, varying from universal (ANXA1, 2, 4–7 and -11) to selective, like ANXA3 in neutrophils and liver or ANXA13 in the small intestine. Annexins are localized in the cytosol and can be found in stable or soluble form. They are reversibly associated with proteins mediating interactions with the extracellular matrix or with components of the cytoskeleton. Annexins can also translocate from the cytosol to the cell surface (e.g. ANXA1) [Sol94, Mir16].



Interestingly, several Annexins have already been identified as viral host factors. Influenza A virus (IAV) recruits ANXA5 to viral budding sites, where ANXA5 is incorporated into nascent viral particles. This represents a viral strategy to escape from immune surveillance, as ANXA5 inhibits the interferon gamma signaling pathway [Ber14]. IAV also induces ANXA1 expression leading to enhanced viral replication, viral binding to target cells and an increase of endosomal trafficking of viral particles to the nucleus [Aro16]. Besides IAV, also HCV has been linked to several Annexins. HCV RNA replication is significantly reduced in cells expressing ANXA1, suggesting that ANXA1 negatively regulates HCV replication [Hir15]. Endogenous ANXA2 interacts with NS3/4A, NS4B, NS5A and NS5B in Huh7.5 cells transfected with plasmids encoding HA-tagged NS proteins. Furthermore, silencing of ANXA2 impaired MW formation and thereby viral RNA replication, suggesting that ANXA2 is important for NS protein recruitment to induce MW formation [Sax12]. Of note ANXA2, -4 and -5 were also identified to participate in the formation of crude replication complexes. A different group reported that ANXA2 acts as a HCV host factor for viral assembly, rather than for viral RNA replication [Bac10]. These findings illustrate the multifunctionality of ANXA2 and indicate that ANXA2 might act at different steps of the viral life cycle, ranging from RNA replication to particle assembly.

### 1.9.1. Annexin A3

The ANXA3 core domain shows large structural homologies to ANXA5, however, the N-terminal region is 3 amino acids longer than the corresponding ANXA5 region. ANXA3 can be secreted and internalized via caveolae-mediated endocytosis [Ton15]. Little is known about the functional role of ANXA3. Dysregulation of ANXA3 expression seems to be involved in the development, progression and drug resistance for several cancers. An upregulation of ANXA3 expression supports the development of colorectal adenocarcinoma and pancreatic carcinoma, correlates with elevated drug resistance in ovarian cancer patients and facilitates progression of lung adenocarcinoma and HCC. In contrast, repression of ANXA3 expression facilitates renal- and prostatic carcinoma formation [Wu13]. In HCC tissue, upregulated ANXA3 expression correlated with advanced tumor stages. Furthermore it has been shown that ANXA3 effects DNA synthesis and thereby participates in the growth regulation of rat hepatocytes *in vitro* and *in vivo*, suggesting an impact of ANXA3 on rat liver regeneration [Har08]. Interestingly, silencing of ANXA3 in 3T3-L1 cells (a fibroblast cell line, which can be differentiated into adipocytes) resulted in an accumulation of LDs accompanied by elevated peroxisome proliferator-activated receptor  $\gamma$ 2 (PPAR $\gamma$ 2) mRNA levels and progressive differentiation into adipocytes [Wat12].



## 2. Aim of the dissertation

The development of the JFH1-based fully infectious cell culture model system in 2005 has enabled the investigation of the entire HCV life cycle. Since then, important contributions regarding viral replication have been made. However, the late steps of the viral life cycle like assembly, maturation and release are still poorly understood.

In this late stage of the viral life cycle, LDs play an essential role, acting as viral assembly platforms. It has already been shown that expression of the HCV core protein influences the LD proteome in HepG2 cells, implying that HCV has to change the LD proteome in order to create an environment, suitable for viral replication [Sat06]. If and how HCV modifies the LD proteome during infection with a replication-competent virus is not known. Therefore, the first aim of the dissertation was a quantitative LD proteome analysis of HCV-infected hepatoma cells to identify putative HCV host factors involved in viral replication. Subsequently, the functional relevance of identified LD-associated proteins was investigated. Thus, knockdown cell lines were generated and challenged with a HCV reporter virus to analyze their impact on viral replication. A novel HCV-host factor, identified by this experimental approach, was further characterized in more detail to elucidate its molecular mechanism during viral replication.

Due to the limited resolution of microscopy techniques used and the scarcity of HCV assembly events, visualization of this process was largely unsuccessful so far. At early stages of viral assembly, the LD-associated viral proteins core and NS5A interact to recruit newly synthesized viral RNA to the surface of LDs or LD-associated ER-membranes, where encapsidation occurs and budding is initiated. At these putative assembly sites, core and NS5A have to be in close contact with the viral envelope E1/E2 complex. Therefore, the second aim of this dissertation was the visualization of core or NS5A together with E2 at LDs or surrounding ER-structures of HCV-infected cells by super-resolution microscopy (dSTORM). Afterwards, putative viral assembly events were reconstructed and analyzed in 3D.



## 3. Results

### 3.1. Quantitative LD proteome analysis of HCV-infected hepatoma cells

In order to perform a quantitative LD proteome analysis of HCV-infected cells, stable isotope labeling by heavy amino acids in cell culture (SILAC) was used. In this SILAC-based approach, the LD proteome of two cell populations (HCV-infected vs. non-infected) were compared: one labeled with “heavy” amino acids and one labeled with “light” (normal) amino acids. The incorporation of heavy amino acids leads to a defined mass shift of all corresponding peptides compared to the control. Due to the molecular weight, the two proteomes can be distinguished and quantified by mass spectrometry (MS) [Man06].

#### 3.1.1. SILAC labeling of Huh7.5 cells

Huh7.5 cells were cultured in media containing heavy  $^{13}\text{C}_6$  L-lysine-2HCl and  $^{13}\text{C}_6$  L-arginine-HCl amino acids or light L-lysine-2HCl and L-arginine-HCl amino acids, which served as a control. Incorporation of heavy isotopes was confirmed by mass spectrometry. Therefore, Huh7.5 cells were cultured in media containing heavy or light amino acids for six passages. Afterwards, cells were harvested and sonicated in LD isolation buffer (50 mM potassium phosphate buffer (PPB) pH 7.4, 100 mM KCl, 1 mM EDTA and protease inhibitor cocktail). 100  $\mu\text{g}$  protein was separated by SDS-PAGE, gels were stained with Coomassie blue and protein bands were excised. In-gel tryptic digestions were performed and peptides were analyzed by liquid chromatography-electrospray ionization-tandem mass spectrometry (LC-ESI-MS/MS). As an example the precursor ion spectrum of the SILAC labeled tryptic peptide DLTDYLMK with the mass to charge ratio ( $m/z$ ) 502.76 of human actin is shown (Figure 3.1 A). Peptides containing heavy isotopes were shifted by three  $m/z$  compared to light peptides. The spectrum confirmed that SILAC labeling was completed, since no signal for the “light“-SILAC peptide at  $m/z$  499.76 was observed. The fragment ion mass spectrum of the SILAC labeled tryptic peptide DLTDYLMK confirmed the actin peptide sequence (Figure 3.1 B). The data indicate that all corresponding amino acids were replaced by a heavy amino acid version after six passages of cell culture.

#### 3.1.2. Quantification of LD-associated proteins

After exchange of lysine and arginine by their heavy  $^{13}\text{C}_6$  L-lysine-2HCl and  $^{13}\text{C}_6$  L-arginine-HCl versions was confirmed by LC-ESI-MS/MS, Huh7.5 cells were labeled for LD proteome analysis. At the same time, control Huh7.5 cells were infected with an HCV Jc1<sup>NS5A-NS5B-mKO2-BSD</sup> reporter virus, which contains a monomeric kusabria orange (mKO2) fluorescence reporter protein as well as a blasticidin S deaminase (BSD) gene (which serves as selection marker) in-between a duplicated NS5A-NS5B cleavage site. Five to ten days after infection, cells were selected with 10  $\mu\text{g}/\text{ml}$  blasticidin for six to ten days. Afterwards viral infection rates were measured by flow cytometry. For each experiment, HCV-infected cells were used that showed infection rates

### 3. Results

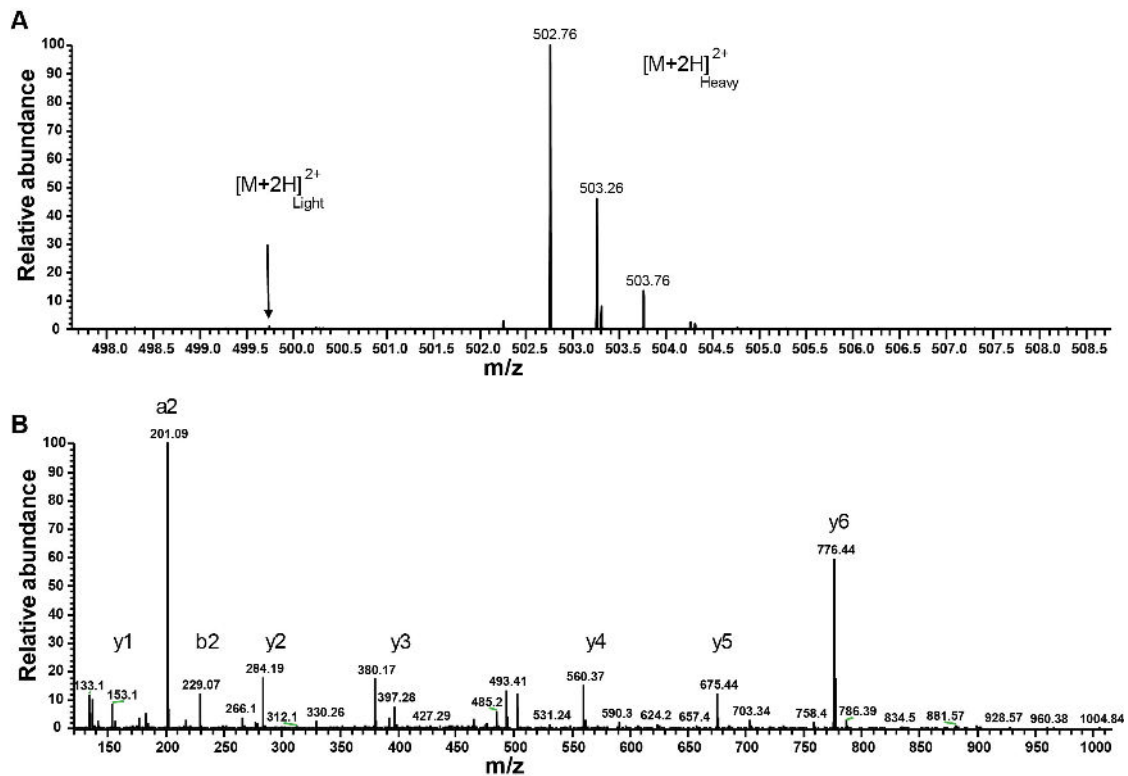


**Figure 3.1.:** Precursor ion and fragment ion mass spectrum of the SILAC labeled peptide DLTYLMK. A) Precursor ion spectrum of the SILAC labeled tryptic peptide DLTDYLMK. The spectrum shows a signal for the doubly charged peptide with m/z 502.76 and confirmed complete SILAC labeling, since no signal for the “light“-SILAC peptide at m/z 499.76 was detectable. B) Fragment ion spectra of the SILAC labeled peptide DLTDYLMK. The fragment ion spectra showed a complementary b- and y-ion series, confirming the peptide sequence DLTDYLMK. MS analysis was performed by Marcel Kwiatkowski.

higher than 95%, thereby minimizing the contribution of non-infected cells to the proteomic data. One day prior LD isolation, naïve cells (labeled with heavy amino acids) and HCV-infected cells (labeled with light amino acids) were seeded at the same density. The next day, cells were counted and  $5 \times 10^7$  cells from each cell population were mixed and lysed in sucrose buffer (0.25 M sucrose, 1 mM EDTA, 1 mM DTT and protease inhibitor cocktail) using a Dounce homogenizer. Nuclei and cell debris were removed by centrifugation at 1000 g and 4 °C. Post-nuclear fractions were loaded into 4 ml ultra-clear thinwall centrifuge tubes and overlaid with LD isolation buffer. After two sequential centrifugations in an SW60 Ti rotor for 2 h at 100.000 g and 4 °C, LDs were visible as a white band floating on top of the gradient. LDs were harvested and washed three times in LD isolation buffer. Protein concentration was determined by DC assay (Biorad). Afterwards, LD fractions were separated by SDS-PAGE, followed by Coomassie blue staining to visualize LD-associated proteins. Protein bands were excised and tryptically digested in order to analyze peptides by LC-ESI-MS/MS (Figure 3.2 A). To exclude differences due to the SILAC labeling conditions, one experiment was performed with HCV-infected cells labeled with heavy amino acids mixed together with naïve cells cultured in media containing light amino acids. In order to confirm an enrichment of LDs with this experimental approach, post nuclear- and LD-fractions were analyzed by SDS-PAGE and western blotting.

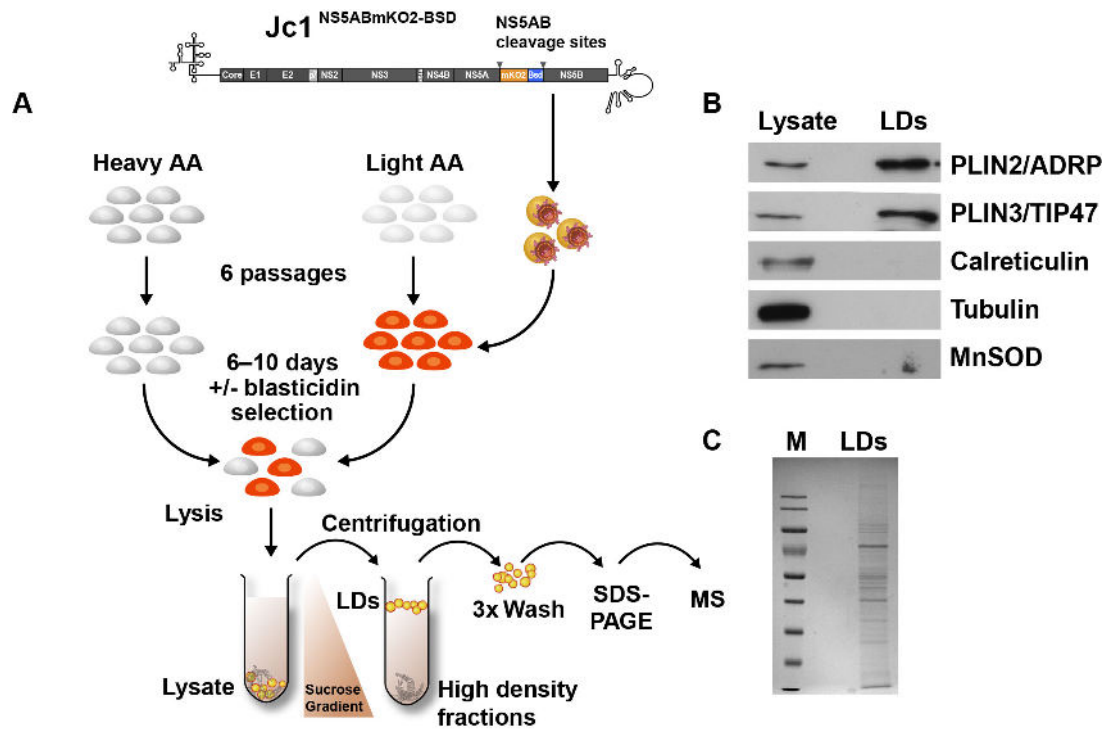


**Figure 3.2.: Experimental outline of quantitative LD proteome analysis.** A) Naïve Huh7.5 cells were labeled with heavy amino acids or light amino acids. Cells carrying light amino acids were infected with a Jc1<sup>NS5AB-mKO2-BSD</sup> reporter virus. After selection with blasticidin nearly 100% of cells were HCV positive. Then light and heavy-labeled populations were mixed in the same ratio and LDs were isolated, separated by SDS-PAGE and analyzed by LC-ESI-MS/MS. MS analysis was performed by Marcel Kwiatkowski. B) Western blot analysis of post-nuclear and LD fractions shows an enrichment of LD-marker proteins in LD fractions, as well as the purity of these fractions. C) Coomassie blue staining of LD fractions separated by SDS-PAGE.

Analysis of LD-marker proteins like PLIN2/ADRP or PLIN3/TIP47 confirmed enrichment in LD fractions. Furthermore, the purity of LD fractions was verified by detection of marker proteins of other cellular compartments, like calreticulin (ER),  $\beta$ -tubulin (microtubuli) or mitochondrial manganese-dependent superoxide dismutase (MnSOD) (mitochondria). Using this experimental approach, no contamination of other cellular compartments was detectable in LD fractions, suggesting that proteins identified by LC-ESI-MS/MS are LD-associated (Figure 3.2 B). Moreover, Coomassie blue staining of LD fractions visualized the range of proteins associated with LDs (Figure 3.2 C).

Four independent experiments on two different MS platforms were performed. Around 1500 proteins were identified and 316 proteins were recognized by multiple peptides in each of the experiments (Figure 3.3 A, 8.3 Supplementary data Table S1). Next, the detection ratios of light over heavy peptides (L/H) or vice versa in swapped labeling conditions (H/L) were centered by dividing through the median of identified proteins, to exclude difference caused by different cell numbers or variations in the amount of LDs. Correlation analysis over all identified proteins revealed a reproducible protein quantification with a mean Pearson's correlation coefficient of  $r = 0.54$  for all experiments, independently of the labeling conditions, blasticidin selection, or MS platform (Figure 3.3 B,C).

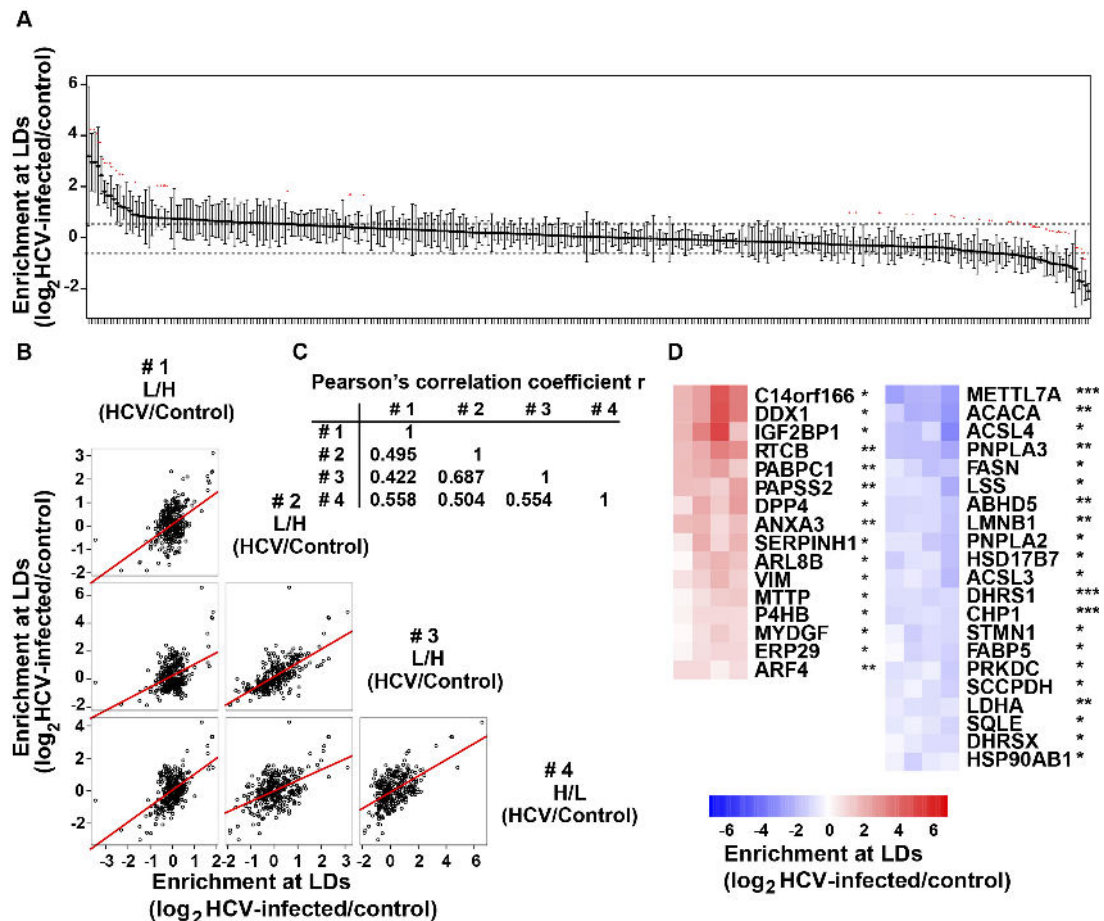


**Figure 3.3.: Quantitative analysis of identified LD-associated proteins.** A) Plot of the LD-associated proteins ranked according to their mean enrichment ratio ( $\log_2$  HCV-infected/control) and centered around the median (Mean  $\pm$  SD,  $n = 4$ , \* $p < 0.05$ , \*\* $p < 0.01$ , \*\*\* $p < 0.001$ ). Lines indicate 1.5-fold cut-off values in fold enrichment/depletion used for further analysis. B) Scatterplot and regression analysis of all proteins identified in four independent experiments, in #1–#3 HCV-infected cells were cultured in light amino acids and control cells in heavy amino acids; in #4 culturing conditions were switched. Shown is the enrichment score at LDs as  $\log_2$  HCV-infected over control normalized to the median. C) Pearson's correlation coefficient  $r$  between the different experiments. D) Heatmap showing significantly enriched or depleted proteins (1.5-fold cutoff, \* $p < 0.05$ , \*\* $p < 0.01$ , \*\*\* $p < 0.001$ ).



Next, the detection ratios of the identified proteins were arranged according to their mean enrichment at LDs. To classify identified proteins, a cut-off ratio greater than 1.5-fold enrichment or depletion was defined (Figure 3.3 A). Following the statistical evaluation a list of 16 proteins that were significantly enriched at LD fractions of HCV-infected cells and 21 proteins that were significantly depleted was generated (Figure 3.3 D). For follow up studies PubMed searches were used to analyze whether the identified LD-associated proteins were already linked to search terms like “HCV” or “lipid droplet”. 35% of the proteins detected in LD fractions have previously been annotated with the term “lipid droplet”, while 37% were annotated together with term “HCV” (Figure 3.4 A). Intriguingly, around one quarter was found together with both search terms. Additionally the LD proteome dataset was compared to other genome-wide datasets generated in HCV-infected cells. Comparison revealed a significant overlap with HCV-interaction networks [Ram15] and three RNAi screens for HCV host dependency and restriction factors [Tai09], [Li09], [Poe15] (Figure 3.4 B). In this approach the whole dataset was included as even unaltered proteins associated with LDs or surrounding membranes might act as HCV host factors.

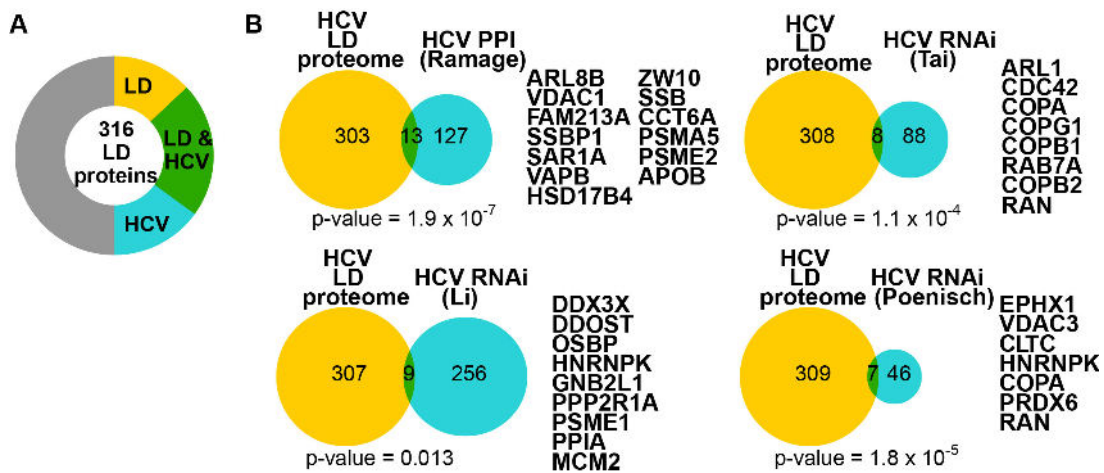


**Figure 3.4.: Characterization of LD proteome of HCV-infected cells.** A) PubMed searches were performed to assess the proportion of the 316 identified LD-associated proteins that have already been linked to either “lipid droplet” or “HCV” search terms. 35% of the identified proteins have previously been linked to the term “lipid droplet” and 37% were annotated together with “HCV”. B) Venn diagrams indicting an overlap between identified LD-associated proteins and previously identified HCV interaction partners [Ram15] or host dependency or restriction factors identified by siRNA screens [Tai09, Li09, Poe15]. P-values were calculated using GeneOverlap package in R.

In order to connect identified LD-associated proteins to a putative molecular function, gene ontology (GO) enrichment analysis was performed. Proteins that are enriched at LDs in HCV-infected cells are usually not associated with LD functions, like RNA-binding proteins or proteins associated with the formation of vesicles or stress granules. Intriguingly, proteins depleted from LDs in HCV-infected cells, are all involved in LD-associated functions, such as biosynthetic/metabolic processing of cholesterol, triglycerides or fatty acids (Figure 3.5 A). The data indicate that HCV disconnects LDs from their normal metabolic function. Furthermore, a protein network analysis was performed, highlighting the protein clusters of significantly enriched or depleted proteins (Figure 3.5 B).

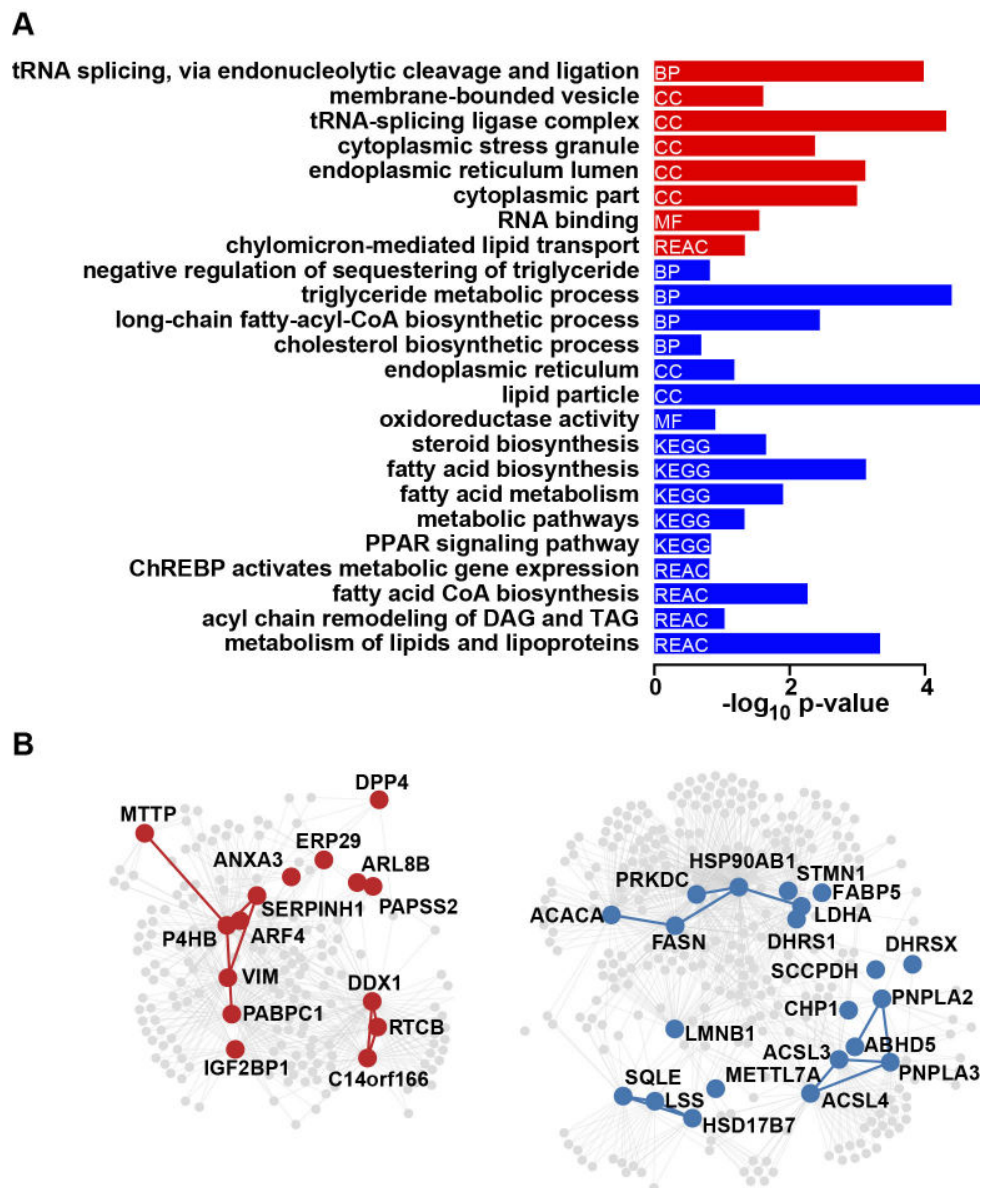


**Figure 3.5.: Gene ontology enrichment analysis and protein interaction network of dysregulated proteins.** A) Gene ontology (GO) enrichment analysis of annotations for molecular function (MF), cellular compartment (CC), biological process (BP) and biological pathways through Kyoto Encyclopedia of Genes and Genomes (KEGG) and the Reactome database (REAC). Shown are annotations significantly enriched and hierarchically filtered for enriched (red) or depleted (blue) LD-associated proteins. Analysis was performed using the gProfileR package in R. B) Protein interaction networks of dysregulated LD-associated proteins. Shown are the interaction networks of significantly enriched (red) or depleted (blue) proteins. Analysis was performed using the cisPath package in R.

### 3.1.3. Validation of LD-associated host proteins

In order to corroborate the proteomics data, eight cellular candidate proteins were validated in follow up studies. These host proteins were selected based on the following criteria: 1) number of unique peptides ( $n \geq 2$ ); 2) enriched in LD fractions of HCV-infected cells; 3) no previous description as HCV host factor, based on PubMed search. Lentiviral particles encoding either irrelevant non-targeting (NT) shRNA or a target-specific shRNA were generated to create stable knockdown cell lines. These constructs also expressed mCherry that allows monitoring the transduction efficacy by flow cytometry. Huh7.5 cells were transduced and knockdown efficacy was measured via quantitative reverse transcription PCR (RT-qPCR) at day three and day five post transduction (Figure 3.6). All experiments were performed with cells that showed transduction efficacies of more than 90% (measured by flow cytometry).

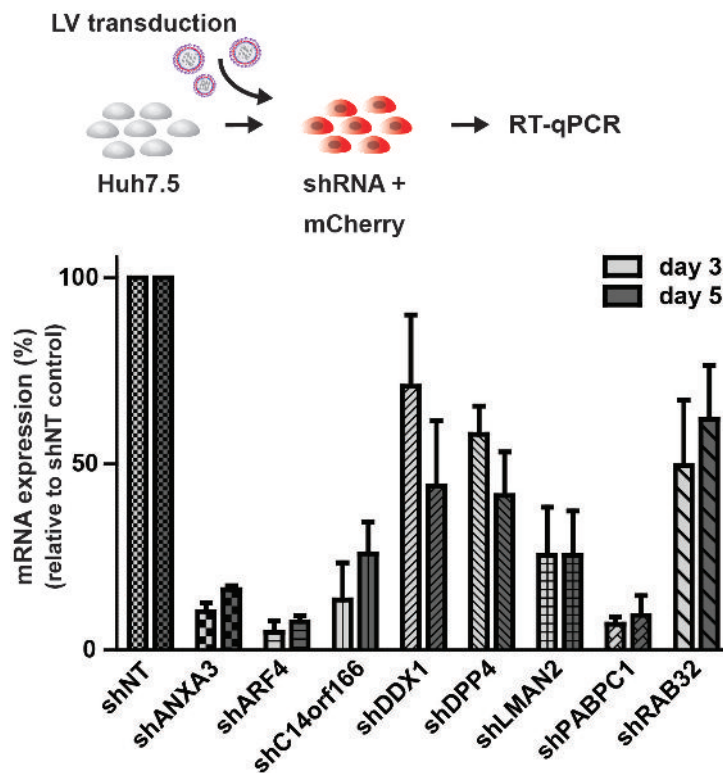


**Figure 3.6.:** mRNA knockdown of candidate LDs-associated host factors. Huh7.5 cells were transduced with lentiviral particles carrying target specific shRNA. Knockdown efficacy was measured by RT-qPCR at day three and day five post transduction. Percentage of downregulation was compared to the shNT control (Mean  $\pm$  SEM,  $n = 3$ ). Values were normalized to glyceraldehyde 3-phosphate dehydrogenase (GAPDH) levels.

Compared to control cells, a shRNA-mediated knockdown on mRNA level was observed for all lentiviral constructs at day three and day five post transduction. shRNAs targeting annexin A3 (ANXA3), ADP-ribosylation factor 4 (ARF4) and polyadenylate-binding protein 1 (PABPC1) showed the strongest knockdown efficacy with  $> 90\%$  at day three and  $> 85\%$  at day five post transduction (knockdown of ANXA3 was also confirmed on protein level by western blotting (Figure 3.11)). Furthermore, a stable knockdown  $> 75\%$  was observed for UPF0586 protein C14orf166 (C14orf166) and lectin mannose-binding 2 (LMAN2). At day three after transduction, expression of ATP-dependent RNA helicase DDX1 (DDX1) and dipeptidyl peptidase 4 (DPP4)

### 3. Results

was reduced by ~30% (DDX1) and ~40% (DPP4). 48 h later, mRNA levels were further reduced by ~20%, respectively. In contrast, mRNA expression of ras-related protein RAB-32 (RAB32) was reduced by ~50% (day three) and ~38% (day five) indicating only a transient knockdown. After knockdown on mRNA level was confirmed for all cell lines, HCV spreading infection assays were performed. Three days post shRNA transduction, cells were challenged with a fluorescently-labeled HCV Jc1<sup>NS5AB-eGFP</sup> reporter virus at a low multiplicity of infection (MOI). At day two, four and six after infection, cells were harvested and the amount of mCherry and enhanced green fluorescence protein (eGFP) double positive cells were analyzed by flow cytometry (Figure 3.7).

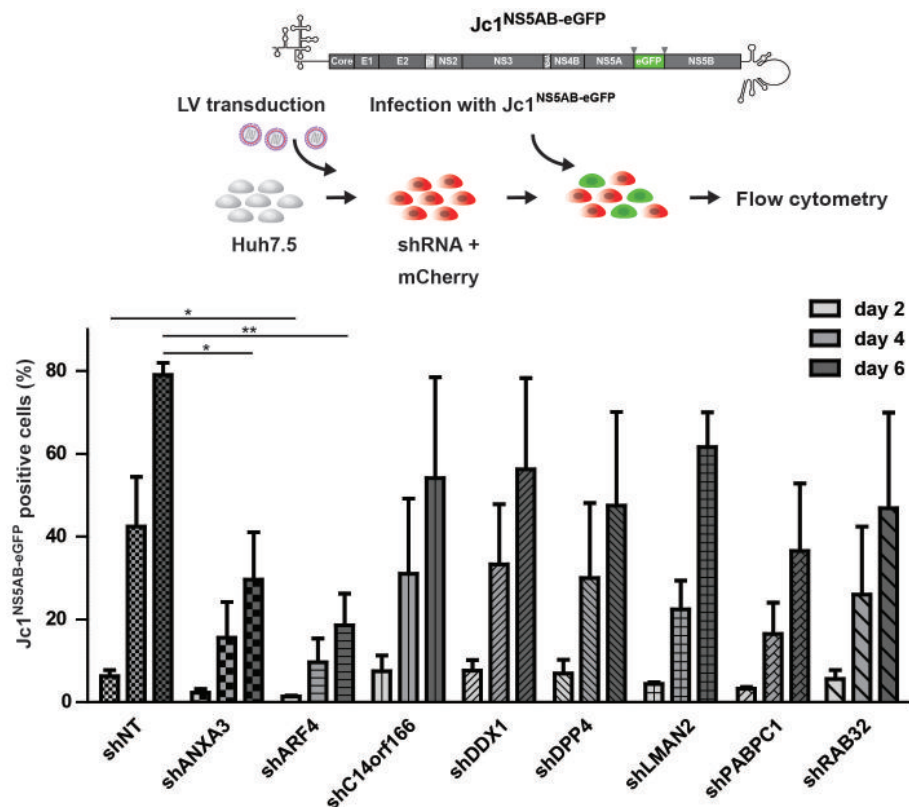


**Figure 3.7.: Depletion of ANXA3 and ARF4 inhibits HCV spreading infection.** At day three post transduction, Huh7.5-knockdown cell lines were infected with an HCV Jc1<sup>NS5AB-eGFP</sup> reporter virus. At day two, four and six after infection, cells were harvested and mCherry/eGFP double positive cells were measured by flow cytometry (Mean  $\pm$  SEM, n = 3, \*p < 0.05, \*\*p < 0.01).

HCV spreading infection was detectable in all cell lines. However, a remarkable decrease in the number of infected cells was observed in cells silenced for ANXA3 and ARF4. Silencing of ANXA3 led to a reduction of infection by ~70% at day six post infection. Compared to the control, silencing of ARF4 resulted in a ~80% decrease in HCV infection. Furthermore, a moderate inhibition by ~60% was observed in cells where PABPC1 was down-regulated. Notably, silencing of RAB32 also impaired an HCV infection by ~50% despite two times less knockdown efficiency, suggesting a proviral activity for RAB32. A delay in viral spreading was noticed in cells targeting LMAN2 at day two and day four post infection. However, a delayed viral spread was not detectable at day six, where LMAN2 reached infection levels comparable to RAB32, indicating that LMAN2 acts at the early steps of viral infection. Finally, silencing of C14orf166, DDX1 and DPP4 showed only a slight reduction or no effect on viral spreading.

As silencing of ANXA3 showed a strong phenotype in HCV spreading infection assays and members of the Arf family have already been described as HCV host factors [Mat11a], follow up studies were focused on the impact of ANXA3 on HCV replication. Previous studies reported Annexin A2 (ANXA2) as a HCV host factor, mainly involved in viral RNA replication [Sax12] or HCV assembly [Bac10]. The LD proteome study also identified Annexin A2, A4 and A5 in LD fractions, however only ANXA3 was enriched in HCV-infected cells. To clarify a potential impact of the identified annexins on viral replication, shRNA-transduced knockdown cell lines were generated and viral spreading was analyzed as described before. Analysis of RT-qPCR experiments revealed a reduction on mRNA level for all annexin shRNA constructs tested in this approach (Figure 3.8). Silencing of ANXA2 and ANXA5 showed the strongest reduction by ~95% on mRNA level at day three and day five post transduction. Again, transduction of a shRNA targeting ANXA3 reduced the mRNA by 85% at day five. In contrast, silencing of ANXA4 was slightly delayed and less efficient as RT-qPCR results revealed a reduction by ~65% at day five post transduction. Nevertheless, shANXA4 was also included in follow up spreading infection assays.

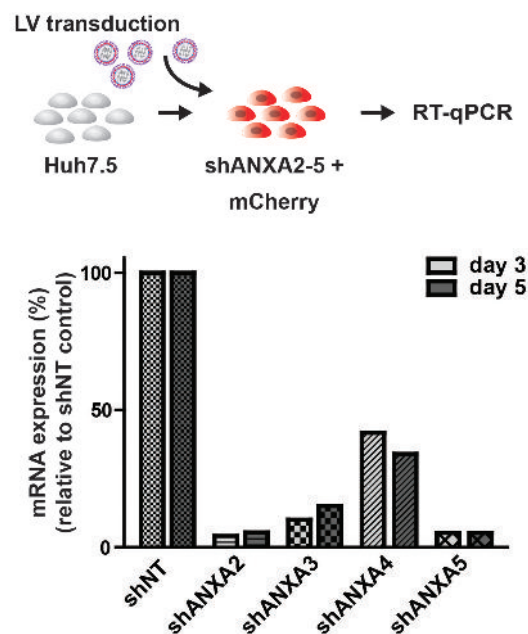


**Figure 3.8.: RNAi validation of Annexin A2–A5.** Huh7.5 cells were transduced with lentiviral particles carrying Annexin A2–A5 specific shRNAs. Knockdown efficacy was measured by RT-qPCR at day three and day five post transduction. Percentage of downregulation was compared to the NT control ( $n = 1$ ). Values were normalized to GAPDH levels.

As described before, spreading infection assays were performed with control and knockdown cell lines and analyzed by flow cytometry (Figure 3.9). At day 2 post infection, no difference in the amount of HCV-infected cells was observed, suggesting no influence on viral entry efficacy. 48 h after infection, a reduction in viral spread was noticed in shANXA3 and shANXA4 cells. At day six post infection, no difference in viral infection rates was detectable between control and ANXA4 knockdown cells, indicating a delay in viral replication in the absence of ANXA4. In this experimental approach, only ANXA3 silencing efficiently blocked HCV spreading.

To analyze an impact of ANXA3 on viral life cycle in more detail, clonal ANXA3 knockout cell lines were generated using the CRISPR/Cas9 system. In contrast to the shRNA-mediated



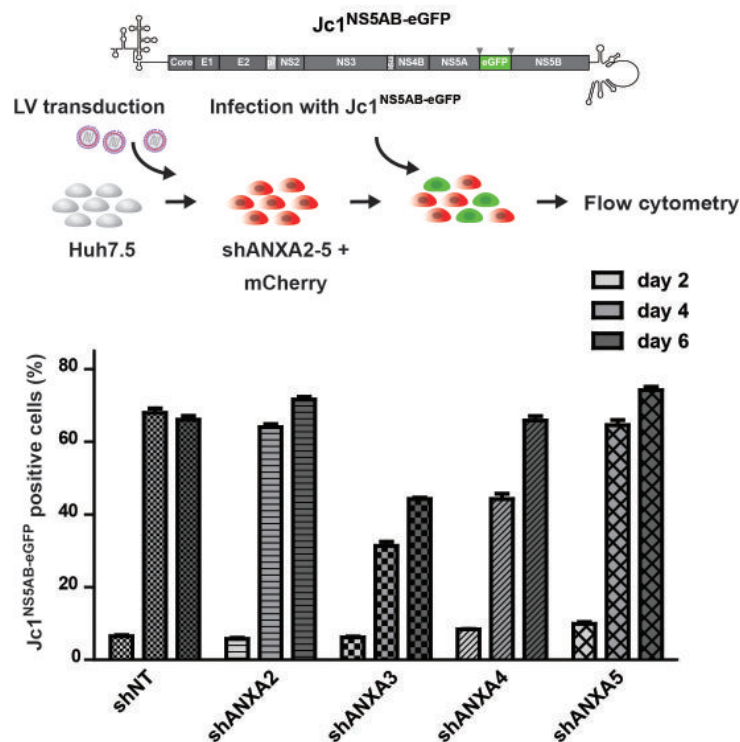


**Figure 3.9.:** HCV spreading infection in Annexin A2–A5 knockdown cells. At day three post transduction, Huh7.5 knockdown cell lines were infected with a HCV Jc1<sup>NS5AB-eGFP</sup> reporter virus. At day two, four and six after infection, cells were harvested and eGFP positive cells were measured by flow cytometry. Shown is one experiment performed in triplicate (Mean  $\pm$  SD).

knockdown cell line, where gene expression is post-transcriptionally downregulated, a knockout cell line allows observations in the context of a completely eliminated gene function. To generate ANXA3 knockout cell lines, Huh7.5 cells were transiently transfected with a plasmid encoding the RNA guided nuclease Cas9 and guide RNA (sgRNA) targeting the ANXA3 locus close to the translation start codon. Single cell clones were expanded and sequenced in order to identify insertions or deletions of bases into the coding region of the ANXA3 gene (Figure 3.10). Analysis of CRISPR/Cas9 treated cell lines revealed that three out of four clones were ANXA3 knockout cell lines (clone one to three). In contrast, clone four (WT) transiently expressed the Cas9 plasmid but nevertheless harbors the wild type alleles.

Next, viability of ANXA3 knockdown and knockout cell lines was measured to exclude any cytotoxic effects caused by ANXA3 silencing or deletion, transduction with lentiviruses or transfection with Cas9 expression plasmid. Cell viability of shANXA3- or knockout cell lines was comparable to parental Huh7.5 or control cells, indicating that ANXA3-knockdown or knockout or transduction/transfection had no cytotoxic side effects (Figure 3.11 A). Then, ANXA3 protein expression in shRNA- and Cas9- treated cell lines was analyzed by western blotting (Figure 3.11 B,C). Compared to shNT cells, ANXA3-knockdown cells showed a reduction by 85% on ANXA3 protein expression level. Regarding  $\Delta$ ANXA3 cell lines, no ANXA3 protein expression was detectable in clone one to three. However, compared to parental Huh7.5 cells, a slight reduction of 22% in ANXA3 protein expression level was observed in WT cells (clone four). Therefore, clone four was used as a control in follow up studies.

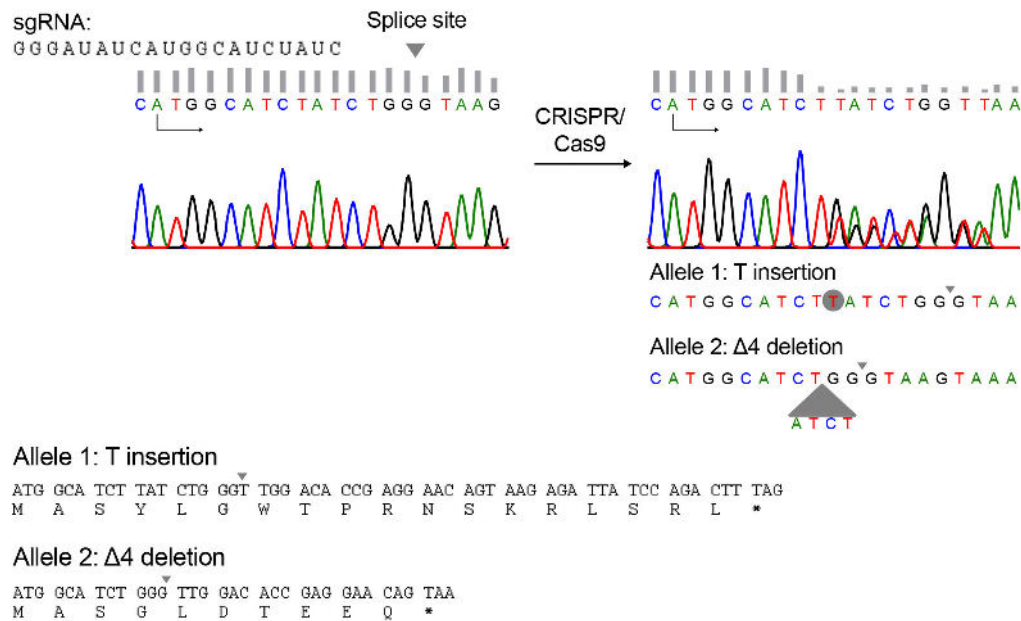


**Figure 3.10.: CRISPR/Cas9 mediated ANXA3 knockout.** Sequencing results of single ANXA3 knockout cell lines and parental Huh7.5 cells. The binding site of the sgRNA is indicated. One allele harbors a T insertion while the second allele carries a 4 nucleotide deletion mutation. Both mutations leave the splicing site intact and, if translated, would lead to the production of an 18 or 10 amino acid peptide respectively.

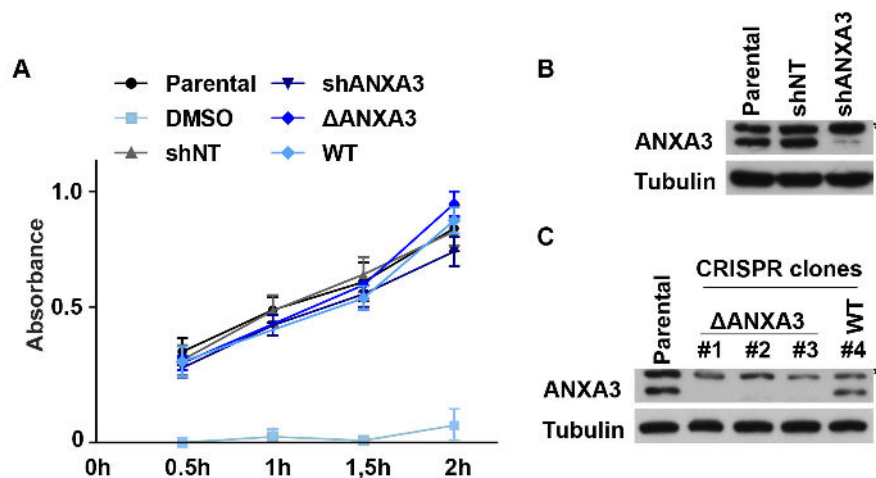


**Figure 3.11.: Viability of ANXA3-knockdown and -knockout cell lines and ANXA3 protein expression.** A) Viability of shRNA-transfected or CRISPR/Cas9-treated cell lines. Viability was measured as the quantity of produced formazan by absorbance at 490 nm. Treatment with 10% DMSO served as negative control. Shown is one experiment performed in triplicate (Mean  $\pm$  SD). B) ANXA3 protein expression in parental Huh7.5, shNT and ANXA3-knockdown cells analyzed by western blotting. C) ANXA3 protein expression in three ANXA3 knockout cell clones (clone #1-3), as well as one WT clone (clone #4) and parental Huh7.5 cells. Quantification of ANXA3 expression was performed by densitometric analysis of western blots. Asterisk marks an unspecific band.

### 3. Results

---

Afterwards, Huh7.5,  $\Delta$ ANXA3 and WT cells were challenged with a fluorescently labeled HCV Jc1<sup>NS5AB-mKO2</sup> reporter virus. Viral spread was analyzed by immunofluorescent staining of the viral NS5A protein and additionally measured by flow cytometry (Figure 3.12). Therefore, cell monolayers were fixed and stained for HCV NS5A at day three post infection. According to the NS5A staining, HCV-infected cells per infection foci were counted. Compared to the cell number per foci observed in parental Huh7.5 or WT cultures, cell numbers decreased  $\sim 4$  fold and  $\sim 2.7$  fold respectively, in  $\Delta$ ANXA3 cells (Figure 3.12 A). This phenotype was also confirmed by flow cytometry. When  $\Delta$ ANXA3 cells were infected with Jc1<sup>NS5AB-mKO2</sup> reporter virus, viral spreading infection was almost completely blocked compared to parental Huh7.5 or WT cells (Figure 3.12 B). The results of both experiments indicate a block or delay in HCV cell-to-cell transmission in the absence of ANXA3. However, WT cells that transiently expressed the Cas9 plasmid showed also a slight decrease in viral spreading compared to parental Huh7.5 cells (Figure 3.12 B). This could be due to the slightly reduced ANXA3 protein expression observed in these cells (Figure 3.11 C) or to the single cell clone expansion of the cell line.

Then, the expression of known HCV host factors was analyzed in parental-,  $\Delta$ ANXA and WT cells, ensuring that single cell expansion doesn't select for cells which are different in the expression of these proteins from parental Huh7.5 cells. First, the expression of surface receptors, which are important for viral entry, was analyzed by flow cytometry. Therefore Huh7.5, WT and  $\Delta$ ANXA cells were fixed and fluorescently labeled with antibodies recognizing CLDN1, CD81 and SR-B1. Flow cytometry analysis revealed a distinct shift from negative controls (cells stained with the secondary antibody alone, shown in grey) to cells labeled with specific antibodies, confirming the specificity of the antibodies. In addition, compared to parental cells, a slight increase in the expression of these entry factors was observed in Cas9 treated cells (Figure 3.12 D). The tight junction protein OCLN is also important for viral entry; however the OCLN-specific antibody was not suitable for flow cytometry. Thus, expression was analyzed by western blotting. Furthermore, the expression of ApoE (important for viral assembly) was also analyzed in this approach. However, no major differences in the expression of OCLN or ApoE were detected in Huh7.5, WT or  $\Delta$ ANXA3 cells (Figure 3.12 C). Finally, RT-qPCRs were performed to measure the expression of miR122, an essential host factor for viral RNA-translation and -replication. WT and  $\Delta$ ANXA3 cells showed a reduction by  $\sim 40$ – $50\%$  in miR122 expression compared to parental Huh7.5 cells (Figure 3.12 E). Although WT cells showed a drop of miR122 expression, only a slight reduction in viral spreading was observed, indicating that the reduced miR122 expression does not account for the phenotype observed in the  $\Delta$ ANXA3 cells.

Next, rescue experiments were performed as they represent the gold standard for validation of RNAi screens. Therefore, a non-targetable ANXA3 mutant (carrying a silent mutation that abolishes complementarity to the shRNA) or a targetable ANXA3 WT version of HA-tagged ANXA3 was generated and cloned into a lentiviral plasmid. This plasmid also contains the fluorescence marker protein cerulean (ANXA3-HA-IRES-cerulean). Afterwards, shANXA3 or control cells were transduced with lentiviral particles encoding these constructs to test whether expression of a silencing-resistant ANXA3 variant is sufficient to rescue the shANXA3 phenotype. Usage of two different colors gave the opportunity to distinguish between shRNA transduction efficacy (monitored by mCherry expression) and restored ANXA3 expression (observed by cerulean expression). Then, silencing and reconstitution efficacy was analyzed by flow cytometry (Figure 3.13 A). Comparable levels of mCherry expression were measured in shNT as well as in shANXA3, indicating an efficient lentiviral transduction. shANXA3 cells co-transduced with the ANXA3 WT version showed an efficient silencing of ANXA3 WT construct, compared to shNT cells where the ANXA3 WT construct was expressed. In contrast, co-transduction with



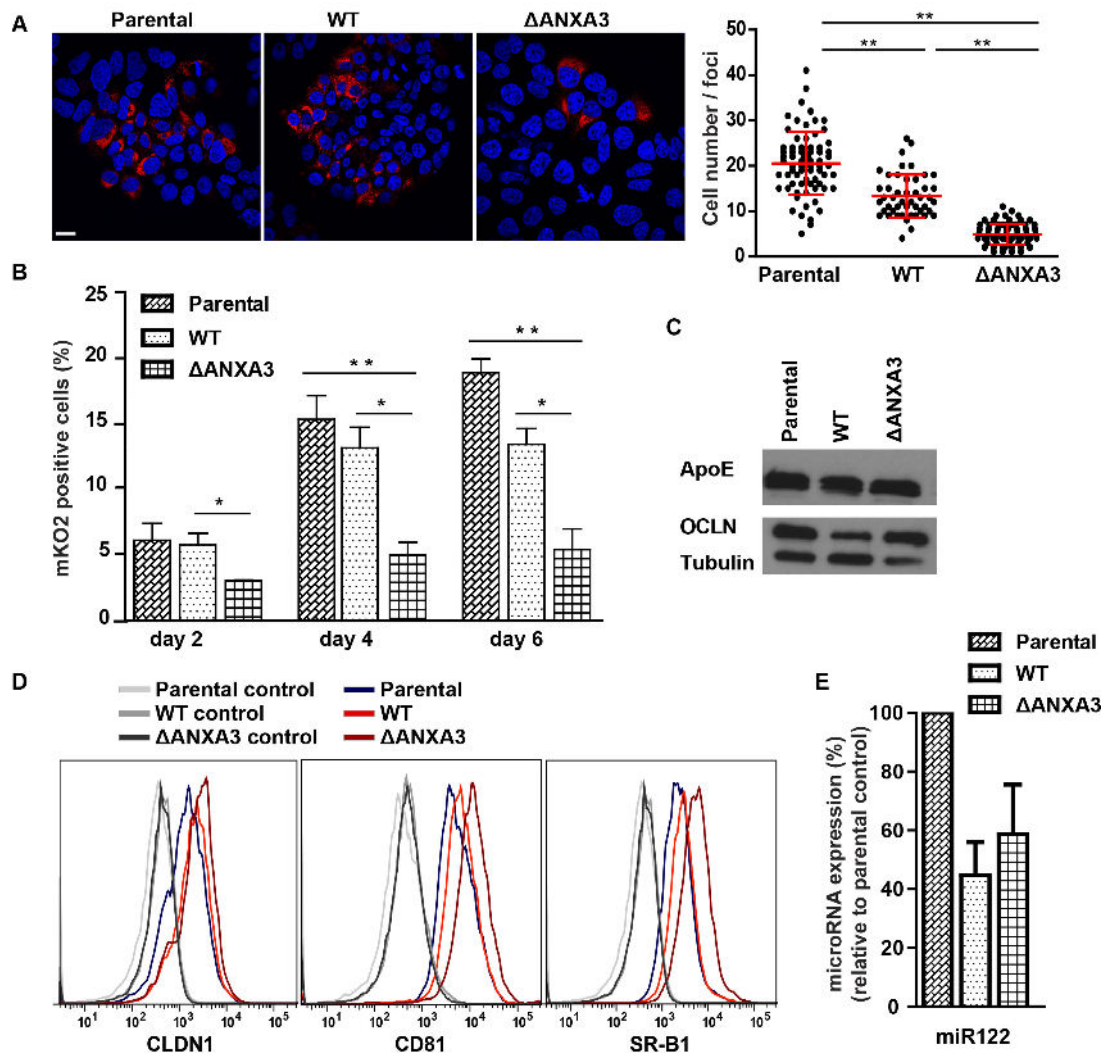


**Figure 3.12.: Knockout of ANXA3 severely reduces viral spreading.** A) Confocal microscopy of parental Huh7.5,  $\Delta$ ANXA3 (clone #3) and WT (clone #4) cells, infected with a low MOI of Jc1<sup>NS5AB-mKO2</sup>. At day three post infection, cells were fixed and stained, using an NS5A antibody, for microscopy. Nuclei were counterstained with Hoechst (scale bar 10  $\mu$ m). To analyze the number of infected cells per foci, cells were counted in two independent experiments with 2–3 wells respectively (Mean  $\pm$  SEM, \*p < 0.5, \*\*p < 0.01). B) HCV spreading infection in  $\Delta$ ANXA3 cells. Parental Huh7.5,  $\Delta$ ANXA3 and WT cells were infected with a Jc1<sup>NS5AB-mKO2</sup> reporter virus. Viral spreading was measured by flow cytometry at day two, four and six post infection (Mean  $\pm$  SEM, n = 3, \*p < 0.5, \*\*p < 0.01). C) ApoE and OCLN expression in Huh7.5, WT and  $\Delta$ ANXA3 cells analyzed by western blotting. D) Flow cytometry of Huh7.5, WT and  $\Delta$ ANXA3 cells stained with antibodies targeting CLDN1, CD81 and SR-B1 and a secondary Alexa-647 antibody. Staining with the Alexa-647 antibody alone served as a secondary antibody control (shown in grey). E) miR122 expression in Huh7.5, WT and  $\Delta$ ANXA3 cells analyzed by RT-qPCR. Percentage of downregulation was compared to Huh7.5 cells (Mean  $\pm$  SEM, n = 4). Values were normalized to 18S RNA levels.

### 3. Results

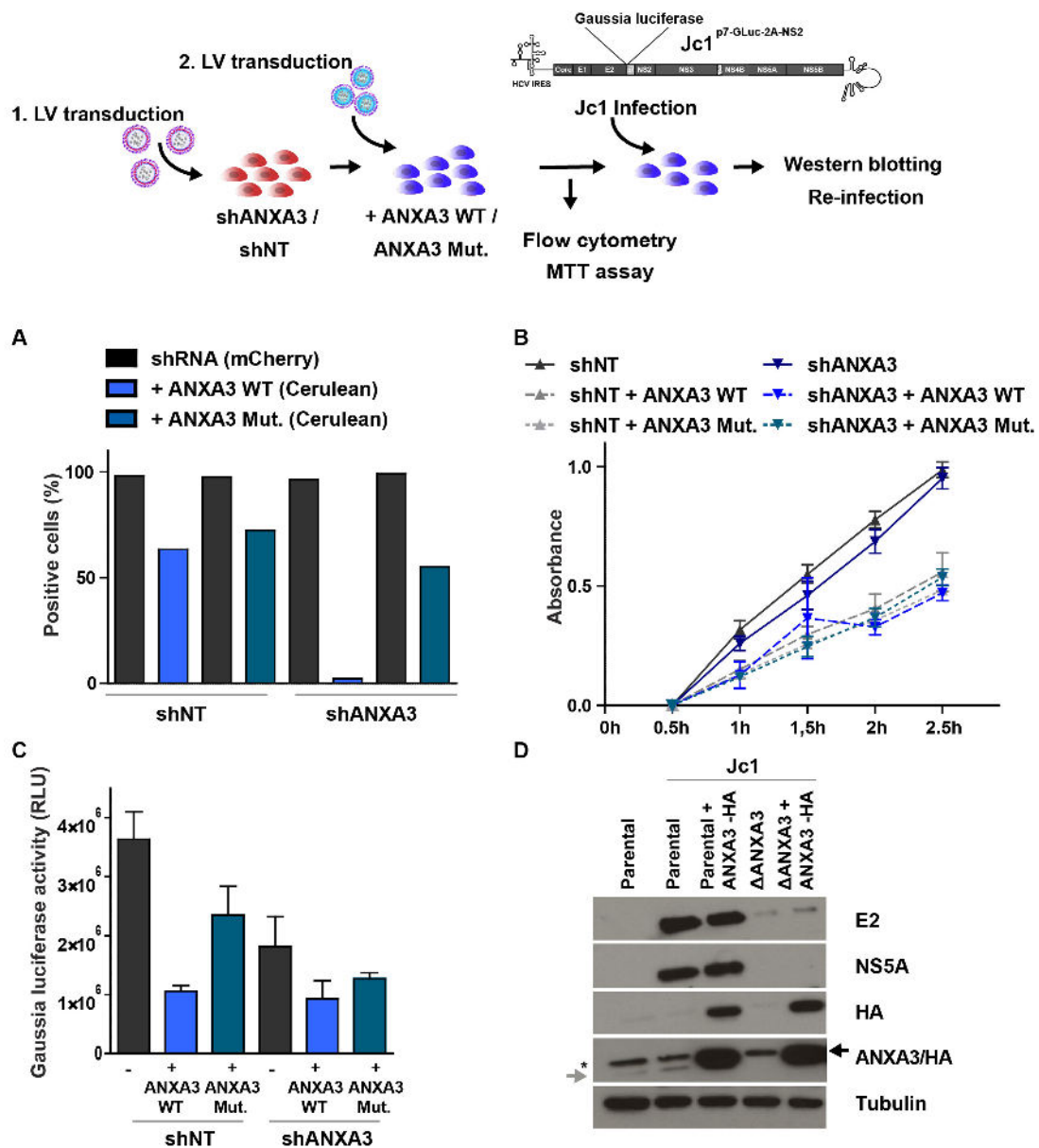


**Figure 3.13.: Overexpression of ANXA3 decreases cell viability and consequently HCV replication.** A) Huh7.5 cells were transduced with lentiviruses expressing mCherry and the indicated shRNAs together with a WT or silencing-resistant ANXA3 mutant construct expressing cerulean. Transduction efficacy was measured by flow cytometry, shown is one experiment. B) Cell viability was assessed by MTT assays. Shown is one experiment performed in triplicate (Mean  $\pm$  SD). C) Transduced cells were infected with Jc1<sup>p7-GLuc-2A-NS2</sup> virus stocks. Supernatant of infected cells was used to re-infect naïve Huh7.5 cells. Two days later, viral replication was analyzed by luciferase assays. Shown is the Gaussia luciferase activity (relative light units, RLU) (Mean  $\pm$  SEM, n = 3). D) Parental Huh7.5 and  $\Delta$ ANXA3 cells were transfected with HA-tagged ANXA3 WT constructs or an empty control plasmid and infected with a Jc1<sup>NS5AB-mKO2</sup> reporter virus. Seven days later, cells were lysed and expression of indicated proteins was analyzed by western blotting. Specific ANXA3 bands are marked by arrows, grey for endogenous ANXA3, black labels ANXA3-HA. Asterisk marks an unspecific band.

the silencing-resistant ANXA3 mutant version restored ANXA3 expression in 55% of shANXA3 cells, indicating a rescue of ANXA3 expression in these cells. To analyze, whether overexpression of ANXA3 in shNT and shANXA3 cells influences cell viability, MTT assays were performed. Overexpression of both ANXA3 constructs severely impaired cell viability in shANXA3 and control cells (Figure 3.13 B). Next, shANXA3 and control cells transduced with the ANXA3 overexpression constructs, were infected with a Jc1<sup>p7-GLuc-2A-NS2</sup> virus to analyze if HCV particle production can be restored by overexpression of ANXA3. The Jc1<sup>p7-GLuc-2A-NS2</sup> virus carries a Gaussia luciferase reporter between a duplicated cleavage site, leading to the secretion of Gaussia luciferase which can be used to assess viral replication. 4 h after infection, cells were washed three times and cultured for 72 h. Supernatant was harvested to re-infect naïve Huh7.5 cells. Again, cells were washed 4 h post inoculation and cultured for 48 h. Then luciferase assays were performed using the supernatant of re-infected Huh7.5 cells. However, HCV progeny production was negatively affected by ANXA3 overexpression in shANXA3 and control cells (Figure 3.13 C). Besides lentiviral-based overexpression also plasmid-based overexpression of ANXA3 was performed. Therefore,  $\Delta$ ANXA3 and parental Huh7.5 cells were transfected with plasmids encoding HA-tagged ANXA3 WT and infected with a Jc1<sup>NS5AB-mKO2</sup> reporter virus. Seven days later, cells were lysed and viral protein expression, as well as ANXA3-HA expression was analyzed by western blotting. Analysis of ANXA3-HA revealed comparable protein expression levels in control and  $\Delta$ ANXA3 cells. However, overexpression of ANXA3 had no effect on viral replication, as both  $\Delta$ ANXA3 cell lines (+/- ANXA3-HA) showed much lower viral protein expression levels than control cells. Furthermore, rescue of ANXA3 induced a massive increase in ANXA3-HA expression (Figure 3.13 D, marked by black arrow) as compared to endogenous ANXA3 expression in parental Huh7.5 cells (Figure 3.13 D, labeled by grey arrow). The results indicate that ANXA3 overexpression constructs were not expressed at physiological levels which was not well-tolerated, leading to severely impaired cell viability and thereby limiting the validity of the rescue experiments.

#### 3.1.4. ANXA3 is recruited to LDs in HCV-infected cells

In order to confirm the re-localization of ANXA3 to LDs in HCV-infected cells, identified by mass spectrometry analysis, LDs of HCV-infected and naïve Huh7.5 cells were isolated and ANXA3 expression was analyzed by western blotting. Huh7.5 cells were infected with a Jc1<sup>NS5AB-eGFP-BSD</sup> reporter virus. Seven days post inoculation, cells were selected with blasticidin for 10 days. Afterwards LDs of HCV-infected or naïve Huh7.5 cells were isolated by sucrose gradient centrifugation and analyzed by western blotting. ANXA3 was detectable in LD fractions isolated from HCV-infected cells, while LD fractions isolated from naïve Huh7.5 cells were ANXA3 negative (Figure 3.14 A). PLIN2/ADRP served as a LD loading control and confirmed equal amounts of protein analyzed by western blotting. To further verify the recruitment of ANXA3 to LDs in the context of HCV replication, LDs of cells harboring a bicistronic Con1 subgenomic replicon (Con1 SGR) were isolated and analyzed. This replicon system lacks all structural HCV proteins and only the viral non-structural proteins NS3–NS5B as well as a neomycin resistance gene are expressed. As a consequence only active viral RNA replication, but no virus production, can occur in these cells [Cho04]. Again, LDs were isolated and ANXA3 expression was analyzed by western blotting (Figure 3.14 B). Western blot analysis demonstrated an enrichment of ANXA3 in LD fractions of replicon cells, despite more protein was loaded from LD fractions of naïve cells (according to the PLIN2/ADRP loading control). These results confirmed an enrichment of ANXA3 in LD fractions of HCV-infected cells and cells that actively replicate viral RNA.

### 3. Results

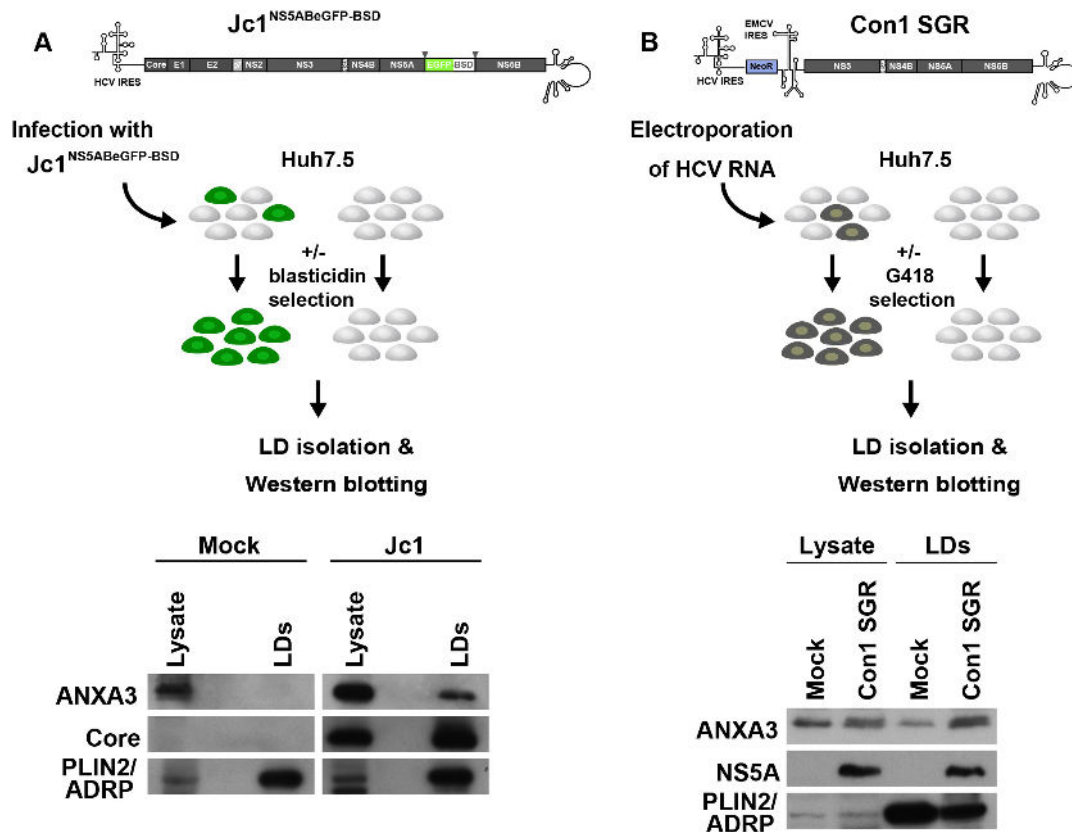


**Figure 3.14.: ANXA3 is recruited to LDs in Con1 SGR- or HCV-infected cells.** LDs isolated from HCV-infected or Con1 replicon cells. A) Huh7.5 cells were infected with an HCV Jc1<sup>NS5AB-eGFP-BSD</sup> reporter virus. Infected cells were selected with 10  $\mu$ g/ml blasticidin for 10 days. LDs of naïve and HCV-infected/selected cells were isolated by sucrose gradient centrifugation. ANXA3 expression was analyzed by western blotting. B) LD fractions of naïve Huh7.5 and cells harboring a Con1 SGR selected for active RNA replication by G418 treatment were analyzed by western blotting. PLIN2/ADRP expression served as a loading control.

To analyze whether HCV specifically recruits ANXA3 to LDs or lead to an overall induction of ANXA3 protein expression, ANXA3 expression levels were analyzed in the absence or presence of HCV. Huh7.5 cells were infected with a Jc1<sup>NS5AB-eGFP-BSD</sup> reporter virus or left untreated. At day two, four and six post infection cells were harvested and ANXA3 expression was analyzed by western blotting and RT-qPCR (Figure 3.15 A,B). Antibodies detecting HCV core and  $\beta$ -tubulin served as infection and loading control, respectively. ANXA3 protein expression was independent of HCV infection rates and remained unchanged in infected cells as compared to non-infected Huh7.5 cells. On mRNA level, a slight increase in ANXA3 expression was observed, indicating a tight regulation of ANXA3 protein levels in the cells (Figure 3.15 B).

Previous reports have shown that ANXA3 expression was significantly enriched in cells derived from hepatocellular carcinoma (HCC) and an increase in secretion of ANXA3 in HCC patient sera correlated with aggressive clinical features. Thus ANXA3 is noticed so far as a marker gene, involved in cancer progression [Pan15, Ton15]. To ensure that the identification of ANXA3 as a potential HCV host factor was not due to a side effect attributed to the hepatocellular carcinoma cell line Huh7.5 used in the SILAC approach, the ANXA3 protein expression was

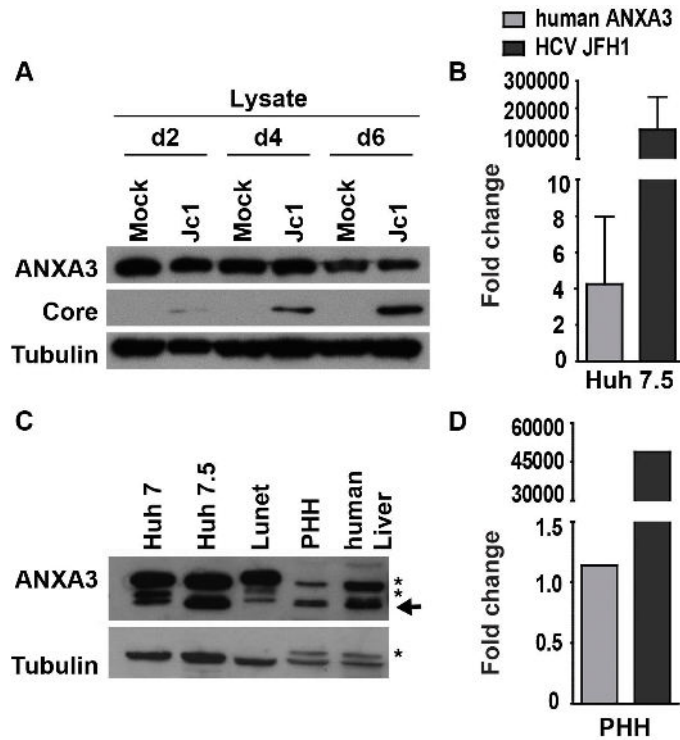


**Figure 3.15.: ANXA3 expression is not influenced by HCV infection.** A) Huh7.5 cells were seeded in equal densities in a six-well plate. 24 h later, three wells were infected with a Jc1<sup>NS5AB-eGFP-BSD</sup> reporter virus. At day two, four and six post infection one non-infected and one infected well were lysed in RIPA lysis buffer. Protein expression was analyzed by western blotting using antibodies detecting ANXA3, HCV core and  $\beta$ -tubulin. B) RT-qPCR analysis of ANXA3 mRNA in HCV-infected and non-infected Huh7.5 cells. Shown is the fold change of ANXA3 mRNA expression in HCV-infected cells over naïve Huh7.5 cells, normalized to 18S RNA levels. Detection of HCV genomes served as HCV infection control (Mean  $\pm$  SEM, n = 3). C) ANXA3 protein expression in different cell lines, PHH and whole human liver tissue analyzed by western blotting. Arrow indicates the specific ANXA3 band. Asterisks mark unspecific bands. D) RT-qPCR analysis of human ANXA3 mRNA in HCV-infected and non-infected PHHs, harvested from human liver chimeric mice. Shown is the fold change of ANXA3 mRNA expression in HCV-infected cells over naïve cells, normalized to 18S RNA levels. Detection of HCV genomes served as HCV infection control. Human liver chimeric mice were generated and infected with HCV as described [Meu05]. Samples were provided by Tassilo Volz (n = 1).

analyzed in different cell lines generated from HCC, and in PHHs or human liver tissue of HCC negative patients. Western blot analysis revealed a high variability of ANXA3 protein expression between the different cell lines. Huh7 and Huh7 Lunet cell lines expressed less ANXA3 compared to the Huh7.5 cell line. In addition, ANXA3 expression was detectable in PHHs as well as in whole human liver tissue, supporting a potential relevance of ANXA3 during HCV infection *in vivo* (Figure 3.15 C). Furthermore, ANXA3 mRNA expression was analyzed in human hepatocytes harvested from HCV-inoculated or untreated chimeric mice (uPA/SCID). This immunodeficient mouse model carries a mouse-specific urokinase-type plasminogen activator gene (uPA) controlled by a mouse albumin enhancer/promotor, leading to a severe transgen-induced liver damage. However, soon after birth these mice can be transplanted with PHHs, resulting in a robust engraftment and repopulation of the mouse liver with human hepatocytes. Thus, allowing to study HCV replication *in vivo* [Meu08]. Of note, due to limitations in the



### 3. Results

availability of such samples only one experiment was performed. Detection of HCV genomes displayed a robust HCV infection in these cells, but no increase in ANXA3 mRNA expression was observed (Figure 3.15 D). Taken together the results indicate a specific recruitment of ANXA3 to LDs in HCV-infected cells.

To further verify the ANXA3 recruitment to LDs in Con1 replicon cells, membrane floatation assays were performed. Membrane floatation assays have already been used to characterize HCV host factors, recruited to low-density lipid-rich cellular membranes [Vog13]. Naïve Huh7.5 and Con1 replicon cells were mechanically broken up using a Dounce homogenizer. Post nuclear cellular lysates were overlaid with a self-forming Iodixanol gradient and separated by centrifugation. From top to bottom eight fractions were harvested and analyzed by western blotting (Figure 3.16). PLIN2/ADRP served as a control, localizing to LDs on top of the gradient. Compared to mock cells, less PLIN2/ADRP was detectable in LD-containing fractions one and two harvested from replicon cells, indicating less LDs in these fractions. Nevertheless, in cells actively replicating the Con1 replicon, more ANXA3 co-fractionated together with NS5A in low-density lipid-rich membranes. Hence, active HCV RNA-replication and/or expression of NS3–NS5B are sufficient to re-localize ANXA3 to LDs or LD-associated membranes.

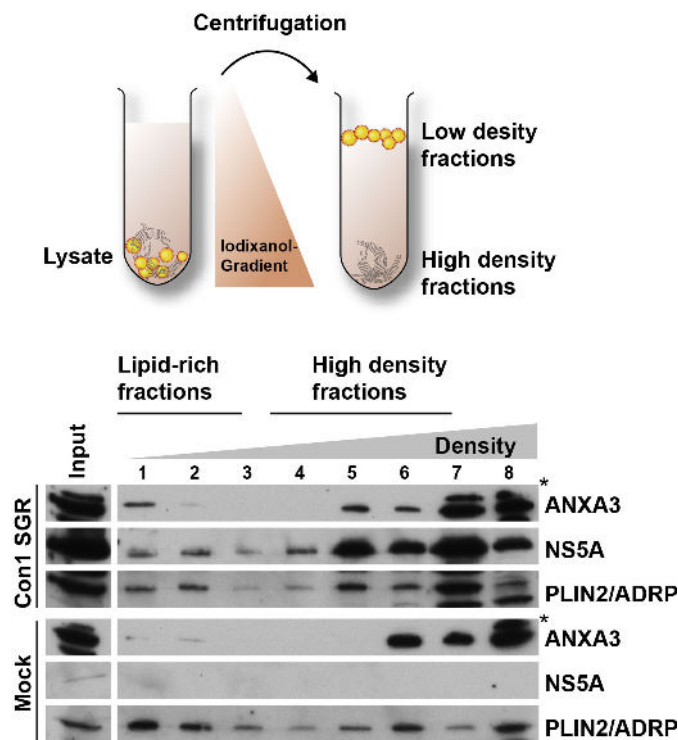


**Figure 3.16.: ANXA3 co-localizes with NS5A in LD-associated membranes.** Membrane floatation assay of naïve Huh7.5 and Con1 SGR replicating cells. Cells were lysed using a Dounce homogenizer. Equal amounts of post nuclear cellular lysates were overlaid with a self-forming Iodixanol gradient and separated by centrifugation. From top to bottom eight fractions were harvested and analyzed by western blotting. Asterisk marks an unspecific band.

In order to assess which viral protein re-localizes ANXA3 to LDs, Huh7.5 cells were co-transfected with plasmids encoding the single Flag-tagged HCV proteins and HA-tagged ANXA3. An ANXA3-HA expression plasmid was used due to the fact that no antibody detecting endoge-

nous ANXA3 was reliably working for immunofluorescence analysis. Three days post transfection co-localization of HCV-Flag and ANXA3-HA was analyzed by immunofluorescence analysis (Figure 3.17). Single expression of ANXA3-HA showed a broad cytoplasmic distribution, similar to co-transfections with plasmids encoding for the structural protein E1-Flag and E2-Flag as well as the non-structural proteins NS2-NS4B. When Flag-core, p7-Flag or NS5A-Flag were co-transfected with ANXA3-HA, ANXA3-HA was not diffusely distributed throughout the cytoplasm, but rather appeared in distinct regions. These regions were also occupied by the viral proteins. However, only core and NS5A localized to ring-like structures, most likely reflecting LDs, as it has already been shown that core and NS5A are the only viral proteins targeting LDs independently of viral replication [Cam13]. Of note, the NS5B-Flag plasmid was not expressed in Huh7.5 cells and therefore could not be analyzed.

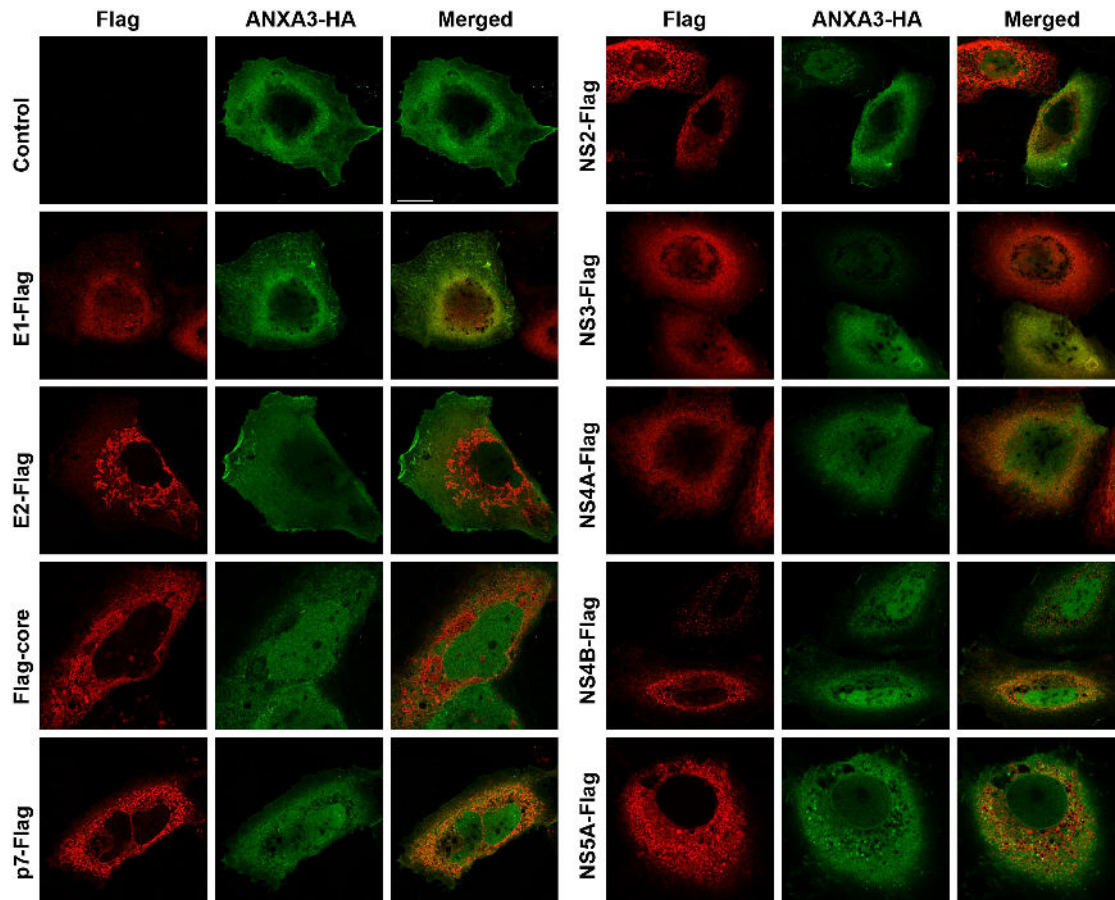


**Figure 3.17.: Co-localization of Flag-tagged HCV proteins and HA-tagged ANXA3.** Huh7.5 cells were transfected with plasmids encoding Flag-tagged HCV proteins and HA-tagged ANXA3. At day three post transfection, cells were fixed and stained with antibodies detecting Flag (red channel) and HA (green channel). Merged pictures show an overlay of both channels (scale bar 10  $\mu\text{m}$ ).

To determine whether endogenous ANXA3 can directly interact with HCV proteins, co-immunoprecipitation assays were performed. Huh7.5 cells were transfected with plasmids encoding single Flag-tagged HCV proteins. 72 h later, cells were lysed and subjected to Flag-specific co-immunoprecipitation and analyzed by western blotting. Flag-specific co-immunoprecipitation led to an enrichment of Flag-tagged HCV proteins, except for E2-Flag, which was not recovered

### 3. Results

by Flag agarose beads. Analysis of endogenous ANXA3 expression revealed no direct interaction of ANXA3 with Flag-tagged HCV proteins tested in this approach (Figure 3.18 A).

The viral envelope proteins are facing the luminal side of the ER and are highly glycosylated. To ensure that E2 localizes correctly and undergoes this post-translational modification in transfected cells, a lentiviral construct expressing the E1/Flag-E2 coding sequence (containing the signal peptide of core to ensure correct subcellular localization) was generated. Huh7.5 cells were transduced with these lentiviral particles and cultured for three days. Afterwards, cells were lysed, subjected to Flag-specific co-immunoprecipitation and analyzed by western blotting (Figure 3.18 B). However, even under those conditions no direct interaction between Flag-E2 and endogenous ANXA3 was observed.

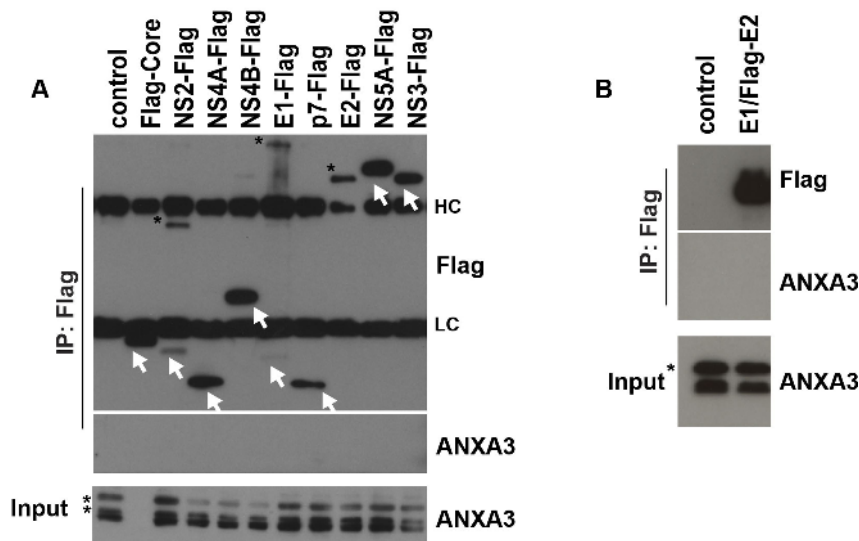


**Figure 3.18.: ANXA3 does not show a direct interaction with Flag-tagged HCV proteins.** A) Huh7.5 cells were transfected with plasmids expressing single Flag-tagged HCV proteins. 72 h later cells were lysed, subjected to Flag-specific co-immunoprecipitation and analyzed by western blotting. HC: heavy chain, LC: light chain. Specific bands are marked by arrows. B) Co-immunoprecipitation of Flag-E2 and endogenous ANXA3. Huh7.5 cells were transduced with lentiviral particles carrying E1/Flag-E2. 72 h later, cells were lysed, subjected to Flag-specific co-immunoprecipitation and analyzed by western blotting. Asterisk marks an unspecific band.

Core and NS5A localize to LDs in the absence of virus infection [Cam13]. To verify whether expression of core or NS5A is sufficient to re-localize ANXA3 to LDs, lentiviral particles encoding for Flag-core or NS5A-Flag were generated. These constructs also expressed the fluorescence marker protein cerulean for monitoring the transduction efficacy. Huh7.5 cells were transduced and co-localization of Flag-core or NS5A-Flag together with ANXA-HA was analyzed by immunofluorescence microscopy. As indicated by LD staining, Flag-core and NS5A-Flag mainly localized at LDs. In contrast, overexpressed ANXA3-HA showed a broad cytoplasmic staining. In order to quantify the degree of co-localization; Pearson's correlation coefficients (PCCs) were used, indicating the correlation of the intensities of both channels (ANXA-HA and Flag) across the entire image. PCCs can reach from 1 (both channel intensities are perfectly linearly related) to -1 (both channel intensities are perfectly, but inversely related). PCCs close to 0 reflect a non-correlated distribution. Additionally, Manders' colocalization coefficients (MCCs) were calculated, representing the fraction of fluorescence in each channel overlapping with the signals of



the second channel. Quantifying the co-localization of ANXA3 with viral proteins according to Manders and Pearson demonstrated that ANXA3 partially co-localized with both viral proteins (Figure 3.19).

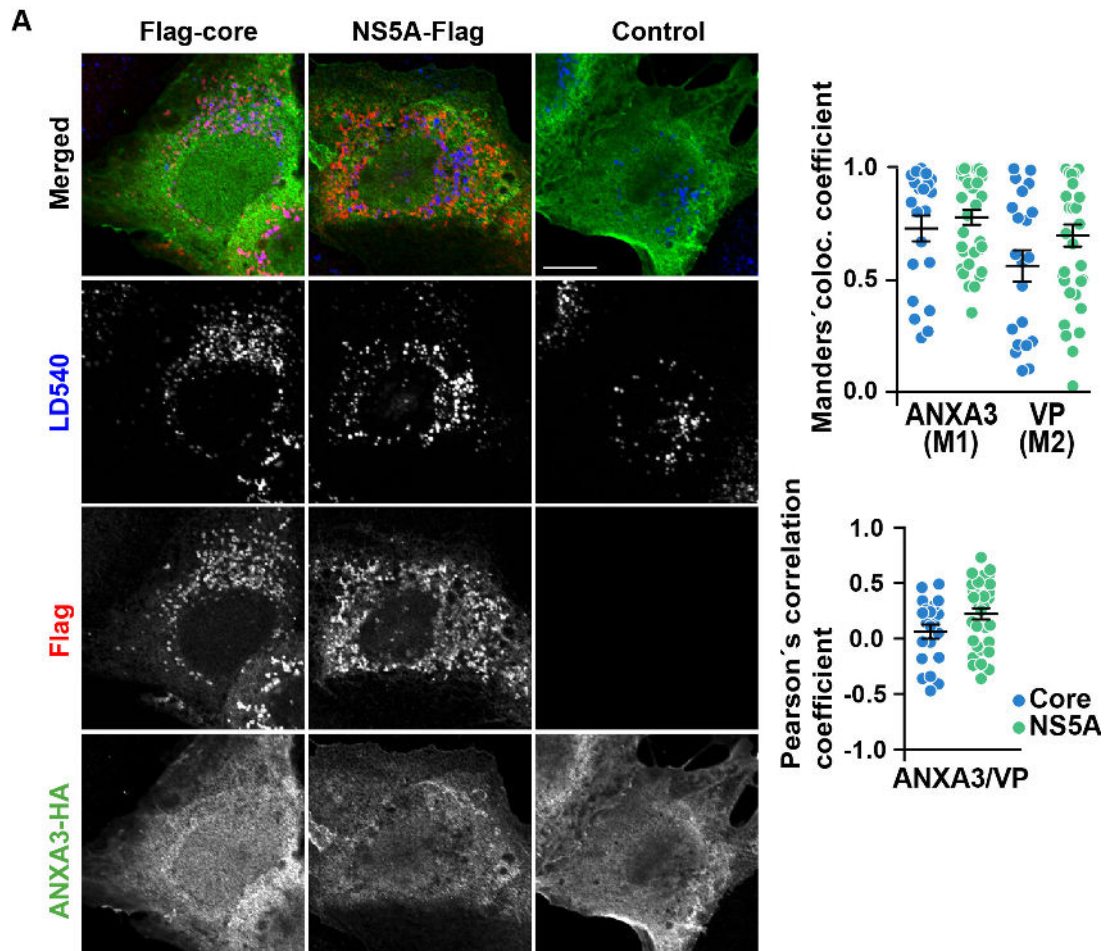


**Figure 3.19.: ANXA3 co-localizes with core or NS5A at LDs.** Confocal analysis of Huh7.5 cells transfected with constructs expressing Flag-core/NS5A-Flag and ANXA3-HA. At day three post transfections cells were fixed and stained with antibodies detecting Flag and HA followed by LD540 staining to visualize LDs. Merged pictures show an overlay of all channels (scale bar 10  $\mu$ m). Co-localization analysis of viral proteins (VP) with ANXA3 was performed using Coloc2 in Fiji [Sch12]. Individual cells of three independent experiments were analyzed (Mean  $\pm$  SEM).

To verify the results obtained by immunofluorescence analysis, Huh7.5 cell lines stably expressing an empty plasmid, Flag-core or NS5A-Flag were generated, LDs were isolated and fractions analyzed by western blotting for endogenous ANXA3 expression. ANXA3 was not detectable in LD fractions of cells harboring the empty cerulean control. However, ANXA3 re-localized to LD fractions in cells expressing Flag-core or NS5A-Flag (Figure 3.20). Taken together, the data indicate that ANXA3 is specifically recruited to LDs by the viral proteins core and NS5A during HCV infection.

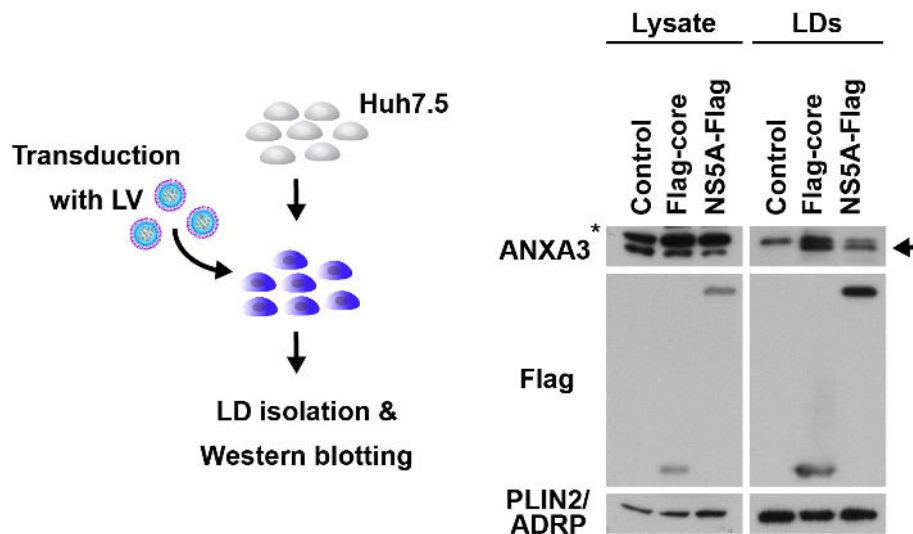


**Figure 3.20.:** Expression of core or NS5A is sufficient to re-localize ANXA3 to LDs. Huh7.5 cells were transduced with lentiviral particles encoding an empty control, Flag-core or NS5A-Flag. LDs were isolated and analyzed by western blotting. Arrow labels ANXA3; asterisk marks an unspecific band.

### 3.1.5. ANXA3 has no impact on viral RNA replication and translation

As silencing of ANXA3 had no effect on viral entry (shown by spreading infection experiments), viral RNA replication and translation was analyzed in the absence of ANXA3 to dissect the step of the viral life cycle influenced by ANXA3. Therefore, viral protein expression was analyzed in cells where ANXA3 expression was repressed. *In vitro* transcribed JFH1<sup>WT</sup> RNA was transfected in control and shANXA3 cells. Three days post transfection, expression levels of core and NS5A were analyzed by western blotting (Figure 3.21 A). No differences in protein expression of core and NS5A were detectable, indicating that viral RNA-replication and -translation as well as polyprotein processing was unaffected by ANXA3 silencing. In addition, *in vitro* transcribed Con1 SGR RNA was transfected in Huh7.5 cells expressing shANXA3 or shNT constructs. Cells were cultured in media containing 1  $\mu\text{g}/\text{ml}$  G418 for three weeks. Growing cell colonies were fixed and stained with crystal violet. Compared to control cells, shANXA3-expressing cells showed a slight decrease in the number of colonies replicating viral RNA (Figure 3.21 B). To further elucidate an effect on viral RNA replication, a monocistronic genotype 2a replicon system containing a firefly luciferase in between a duplicated NS5A-NS5B cleavage site was used. This construct was also partially deleted in E1 and E2 to prevent viral spreading (Jc1 $\Delta\text{E1E2-NS5AB-Fluc}$ ) [Web13a]. Compared to the Con1 SGR system, this system is much more sensitive and allows investigations at early time points post transfection. shANXA3 and control cells were transfected with *in vitro* transcribed Jc1 $\Delta\text{E1E2-NS5AB-Fluc}$  RNA. Viral RNA replication was analyzed by luciferase assays at different time points post transfection (Figure 3.21 C). To correct for different transfection efficiencies, all values were expressed as fold increase of luciferase activity (relative light units, RLU) per  $\mu\text{g}$  protein over a 4 h post transfection time point, before viral RNA replication started. Again, no significant difference in luciferase activity was observed between shANXA3 or control cells, indicating that ANXA3 doesn't impact viral RNA replication.

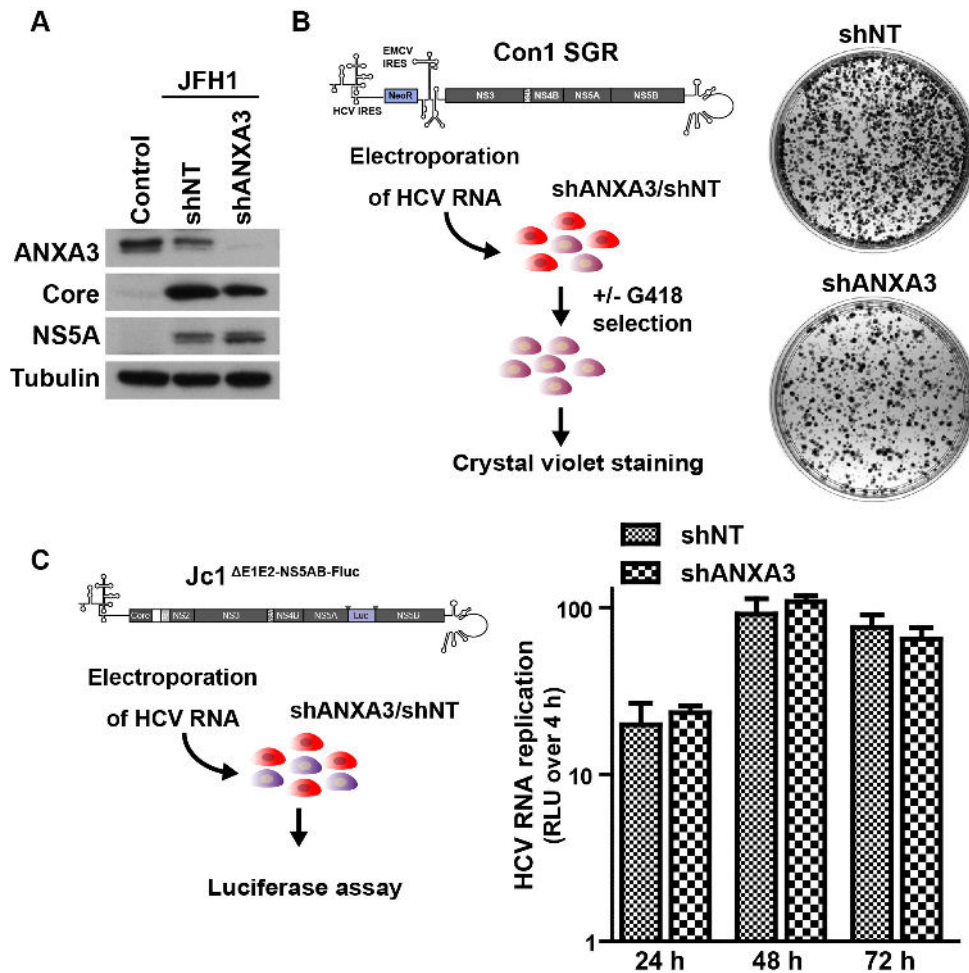


**Figure 3.21.: HCV RNA replication and viral protein expression is not affected by ANXA3.** A) *In vitro* transcribed JFH1<sup>WT</sup> RNA transfected in ANXA3-knockdown and control cells. Viral protein expression was analyzed by western blotting. B) shANXA3 or control knockdown cells were transfected with *in vitro* transcribed Con1 SGR RNA. Cells harboring the SGR and actively replicating viral RNA were cultured in media containing 1  $\mu$ g/ml G418 for three weeks. Growing cell colonies were fixed and stained with crystal violet. Shown is one representative experiment. C) shANXA3-expressing or control cells were transfected with *in vitro* transcribed Jc1 $\Delta$ E1E2-NS5AB-Fluc RNA. 4 h, 24 h, 48 h and 72 h post transfection luciferase activity was measured. Luciferase activity (relative light units, RLU) was normalized per  $\mu$ g protein standardized to the 4 h time point (Mean  $\pm$  SEM, n = 3).

### 3.1.6. ANXA3 influences late steps of viral replication

To investigate, whether ANXA3 acts at later steps of the viral life cycle, ANXA3-knockdown and control cells were transfected with *in vitro* transcribed Jc1<sup>NS5AB-eGFP</sup> RNA and seeded at the same density. Comparable transfection efficacies were confirmed by measuring eGFP expression by flow cytometry at day three post transfection. The amount of intracellular and secreted HCV RNA genomes was analyzed by RT-qPCR at day three and day six post transfection. As shown in replicon experiments, shRNA-mediated knockdown of ANXA3 had no effect on viral RNA replication (Figure 3.22 A), but significantly reduced extracellular HCV RNA genomes (Figure 3.22 B). This is in line with a significantly reduced secretion of the capsid protein core, as measured by core ELISA (Figure 3.22 C).

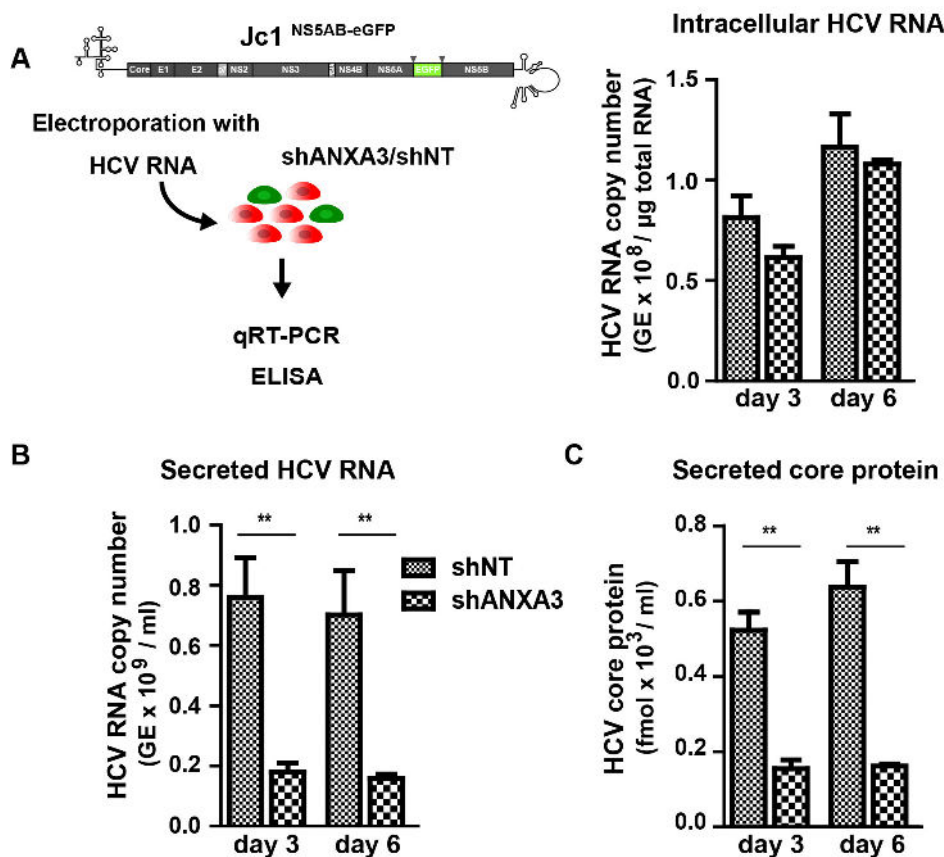


**Figure 3.22.: Knockdown of ANXA3 expression significantly reduced secretion of HCV RNA genomes.** ANXA3-knockdown and control cells were transfected with *in vitro* transcribed Jc1<sup>NS5AB-eGFP</sup> RNA and seeded at the same density. At day three and six post transfection, HCV copy numbers were determined by RT-qPCR intracellularly (A) as well as extracellularly (B). Shown is the absolute quantification of HCV copy numbers (genome equivalents, GE) per  $\mu\text{g}$  total RNA (intracellular) or ml supernatant (extracellular) (Mean  $\pm$  SEM, n = 3, \*\* p < 0.01). C) Quantification of core protein released into the supernatant measured by ELISA (Mean  $\pm$  SEM, n = 3, \*\* p < 0.01).

Next, the intra- as well as the extracellular 50% tissue culture infective dose (TCID<sub>50</sub>) was measured to determine whether the reduction of extracellular virus was due to defects in release or the assembly of HCV particles. To this end, ANXA3-knockdown and control cells were transfected with *in vitro* transcribed Jc1<sup>NS5AB-eGFP</sup> RNA. 48 h later, equal transfection efficacies were

confirmed by flow cytometry. Afterwards, cells were seeded at the same density and in the same volume of media. 24 h later, supernatant was harvested to determine extracellular TCID<sub>50</sub>/ml supernatant (Figure 3.23 B). Furthermore,  $1 \times 10^5$  cells were lysed by multiple cycles of freeze and thaw, to measure the intracellular TCID<sub>50</sub>/ $1 \times 10^5$  cells. Regarding intracellular infectivity, a slight but non-significant decrease was observed in ANXA3-knockdown cells, suggesting no block of virion release in the absence of ANXA3 (Figure 3.23 A). However, the infectivity of viral particles secreted from ANXA3-knockdown cells was severely reduced in comparison to control cells (Figure 3.23 B). Thus implicating that ANXA3 affects viral assembly or maturation.

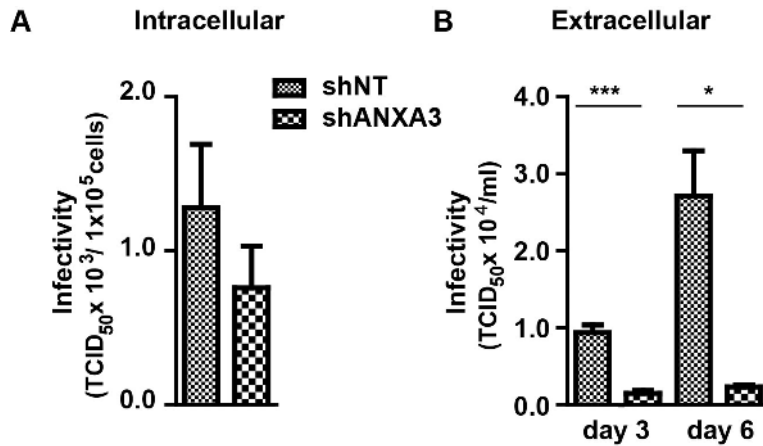


**Figure 3.23.: ANXA3 regulates HCV progeny virion production.** A) ANXA3-knockdown and control cells were transfected with *in vitro* transcribed Jc1<sup>NS5AB-eGFP</sup> RNA. 48 h later, cells were seeded at the same density and cultured with 1 ml media for 24 h.  $1 \times 10^5$  cells were lysed by multiple cycles of freeze and thaw and intracellular TCID<sub>50</sub>/ $1 \times 10^5$  cells was determined by titration on naïve Huh7.5 cells (Mean ± SEM, n = 5). B) Infectivity of supernatant was determined by TCID<sub>50</sub>/ml at day three and six post transfection (Mean ± SEM, n = 3–5, \*p < 0.05, \*\*\*p < 0.001).

### 3.1.7. ANXA3 has no effect on capsid assembly and envelopment

To assess whether a defect in viral assembly contributes to the ANXA3 phenotype, the assembly process was subdivided into trafficking of core to the surface of LDs, core oligomerization/capsid formation and core envelopment. First, translocation of core and NS5A to LDs was investigated by confocal microscopy (Figure 3.24 A,B). Control and shANXA3-expressing cells or  $\Delta$ ANXA3 and WT cells were infected with a Jc1<sup>WT</sup> strain. At day three post infection, cells were fixed and stained with antibodies detecting core or NS5A. LDs were stained using the neutral lipid stain BODIPY. Core localized to LDs in 70–90% of Jc1-infected cells independently of the cell line used. Compared to core, NS5A was more diffusely distributed within the cells. However, NS5A was also detected around LDs in ~70% of Jc1-infected cells. Regarding the co-localization of core and NS5A to LDs, no differences between control and ANXA3-knockdown or -knockout cells were observed (Figure 3.24 C,D). These results were supported by western blot analysis of LD fractions. No differences in core and NS5A levels in LD fractions were detectable in Jc1 transfected ANXA3-knockdown or control cells (Figure 3.24 E). The data exclude a defect in core or NS5A trafficking to LDs in absence of ANXA3.

Next the formation of high molecular mass (HMM) core complexes was analyzed. ANXA3-knockdown and control cells were transfected with Jc1<sup>WT</sup> RNA. Cells were lysed in native lysis



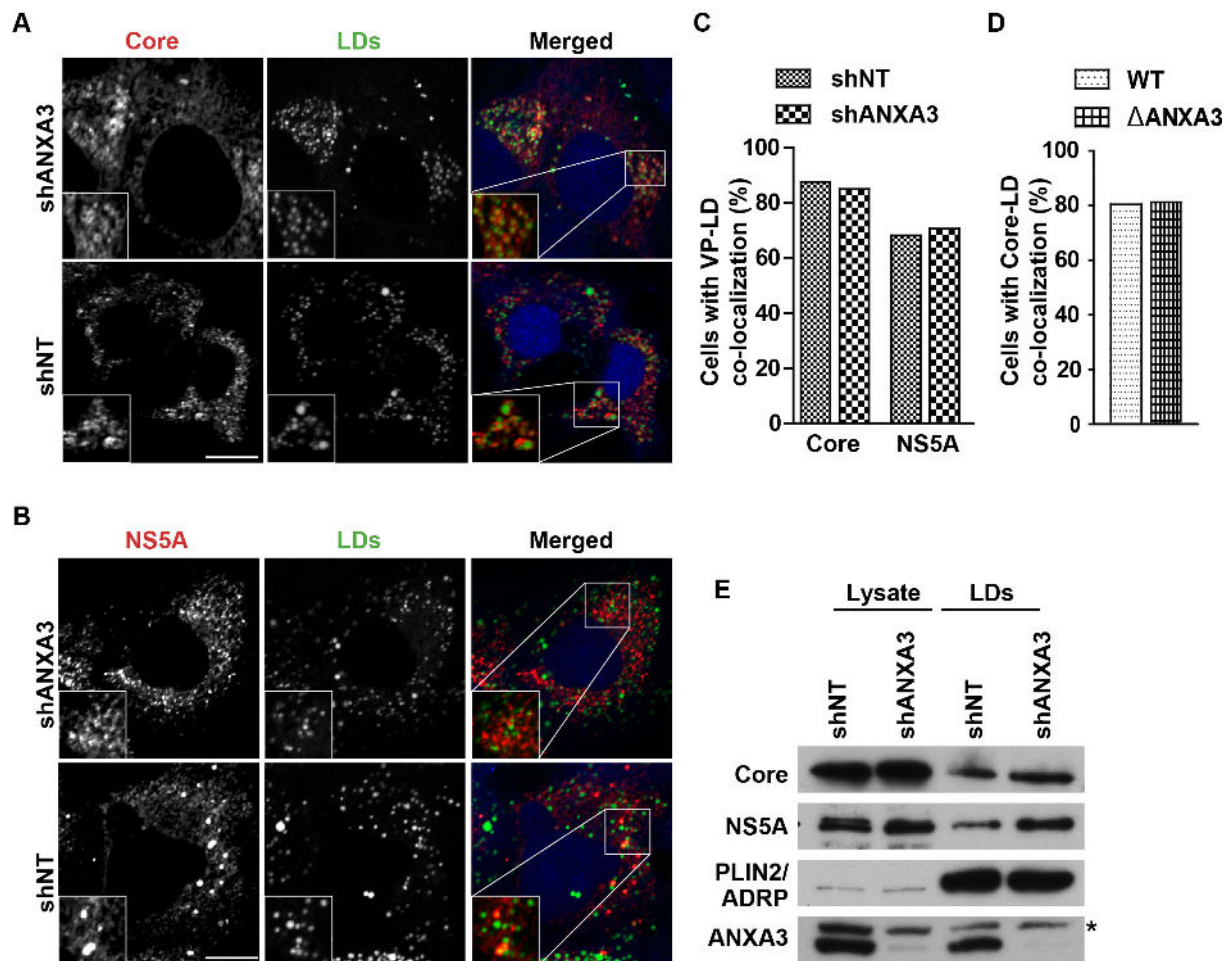


**Figure 3.24.: Trafficking of core and NS5A to LDs works independently of ANXA3.** ANXA3-knockdown and control cells were infected with a Jc1<sup>WT</sup> strain. At day three post infection, cells were fixed and labeled with antibodies detecting core (A) and NS5A (B). LDs were stained with BODIPY and samples were analyzed by confocal microscopy. Single channels are shown in black and white, merged pictures are pseudocolored as indicated. The blue signal in the merged image represents mCherry of shRNA constructs (scale bar 10  $\mu$ m). C) Percentage of Jc1-infected ANXA3-knockdown or control cells in which LDs were surrounded by the viral proteins (VP) core or NS5A. Cells that have LDs surrounded by viral proteins were counted as positive. The number of these cells was divided by the total number of HCV-infected cells. 40–100 cells were analyzed per construct and antigen. D) Percentage of Jc1-infected  $\Delta$ ANXA3 and WT cells in which LDs were surrounded by core. 30–50 cells were analyzed. E) ANXA3-knockdown and control cells transfected with a Jc1<sup>NS5AB-eGFP-BSD</sup> and selected with blasticidin. LDs were isolated and analyzed by western blotting. Asterisk marks an unspecific band.

buffer and analyzed by 2D blue native SDS-PAGE (Figure 3.25 A). No differences in the formation of HMM core complexes were detected. To further verify the results,  $\Delta$ ANXA3 and WT cells were also transfected with JFH1<sup>WT</sup> RNA and tested for their ability to form HMM core complexes. Again, no differences were observed, indicating that the formation of HMM core complexes does not involve ANXA3 expression, independently of the ANXA3 inactivation method and the viral strain used in this approach.

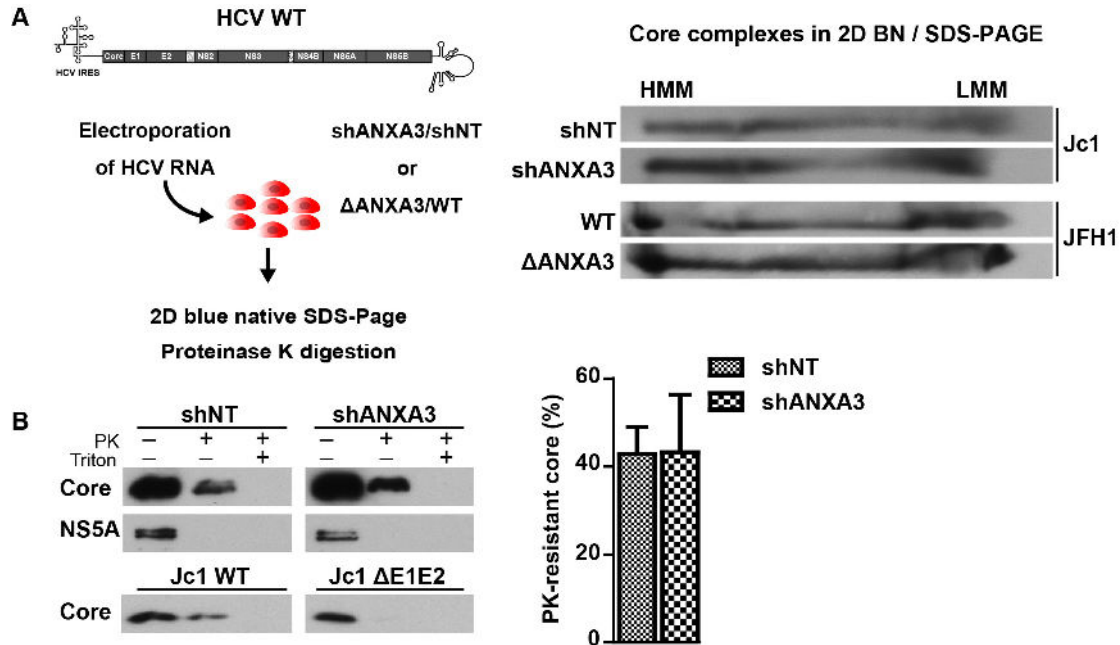


**Figure 3.25.: ANXA3 is not involved in the formation of HMM core complexes and core envelopment.** A) Formation of high molecular mass (HMM) and low molecular mass (LMM) core complexes in ANXA3-knockdown or -knockout and control cells. Cell lines were transfected with Jc1<sup>WT</sup> or JFH1<sup>WT</sup> RNA. 48 h post transfection cells were lysed and formation of HMM and LMM core complexes was analyzed by 2D native blue/SDS-PAGE. B) shANXA3-expressing and control cells were transfected with Jc1<sup>WT</sup> RNA and lysed without detergents at day three post transfection. Lysates were divided into three portions; left untreated, treated with 25  $\mu$ g/ml proteinase K for 20 min on ice or pretreated with 5% Triton X-100 prior to proteinase K treatment. The amount of core protein protected from proteinase K digestion was analyzed by western blotting. Signal intensities of core were quantified using Fiji to determine the percentage of protected core compared to untreated control (Mean  $\pm$  SEM, n = 6).

To determine, whether ANXA3-knockdown contributes to a defect in core envelopment, protection of core protein from proteinase K digestion was assessed. Envelopment of core protein into membranes is expected to protect the protein from proteolytic proteinase K digestion. shANXA3-expressing and control cells were transfected with Jc1<sup>WT</sup> RNA and lysed by multiple cycles of freeze and thaw at day three post transfection. Lysates were divided into three fractions: one portion left untreated, one treated with proteinase K and one treated with Triton X-100 prior to proteinase K digestion. Triton X-100 treatment was used as a control to solubilize all membranes and therefore abolish core protection. The amount of core protein protected by envelopment from proteinase K digestion was then analyzed by western blotting (Figure 3.25 B). Besides core, the expression of NS5A, which should not be resistant to proteinase K digestion, was also analyzed. Indeed, NS5A was completely degraded in samples treated with proteinase K, confirming entire digestion of non-enveloped proteins. It has already been published that the coding region of E1

### 3. Results

and E2 is necessary for proper core envelopment [Gen13]. Therefore, transfection of Jc1<sup>ΔE1E2</sup> RNA was used as a further control. Quantification of core intensities revealed that in both control and ANXA3-knockdown cell lines ~43% of core protein was resistant to proteinase K digestion and thus already acquired an envelope. As expected, core was not protected in the envelope-deleted strain. The comparable levels of core protection in ANXA3-knockdown and control cells illustrate that ANXA3 doesn't impact envelopment of core.

Previous studies have shown that Annexins can influence cPLA2 activity [Ger02, Kim01] and suppression of cPLA2 activity severely repressed HCV replication and assembly [Xu12]. To investigate whether silencing of ANXA3 modulates cPLA2 expression or localization, LDs of shANXA3 and control cells were isolated and analyzed by western blotting (Figure 3.26 A). Independently of ANXA3 expression, equal cPLA2 levels were detected in LD fractions as well as in lysates of both cell lines. Furthermore, cPLA2 activity was analyzed in Jc1<sup>NS5AB-eGFP</sup> infected shANXA3 and control cells (Figure 3.26 B). Again, no differences were observed, suggesting no impact of ANXA3 on cPLA2 expression or activity.

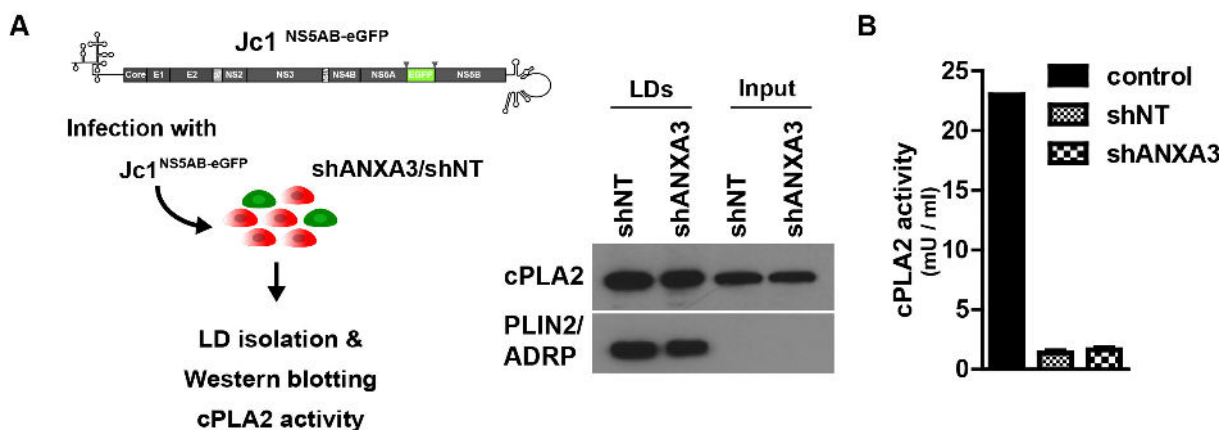


**Figure 3.26.: cPLA2 activity is not affected by ANXA3-knockdown.** A) cPLA2 levels in LD fractions and lysates of ANXA3-knockdown and control cells analyzed by western blotting. B) cPLA2 activity measured in Jc1<sup>NS5AB-eGFP</sup> infected ANXA3-knockdown and control cells at day six post infection. cPLA2 activity is shown in milliunits (mU) per ml cell lysate. Bee venom was used as positive control (Mean  $\pm$  SEM, n = 3).

#### 3.1.8. Density and specific infectivity of virions is affected by ANXA3 expression

ANXA3 is required for HCV spreading infection (Figure 3.12) and for efficient HCV virion production, as demonstrated by shRNA knockdown of ANXA3 expression and consequent suppression of HCV virion production (Figure 3.23). To elucidate whether viral particles produced from ANXA3-knockdown cells are less infectious than particles produced from control cells, the specific infectivity (focus forming units, FFU per released HCV core) was analyzed.

ANXA3-knockdown and control cells were transfected with Jc1<sup>NS5AB-eGFP</sup> RNA. At day two post transfection, equal transfection efficacies were confirmed by flow cytometry and cells were seeded at the same cell density per well. At day three and day six post transfection, supernatant



was harvested and the specific infectivity was analyzed by measuring the amount of HCV core and determine the TCID<sub>50</sub>.

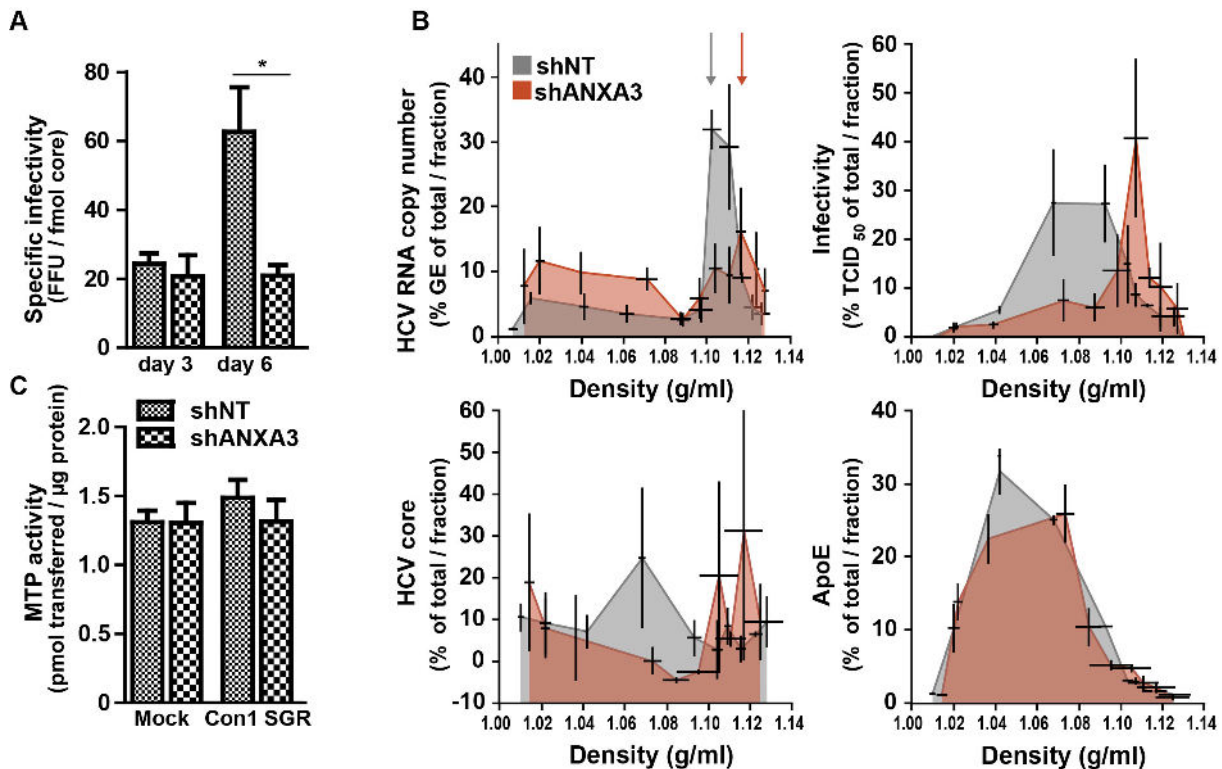


**Figure 3.27.:** ANXA3 influences the specific infectivity and the density of HCV virions. A) Specific infectivity was calculated by dividing focus forming units (FFU) by the amount of core protein at day three and six post transfection (Mean  $\pm$  SEM, n = 3, \*p < 0.05). B) Density of secreted viral particles was analyzed by Iodixanol gradient centrifugation. Viral RNA copy numbers, infectivity, core and ApoE protein levels were determined in each fraction (Mean  $\pm$  SEM, n = 3). C) MTP activity was measured in shANXA3 and control cells left untreated or harboring Con1 SGR system. MTP activity is shown as pmol transferred fluorescence substrate per  $\mu$ g protein (Mean  $\pm$  SEM, n = 10).

At day six post transfection, particles produced in shANXA3 cells exhibited a lower specific infectivity compared to particles released from control cells, suggesting that ANXA3 influences infectivity of viral particles (Figure 3.27 A). The specific infectivity of HCV clearly correlates with the density of LVPs [Gas10]. Therefore, the density of HCV particles produced in shANXA3 and control cells was analyzed to answer whether they are physically different from each other. Supernatant (produced as described above) was fractionated by Iodixanol density gradient centrifugation and HCV copy numbers were analyzed in each fraction by RT-qPCR (Figure 3.27 B). Compared to control cells, secreted HCV RNA genomes produced by shANXA3 cells showed a slight shift towards higher densities (indicated by arrows). Of note, a higher plateau at lower densities most likely reflects lower viral RNA levels in supernatant of shANXA3 cells. Therefore, when shown as percentage of total RNA, the plateau seems higher than in control cells. However, infectious viral particles produced in shANXA3 cells showed a reproducible shift towards higher densities (> 1.10 g/ml) compared to control cells, where infectious particles peaked at lower densities (1.06–1.09 g/ml). The results are in line with the amount of secreted core protein, which peaked at  $\geq$  1.06 g/ml in control samples and > 1.10 g/ml in the absence of

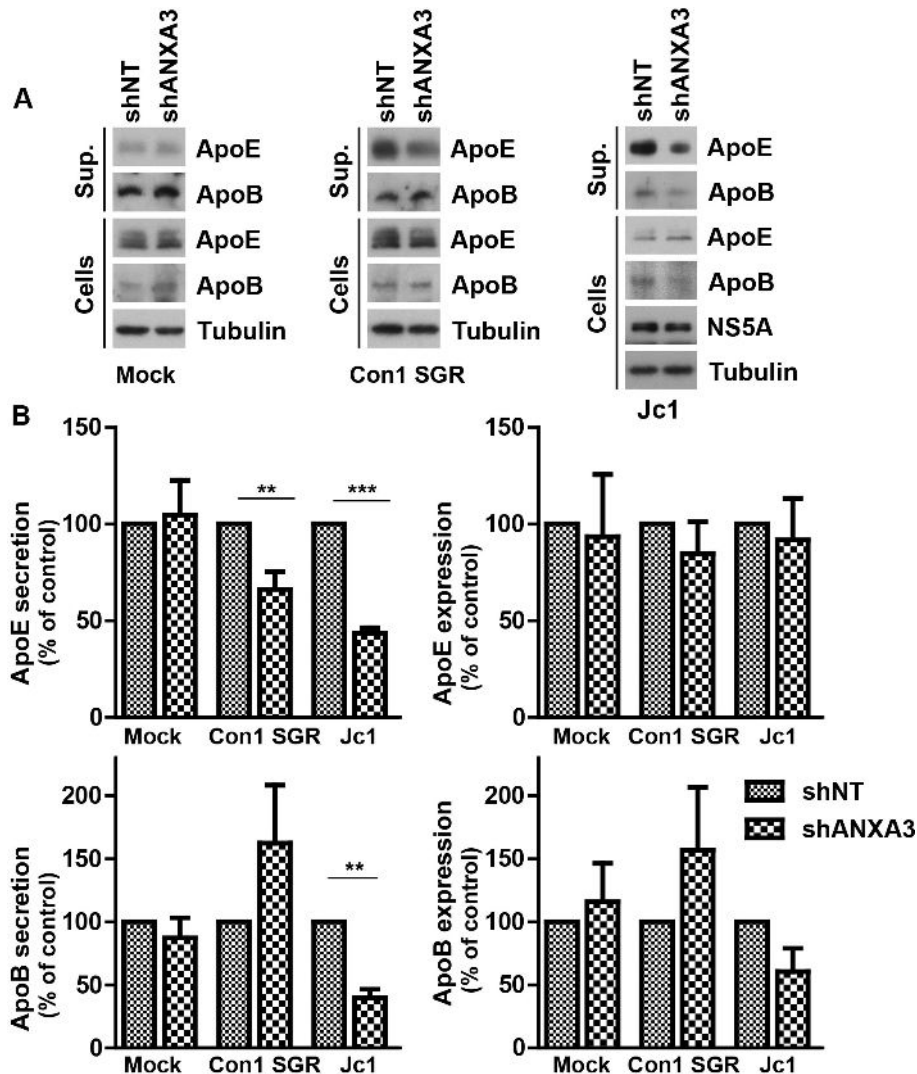


**Figure 3.28.: ANXA3 contributes to ApoE and ApoB secretion in HCV replicating cells.** A) Effect of ANXA3 silencing on ApoE and ApoB expression and secretion was verified by western blotting. shANXA3 and control cells were transfected with Con1 SGR, infected with Jc1<sup>NS5AB-eGFP-BSD</sup> or left untreated. Equal cell numbers were seeded in 1 ml OptiMEM and cultured for 12 h. Supernatant was harvested and cells were lysed in RIPA lysis buffer. Lipoprotein levels were analyzed by western blotting. B) Quantification of ApoE and ApoB expression and secretion by densitometric analysis of western blots (Mean  $\pm$  SEM, n = 3-10, \*\*p < 0.01, \*\*\*p < 0.001).

ANXA3. As mentioned above, ApoE is one major component of LVPs, but it is also secreted as VLDLs from HCV-infected cells. To analyze if ANXA3-knockdown influences the density of total secreted ApoE, gradient fractions were analyzed by ApoE ELISA (Figure 3.27 B). Secreted ApoE peaked at comparable densities in both samples. Besides ApoE, viral particles also may contain apolipoprotein B (ApoB) [Lus16]. Assembly and secretion of ApoB is tightly connected to the function of MTP and it has already been shown that knockdown of ApoB or inhibition of MTP activity suppresses HCV secretion [Hus12]. Therefore, MTP activity was probed in naïve and Con1 SGR cells to determine if shANXA3-mediated knockdown affects MTP activity (Figure 3.27 C). MTP activity was not affected by ANXA3-knockdown in the presence or absence of HCV replication. Of note, due to the technical setup, MTP activity could not be measured under S3\*\*-biosafety level, required for working with infectious HCV. Because of the strong connection of HCV particle maturation and the VLDL pathway, ApoE and ApoB secretion was further analyzed in the absence or presence of ANXA3 in HCV-replicating or naïve cells. shANXA3 or control cells were transfected with Con1 SGR system or infected with Jc1<sup>NS5AB-eGFP-BSD</sup> or left untreated. Cells were seeded at the same density and cultured in the same volume of media for 12 h. ApoE and ApoB secretion and expression levels were then quantified in cell lysates and culture supernatant by western blotting (Figure 3.28). Compared to the control, ApoE and ApoB secretion was not affected by ANXA3-silencing in naïve cells. However, shANXA3 cells replicating Con1 SGR RNA showed a reduction of ApoE secretion by 30%. ANXA3 downregulation in cells infected with replication-competent HCV led to a ~50% reduction of ApoE secretion, even though cellular ApoE expression was not impaired. In addition, ApoB secretion was reduced by ~55% in shANXA3 cells replicating the HCV full length genome. However, compared to control cells, a slight decrease in ApoB expression was detected in these cells, which could be responsible for the reduced ApoB secretion.

In summary, the results indicate that silencing of ANXA3 leads to the production of HCV particles of higher density, correlating with a lower specific infectivity, thus suggesting that ANXA3 influences maturation of HCV progeny. ApoE secretion was severely impaired in HCV-infected shANXA3 cells, demonstrating that ANXA3 contributes to ApoE secretion, but not lipidation. Furthermore, the reduced ApoE secretion caused by silencing of ANXA3 has to be HCV specific, because in non-infected cells lipoprotein secretion worked independently of the ANXA3 expression.

### 3.1.9. ANXA3 is not part of the lipovirions

In order to verify whether ANXA3 directly influences virion infectivity, the incorporation of ANXA3 into HCV particles was analyzed. Hence, Huh7.5 cells were infected with a Jc1<sup>Flag-E2-NS5AB-eGFP</sup> reporter virus. 1.3 l culture supernatant was harvested and concentrated to 17 ml by polyethylene glycol precipitation. The concentrate was loaded on top of a 10–60% Iodixanol gradient and centrifuged at ~100.000 g for 20 h. Afterwards, the first 27 ml of the gradient were discarded and leftover was harvested in 1 ml fractions. Fraction seven and eight were subjected to Flag-specific immunoprecipitation and analyzed by western blotting. As part of mature virions, viral core protein and the host protein ApoE were co-immunoprecipitated with Flag-E2, indicating an efficient purification of secreted HCV particles. However, no attachment of ANXA3 to HCV particles was observed (Figure 3.29).

Furthermore, neutralization assays were performed to confirm the results obtained by affinity purification. Equal amounts of Jc1<sup>P7-GLuc-2A-NS2</sup> viral particles were incubated with different concentrations of the indicated antibodies. After 1 h incubation, naïve Huh7.5 cells were inocu-

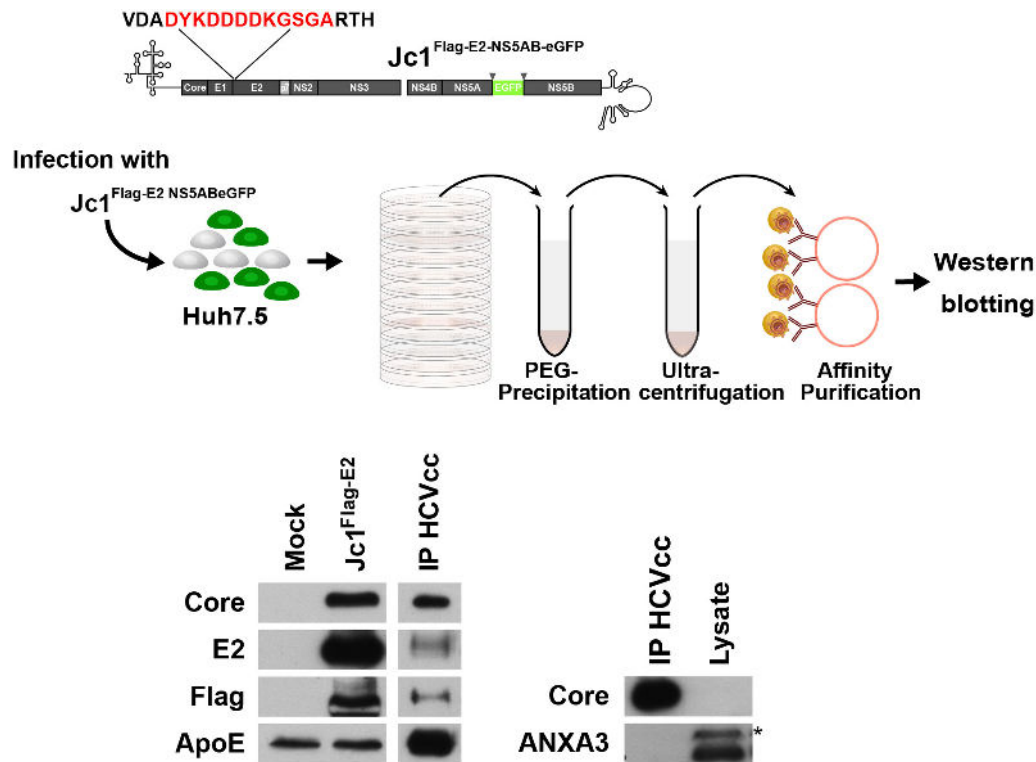


**Figure 3.29.: ANXA3 is not a component of the HCV virion.** Experimental outline of the HCV particle purification assay. Huh7.5 cells were infected with Flag-tagged E2 constructs (Jc1<sup>Flag-E2-NS5AB-eGFP</sup>). Cell supernatant was harvested, concentrated by polyethylene glycol precipitation and ultracentrifugation, followed by affinity purification with anti-Flag agarose. Purified HCVcc particles were analyzed by western blotting using core, E2, Flag, ApoE, and ANXA3 antibodies. Of note, purified particles were re-loaded (right panel) and probed with an ANXA3 antibody on a fresh membrane. Asterisk marks an unspecific band. Experiments were performed by Sarah Hofmann.

lated und incubated for 4 h. Then, cells were washed and cultured for 48 h. HCV infection rates were determined by measuring luciferase activity in the supernatant. Consistent with results obtained by affinity purification, two different antibodies detecting ANXA3 failed to neutralize HCV. In contrast, antibodies targeting viral E2 or the host entry factor CD81 efficiently neutralized HCV, indicating dependency of HCV entry on these proteins (Figure 3.30). The results further substantiated that ANXA3 is not associated to mature virions.

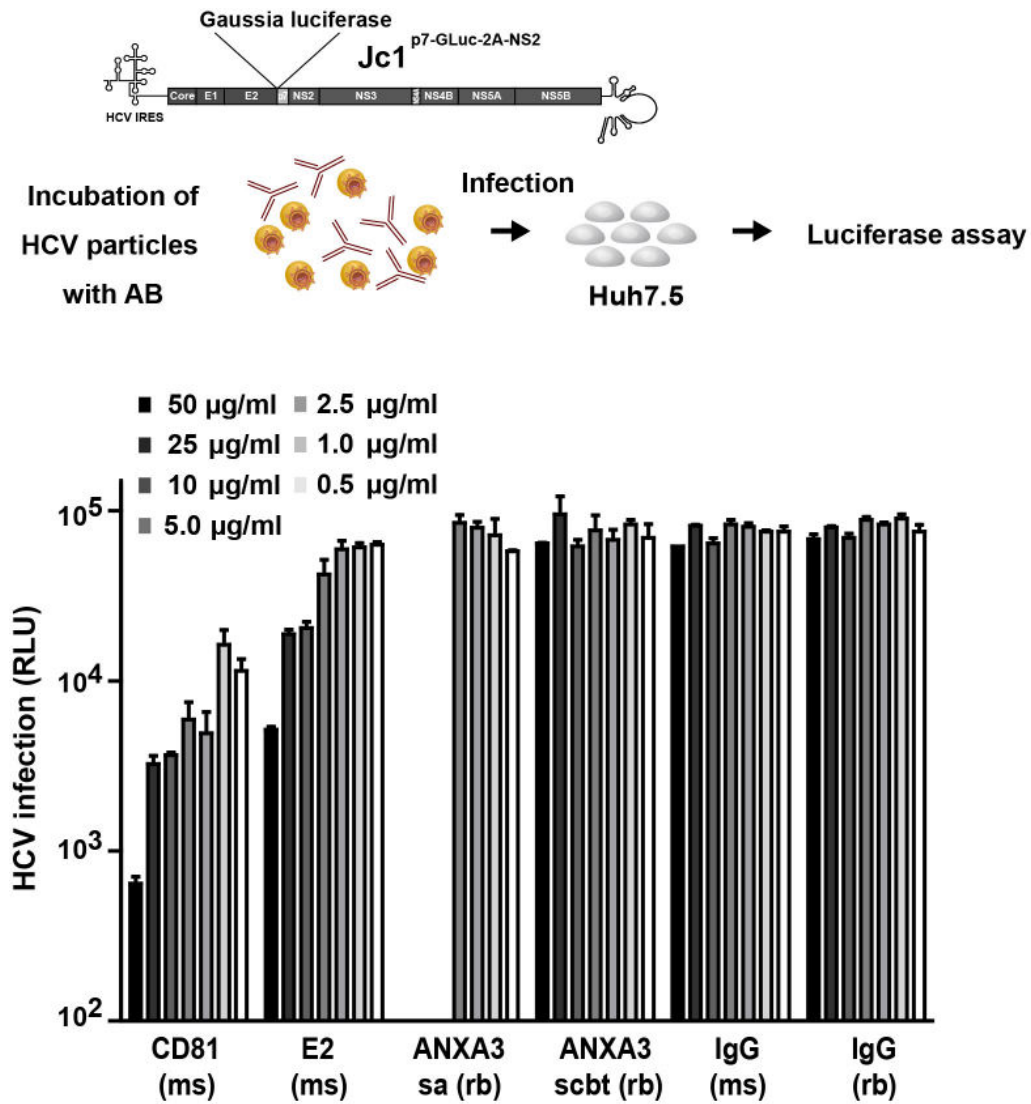


**Figure 3.30.:** Neutralization assay of HCV particles. Neutralization assay of Jc1<sup>p7-GLuc-2A-NS2</sup> virions incubated with indicated antibodies prior infection of naïve Huh7.5 cells. Two days post infection HCV replication was analyzed by measuring the activity of secreted Gaussia luciferase in the cell culture supernatant (Mean ± SD, assay in duplicate).

### 3.1.10. ANXA3 contributes to HCV virion maturation by facilitating incorporation of ApoE

As part of the viral particle, the viral glycoprotein E2 directly interacts with ApoE to allow attachment of the lipoprotein to the virion [Lee14]. Whether E2 is still able to interact with ApoE in the absence of ANXA3 was next probed by co-immunoprecipitation experiments. shANXA3 and control cells were transfected with Jc1<sup>Flag-E2</sup> RNA. At day three post transfection, cells were lysed and subjected to Flag-specific immunoprecipitation. Western blot analysis of co-immunoprecipitation from control cells confirmed an interaction of Flag-E2 and ApoE. However, in the absence of ANXA3, this interaction was nearly abolished (Figure 3.31 A). This experiment was also repeated in  $\Delta$ ANXA3 and WT cells and again no interaction of Flag-E2 and ApoE was detectable in  $\Delta$ ANXA3 cells (Figure 3.31 B). Additionally, the data indicate that ANXA3 expression was also required for the interaction of Flag-E2 with core. Then Huh7.5 cells were transduced with lentiviral constructs expressing core and E1/Flag-E2 (containing the signal peptide of core to ensure correct subcellular localization) to clarify whether an interaction between Flag-E2/ApoE and Flag-E2/core occurs independently of full viral replication. Again, co-immunoprecipitation experiments were performed. In absence of full viral replication, no interaction between Flag-E2 and core was observed and also no interaction between Flag-E2 and endogenous ApoE was detectable (Figure 3.31 C). The data indicate that ANXA3 as well as other viral proteins than core and E1/E2 are needed for proper virion assembly.

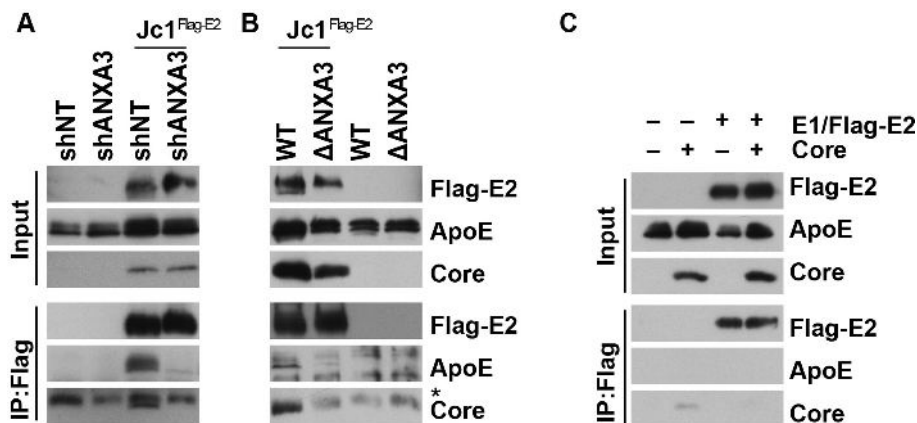


**Figure 3.31.: ANXA3 facilitates the interaction of ApoE with E2.** A) Interaction of Flag-E2 with ApoE and core in shANXA3 cells was analyzed by co-immunoprecipitation experiments. ANXA3-knockdown and control cells were transfected with Jc1<sup>Flag-E2</sup> RNA. 72 h later, cells were harvested and subjected to Flag-specific immunoprecipitation. Co-immunoprecipitations were analyzed by western blotting. B) Co-immunoprecipitations performed in  $\Delta$ ANXA3 and WT cells. C) Interaction between Flag-E2 and ApoE/core in cells expressing core and E1/Flag-E2 proteins. Huh7.5 cells transduced with lentiviruses expressing core and E1/Flag-E2. Cells were harvested and subjected to Flag-specific immunoprecipitation. Co-immunoprecipitations were analyzed by western blotting.

HCV assembly can be subdivided into two tightly connected processes: an initiation phase, which occurs at LDs close to replication complexes on the cytosolic side of the ER membrane and the assembly, maturation and release which occurs on the luminal side of the ER membrane and/or during secretion. Previous reports have shown that during the initiation process an interaction between ApoE and NS5A takes place. This occurs close-by replication complexes in order to recruit ApoE to viral assembly sites and thereby impact generation of HCV parti-

cles [Ben10, Jon10b]. To answer whether ANXA3 acts on the cytosolic initiation process or on the luminal assembly, maturation and release of virions, the interaction between ApoE and NS5A was analyzed in the absence of ANXA3. shANXA3 or control cells were transfected with Jc1<sup>NS5A-HA</sup> RNA. 72 h later, cells were harvested and subjected to HA-specific co-immunoprecipitation. No change in the level of ApoE interacting with NS5A was observed, indicating that ANXA3 acts either on the cytosolic side but after the NS5A/ApoE interaction or supports virion assembly on the luminal side of the ER membrane (Figure 3.32 A). Furthermore, co-immunoprecipitation experiments were performed to answer if ANXA3 directly interacts with NS5A in viral RNA replication competent cells. Therefore, Huh7.5 cells were transfected with Jc1<sup>ΔE1E2-NS5A-HA</sup> RNA, encoding a HA-tagged NS5A variant. 72 h post transfection, cells were lysed and subjected to HA-specific co-immunoprecipitation. However, western blot analysis revealed no direct interaction between NS5A and endogenous ANXA3 (Figure 3.32 B).

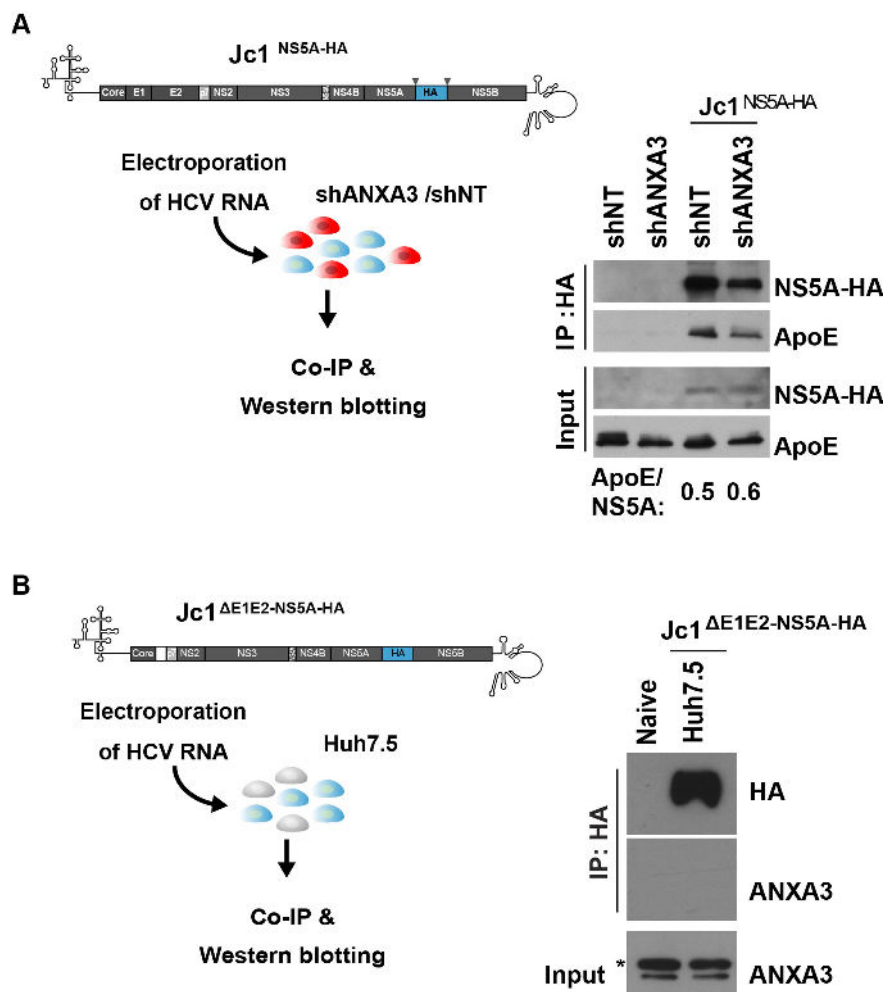


**Figure 3.32.: ANXA3 acts on the luminal side of the ER and doesn't interact directly with NS5A.** A) Co-immunoprecipitation performed in shANXA3 and control cells, transfected with Jc1<sup>NS5A-HA</sup> RNA, 72 h post transfection. Cells were lysed using low-stringency lysis buffer and subjected to HA-specific immunoprecipitation. Co-immunoprecipitations were analyzed and quantified by western blotting. B) Co-immunoprecipitation of NS5A-HA and endogenous ANXA3. Huh7.5 cells were mock-transfected or transfected with Jc1<sup>ΔE1E2-NS5A-HA</sup> RNA. 72 h later, cells were lysed, subjected to HA-specific co-immunoprecipitation and analyzed by western blotting. Asterisk marks an unspecific band.



### 3. Results

To further verify the results generated by co-immunoprecipitation, co-localization of Flag-E2 and core in the absence of ANXA3 was analyzed by immunofluorescence microscopy. ANXA3-knockdown and control cells were infected with Jc1<sup>Flag-E2</sup>. 72 h post infection, cells were fixed and stained with antibodies detecting core and Flag. Then co-localization of core and Flag-E2 was probed by confocal microscopy. In both cell lines Flag-E2 showed a broad reticular distribution throughout the cell. In contrast, core either appeared in ring-like structures most likely reflecting LDs or in a reticular pattern most likely representing the ER. Compared to the control, silencing of ANXA3 had no severe effect on the cellular distribution of both proteins, but co-localization of core and Flag-E2 was significantly reduced in the absence of ANXA3 (Figure 3.33).

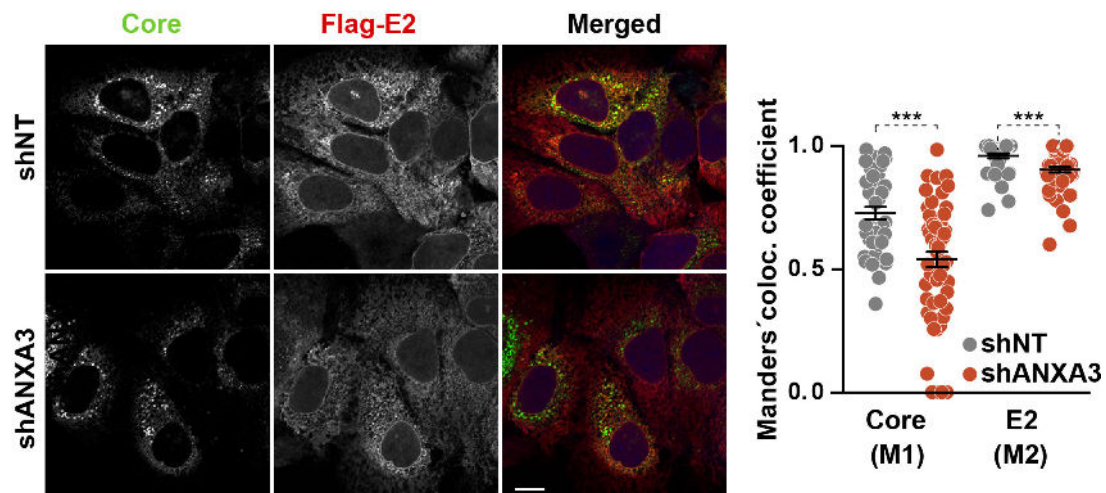


**Figure 3.33.: Silencing of ANXA3 affects the co-localization of core and Flag-E2.** Subcellular distribution and co-localization of core and Flag-E2 in Jc1<sup>Flag-E2</sup>-infected ANXA3-knockdown and control cells. 72 h post infection, cells were fixed and analyzed by immunofluorescence using specific antibodies. Single channels are showed in black and white, merged pictures are pseudocolored as indicated. The blue signal in the merged image represents mCherry of shRNA constructs (scale bar 10  $\mu$ m). The degree of co-localization was quantified using Coloc2 in Fiji [Sch12], with each dot corresponding to one cell. Individual cells of three independent experiments were analyzed (Mean  $\pm$  SEM, \*\*\*p < 0.001).

Next, co-localization of core/Flag-E2 with endogenous ApoE was analyzed in HCV-infected shANXA3 and control cells by immunofluorescence microscopy. In non-infected cells ApoE mainly localized to the Golgi compartment. While an HCV infection caused a scattered punctuate pattern of ApoE co-localizing with Flag-E2 throughout the cytoplasm (Figure 3.34 A). In contrast to the control, ApoE persisted in the Golgi compartment in HCV-infected as well as in non-infected ANXA3-knockdown cells. In the absence of ANXA3 less co-localization between Flag-E2 and ApoE was detectable, supporting the reduced interaction of these proteins in ANXA3-knockdown- and  $\Delta$ ANXA3 cells detected by co-immunoprecipitation experiments (Figure 3.31 A,B). However, compared to the control, silencing of ANXA3 had no effect on the co-localization of core and ApoE (Figure 3.34 B). The results perfectly fit to the idea that ANXA3 act on the luminal side on the ER membrane, because silencing of ANXA3 severely influenced the co-localization of Flag-E2 and ApoE, but had no effect on the co-localization of core and ApoE (which may partially take place on the cytosolic side of the ER or within HCV particles on the luminal side of the ER).

To address a possible direct interaction of ANXA3 with ApoE, E2 or core in HCV replication competent cells, co-immunoprecipitation experiments were performed. Huh7.5 cells expressing



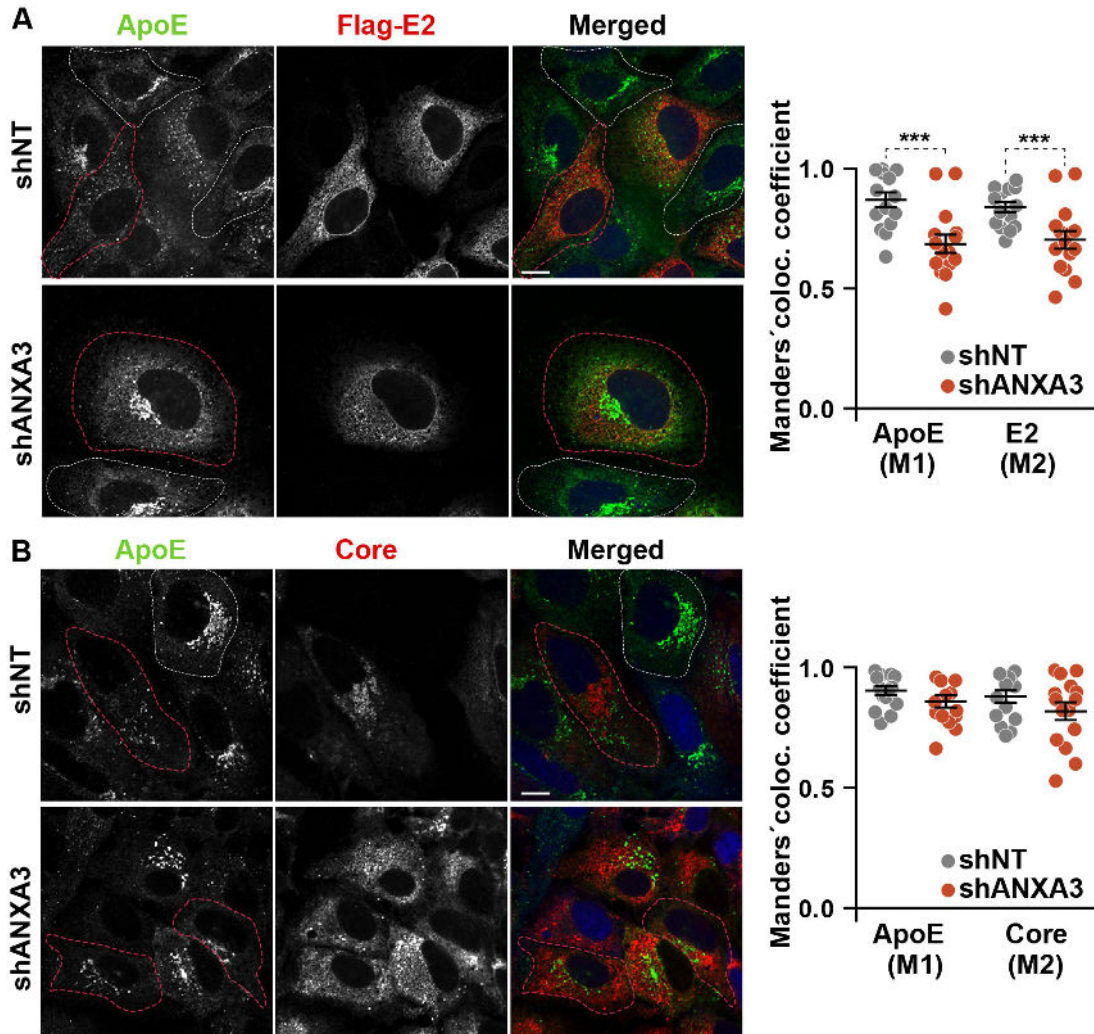


**Figure 3.34.: Silencing of ANXA3 reduces the co-localization of Flag-E2 and ApoE.** Subcellular distribution and co-localization of Flag-E2 (A) or core (B) with endogenous ApoE was analyzed in Jc1<sup>Flag-E2</sup>-infected ANXA3-knockdown and control cells. Co-localization was analyzed by immunofluorescence using specific antibodies. The degree of co-localization was quantified using Coloc2 in Fiji [Sch12]; each dot corresponds to one cell. Single channels are showed in black and white, merged pictures are pseudocolored as indicated. The blue signal in the merged image represents mCherry of shRNA constructs (scale bar 10  $\mu$ m). HCV-infected cells are labeled with red dashed lines, naïve cells are labeled with white dashed lines. Individual cells of three independent experiments were analyzed (Mean  $\pm$  SEM, \*\*\*p < 0.001).

### 3. Results

ANXA3-HA or carrying an empty control plasmid were infected with a Jc1<sup>WT</sup> strain. Five days later, cells were lysed and subjected to HA-specific co-immunoprecipitation. In this experimental approach, no direct interaction between ANXA3 and ApoE or the viral proteins E2 and core was detectable, arguing for an indirect interaction of ANXA3 with these proteins (Figure 3.35).

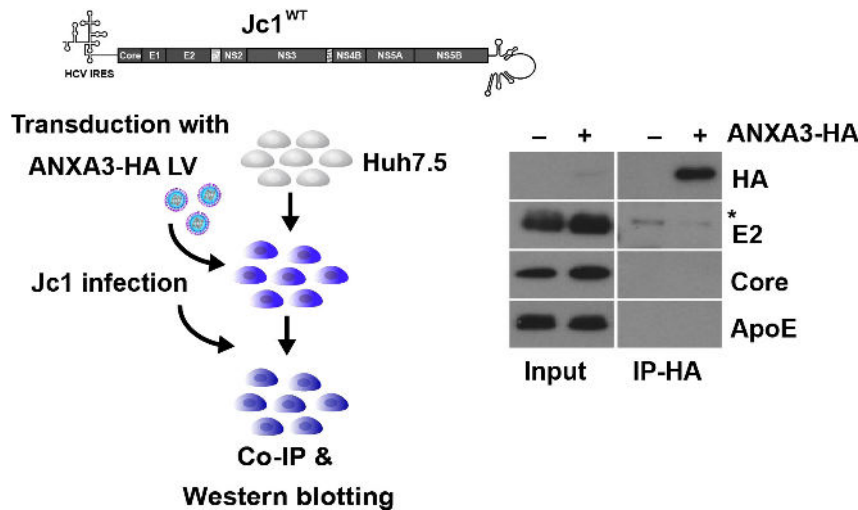


**Figure 3.35.: ANXA3-HA does not interact with core, E2 or ApoE in HCV-infected cells.** Co-immunoprecipitation of ANXA3-HA with E2 or ApoE/core. Huh7.5 cells were transduced with lentiviral particles expressing ANXA3-HA or an empty vector control. Two days later, cell lines were infected with a Jc1<sup>WT</sup> strain. Five days post infection, cells were lysed and subjected to HA-specific co-immunoprecipitation. Co-immunoprecipitations were analyzed by western blotting. Asterisk marks an unspecific band.

In order to verify whether an association of core, E2 and ApoE with cellular membranes was different in shANXA3 cells compared to shNT cells, membrane floatation assays were performed. shANXA3- and shNT cells were infected with Jc1<sup>Flag-E2-NS5AB-eGFP-BSD</sup>. After blasticidin selection, cells were mechanically lysed using a Dounce homogenizer. Equal amounts of protein were overlaid with a 30–10% Iodixanol gradient and centrifuged for 16 h at 200.000 g. From top to bottom, 1 ml fractions were harvested and the expression of indicated proteins was analyzed in each fraction by western blotting (Figure 3.36). Cell lysates were also analyzed to assess the overall expression of these proteins.

Compared to the control, no significant differences in the expression levels of core, Flag-E2 and ApoE were found in lysates of HCV-infected shANXA3 cells, indicating comparable levels of viral replication. Based on their density, gradient fractions can be divided into lipid-rich, low density areas (fraction one to six, high PLIN2/ARDP expression), ER-rich areas containing high density membranes (fraction seven to fourteen, high calreticulin expression) and areas which contained aggregated proteins (fifteen to twenty five). Low density membrane fractions were enriched in ApoE and PLIN2/ADRP in both cell lines and also core and Flag-E2 were highly associated with these membranes. A change in the distribution of viral proteins and ApoE within ER-enriched areas was not observed in shANXA3 cells compared to the control. In summary, no significant differences in the association of ApoE and viral proteins with cellular membranes was observed in the absence or presence of ANXA3. Of note, this assay is not suitable to separate ER- and Golgi- enriched fractions.

In order to confirm that large amounts of endogenous ApoE remained in the Golgi compartment in HCV-infected ANXA3-knockdown cells, immunofluorescence analysis using a Golgi-

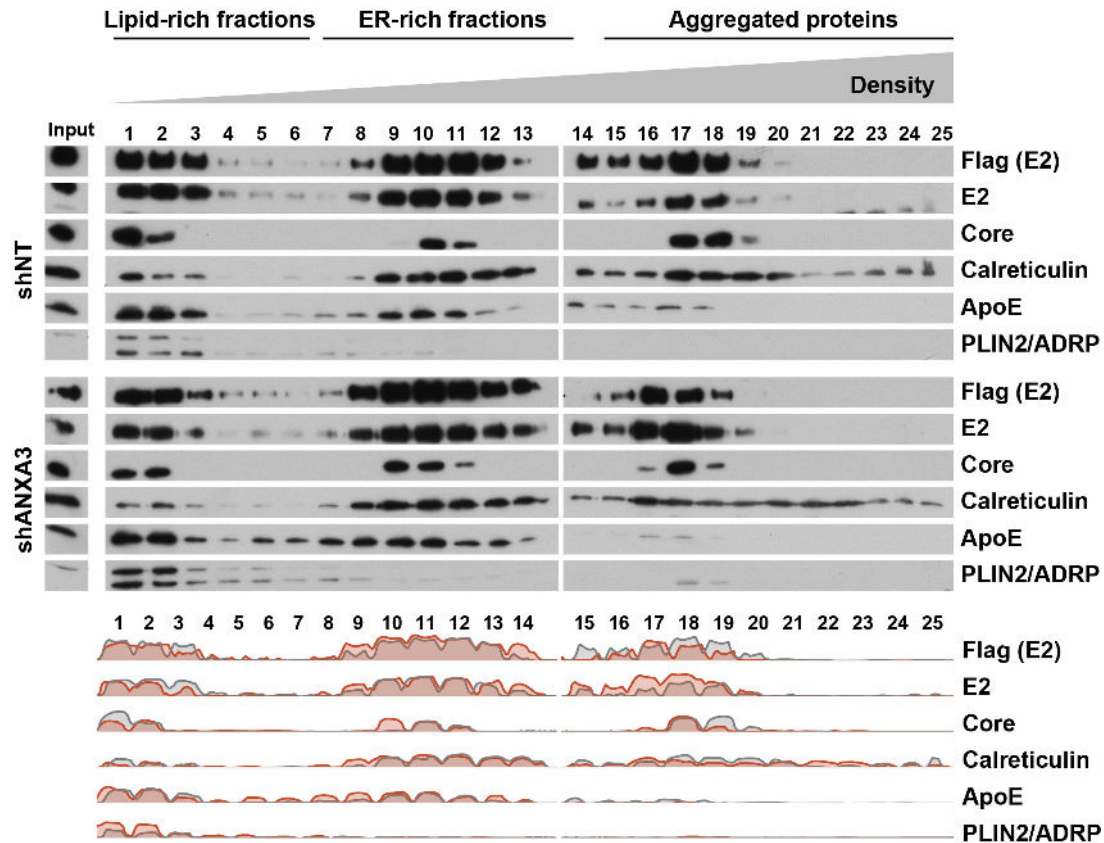


**Figure 3.36.:** No differences in membrane- association of ApoE, core and Flag-E2 in shANXA3 cells. Membrane floatation assay of HCV-infected shANXA3 and control cells. Cells were lysed using a Dounce homogenizer. Equal amounts of post nuclear cellular lysates were overlaid with a 30–10% Iodixanol gradient and separated by centrifugation for 16 h at 200.000 g. From top to bottom 25 fractions were harvested and analyzed by western blotting. Density profile of protein expression in each fraction was plotted and overlaid using ImageJ. Shown is one representative experiment.

specific antibody was performed. Here, shRNA-expressing lentiviruses were used that carry a puromycin selection marker instead of mCherry to enable detection of three different channels by confocal microscopy. ANXA3-knockdown and control cells were selected with puromycin and infected with Jc1<sup>Flag-E2</sup>. 72 h later, co-localization of ApoE, GM130 (Golgi marker) and Flag-E2 was probed by specific antibodies (Figure 3.37 A). Comparison of HCV-infected and non-infected control cells showed less ApoE/Golgi co-localization in HCV-infected cells, which was partially attended by a distorted/scattered distribution of the Golgi compartment (Figure 3.37 A,B). Silencing of ANXA3 partially restored the Golgi fragmentation in HCV-infected cells accompanied by an increase in the co-localization of ApoE and GM130. Here, no significant difference in the ApoE/GM130 co-localization between HCV-infected and naïve cells was observed. Co-localization analysis of ApoE and calnexin, which served as an ER marker, revealed no differences in HCV-infected or non-infected cells in the absence or presence of ANXA3, indicating a specific interplay between ANXA3 and viral maturation inside the Golgi compartment (Figure 3.37 C).

The analysis of the frequency of Golgi fragmentation revealed that more than 70% of HCV-infected control cells showed a distorted/scattered Golgi pattern. In non-infected control cells only 7% of cells showed a Golgi fragmentation, indicating a HCV contributes to the fragmen-

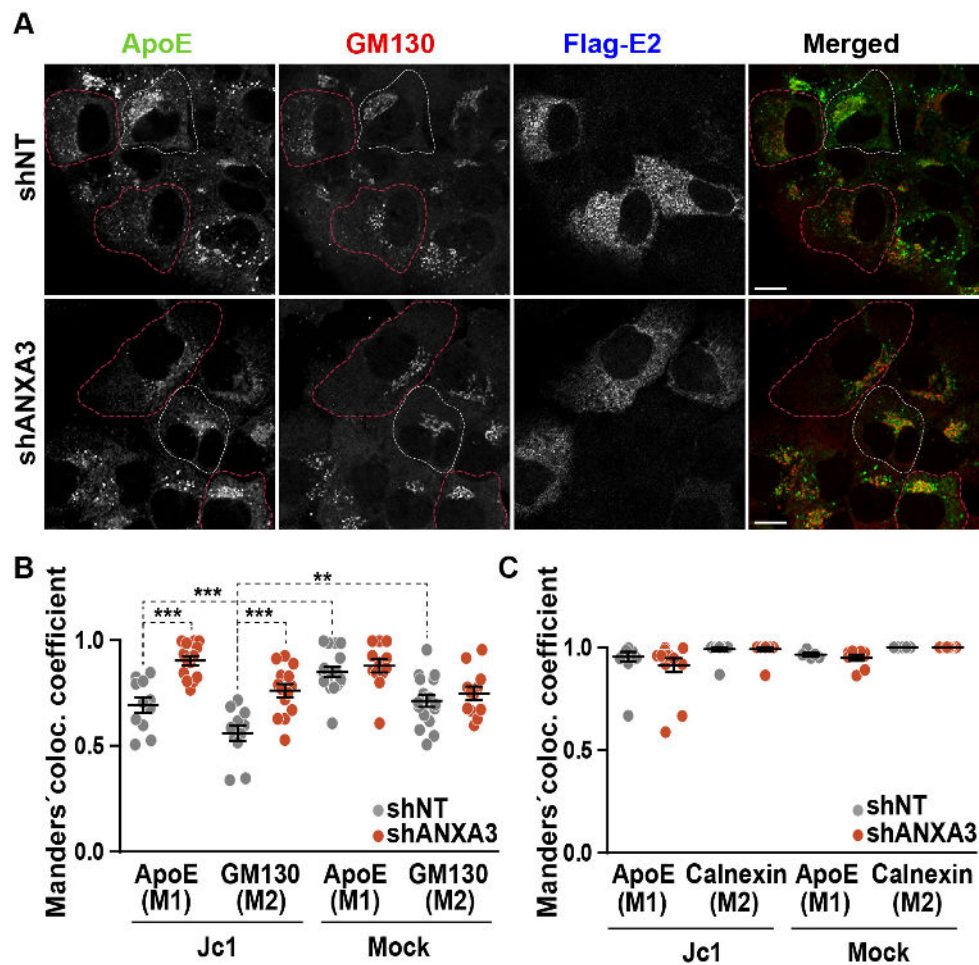


**Figure 3.37.: HCV-induced morphological changes of the Golgi compartment are less pronounced in shANXA3 cells.** A) Subcellular distribution and co-localization of endogenous ApoE and GM130 in Jc1<sup>Flag-E2</sup>-infected ANXA3-knockdown and control cells. 72 h post infection, cells were fixed, stained with antibodies detecting ApoE, GM130 and Flag and analyzed by confocal microscopy. The degree of co-localization was quantified using Coloc2 in Fiji [Sch12], each dot corresponds to one cell. Single channels are showed in black and white, merged pictures are pseudocolored as indicated (scale bar 10  $\mu$ m). HCV-infected cells are labeled with red dashed lines, naïve cells are labeled with white dashed lines. B) Quantitative analysis of co-localization of ApoE and GM130. Individual cells of two–three independent experiments were analyzed with Coloc2 in Fiji [Sch12], each dot corresponds to one cell. Mean  $\pm$  SEM, \*\* $p < 0.01$ , \*\*\* $p < 0.001$ . C) Quantitative analysis of co-localization of ApoE and calnexin. Individual cells of two independent experiments were analyzed with Coloc2 in Fiji [Sch12], each dot corresponds to one cell (Mean  $\pm$  SEM).



tation of the Golgi apparatus. In the absence of ANXA3, 68% of HCV-infected cells showed perinuclear Golgi apparatus. In contrast to HCV-infected control cells, only ~30% of shANXA3 cells showed a distorted Golgi compartment, suggesting that an HCV-induced disorganization of the Golgi compartment was less efficient in the absence of ANXA3 (Figure 3.38). The results are in line with a previous report showing that up to 90% of HCV-infected cells showed a Golgi fragmentation [Ama11].

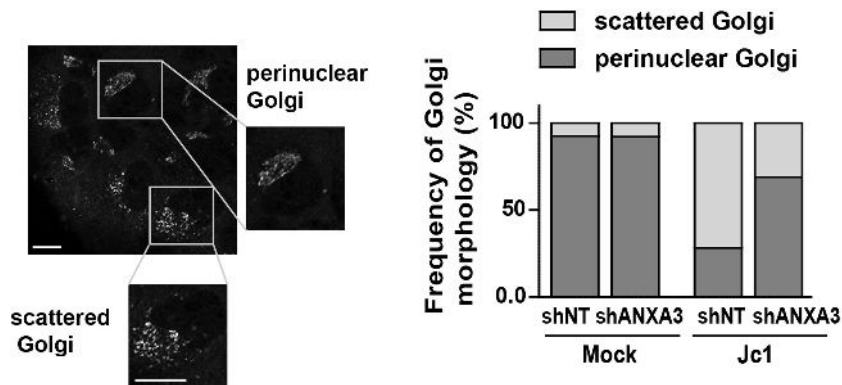


**Figure 3.38.: ANXA3 affects Golgi scattering in HCV-infected cells.** Analysis of HCV induced Golgi fragmentation. Subcellular distribution of the Golgi compartment was analyzed in HCV-infected and naïve shANXA3/control cells according to the GM130 staining. Shown is one representative example of the two Golgi phenotypes which were distinguished as perinuclear Golgi- and scattered Golgi patterns (scale bar 10  $\mu$ m). Two individual experiments were analyzed. At least 120 cells per condition (infected vs. non-infected, control vs. shANXA3) were manually analyzed to determine the frequency of a perinuclear or scattered Golgi pattern.

## 3.2. Visualization of viral proteins at LDs by super-resolution microscopy (dSTORM)

In the second part of the dissertation, the spatial distribution of core/NS5A and E2 at LDs of HCV-infected cells was analyzed by dSTORM, in order to visualize putative viral assembly events.

### 3.2.1. Generation and validation of Flag-E2 tagged viral strains

Due to the lack of suitable commercially available antibodies of the right species that detect the viral envelope protein E2 of the JFH1 and the Jc1 strain, infectious HCV viral strains with tagged E2 were generated. Thus, allowing the visualization of E2 together with the capsid protein core or the phosphoprotein NS5A. Therefore, a Flag tag sequence (amino acids: DYKDDDDK) was inserted in the N-terminal region of E2 [Pre11]. Two infectious HCV constructs carrying the Flag-E2 fusion protein were generated, the original isolate JFH1 and the cell culture adapted Jc1 strain, which replicates to high titers in cell culture. Afterwards, protein expression, infectivity, and the subcellular localization of the Flag-E2 fusion protein was characterized for JFH1<sup>Flag-E2</sup>- and Jc1<sup>Flag-E2</sup>-strains (Figure 3.39). First, the expression of E2 and Flag was analyzed by western blotting. Therefore, Huh7.5 cells were transfected with *in vitro* transcribed viral RNA. At day three post transfection, cells were harvested and analyzed. The Flag-E2 fusion protein was

### 3. Results

detectable by antibodies targeting E2 as well as Flag in JFH1<sup>Flag-E2</sup>- and Jc1<sup>Flag-E2</sup>-transfected cells, confirming the Flag-tag insertion into E2 and a correct translation and folding as well as glycosylation of the protein (Figure 3.39 A). In addition, the supernatant of transfected cells was harvested to investigate the infectivity of these modified viral strains. Viral titers were determined by calculating the TCID<sub>50</sub>/ml, at days six and ten after transfection. Viral titers reached up to  $4 \times 10^4$  TCID<sub>50</sub>/ml for JFH1<sup>Flag-E2</sup> and  $4 \times 10^7$  TCID<sub>50</sub>/ml for Jc1<sup>Flag-E2</sup> (Figure 3.39 B). These viral titers are comparable to viral titers produced from Jc1 or JFH1<sup>WT</sup>-strains, suggesting that the insertion of the Flag-tag does not influence properties that determine infectivity.

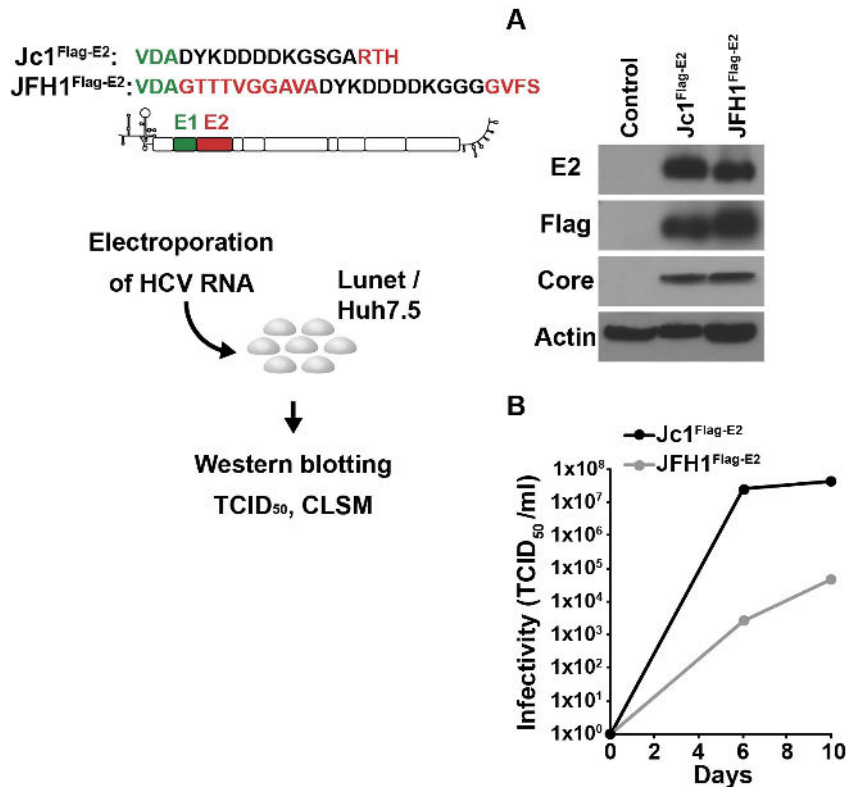


**Figure 3.39.: Characterization of Jc1<sup>Flag-E2</sup> and JFH1<sup>Flag-E2</sup> HCVcc constructs.** Jc1<sup>Flag-E2</sup> and JFH1<sup>Flag-E2</sup> HCVcc constructs were generated by overlap extension PCR, leading to the fusion of a Flag tag (amino acids sequence shown in black) with the N-terminal region of E2 (sequence shown in red). Huh7.5 cells were transfected with Jc1<sup>Flag-E2</sup> or JFH1<sup>Flag-E2</sup> RNA to analyze protein expression and infectivity of these strains. A) Western blot analysis of Huh7.5 cells transfected with *in vitro* transcribed Jc1<sup>Flag-E2</sup> and JFH1<sup>Flag-E2</sup> RNA. Naïve Huh7.5 cells served as a control, confirming the antibody specificity.  $\beta$ -actin served as loading control. B) Infectivity (shown as TCID<sub>50</sub>/ml) of Jc1<sup>Flag-E2</sup> and JFH1<sup>Flag-E2</sup> viral strains.

Next, the subcellular localization of E2 and Flag was analyzed by confocal microscopy. Therefore, Huh7 Lunet cells were infected with JFH1<sup>Flag-E2</sup>- or Jc1<sup>Flag-E2</sup>-viral strains and immunofluorescence staining using antibodies detecting E2 and Flag were performed. Furthermore, two different permeabilization methods were compared: 0.1% Triton X-100 for 5 min and 0.5% Saponin for 5 min, to investigate whether the permeabilization method influences the detection of the subcellular localization of the proteins. The immunofluorescence analysis showed a reticular pattern of the Flag-E2 fusion protein independently of the permeabilization method or viral

### 3.2. Visualization of viral proteins at LDs by super-resolution microscopy (dSTORM)

strain (Figure 3.40). However, compared to cells permeabilized with Saponin, treatment with Triton X-100 resulted in a brighter signal, probably due to the fact that Saponin permeabilization is considered less harsh than Triton X-100 treatment. To quantitate the results, the degree of co-localization of E2 and Flag was analyzed. Pearson's correlation coefficients (PCCs) were calculated between E2 (green channel) and Flag (red channel). PCC analysis of E2 and Flag indicated a strong correlation (0.92 and 0.77 in Jc1<sup>Flag-E2</sup>- and 0.85 and 0.68 in JFH1<sup>Flag-E2</sup>-infected cells) of both channels. In addition, Manders' colocalization coefficient (MCC) analysis also confirmed the co-localization of both channels, independently of the viral strain or permeabilization method.

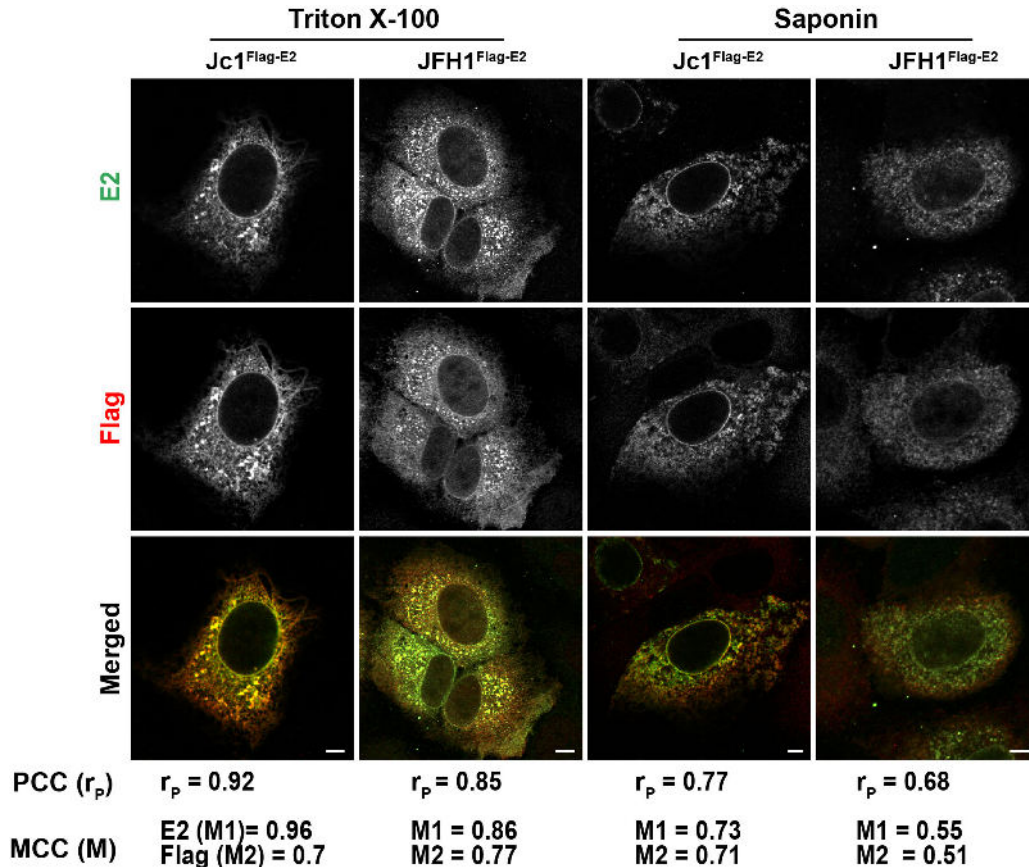


**Figure 3.40.:** Subcellular localization of Flag and E2. Confocal microscopy of Huh7 Lunet cells infected with Jc1<sup>Flag-E2</sup> and JFH1<sup>Flag-E2</sup> strains. Cells were permeabilized with 0.1% Triton X-100 or 0.5% Saponin and stained with antibodies detecting E2 and Flag. Single channels are shown in black and white; merged pictures are shown in color (scale bar 5  $\mu$ m). PCC as well as MCC were calculated using JACoP (Just Another colocalization Plugin) plugin for Image J.

#### 3.2.2. Confocal microscopy of JFH1<sup>E2-Flag</sup> / Jc1<sup>E2-Flag</sup>-infected cells

Next, the localization of core or NS5A with Flag-E2 at LDs was analyzed by confocal microscopy. Therefore, Huh7 Lunet cells were infected with JFH1<sup>Flag-E2</sup> or Jc1<sup>Flag-E2</sup> strains and further processed for co-immunofluorescence staining with specific antibodies, detecting the viral capsid protein core or NS5A, as well as Flag-E2. Furthermore, cells were also stained with LipidTox

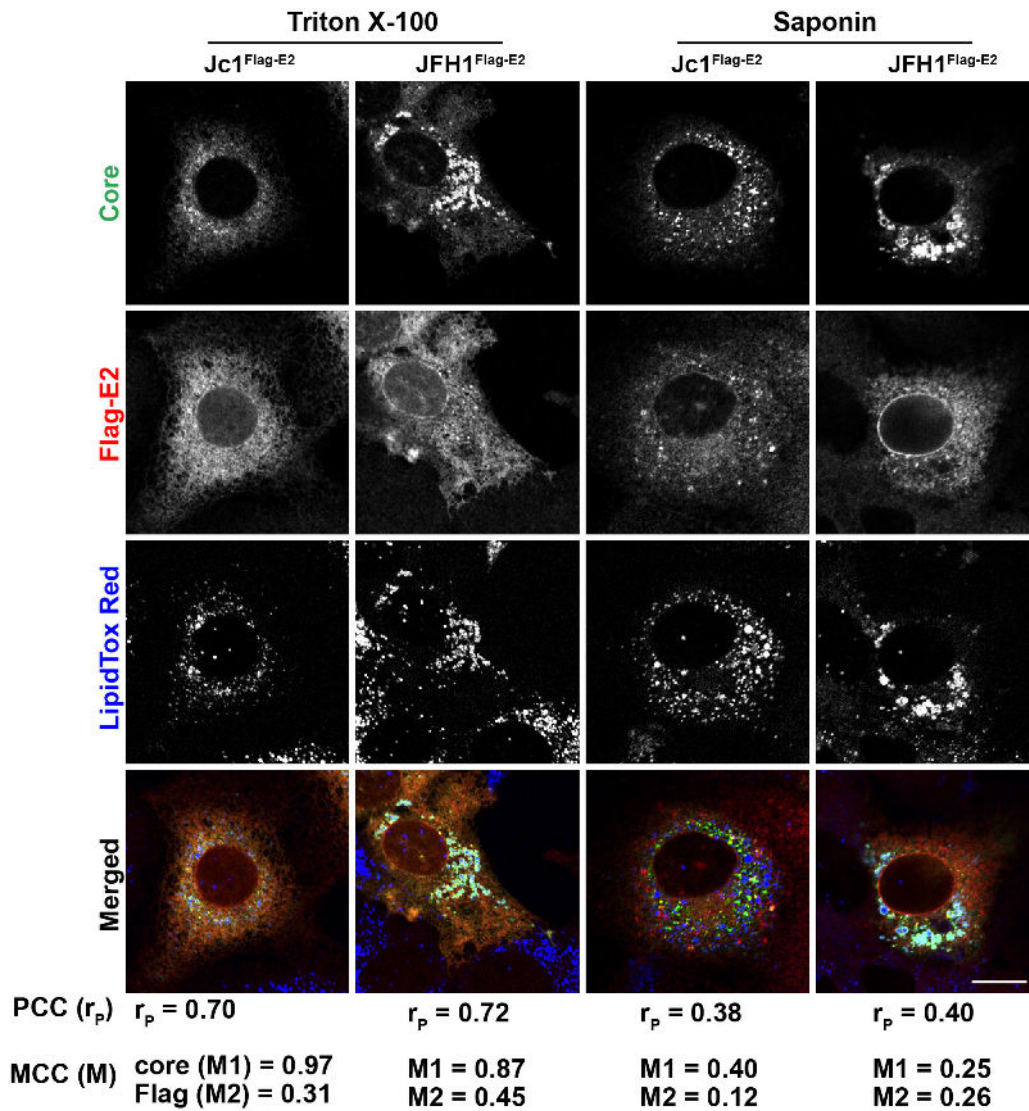


**Figure 3.41.:** Subcellular localization of core and Flag-E2 in Jc1<sup>Flag-E2</sup>- and JFH1<sup>Flag-E2</sup>-infected cells. Huh7 Lunet cells were infected with Jc1<sup>Flag-E2</sup> or JFH1<sup>Flag-E2</sup> viral stocks. Three days after infection, cells were fixed with 4% paraformaldehyde and permeabilized with 0.1% Triton X-100 or 0.5% Saponin. Afterwards, co-immunostainings were performed using antibodies detecting core and Flag. LDs were stained with LipidTox Red neutral lipid stain. Single channels are shown in black and white; merged pictures are shown in color (scale bar 5  $\mu$ m). PCC and MCC were calculated using JACoP plugin for Image J.



Red to trace LDs. Others have shown that fixation and permeabilization methods can influence the detection of LD-associated proteins [Ohs05]. Thus, permeabilization with 0.1% Triton X-100 for 5 min. was compared to 0.5% Saponin for 5 min. and additional 0.1% Saponin added to all subsequent incubation and washing steps. In Jc1<sup>Flag-E2</sup>-infected cells, core showed a broad distribution pattern mainly localized at the ER and partially LD-associated. In contrast to Jc1<sup>Flag-E2</sup>-infected cells, an accumulation of core in ring-like structures was observed in JFH1<sup>Flag-E2</sup>-infected cells. Co-localization of core with LipidTox Red revealed that these ring-like shapes reflect LDs. As shown before, JFH1 strains induce an accumulation of core at LDs most likely caused by an inefficient viral assembly process [Sha07]. In contrast to core, Flag-E2 appeared as a predominantly broad reticular structure that might reflect an ER-association, independently of the viral construct. Compared to Triton X-100 permeabilization, cells treated with Saponin exhibited a weaker Flag-E2 staining. In order to measure the level of co-localization of core and Flag-E2, quantification according to Pearson and Manders were performed. PCC analysis of core and Flag-E2 indicated a strong correlation (0.7 in Jc1<sup>Flag-E2</sup>- and 0.72 in JFH1<sup>Flag-E2</sup>-infected cells) in cells treated with Triton X-100. Quantification according to MCC revealed that most of the core co-localized with Flag-E2 ( $M1 = 0.97$  for Jc1<sup>Flag-E2</sup> and  $M1 = 0.87$  for JFH1<sup>Flag-E2</sup>) while Flag-E2 only partially co-localized with core ( $M2 = 0.31$  for Jc1<sup>Flag-E2</sup> and  $M2 = 0.45$  for JFH1<sup>Flag-E2</sup>). These differences are most likely caused by the broad distribution of Flag-E2, resulting in less overlap with the more distinct core signals. Compared to Triton X-100-treated cells, co-localization of core and Flag-E2 observed in Saponin-permeabilized cells was much lower (Figure 3.41).

JFH1<sup>Flag-E2</sup>- and Jc1<sup>Flag-E2</sup>-infected cells were also stained for Flag, NS5A, and LDs. NS5A showed less distinct LD-localization than core, independently of the viral strain used for infection. PCC analysis illustrated an intermediate co-localization of NS5A with Flag-E2 (0.6 in Jc1<sup>Flag-E2</sup>- and 0.44 in JFH1<sup>Flag-E2</sup>-infected cells) in cells treated with Triton X-100. In the MCC analysis most of the NS5A signals overlapped with Flag-E2 ( $M1 = 0.97$  for Jc1<sup>Flag-E2</sup> and  $M1 = 0.79$  for JFH1<sup>Flag-E2</sup>) whereas co-localization of Flag-E2 with NS5A was much lower ( $M2 = 0.19$  for Jc1<sup>Flag-E2</sup> and  $M2 = 0.17$  for JFH1<sup>Flag-E2</sup>), indicating that the broad distribution of Flag-E2 leads to less co-localization with the more specifically localized NS5A. Again, treatment with Saponin resulted in less co-localization between NS5A and Flag-E2 (Figure 3.42).

However, a statistically significant difference of viral protein co-localization between the two viral strains was not observed. Overall, Triton X-100 permeabilization leads to much stronger fluorescence intensities than Saponin, which might result in an enlarged overlap of both channels, suggesting that Saponin inadequately permeabilized intracellular membranes. Furthermore, core as well as NS5A co-localized with Flag-E2 at LDs in Jc1<sup>Flag-E2</sup>- and JFH1<sup>Flag-E2</sup>-infected cells, which might reflect putative viral assembly sites. Therefore, the generated Jc1<sup>Flag-E2</sup>- and JFH1<sup>Flag-E2</sup>-strains and the established co-immunofluorescence staining approach should be appropriate for the analysis of viral assembly sites in dSTORM.

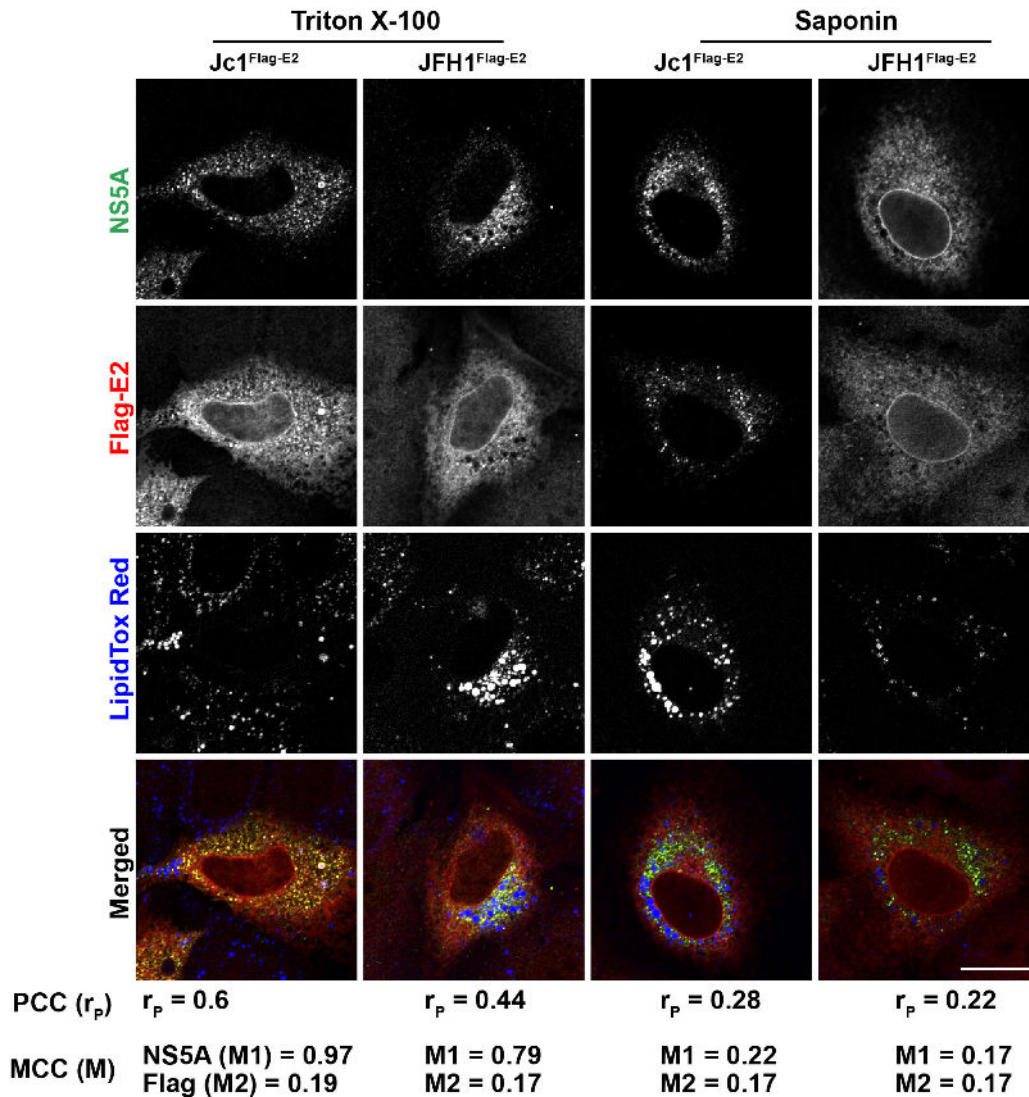


**Figure 3.42.: Subcellular localization of NS5A and Flag-E2 in Jc1<sup>Flag-E2</sup>- and JFH1<sup>Flag-E2</sup>-infected cells.** Huh7 Lunet cells were infected with Jc1<sup>Flag-E2</sup> or JFH1<sup>Flag-E2</sup> viral stocks. Three days after infection, cells were fixed with 4% paraformaldehyde and permeabilized with 0.1% Triton X-100 or 0.5% Saponin. Afterwards co-immunostainings were performed using a NS5A antibody and a Flag antibody. LDs were stained with LipidTox Red neutral lipid stain. Single channels are shown in black and white; merged pictures are shown in color (scale bar 5  $\mu$ m). PCC and MCC were calculated using JACoP plugin for Image J.

### 3.2.3. Visualization of LDs by dSTORM

To analyze LDs by dSTORM, a lipophilic fluorescence dye is needed that has the ability to “blink”, meaning the activation of dye molecules into a fluorescence state and switching them off into a dark state. Thus, different lipophilic fluorescence dyes (BODIPY, LipidTox Red, and LipidTox Green) were tested for their ability to blink under dSTORM buffer conditions. Huh7 Lunet cells were fixed and stained with the lipophilic fluorescence dyes. Then dSTORM analysis was performed to demonstrate the ability of these dyes to switch between the “on” and “off” state of single fluorescence molecules over time. Of the dyes tested, LipidTox Red showed the best capacity for dSTORM imaging. To verify the blinking properties of LipidTox Red, signal intensities were plotted over time, illustrating the switch between the “on” and “off” state of single LipidTox Red molecules (Figure 3.43 A).

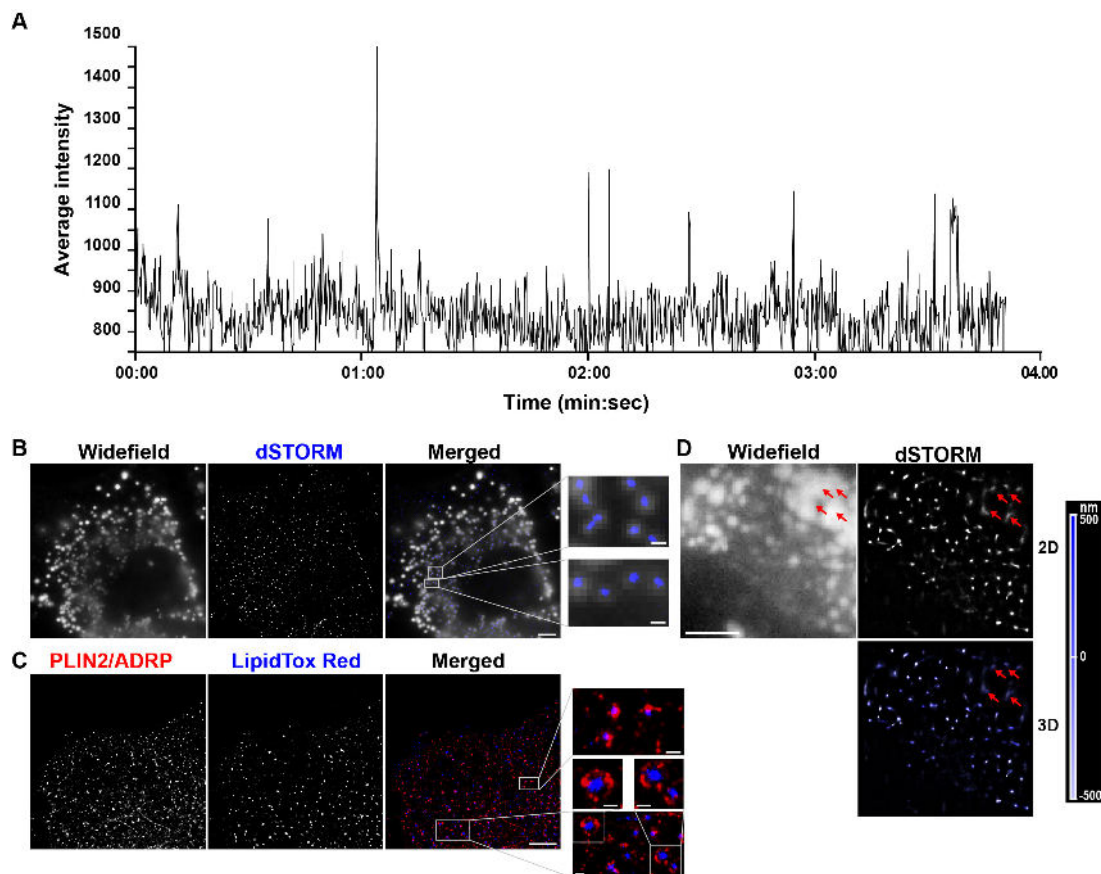


**Figure 3.43.: Visualization of LDs in dSTORM.** A) Single molecule time traces of LipidTox Red. Huh7 Lunet cells were stained with LipidTox Red neutral lipid stain. The “on” and “off” switch of single molecules was analyzed by dSTORM over time. B) Correlative widefield microscopy / dSTORM was performed of Huh7 Lunet cells stained with LipidTox Red neutral lipid stain. C) dSTORM image of Huh7 Lunet cells stained with an PLIN2/ADRP antibody and LipidTox Red neutral lipid stain. D) Visualization of small LDs by dSTORM. Huh7 Lunet cells were stained with LipidTox Red neutral lipid stain. dSTORM and widefield microscopy was performed. Shown are the single channel 2D and 3D images with the axial position color-coded according to the scale on the right together with the corresponding widefield image. Arrows highlight large LDs observed in widefield microscopy. Single channels are shown in black and white; merged pictures are shown in color (scale bar  $5 \mu\text{m}$ , in magnified images  $0.5 \mu\text{m}$ ). dSTORM analysis was performed by Dennis Eggert.

In addition, widefield fluorescence images were recorded and correlated with the corresponding dSTORM image, to secure that blinking events of LipidTox Red represents LDs. The signals detected with widefield fluorescence microscopy completely overlapped with the signals in dSTORM images, suggesting that LipidTox Red signals in dSTORM mode represent LDs (Figure 3.43 B). To further characterize dSTORM images, Huh7 Lunet cells were stained with LipidTox Red and an antibody detecting the LD-marker protein PLIN2/ADRP. Two-dimensional dSTORM images indicated that almost every LD (shown in blue) was tightly surrounded by PLIN2/ADRP (shown in red) confirming that LipidTox Red staining was suitable for LD visualization by dSTORM (Figure 3.43 C). Of note, LDs, which are observed via dSTORM are generally small ( $< 0.5 \mu\text{m}$  in diameter), as only LDs within  $2 \mu\text{m}$  in axial distance from the coverslip can be detected. Large LDs additionally observed in widefield images were mainly more than  $2 \mu\text{m}$  above the coverslip so of those large LDs only the edge could be detected with dSTORM (Figure 3.43 D).

#### 3.2.4. 2D and 3D dSTORM analysis of Jc1<sup>Flag-E2</sup>- and JFH1<sup>Flag-E2</sup>-infected cells

Next, 2D super resolution microscopy of Jc1<sup>Flag-E2</sup>- and JFH1<sup>Flag-E2</sup>-infected cells was performed. Therefore, Huh7 Lunet cells were infected with JFH1<sup>Flag-E2</sup> or Jc1<sup>Flag-E2</sup> and permeabilized with Triton X-100 or Saponin. Core, NS5A, Flag-E2 as well as LDs were stained as described before. Super-resolution datasets were then acquired on a custom modified Nikon N-STORM microscope in dSTORM mode [Ama11, Pre11, Hua08]. Shown are examples of 2D dSTORM images, of cells either stained for core (Figure 3.44) or NS5A (Figure 3.45) together with Flag-E2 and LipidTox Red. In all experiments a partial co-localization of core and NS5A with Flag-E2 at LDs can be observed, irrespective of the viral strain. However, a complete co-localization of all three channels was rarely observed. Furthermore, core and NS5A showed a more defined LD-associated pattern than Flag-E2, which was mostly detectable in the periphery of LDs. LDs itself, were visible as tight round spots.

The degree of co-localization of core or NS5A with Flag-E2 at LDs was calculated according to Manders (Figure 3.46). Therefore, cytosolic regions were analyzed for co-localization of: core/NS5A with LDs, Flag-E2 with core/NS5A, and Flag-E2 with LDs. Co-localization coefficients were very low in all analyzed dSTORM datasets, reflecting the high resolution of dSTORM images. No significant differences in the co-localization of core or NS5A with Flag-E2 were observed. Furthermore, comparable levels in core/NS5A co-localization with LDs were monitored. However, a slight decrease in the overlap of LD signals with NS5A was detectable in JFH1<sup>Flag-E2</sup>-infected cells, which could be caused by a broader NS5A distribution in these cells. MCC analysis of Flag-E2 and LDs showed an elevated overlap in Jc1<sup>Flag-E2</sup>-infected cells, indicating a tight Flag-E2 distribution around LDs. But these results were only observed in cells co-stained with core and not with NS5A.

For 3D dSTORM an astigmatism imaging was used as described [Hua08]. dSTORM images were reconstructed from a series of 5,000–15,000 widefield images per channel using the N-STORM v. 2.0 module of NIS Elements AR v. 4.0 (Nikon). For 3D dSTORM, cytosolic regions were selected, where core or NS5A overlapped with the Flag-E2 staining in close proximity to LDs. These regions of interest (ROIs) were reconstructed in 3D with the axial position information encoded according to the color-coded bar. Shown is one example of 2D and 3D dSTORM images, either generated from Jc1<sup>Flag-E2</sup>- and JFH1<sup>Flag-E2</sup>-infected cells, stained for core, Flag-E2, and LDs (Figure 3.47).

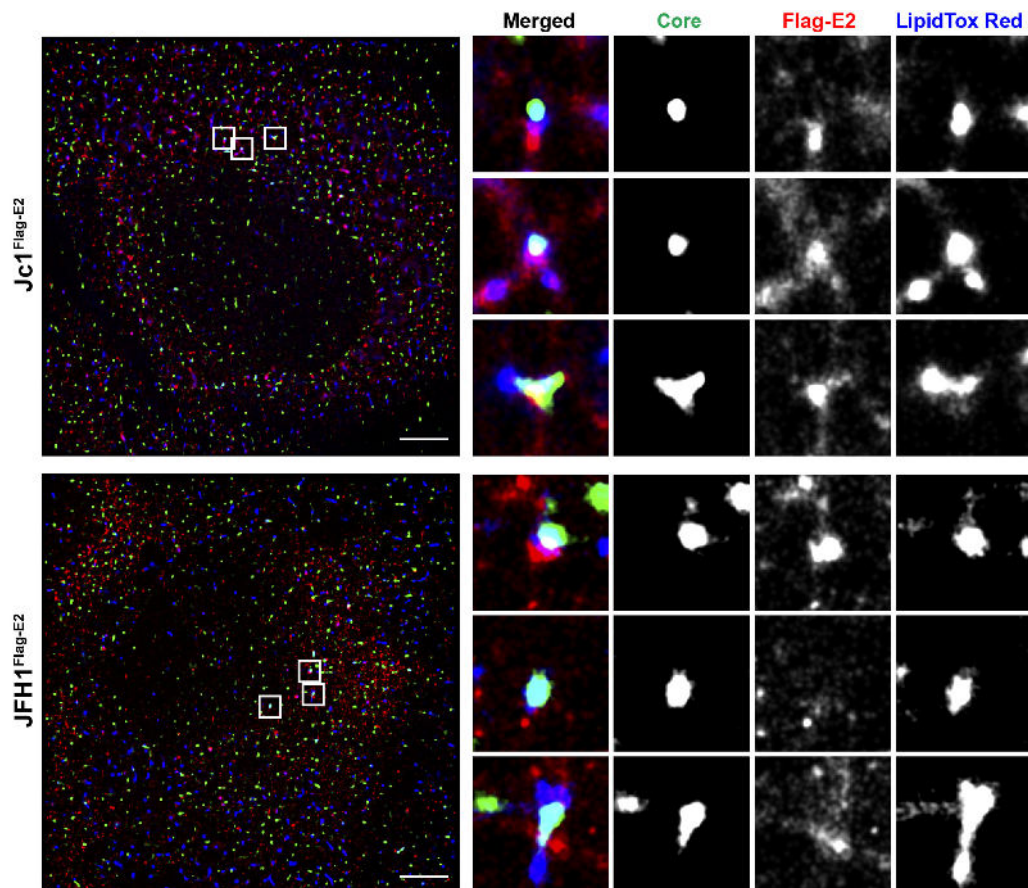


**Figure 3.44.:** dSTORM images of core overlapping with Flag-E2 and LipidTox Red. Huh7 Lunet cells were infected with Jc1<sup>Flag-E2</sup> or JFH1<sup>Flag-E2</sup> viral stocks. At day three post infection, cells were permeabilized with 0.1 % Triton X-100 followed by incubation with antibodies detecting core and Flag. LDs were visualized using LipidTox Red neutral lipid stain and analyzed by dSTORM. Super resolution images were reconstructed from a series of 5000-15000 images per channel (scale bar 5  $\mu\text{m}$ ). Selected ROIs are shown in enlarged images. Single channels are shown in black and white; merged pictures are shown in color (scale bar 0.5  $\mu\text{m}$ ). dSTORM analysis was performed by Dennis Eggert.



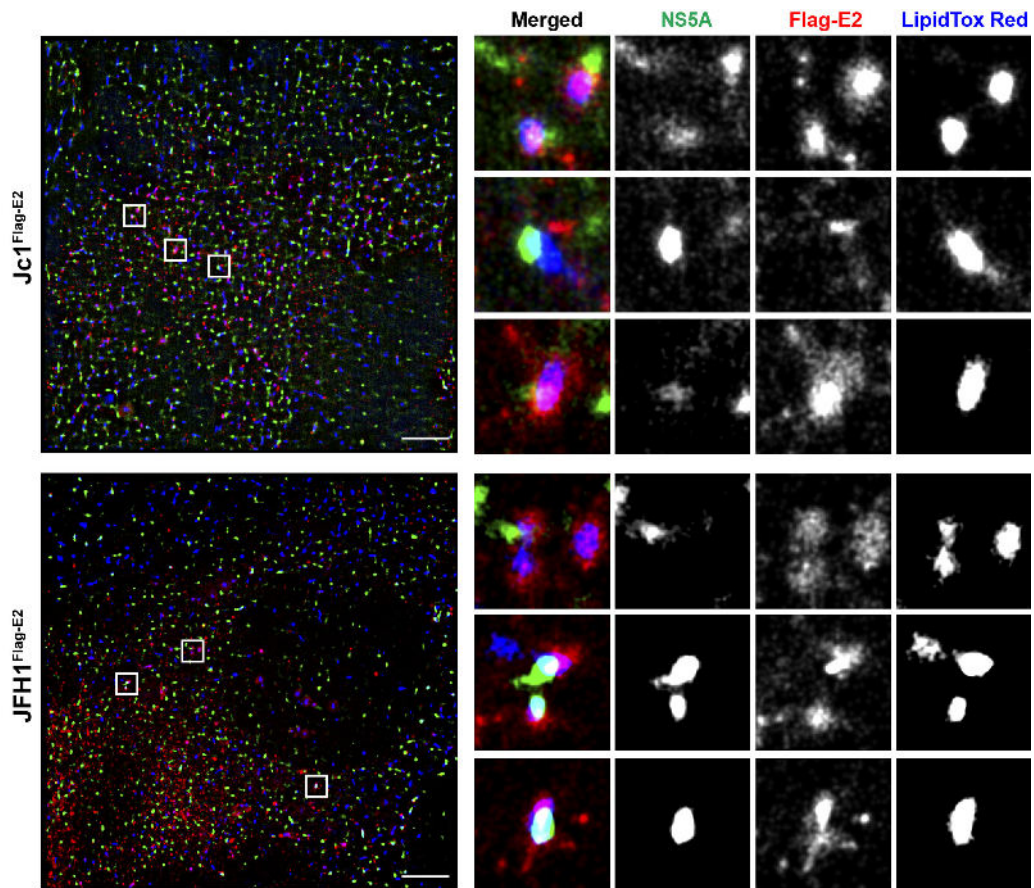


**Figure 3.45.: dSTORM images of NS5A overlapping with Flag-E2 and LipidTox Red.** Huh7 Lunet cells were infected with Jc1<sup>Flag-E2</sup> or JFH1<sup>Flag-E2</sup> viral stocks. At day three post infection, cells were permeabilized with 0.1 % Triton X-100 followed by incubation with antibodies detecting NS5A and Flag. LDs were visualized using LipidTox Red neutral lipid stain and analyzed by dSTORM. Super resolution images were reconstructed from a series of 5000-15000 images per channel (scale bar 5  $\mu\text{m}$ ). Selected ROIs are shown in enlarged images. Single channels are shown in black and white; merged pictures are shown in color (scale bar 0.5  $\mu\text{m}$ ). dSTORM analysis was performed by Dennis Eggert.

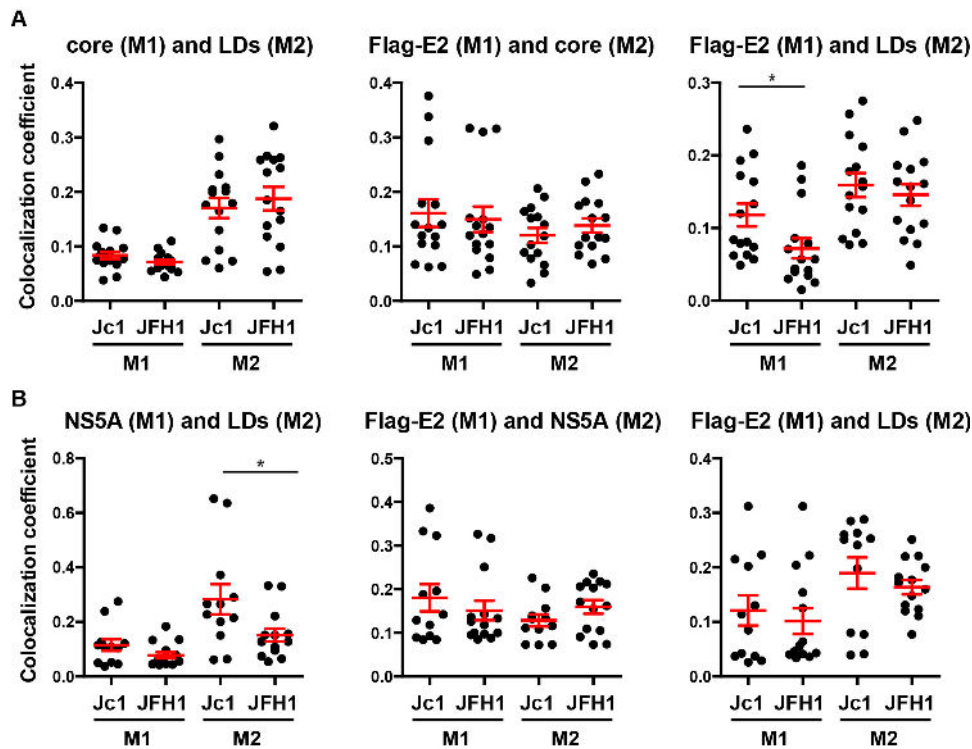


**Figure 3.46.:** Analysis of co-localization according to Manders of core/NS5A with Flag-E2 at LDs visualized by super resolution microscopy. The degree of co-localization of dSTORM datasets was analyzed using the JACoP plugin for Image J. Four independent experiments were performed and ROIs were analyzed in 2D. A) MCC analysis was used to illustrate the degree of co-localization of core and Flag-E2 at LDs. B) Co-localization coefficients of NS5A and Flag-E2 at LDs (Mean  $\pm$  SEM, \* $p < 0.05$ ).

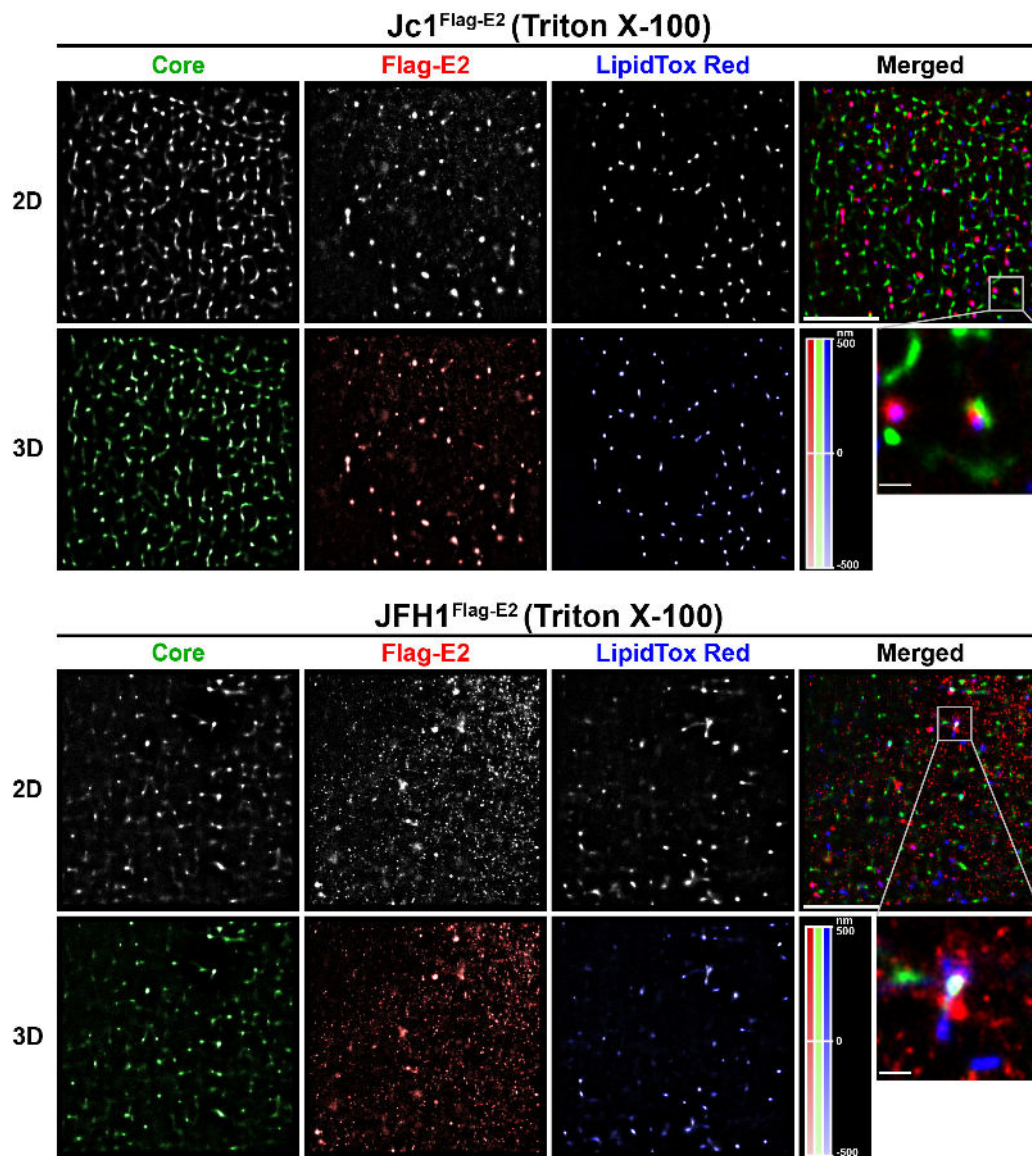


**Figure 3.47.: 2D and 3D dSTORM images of Jc1<sup>Flag-E2</sup>- and JFH1<sup>Flag-E2</sup>-infected cells.** Jc1<sup>Flag-E2</sup>- and JFH1<sup>Flag-E2</sup>-infected Huh7 Lunet cells were permeabilized with Triton X-100 followed by staining with core and Flag antibodies as well as LipidTox Red neutral lipid stain. 3D super-resolution datasets were acquired using astigmatism imaging. dSTORM images were reconstructed from a time series of 10,000–15,000 raw images per channel. Shown are the single channel 2D projections and the overlay as well as 3D images with the axial position color-coded according to the scale (scale bars 5  $\mu\text{m}$ ). Selected ROIs are shown in enlarged images (scale bars 0.5  $\mu\text{m}$ ). dSTORM analysis was performed by Dennis Eggert.



### 3.2.5. Analysis of 3D distribution of core/NS5A and Flag-E2 at LDs

Next, 3D dSTORM analysis was performed in order to gain insights into the spatial distribution of core/NS5A and Flag-E2 in close proximity to LDs. Thus only LDs were selected for analysis where both viral proteins were detected. In order to assess LD co-localization, three different patterns were defined and LDs were classified accordingly: 1) core/NS5A and Flag-E2 both surrounding LDs, 2) Flag-E2 next to core/NS5A and core/NS5A surrounding LDs and 3) core/NS5A next to Flag-E2 and Flag-E2 surrounding LDs. Additionally the degree of co-localization between the viral proteins and LDs was scored as complete, partial, and no co-localization. Two evaluators (KR and DE) performed the analysis independently and counted only matching events (Figure 3.48).

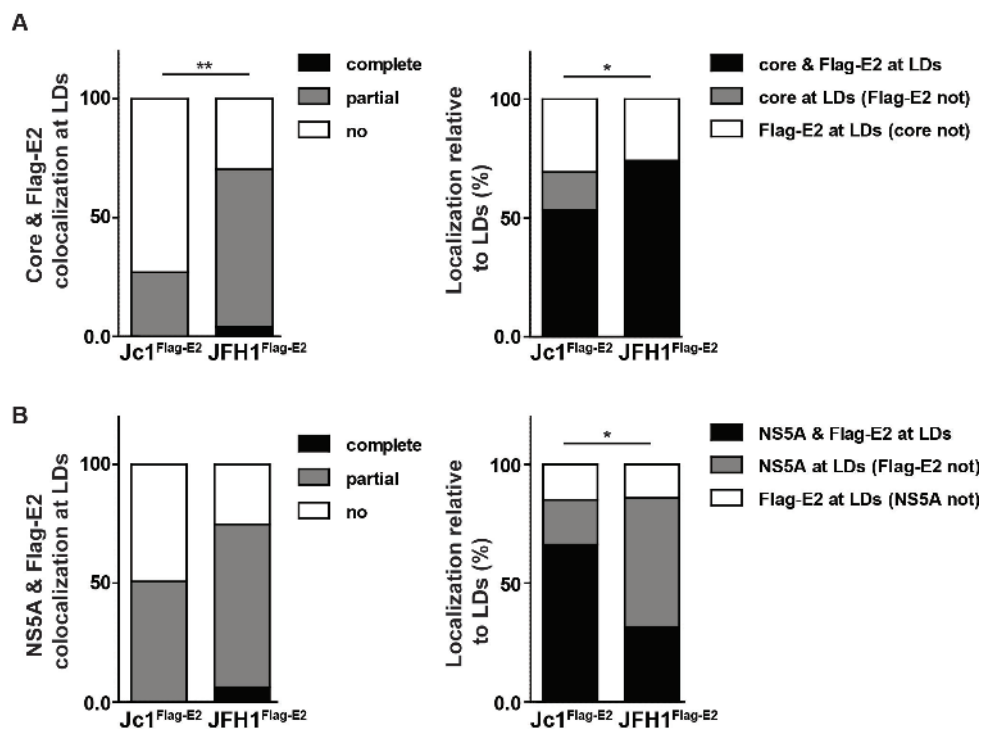


**Figure 3.48.: 3D distribution and co-localization analysis of viral proteins at LDs.** dSTORM datasets were analyzed for the distribution and co-localization of core/NS5A and Flag-E2 at LDs. ROIs were reconstructed in 3D and LDs where core/NS5A and Flag-E2 co-localized in close proximity were analyzed. For reconstruction, three independent experiments of Triton X-100 permeabilized- and one of Saponin treated- cells were used and stained with antibodies detecting core and Flag-E2 (A) or antibodies detecting NS5A and Flag-E2 (B) as well as LipidTox Red neutral lipid stain. In Jc1<sup>Flag-E2</sup>-infected cells 40 LDs and in JFH1<sup>Flag-E2</sup>-infected cells 36 LDs were analyzed. In order to analyze LD co-localization, different criteria were defined; 1) core/NS5A and Flag-E2 both surrounding LDs, 2) Flag-E2 next to core/NS5A and core/NS5A surrounding LDs and 3) core/NS5A next to Flag-E2 and Flag-E2 surrounding LDs. Additionally the degree of co-localization between the viral proteins and LDs was scored as complete, partial, and no co-localization. \* $p < 0.05$ , \*\* $p < 0.01$ .

Analysis of core and Flag-E2 co-localization at LDs showed that most of the viral proteins (~70%) were detectable on opposing sites of LDs. Only 30% of analyzed LDs revealed a partial co-localization of core and Flag-E2 in Jc1<sup>Flag-E2</sup>-infected cells. In JFH1<sup>Flag-E2</sup>-infected cells,

around 4% of analyzed LDs showed a complete co-localization of core and Flag-E2. Approximately 66% exhibited a partial overlap of both viral proteins and only ~30% had no overlap of core and Flag-E2. Additionally, nearly 70–75% of LDs were coated with core in both viral strains, whereas Flag-E2 was present in ~85% of LDs of Jc1<sup>Flag-E2</sup>-infected cells and nearly ~100% in JFH1<sup>Flag-E2</sup>-infected cells, suggesting an enhanced recruitment of Flag-E2 to LDs (Figure 3.48 A). In contrast to core, NS5A showed with ~50% a stronger partial co-localization with Flag-E2 at LDs in Jc1<sup>Flag-E2</sup>-infected cells. In JFH1<sup>Flag-E2</sup>-infected cells approximately 6% of analyzed LDs showed a complete co-localization of NS5A and Flag-E2. Furthermore ~70% of LDs revealed a partial distribution of NS5A and Flag-E2. ~24% of LDs were coated with viral proteins on contrary sites. In addition NS5A occupied more space in areas surrounding LDs with nearly 85% in Jc1<sup>Flag-E2</sup>- and JFH1<sup>Flag-E2</sup>-infected cells resulting in less detected Flag-E2 alone at LDs (Figure 3.48 B).

#### 3.2.6. 3D reconstruction of viral proteins surrounding LDs

Finally, 3D reconstructions of viral proteins in close proximity to LDs were generated by calculating the volumes occupied by core or NS5A together with Flag-E2 and LDs using Imaris software. Shown are examples of 3D reconstructions of areas occupied by core or NS5A, Flag-E2, and LDs in JFH1<sup>Flag-E2</sup>- and Jc1<sup>Flag-E2</sup>-infected cells. The first image stacks were used to do the 3D reconstructions. Then reconstructed volumes of all three channels or volumes of the single viral proteins touching LDs are depicted. LDs are shown in blue, Flag-E2 is shown in red, and core/NS5A is shown in green. The co-localization volumes of both viral proteins at LDs are shown in yellow. In Jc1<sup>Flag-E2</sup>-infected cells core was usually found in distinct spots close to LD volumes. Reconstruction of core and Flag-E2 dSTORM datasets revealed co-localization volumes around or below 100 nm in diameter. In some cases both viral proteins were attached on opposing sites of the LD as already indicated by 2D dSTORM analysis (Figure 3.49). Flag-E2 volumes are more scattered than volumes occupied by core. In JFH1<sup>Flag-E2</sup>-infected cells core accumulated in larger areas surrounding LDs as compared to Jc1<sup>Flag-E2</sup>-infected cells (Figure 3.50). In contrast to core, NS5A showed a more diffuse pattern in Jc1<sup>Flag-E2</sup>-infected cells. As shown before, NS5A and Flag-E2 were also found on opposing sites or partially co-localized at LDs (Figure 3.51). In the analyzed JFH1<sup>Flag-E2</sup>-infected cells, NS5A and Flag-E2 were mostly found on opposing sites of LDs (Figure 3.52).

3.2. Visualization of viral proteins at LDs by super-resolution microscopy (dSTORM)

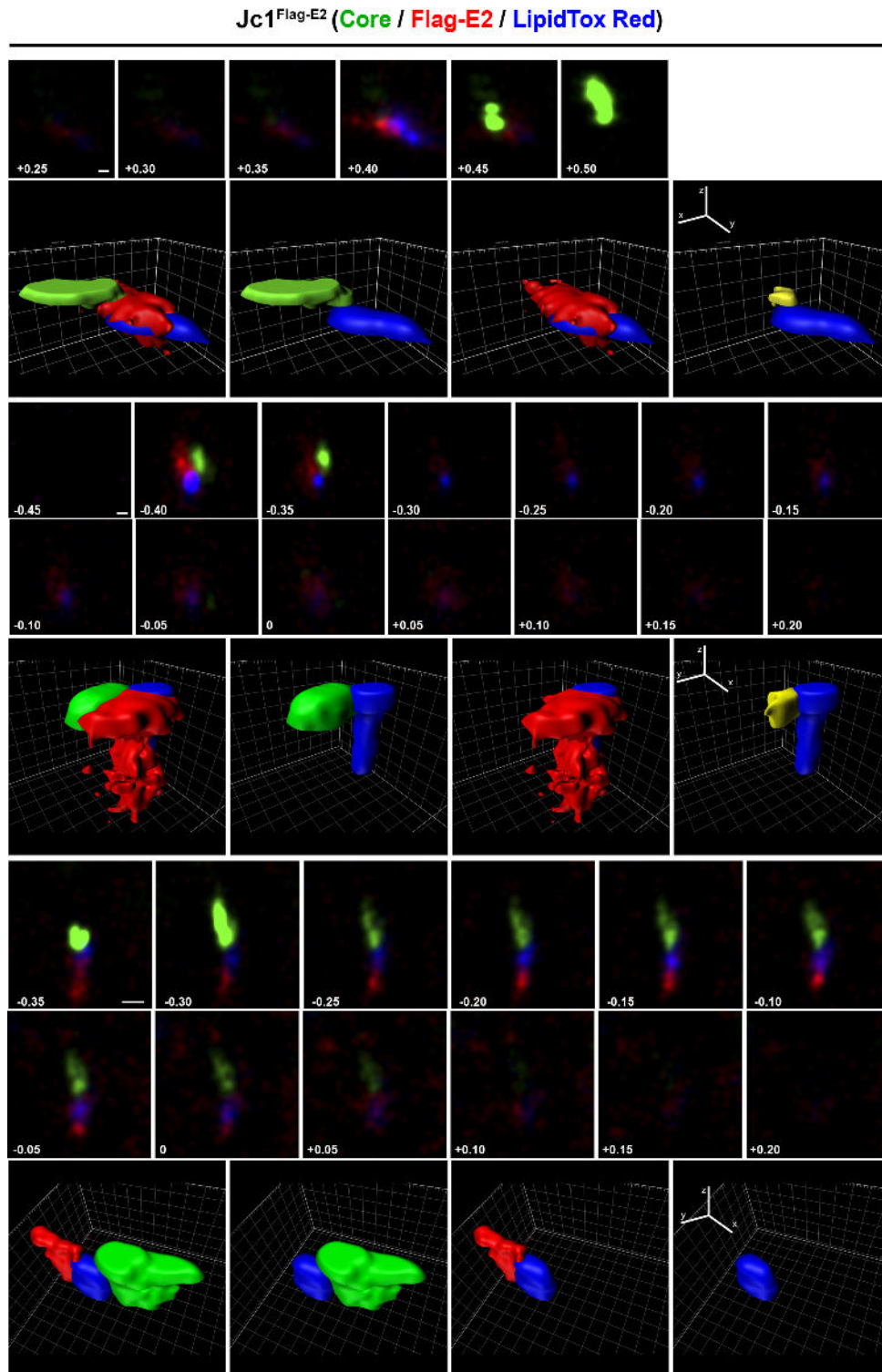


**Figure 3.49.:** 3D reconstruction of core, Flag-E2, and LDs in Jc1<sup>Flag-E2</sup>-infected cells. 3D reconstructions of volumes occupied by core and Flag-E2 attached to LDs in Jc1<sup>Flag-E2</sup>-infected cells. Shown are three examples, first the image stacks used for 3D reconstruction, beneath the 3D reconstruction of all channels, as well as core (shown in green) at the LD (shown in blue) or Flag-E2 (shown in red) at the LD and finally the volume of co-localization between both viral proteins (shown in yellow). Scale bars and ruler hatch marks represent 100 nm. dSTORM analysis was performed by Dennis Eggert.

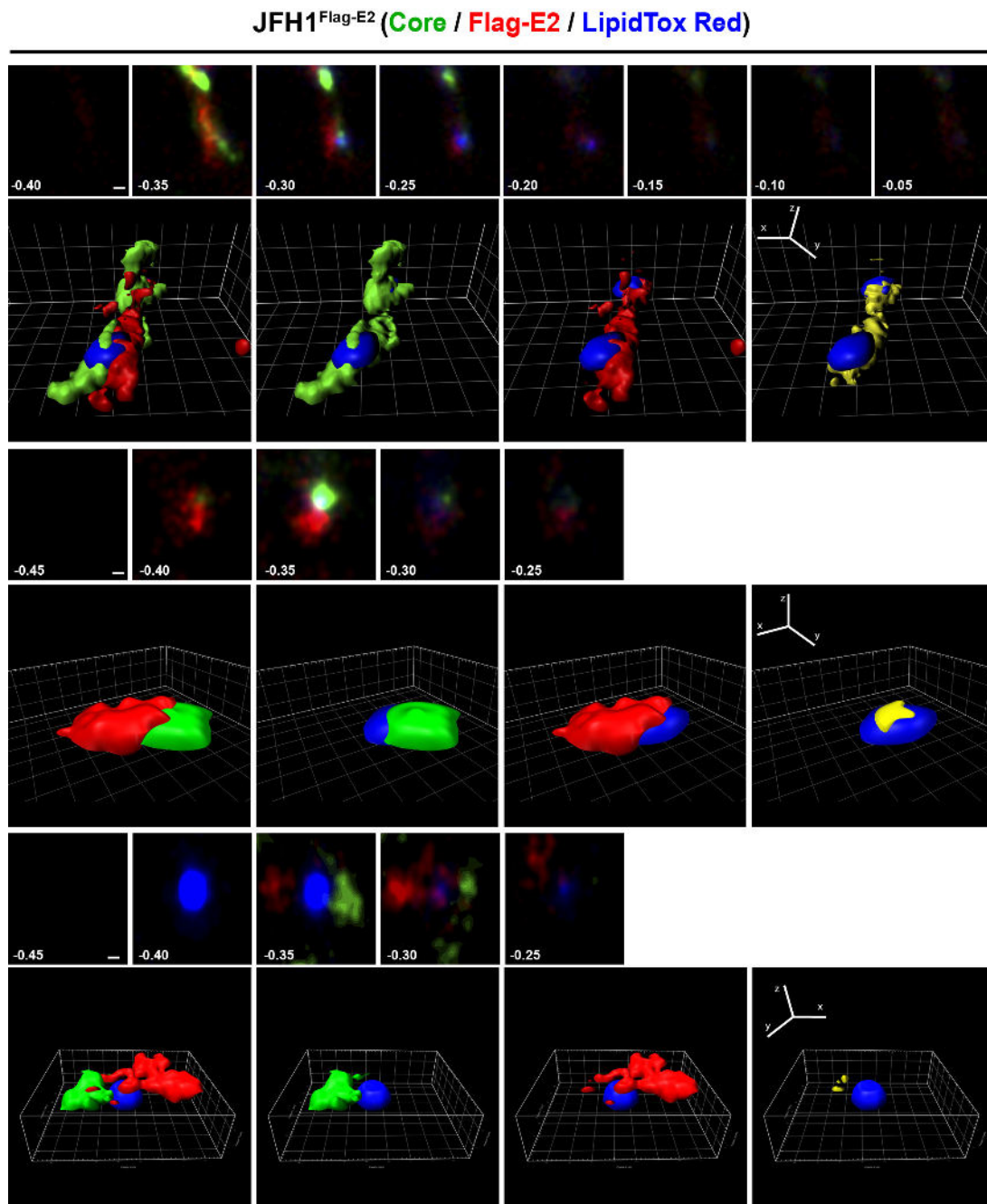


**Figure 3.50.: 3D reconstruction of core, Flag-E2, and LDs in JFH1<sup>Flag-E2</sup>-infected cells.** 3D reconstructions of volumes occupied by core and Flag-E2 attached to LDs in JFH1<sup>Flag-E2</sup>-infected cells. Shown are three examples, first the image stacks used for 3D reconstruction, beneath the 3D reconstruction of all channels, as well as core (shown in green) at the LD (shown in blue) or Flag-E2 (shown in red) at the LD and finally the volume of co-localization between both viral proteins (shown in yellow). Scale bars and ruler hatch marks represent 100 nm. dSTORM analysis was performed by Dennis Eggert.



### 3.2. Visualization of viral proteins at LDs by super-resolution microscopy (dSTORM)

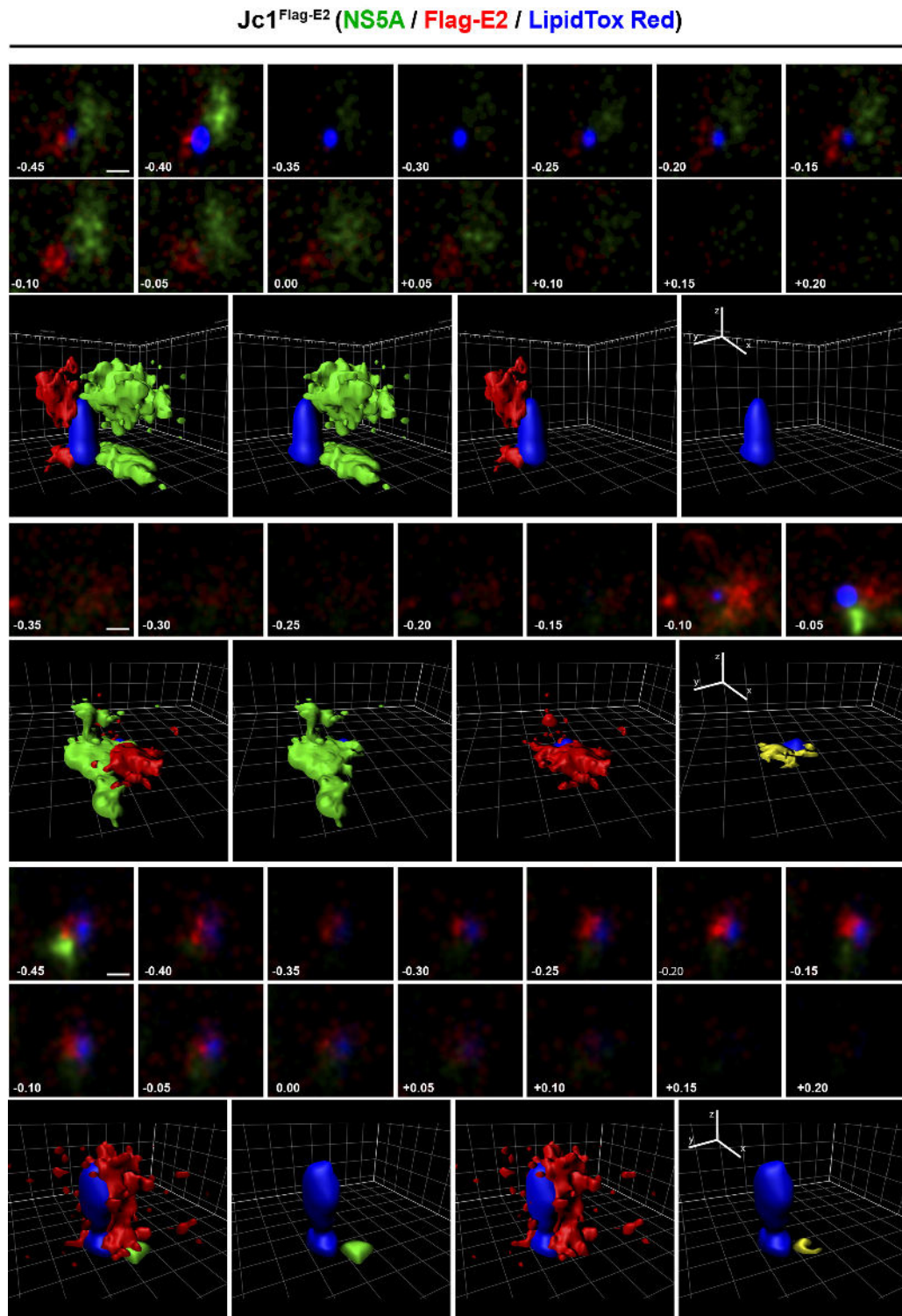


**Figure 3.51.:** 3D reconstruction of NS5A, Flag-E2, and LDs in Jc1<sup>Flag-E2</sup>-infected cells. 3D reconstructions of volumes occupied by NS5A and Flag-E2 attached to LDs in Jc1<sup>Flag-E2</sup>-infected cells. Shown are three examples, first the image stacks used for 3D reconstruction, beneath the 3D reconstruction of all channels, as well as NS5A (shown in green) at the LD (shown in blue) or Flag-E2 (shown in red) at the LD and finally the volume of co-localization between both viral proteins (shown in yellow). Scale bars and ruler hatch marks represent 100 nm. dSTORM analysis was performed by Dennis Eggert.

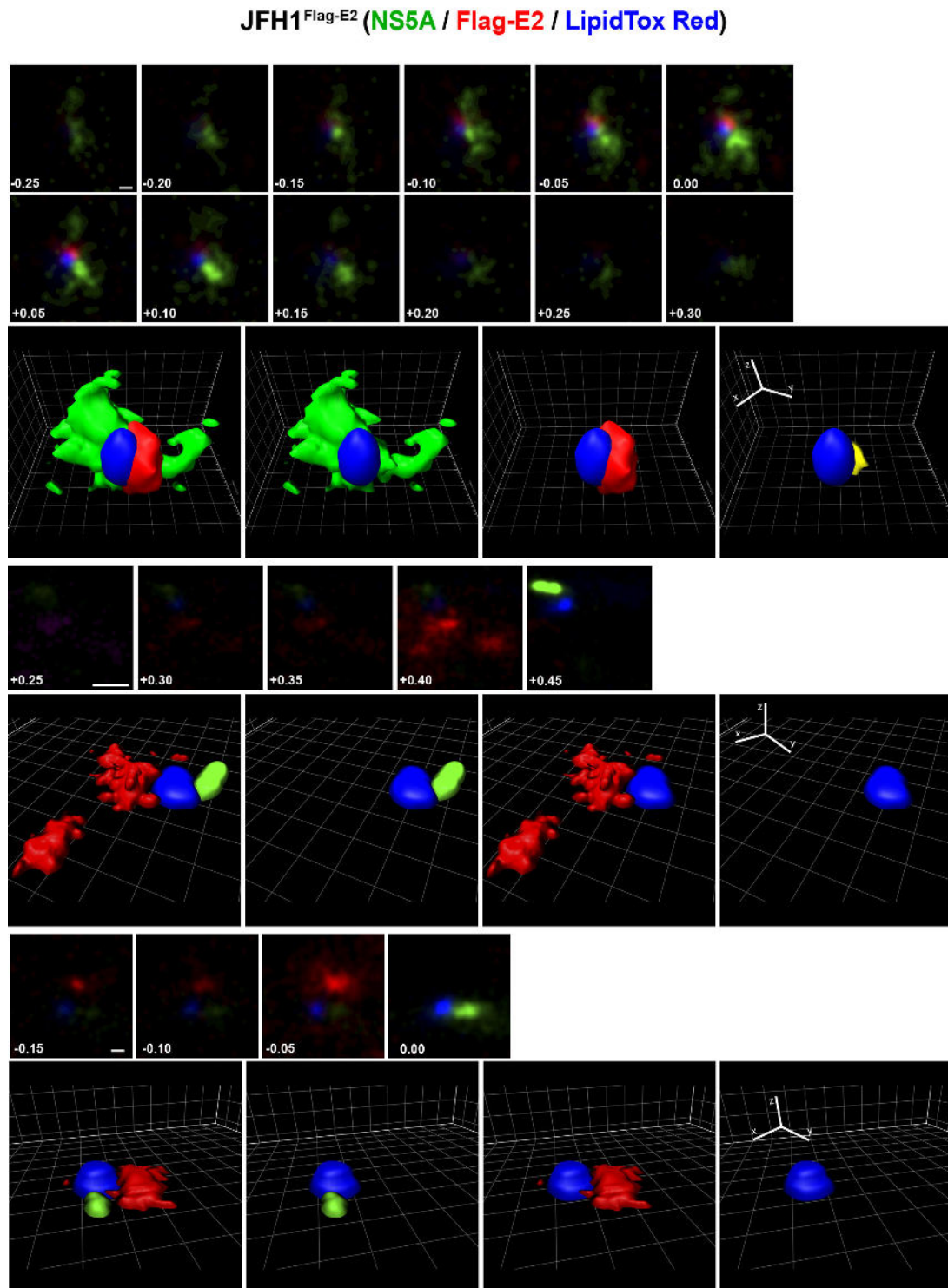


**Figure 3.52.: 3D reconstruction of NS5A, Flag-E2, and LDs in JFH1<sup>Flag-E2</sup>-infected cells.** 3D reconstructions of volumes occupied by NS5A and Flag-E2 attached to LDs in JFH1<sup>Flag-E2</sup>-infected cells. Shown are three examples, first the image stacks used for 3D reconstruction, beneath the 3D reconstruction of all channels, as well as NS5A (shown in green) at the LD (shown in blue) or Flag-E2 (shown in red) at the LD and finally the volume of co-localization between both viral proteins (shown in yellow). Scale bars and ruler hatch marks represent 100 nm. dSTORM analysis was performed by Dennis Eggert.

## 4. Discussion

### 4.1. LD proteome analysis of HCV-infected hepatoma cells

MS-based quantitative proteome analysis has become a powerful approach, used for measuring absolute or relative protein amounts, which is essential for understanding their molecular function and dynamics in biological systems. There are several methods to generate quantitative protein profiles, including 2D gel electrophoresis combined with MS, metabolic labeling (SILAC) or chemical labeling (isobaric tags for relative and absolute quantification (iTRAQ) or tandem mass tag (TMT)) by stable isotopes [Col10, Yan05].

Here, SILAC was used to perform a quantitative proteome analysis of LDs, isolated from HCV-infected and non-infected Huh7.5 cells, to elucidate how HCV changes the expression and/or localization of LD-associated proteins and thereby controls LD functions. Using this approach, 316 proteins were reliably identified as LD-associated. Quantification revealed that 16 proteins were significantly enriched and 21 proteins were significantly depleted from LD fractions of HCV-infected cells. Interestingly, only a few of the significantly enriched proteins were annotated for metabolic processes so far. Most of these proteins are involved in RNA-processing or -binding, thereby illustrating a close spatial proximity of viral RNA replication happening inside the MW and viral assembly occurring at LDs. Numerous proteins identified as highly enriched at LDs of HCV-infected cells have been previously published as HCV host factors (e.g. DEAD box proteins 1 and 3 (DDX1, DDX3) or Insulin-like growth factor-II mRNA-binding protein 1 (IGF2BP1)), indicating the reliability of the SILAC approach. DDX1 binds the 5'UTR as well as the 3'UTR of HCV genomes and silencing of DDX1 leads to a reduction of viral RNA replication [Tin06]. It has been shown that DDX3 binding to core results in enhanced viral RNA replication [Ari07]. Furthermore, interaction of DDX3 with HCV 3'UTR leads to the activation of I $\kappa$ B kinase- $\alpha$  (IKK- $\alpha$ ) and thereby modulates the induction of lipogenic genes, LD formation, enhanced core-LD interaction and promotes viral assembly [Li13]. IGF2BP1 has been reported as HCV host factor, mainly involved in IRES-mediated translation of viral RNA [Wei09]. Furthermore, cathepsin D (CTSD) and Sodium/potassium-transporting ATPase subunit alpha-1 (ATP1A1) were also identified as enriched proteins at LDs of HCV-infected cells. It has recently been shown that both proteins are part of mature HCV virions [Lus16].

Remarkably, proteins that are depleted from HCV-infected LDs are mainly annotated for lipid metabolic functions like biosynthesis of fatty acids, cholesterol and steroids, suggesting that HCV disconnects LDs from their normal metabolic functions to create an environment suitable for viral assembly. This is in line with previous reports showing that expression of core and its localization at LDs reduces the LD triglyceride turnover in NIH/3T3 or Huh7 cells and thereby facilitates LD accumulation [Har11]. Additionally, the expression of core interferes with adipose triglyceride lipase (ATGL), a key enzyme in triglyceride degradation, to inhibit lipolysis of LDs *in vivo* [Cam14]. These observations indicate a functional link between HCV-infections and steatosis, prevalent in 55% of chronically infected patients [ME16].

The phospholipid-binding protein ANXA3 was also significantly enriched in LD fractions of HCV-infected cells. ANXA3 was further studied in detail, as it has not been described as an HCV host factor or LD-associated protein so far. Silencing by RNAi or complete depletion of ANXA3 negatively regulates viral spreading infection, arguing for a pro-viral role of ANXA3 in the HCV life cycle. Viral spreading occurs via cell-to-cell transmission or cell-free transmission. However, it has been shown that cell-to-cell transmission is the more efficient way to promote viral spread *in vivo* and *in vitro* [Mer13]. Several host factors e.g. OCLN, SR-B1, CD81, CLDN1 as well as EGFR and its signal transducer HRas are involved in cell-to-cell transmission, which is also essential for establishing persistence of HCV [Cat13a, Lup11, Xia14]. Knockout of ANXA3 severely impaired viral cell-to-cell transmission, as shown by immunofluorescence analysis of NS5A to determine the size of foci of infection. This effect is likely not due to entry defects as single ANXA3 knockout cell clones had similar expression levels of entry factors involved in cell-to-cell transmission. Additionally, silencing or knockout of ANXA3 had also no effect on cell proliferation, which could also lead to differences in spreading efficiency, suggesting an impact of ANXA3 on cell-to-cell transmission and thereby persistence of HCV.

ANXA3 was recruited to LD-associated membranes in a core- and NS5A-dependent manner. Conversely, no direct interaction between ANXA3 and viral proteins (excluding NS5B, which was not expressed) was observed, indicating an indirect interaction. This might occur via an unknown protein, acting as bridging partner or due to HCV-induced changes of the composition of LDs or LD-associated ER membranes, thus allowing ANXA3 binding. ANXA3 has several known interaction partners, but of these only ANXA4 was also detected in LD fractions. Silencing of ANXA4 resulted in a delay in viral spreading, though it did not block viral spread as efficient as ANXA3 silencing. Of note, knockdown of ANXA4 was not as efficient as of ANXA3, which resulted in a reduction by 65% on mRNA level at day five post transduction. Therefore, ANXA4 might still be expressed at sufficient level to function in HCV-infected cells. Nevertheless, ANXA4 was not enriched in LD fractions of HCV-infected cells, thus arguing against the idea that it might act as bridging partner between ANXA3 and viral proteins.

Recruitment of ANXA3 could also be influenced by HCV-induced changes of the lipid composition of LDs or LD-associated membranes that enable ANXA3 binding. It has already been shown that changes in triglyceride and cholesterol levels in liver tissue of hamsters lead to an increase in ANXA3 protein expression, suggesting that alterations in TG and/or cholesterol levels might modify ANXA3 protein expression [Lia15]. Interestingly, expression of core (genotype 3a) increased the cholesterol ester content in LDs of Huh7 cells, indicating that HCV changes the lipid composition of LDs in infected cells [LM14]. Alternatively, ANXA3 might also be recruited to LDs by a calcium efflux from the ER to LD-associated membranes. NS5A as well as core are capable of inducing ER-stress. As a consequence,  $\text{Ca}^{2+}$  is released from the ER which might trigger ANXA3 binding [Gon01, BF05]. Besides ANXA3 and ANXA4, ANXA2 and ANXA5 were also identified in LD-fractions. But contrary to ANXA3, they were not regulated. Interestingly, ANXA2 has already been published as HCV host factor, facilitating HCV RNA replication or viral assembly [Sax12, Bac10]. In contrast to these studies, no effect on viral replication was observed for ANXA2 silencing, which is in line with data published by Dreux *et al.*, showing that exosomal viral RNA transfer depends on ANXA2 while viral replication works independently of ANXA2 [Dre12]. The discrepancies may partly be based on differences in the experimental approaches: Backes *et al.*, used Huh7 and Lunet cells, whereas Huh 7.5 cells were used in this study. ANXA3 might have a compensatory effect to ANXA2 silencing and as endogenous ANXA3 protein expression is much lower in Huh7 and Lunet cells than in Huh7.5 cells, this might affect different results in these cell lines. Furthermore, most of the work published by Saxena *et al.* was



done with replicon cells. In experiments where full length HCV constructs were used, cells were harvested at early time points post infection and only a slight decrease in viral protein expression in the absence of ANXA2 was observed. Here, effects of ANXA2 silencing on viral spreading were analyzed with a full length viral construct at day 2 to day 6 post infection. Taken together the diverse effects caused by ANXA2 silencing might be due to differences in cell lines, HCV constructs and time points.

Characterization of ANXA3 silencing showed that it had no effect on viral entry, RNA replication, or core envelopment, but particles released from ANXA3 knockdown cells showed a higher density accompanied by a lower specific infectivity. These findings suggest that ANXA3 acts as host factor for late steps of viral assembly or during the maturation of nascent viral particles (Figure 4.1 A). Viral assembly starts at cytosolic LDs, to which all components needed for HCV progeny production are recruited. Recent data revealed that ApoE interacts with NS5A within RCs, thereby ApoE might be transferred to core-coated LDs to get included in the viral assembly process [Cun10, Ben10]. Disruption of the interaction between NS5A and ApoE leads to severe defects in HCV replication. However, if this interaction occurs on the cytosolic side of the ER (where NS5A is located) or within the ER lumen (where ApoE is located) is not known and the topological problem has not been solved yet. Assembly is then thought to be initiated by the NS5A-mediated interaction of viral RNA with core, thereby triggering the formation of viral capsids. Then, viral RNA is encapsidated and the capsid buds into the ER lumen acquiring an envelope with viral glycoproteins. Lipoproteins and lipids associate with immature viral particles either during budding or egress. Co-immunoprecipitation experiments were performed to gain insight where ANXA3 functions are needed during this process. First, ANXA3 knockdown cells were transfected with Jc1<sup>NS5A-HA</sup> RNA. NS5A was captured by HA-specific immunoprecipitation and analyzed for its interaction with endogenous ApoE. An ANXA3-independent interaction of HA-tagged NS5A with endogenous ApoE was observed, indicating that ANXA3 acts either on the cytosolic side of the ER but after the interaction between ApoE and NS5A, or on the luminal side of the ER. Annexins are mainly located in the cytosol [Ger02]. However, it has been shown that ANXA3 can be measured in sera of HCC patients as well as in supernatant of different cell lines, confirming that ANXA3 can be secreted, but the mechanism of ANXA3 secretion is still unknown [Ton15].

Inside the ER lumen, viral particles bind to ApoE (and in non-hepatoma cells ApoB), which influences their density as well as infectivity [Mer11]. Silencing of ANXA3 impaired secretion of ApoE in HCV-replicating cells. The effect observed on ApoB secretion was inconsistent (replicon vs infected cells) and correlated mostly with expression levels. In contrast, no effect on ApoB and ApoE secretion was observed in non-infected cells, arguing for a specific role of ANXA3 in the secretion of ApoE in HCV-infected cells. It also implicates that HCV secretion via the VLDL pathway somehow differs from the VLDL secretion pathway in naïve cells, where ANXA3 is not needed. However, no effect on lipidation of total ApoE was observed, as the density of secreted ApoE containing particles (analyzed by density gradient centrifugation followed by ELISA) was similar in HCV-infected cells expressing or not expressing ANXA3. In addition, no differences in MTP activity were observed (important for transferring lipids to ApoB and ApoE or the generation of luminal LDs). Admittedly, due to similar biophysical properties of LVPs and VLDLs, the experimental approach did not answer if LVPs produced in the absence of ANXA3 are less associated with ApoE or ApoB, if detectable. Catanese *et al.* showed that HCV particles incorporate different amounts of several lipoprotein species; thus, less lipoprotein association of LVPs might contribute to the HCV particle phenotype observed in the absence of ANXA3 [Cat13b]. Perturbation of the lipoprotein secretion by ANXA3 silencing in HCV-

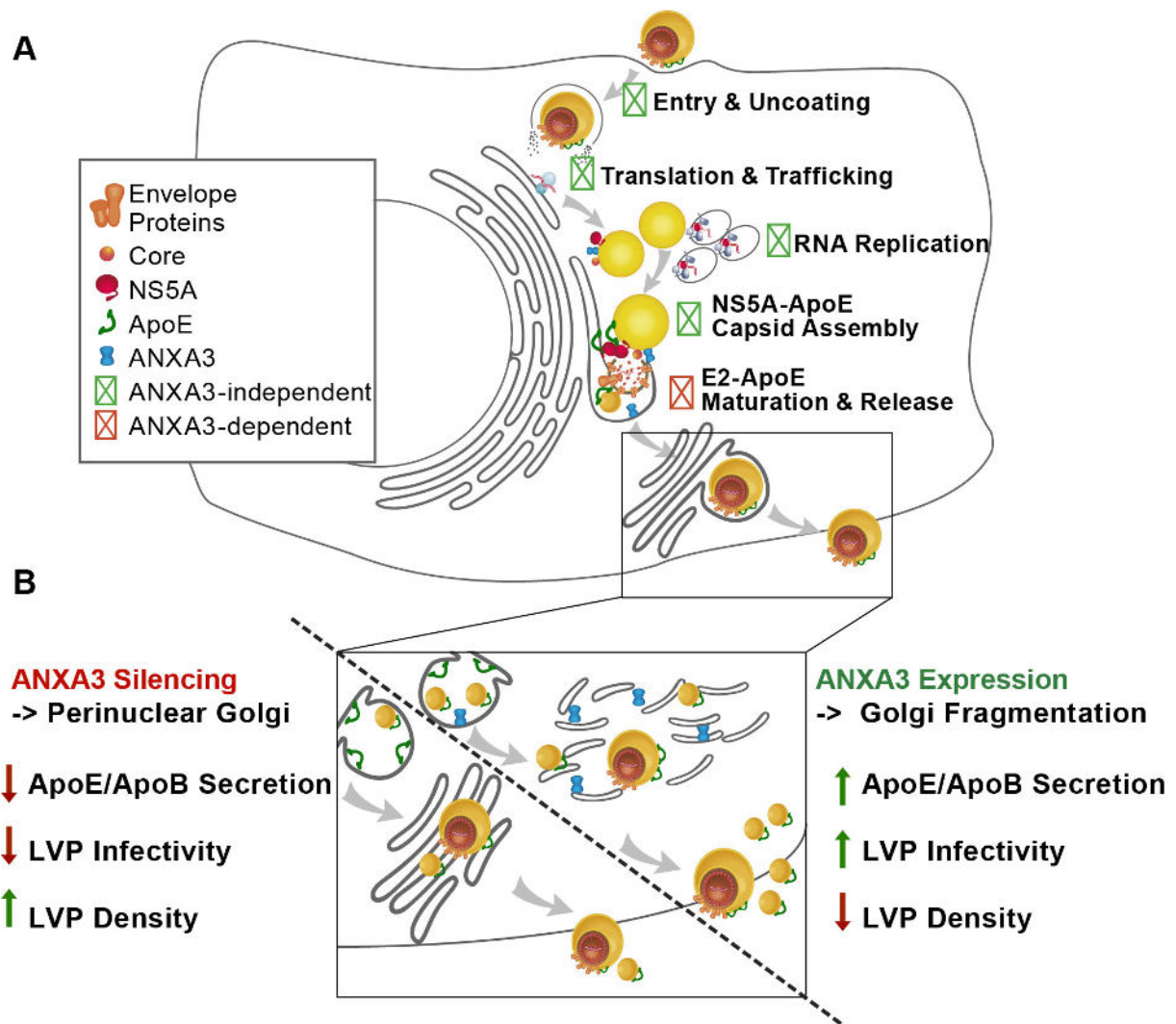


**Figure 4.1.: ANXA3 impacts maturation of nascent viral particles.** A) Silencing of ANXA3 had no impact on viral entry, translation of viral genomes, viral RNA replication and initiation of viral assembly. B) HCV core and NS5A recruit ANXA3 to LD-associated membranes to facilitate the late steps of viral assembly and/or maturation. ANXA3 expression supports disruption of the Golgi network in HCV-infected cells. Thereby ANXA3 facilitates the secretion of lipoproteins and might contribute to the incorporation of ApoE in LVPs.

infected cells might lead to inefficient lipoprotein incorporation into LVPs. This is in line with the observation that ANXA3 silencing results rather in a slight decrease than in an accumulation of intracellular infectious viral particles. Previous reports suggest that immature LVPs are targeted to degradation if they fail to undergo proper maturation within the ER [Lee14, Gas08]. Therefore, the lipoprotein association might function as a quality control, as only LVPs containing adequate lipoprotein amounts are secreted.

Immunofluorescence analysis was performed to further analyze the mechanism of how ANXA3 influences viral particle maturation. Control cells showed co-localization between ApoE and Flag-E2 as well as Flag-E2 and core in HCV-infected cells. Additionally, co-immunoprecipitation of Flag-E2 confirmed an interaction between Flag-E2 and ApoE or core. However, none of these interactions were observed in the absence of ANXA3, indicating that on one side, ANXA3 silencing impaired the interaction and co-localization between core and Flag-E2. It has already been shown that core traffics to LDs, forming a cap on the surface where co-localization of core and E2 can be observed, suggesting that these are viral assembly sites [Cou11]. As this co-localization/interaction was reduced in the absence of ANXA3, it is feasible that ANXA3 silencing causes a defect in late viral assembly steps and incorporation of the glycoproteins into the envelope. On the other side, ANXA3 expression directly influenced the subcellular localization of ApoE in HCV-infected cells even though no direct interaction between endogenous ApoE and ANXA3-HA was observed. Changes in the subcellular localization of ApoE might also be responsible for an abolished interaction between ApoE and Flag-E2 in the absence of ANXA3. Previous reports showed that ApoE mainly interacts with E2 on the luminal side of the ER or in the Golgi apparatus [Lee14]. Consequently, Golgi morphology in ANXA3 knockdown cells was analyzed in more detail.

In general the Golgi apparatus is localized in the perinuclear region of the cell, composed of flat membrane stacks (cisternae) associated with vesicles. Laterally, these cisternae are connected by tubules, establishing a ribbon-like network [Pol04]. It mainly acts in the sorting and transport of proteins or lipids within the cell. Furthermore, post-translational modifications (e.g. glycosylation, sulfation or proteolytic cleavage) of proteins and lipids are triggered within the Golgi apparatus. Several findings directly connect Golgi functions with HCV replication; E2 is highly glycosylated during particle maturation [Vie10]. Treatment with Brefeldin A, an inhibitor of the ER-Golgi transport, leads to intracellular accumulation of HCV particles [Gas08]. Additionally, immunofluorescence analysis of the Golgi marker GM130 revealed a disperse distribution in HCV-infected cells, indicating an important role of the Golgi network to promote HCV secretion [Ama11, Bis12]. Co-localization of ApoE with Flag-E2 and GM130 was analyzed in the absence or presence of ANXA3. Consistent with previous reports, the majority of Jc1<sup>Flag-E2</sup>-infected control cells showed a scattered GM130 staining. In contrast, naïve control cells revealed a perinuclear Golgi morphology, indicating an HCV-induced fragmentation of the Golgi apparatus. Silencing of ANXA3 prevented Golgi fragmentation in most of the HCV-infected cells. In addition naïve ANXA3 knockdown cells showed also a normal Golgi phenotype, suggesting that ANXA3 might influence the Golgi morphology in HCV-infected cells. However, no intracellular accumulation of HCV virions was detectable in ANXA3 silencing cells, indicating that ANXA3 contributes to a Golgi fragmentation that is needed for viral particle morphogenesis or assembly and not for particle secretion. Interestingly, the Golgi morphology directly impacted the subcellular localization of ApoE. In non-infected cells ApoE mainly remained in the perinuclear Golgi compartment and also in HCV-infected ANXA3-knockdown cells, indicating that the subcellular localization of ApoE might be attributed to the Golgi morphology. Thereby, Golgi disruption might affect ApoE secretion in HCV-infected cells or the association of ApoE with nascent viral

particles (Figure 4.1 B).

Golgi fragmentation can be observed during normal cellular processes, e.g. during mitosis to facilitate equal distribution of the Golgi apparatus to daughter cells or during pathological conditions, e.g. in neurons of patients suffering from Amyotrophic Lateral Sclerosis [Sun15]. Furthermore, diverse viruses utilize Golgi fragmentation to facilitate viral replication; Human rhinovirus 1A induces Golgi fragmentation to generate vesicles suitable for viral RNA replication. For this purpose, the expression of the viral 3A protein is sufficient to hijack Golgi membranes. However, mechanistically details are still missing [Qui10]. Rhinovirus 16, another human rhinovirus subtype, also induces disruption of the Golgi apparatus. Interestingly, expression of the single viral proteins 3A, 3B and 2B caused Golgi fragmentation resulting in a decrease in protein secretion. However, infection of cells with rhinovirus 16 particles also disrupts the Golgi apparatus, but does not inhibit protein secretion, suggesting that these phenomena are independent from each other [Mou14]. This is in line with work published by Beske *et al.*, showing that Golgi fragmentation and protein secretion are independent events during a poliovirus infection [Bes07]. During pathological conditions, Golgi fragmentation can be initiated when apoptosis is activated e.g. by the caspase-mediated cleavage of structural Golgi proteins. Interestingly, Golgi fragmentation can be caused by inhibition of phosphatidylinositol 4,5-bisphosphate (PI(4,5)P<sub>2</sub>) or phosphatidic acid (PA) synthesis (shown in rat livers). Inhibition of cPLA<sub>2</sub> also effects Golgi fragmentation, implicating a connection between phospholipid biology and Golgi morphology [Cho00, Swe02]. Intriguingly, NS5A has been found to interact with PI(4,5)P<sub>2</sub> via a specific Basic Amino Acid PI(4,5)P<sub>2</sub> Princer (BAAPP) binding domain within its N-terminal amphipathic helix. Moreover, such a BAAPP domain was also identified in NS4B as well as ApoB. Furthermore, cPLA<sub>2</sub> interacts with NS4B to contribute to the formation of the MW, HCV replication as well as assembly [Xu12]. All this data might suggest a possible link between Golgi morphology and HCV [Cho15]. However, how HCV causes Golgi fragmentation and if ANXA3 itself or viral proteins induce Golgi fragmentation is still elusive. How HCV egress benefits from Golgi disruption also remains to be characterized.

### 4.1.1. Future aspects regarding the functional role of ANXA3 in the HCV life cycle

With respect to elucidate the functional role of ANXA3 during HCV assembly, one key step would be the identification of ANXA3 interaction partners. Tandem affinity purification (TAP) combined with MS has already been used to efficiently identify protein complexes from bacteria, mammalian cells or yeast [Gul03, Bra04, Rig99]. Capturing ANXA3 from HCV-infected cells by co-immunoprecipitation followed by MS analysis would be a powerful approach to identify novel ANXA3 interaction partners. Compared to common co-immunoprecipitations, TAP utilizes two purification steps resulting in a major improvement in the reduction of non-specific protein binding. However, depending on the size and position, TAP-tag insertion might severely affect target protein folding, activity or interaction. Usage of small TAP-tags (e.g. Flag-2xHA or 3xFlag-His both 3 kDa in size) might be suitable to overcome this limitation [Li11]. However, weak or transient interactions might be lost and also solubility of the bait protein can interfere with the experimental approach. The recently described BioID technology relies on proximity dependent labeling of proteins in a living cell. This technique is based on a biotin protein ligase (isolated from *Escherichia coli*) fused to a target protein (e.g. ANXA3). After transfection, the biotin protein ligase biotinylates proteins in close proximity to the target protein [Rou12]. Then, proteins carrying biotin can be isolated and identified by MS. Using this technique, 50%

of identified proteins reside within a 20–30 nm radius of a fusion protein, indicating possible interaction partners. Applying BioID would enable analyzing ANXA3 protein complexes in a native state.

Future investigations that evaluate ANXA3 interaction partners in HCV-infected cells may also help to understand how core/NS5A-induced recruitment of ANXA3 to LD-associated membranes occurs. Further, analysis of ANXA3 expression in LD fractions of cells fed with different fatty acids would be a feasible method to clarify if ANXA3 recruitment is initiated directly by viral proteins or arises as a consequence of HCV-induced changes of the lipid composition.

Due to the lack of suitable antibodies, visualization of endogenous ANXA3 by immunofluorescence analysis was not successful so far. However, the CRISPR/Cas9 system does not only allow depletion of genes but also the insertion of tags in genes. Therefore, cells are transfected with Cas9, a sgRNA targeting the gene of interest (e.g. ANXA3) and a generic donor plasmid containing the tag in-between two identical Cas9 cleavage sites (e.g. the cytotoxic granule-associated RNA binding protein 1, like (*tia11*) gene from zebrafish). Additionally, the donor plasmid contains a sgRNA targeting the *tia11* cleavage sites. After transfection, the tag will be released and integrated by Cas9 at a site specified by the sgRNA. This strategy has already been used to generate cell lines expressing endogenous proteins tagged with GFP or luciferase [Lac15]. Using this experimental approach, endogenous ANXA3 could be labeled by several tags allowing immunofluorescence analysis or live cell imaging (e.g. by tetracycline based protein detection). The incorporation of tetracycline tags could also be used to perform correlative EM analysis or tracing ANXA3 translocation in HCV infected cells by live cell imaging. Moreover, insertion of Flag or HA-tags could also be beneficial for co-immunoprecipitation experiments.

Here, it has been shown that overexpression of ANXA3 leads to a massive increase in ANXA3 protein expression that was not well tolerated by Huh7.5 cells. In these overexpression constructs, ANXA3-HA was cloned under the control of the elongation factor 1 alpha (EF1a) promoter, leading to a strong expression in transfected cells. To express ANXA3 on more physiological levels, ANXA3 could be cloned under the control of weaker promoters. Furthermore, it has been shown that ANXA3 can be secreted (maybe via exosomes) and internalized by caveolin 1 mediated endocytosis [Ton15]. Therefore, conditioned media from ANXA-HA overexpressing cells could be used to transfer ANXA-HA to Huh7.5 cell in more physiological levels.

ANXA3 contributes to an HCV-induced Golgi fragmentation, which might be beneficial for viral maturation. Further immunofluorescence analysis of markers detecting distinct Golgi regions could clarify if silencing of ANXA3 prevents fragmentation of individual areas or the entire Golgi apparatus in HCV-infected cells. Here, a GM130 specific antibody was used to characterize Golgi morphology. GM130 represents a marker of the *cis*-Golgi compartment, which displays the entrance site of the Golgi apparatus, connecting the ER with the Golgi stack. The *trans*-Golgi network (TGN) represents the exit site of the Golgi apparatus, functioning as major protein sorting site [Klu11]. Antibodies detecting TGN marker proteins (e.g. TGN46) might help to describe the entire Golgi architecture in HCV-infected cells and might help to understand how ANXA3 silencing contributes to Golgi morphology.

To further analyze structural differences of the Golgi apparatus in HCV-infected control or ANXA3 silencing cells, serial EM sectioning combined with 3D reconstructions could be performed. Furthermore, combining serial sectioning with 3D electron tomography analysis could be used to further resolve the Golgi architecture in these cells. Additionally, isolation of the Golgi apparatus followed by protein expression analysis might reveal if ANXA3 acts as a structural Golgi protein. Moreover, analysis of resident Golgi proteins might reveal if the Golgi fragments are still functional units in the absence or presence of ANXA3.

Additionally, HCV particles could be analyzed by immunolabeling combined with EM to characterize HCV particles released from ANXA3 knockdown cells. Here, ANXA3 knockdown or control cells could be transfected with Jc1<sup>Flag-E2</sup> RNA, thus allowing purification of Flag-tagged virions from the supernatant of these cells. After purification and fixation, viral particles could be stained with antibodies detecting virion-associated lipoproteins and further processed for EM. This experimental approach might reveal if ANXA3 silencing influences lipoprotein association of HCV particles.

### 4.2. dSTORM analysis of viral protein expression at LDs

Multicolor imaging is one major advantage of fluorescence microscopy and has been widely used for co-localization analysis to map interactions of diverse biological structures. However, the precision of co-localization analysis is limited by the resolution of the image. Taking advantages of its high resolution, dSTORM can be used to overcome this limitation [Bat07]. Dual-color dSTORM has already been used successfully to validate the viral protein distribution during the life cycle of HIV1 [Per12]. Here, three-color dSTORM was employed to analyze the spatial localization of core or NS5A with the viral envelope protein E2 at LDs of HCV-infected cells. For this purpose, two viral strains (JFH1<sup>Flag-E2</sup> and Jc1<sup>Flag-E2</sup>), carrying a Flag insertion at the N-terminal part of E2, were generated, thus allowing detection of E2 by Flag-specific antibodies. The Flag-tag insertion was confirmed by co-immunofluorescence analysis of Flag and E2. Characterization of the modified viral strains revealed that the Flag-E2 insertion had no effect on viral infectivity or the subcellular localization of Flag-E2, as it has already been shown by Prentoe *et al.* [Pre11]. Therefore, Flag-tag insertion into E2 can be used as a valuable tool for different approaches, e.g. particle purification, co-immunoprecipitation or immunofluorescence analysis.

For immunofluorescence co-localization analysis, the method used for fixation and permeabilization can be crucial [Ohs05]. Therefore, permeabilization of Jc1<sup>Flag-E2</sup>- and JFH1<sup>Flag-E2</sup>-infected cells with Triton X-100 and Saponin was compared to visualize Flag together with E2. In HCV-infected cells, E2 was often found in dot-like and reticular structures within the ER, most likely representing viral assembly sites [Cou11, Zay16]. As expected, co-localization was observed in Triton X-100- and Saponin-treated cells. However, signal intensities and co-localization coefficients were much stronger in Triton X-100 permeabilized cells. Moreover, dot-like structures of E2 were also more prevalent in Triton X-100 treated cells, suggesting that Saponin permeabilized intracellular membranes less efficient than Triton X-100. Since treatment with Triton X-100 can lead to solubilization of LD-associated proteins, as it has been shown for PLIN2/ADRP [Ohs05], both permeabilization methods were used for super resolution microscopy.

Fluorophores used in dSTORM have to be photo-switchable. To visualize LDs, different lipophilic dyes were tested for their ability to blink. The yellow absorbing LipidTox Red fluorophores showed the strongest spontaneous activation rate from the dark to the fluorescent state. Additionally, correlation of widefield images with corresponding dSTORM images as well as co-localization with PLIN2/ADRP confirmed that LipidTox Red specifically stained LDs. These data indicate that LipidTox Red is suitable to visualize LDs by dSTORM. For the imaging of viral proteins, a blue-absorbing Alexa 488 and a red-absorbing Alexa 647 dye were used. Both are published as photo-switchable dyes and the combination of these dyes fits for multi-color dSTORM, because due to the distinct spectral ranges of all three dyes, no cross-talk between the

different channels was expected [Dem11]. LDs generally became visible as round or oval shaped structures by dSTORM. In general, only small LDs (0.2–0.5  $\mu\text{m}$  in diameter) were visualized with this approach. A phenomenon attributed to the thickness of the sample, which can be illuminated in dSTORM (1–2  $\mu\text{m}$ ). However, this did not limit the benefit from dSTORM, as core and E2 preferentially co-localize adjacent to small LDs, which might reflect recruitment of core from LDs to nascent viral particles [Cou11].

Then, the cellular spatial distribution of Flag-E2 together with core or NS5A at LDs was analyzed. Therefore, Lunet cells were infected with the Flag-tagged partially cell culture-adapted viral strain Jc1<sup>Flag-E2</sup> or the parental isolate JFH1<sup>Flag-E2</sup>. It has been proposed, that a single amino acid residue in the LD-binding domain (D2) of Jc1 core mediates the more efficient assembly and release of infectious virions [Sha07]. As such, differences in the assembly efficiency of these viral strains might lead to differences in the spatial distribution of Flag-E2 and core/NS5A at LDs. To answer this hypothesis, four independent experiments with cells permeabilized with Triton X-100 or Saponin were analyzed and 3D reconstructions of the viral protein distributions at LDs were performed. Similar co-localization events and staining patterns were observed in cells treated with Triton X-100 or Saponin, indicating that the permeabilization method did not influence the spatial distribution of the viral proteins. Compared to JFH1<sup>Flag-E2</sup>, a slight increase in Flag-E2 co-localizing with LDs was observed in Jc1<sup>Flag-E2</sup>-infected cells, indicating a more efficient recruitment of Flag-E2 to viral assembly sites. Moreover, LDs analyzed in Jc1<sup>Flag-E2</sup>-infected cells showed a slight increase in the co-localization with NS5A, suggesting that NS5A might also be recruited more efficiently to LDs in the cell culture adapted viral strain than in the parental viral strain. Co-localization analysis of core did not reveal any significant differences between Jc1<sup>Flag-E2</sup> and JFH1<sup>Flag-E2</sup>. However, due to the high resolution in dSTORM, co-localization events were quite rare as compared to CLSM analysis [Flo13].

To analyze in greater detail the spatial distribution of viral proteins at single LDs, ROIs were selected, where both viral proteins are in close proximity to LDs. Co-localization events were also quite rare in these ROIs, as already observed in the cellular distribution analysis. The co-localization of Flag-E2 and core at LDs was much lower in Jc1<sup>Flag-E2</sup>- than in JFH1<sup>Flag-E2</sup>-infected cells. On one hand, this might suggest a low number of assembly events in Jc1<sup>Flag-E2</sup>-infected cells. On the other hand, this might confirm a defect in viral assembly leading to the accumulation of core at LDs in JFH1<sup>Flag-E2</sup>-infected cells. Furthermore, it is possible that nascent virions are transported away from LDs in Jc1<sup>Flag-E2</sup>-infected cells, as it has been shown that core is recruited from LDs into motile puncta, most likely representing transport vesicles containing viral particles [Cou11]. Recruitment of E2 to core-containing LDs is affected by proper NS5A function. Additionally, NS5A recruits viral RNA to viral assembly sites by facilitating the interaction of core with the viral RNA. Surprisingly, the interaction of core with viral RNA is also significantly reduced (by 80%) in  $\Delta\text{E1}/\text{E2}$  viral strains, suggesting that capsid formation and envelopment are coupled and that NS5A might act as key player in the coordination of these processes [Zay16]. Therefore, the co-localization of NS5A and Flag-E2 was also analyzed at LDs in Jc1<sup>Flag-E2</sup>- and JFH1<sup>Flag-E2</sup>-infected cells. Nearly 50% of the analyzed LDs showed a partial co-localization of NS5A and Flag-E2, indicating that, compared to core, more space was occupied by NS5A in Jc1<sup>Flag-E2</sup>-infected cells. This might reflect a close connection between viral replication complexes located in the ER-derived MW, and viral assembly at LDs. Additionally, 3D reconstructions of co-localization events revealed that these areas are generally small ( $\sim 100$  nm in diameter). However, no specific distribution pattern was resolved within these small volumes, attributed to the limit in resolution. Furthermore, co-localization events were quite rare, which restricted a quantification of the protein distribution within these areas across different LDs.

### 4.2.1. Future perspectives regarding dSTORM analysis of HCV assembly

dSTORM offers the opportunity to illustrate viral assembly events through a nanoscopic window, thereby providing new insights into this process. Especially in combination with correlative EM or TEM, dSTORM might be a useful tool to identify budding events of nascent viral particles from LDs into the ER. Furthermore, combining RNA labeling techniques (e.g. by fluorescence *in situ* hybridization (FISH) to visualize viral RNA genomes) with labeling of core or Flag-E2 proteins might also contribute to illuminate the viral assembly process. However, antibody-based labeling needs permeabilization of the cell, making the antigen of interest accessible for the antibody. But permeabilization might cause artifacts, as strong permeabilization reagents tend to disturb membrane organization. Additionally, antibodies itself might also cause side effects as they are large (~150 kDa) plasma proteins with a length of 10–15 nm. Therefore, in indirect immunofluorescence the combination of two antibodies might shift the localization of the fluorescence molecule up to 30 nm away from the antigen and the antibody size might also influence the spatial accessibility of the antigen. Thereby permeabilization and usage of antibodies might impact the spatial resolution in dSTORM. It has already been shown, that usage of direct dye-conjugated primary antibodies or direct dye-conjugated Fab fragments are suitable tools to visualize viral particles in dSTORM (e.g. herpes simplex virus 1) and contribute to more precise spatial localization analysis than labeling with primary and secondary antibodies [Lai15]. Furthermore, generation of viral proteins expressing fluorescence proteins (e.g. eGFP) might be another approach to bypass artifacts due to permeabilization or antibody labeling.

## 4.3. Conclusion

The presented thesis illustrates that a quantitative proteome analysis and advanced microscopy can help deciphering molecular mechanisms of virus replication. In summary, HCV profoundly changes the LD proteome and disconnects LDs from their metabolic functions to create an environment facilitating viral replication. Here, several putative HCV host factors have been identified. One of these, ANXA3, was studied in more detail, and discovered to act as novel HCV host factor for late steps of the viral life cycle. ANXA3 facilitates the incorporation of lipoproteins and thereby critically affects HCV assembly and maturation. Thus this study opens new directions to understand in molecular detail virus-host interactions during HCV particle formation.



## 5. Material

### 5.1. Bacteria strains

| Name                       | Genotype   | Company                            |
|----------------------------|--|------------------------------------|
| DH5 $\alpha$ <sup>TM</sup> | F- $\Phi$ 80 <i>lacZ</i> $\Delta$ M15 $\Delta$ ( <i>lacZYA-argF</i> ) U169 <i>recA1 endA1 hsdR17</i> ( $r_k^-$ , $m_k^+$ ) <i>phoA supE44 thi-1 gyrA96 relA1</i> $\lambda^-$ | ThermoFisher Bioscience, Darmstadt |
| Stbl2 <sup>TM</sup>        | F- <i>mcrA</i> $\Delta$ ( <i>mcrBC-hsdRMS-mrr</i> ) <i>recA1 endA1lon gyrA96 thi supE44 relA1</i> $\lambda^-$ $\Delta$ ( <i>lac-proAB</i> )                                  | ThermoFisher Bioscience, Darmstadt |

### 5.2. Eukaryotic cell lines

HEK293T cells were obtained from the American Type Culture Collection, Huh7 and Lunet cells were provided by Ralf Bartenschlager. Huh7.5 cells were from Charles M. Rice. Cells were grown under standard cell culture conditions at 37 °C and 5% CO<sub>2</sub>.

| Name       | Description   | Reference |
|------------|---|-----------|
| HEK293T    | Human cell line, derived from embryonic kidney cells, stably express the SV40 large T antigen to promote replication of vectors carrying the SV40 origin of replication.  | [Leb85]   |
| Huh7       | Human hepatocyte cell line, derived from HCC, permissive for HCV replication.   | [Nak82]   |
| Huh7 Lunet | Huh7 derived cell line (Huh7 carrying a HCV replicon, replication was cured by IFN $\alpha$ treatment), highly permissive for HCV replication, less CD81 expression.  | [Fri05]   |
| Huh7.5     | Huh7 derived cell line (Huh7 carrying a HCV replicon, replication was cured by IFN $\alpha$ treatment), highly permissive for HCV replication, due to a single point mutation in the dsRNA sensor retinoic acid-inducible gene-I (RIG-I). | [Bli02]   |

### 5.3. Media

#### 5.3.1. Media for culturing bacteria

Media ingredients were solubilized and autoclaved (20 min at 120 °C). After cooling at 50 °C antibiotics (100 mg/l ampicillin or 50 mg/l kanamycin) were added.

## 5. Material

| Name                                  | Components   |
|---------------------------------------|--|
| Luria Bertani medium (LB)             | 10 g/l bacto-trypton, 5 g/l yeast extract, 8 g/l NaCl, 1 g/l glucose, pH was adjusted to 7.2 with NaOH.                    |
| Luria Bertani medium (LB) agar plates | LB media plus 15 g/l agar  |
| SOC media                             | 20 g/l bacto-trypton, 5 g/l yeast extract, 2.5 mM NaCl, 10 mM MgCl <sub>2</sub> , 10 mM MgSO <sub>4</sub> , 20 mM glucose. |

### 5.3.2. Media for culturing eukaryotic cell lines

| Name              | Components  |
|-------------------|---|
| DMEM              | Dulbecco's modified Eagle Medium, 10% heat inactivated fetal calf serum, 1× GlutaMAX  |
| Heavy SILAC media | Dulbecco's modified Eagle Medium, 10% dialyzed fetal calf serum, 25 mg/l <sup>13</sup> C <sub>6</sub> L-Arginine-HCl, 25 mg/l <sup>13</sup> C <sub>6</sub> L-Lysine-2HCl, 1× Penicillin / Streptomycin, 1× GlutaMAX |
| Light SILAC media | Dulbecco's modified Eagle Medium, 10% dialyzed fetal calf serum, 25 mg/l L-Arginine-HCl, 25 mg/l L-Lysine-2HCl, 1× Penicillin / Streptomycin, 1× GlutaMAX   |

### 5.3.3. Cell culture media ingredients

| Name  | Company                                |
|---|--|
| <sup>13</sup> C <sub>6</sub> L-Arginine-HCl 50 mg | Life Technologies, Darmstadt           |
| <sup>13</sup> C <sub>6</sub> L-Lysine-HCl 50 mg   | Life Technologies, Darmstadt           |
| Blasticidin S                                     | AppliChem GmbH, Darmstadt              |
| Dialyzed fetal calf serum                         | Life Technologies, Darmstadt           |
| Dulbecco's modified Eagle Medium                  | Life Technologies, Darmstadt           |
| Fetal calf serum                                  | Biochrom GmbH, Darmstadt               |
| G418-Disulfate                                    | Geyer Th. GmbH & Co.KG, Renningen      |
| GlutaMAX, 100x                                    | Life Technologies, Darmstadt           |
| L-Arginine-HCl 50 mg                              | Life Technologies, Darmstadt           |
| L-Lysine-2HCl 50 mg                               | Life Technologies, Darmstadt           |
| OptiMEM   | Life Technologies, Darmstadt           |
| Penicillin / Streptomycin, 100x                   | Sigma-Aldrich Chemie GmbH, Taufkirchen |
| Phosphate-buffered Saline (PBS)                   | Sigma-Aldrich Chemie GmbH, Taufkirchen |
| Puromycin   | Geyer Th. GmbH & Co.KG, Renningen      |

## 5.4. Oligonucleotides

### Primer for cloning ANXA3-HA WT/shRNA resistant mutant

| Name           | Sequence   |
|----------------|--|
| ANXA3-HA fw    | TCGGATCCGCCACCATGGCATCTATCTGGGTTG                                    |
| ANXA3-HA rev   | CTGCGGCCGCTCAAGCGTAATCTGGTACGTCGTATGGGTAACC<br>ACCGTCATCTCCACCACAGAT |
| ANXA3 Mut. fw  | AGAAGCTTCCCCCAGCTGAAACTAACATTTGATGA                                  |
| ANXA3 Mut. rev | TTCAGCTGGGGGAAGCTTCTTAAACACAGGATCTC                                  |

### Primer for cloning lentiviral shRNA constructs

| Name          | Sequence   |
|---------------|--|
| ANXA2 fw      | TGCAAGTCCCTGTACTATTATTCAAGAGATAATAGTACAGGGA<br>CTTGCTTTTTTC      |
| ANXA2 rev     | TCGAGAAAAAAGCAAGTCCCTGTACTATTATCTCTTGAATAAT<br>AGTACAGGGACTTGCA  |
| ANXA3 fw      | TGGAGCTTTCCTCAATTAAATTCAAGAGATTTAATTGAGGAAA<br>GCTCCTTTTTTC      |
| ANXA3 rev     | TCGAGAAAAAAGGAGCTTTCCTCAATTAAATCTCTTGAATTTA<br>ATTGAGGAAAGCTCCA  |
| ANXA4 fw      | TGAAACATTCTGAAGATGTATTCAAGAGATACATCTTCAGAAT<br>GTTTCTTTTTTC      |
| ANXA4 rev     | TCGAGAAAAAAGAAACATTCTGAAGATGTATCTCTTGAATACA<br>TCTTCAGAATGTTTCA  |
| ANXA5 fw      | TGAAAGGTGTTTGACAAGTATTCAAGAGATACTTGTCAAACAC<br>CTTCTTTTTTC       |
| ANXA5 rev     | TCGAGAAAAAAGAAAGGTGTTTGACAAGTATCTCTTGAATAC<br>TTGTCAAACACCTTTCA  |
| ARF4 fw       | TGCAGACATATCTTCATTAATTCAAGAGATTAATGAAGATATG<br>TCTGCTTTTTTC      |
| ARF4 rev      | TCGAGAAAAAAGTACTCCTATGCAATATTATCTCTTGAATAAT<br>ATTGCATAGGAGTACA  |
| C14orf166 fw  | TGGTATGTTCTAGAGATTTATTCAAGAGATAAATCTCTAGAAC<br>ATACCTTTTTTC      |
| C14orf166 rev | TCGAGAAAAAAGTAGCTGTTTCAGGCAATTATCTCTTGAATAAT<br>TGCCTGAACAGCTACA |
| DDX1 fw       | TGAAAGTCTGTAGTCTTAAATTCAAGAGATTTAAGACTACAGA<br>CTTCTTTTTTC       |
| DDX1 rev      | TCGAGAAAAAAGAAAGTCTGTAGTCTTAAATCTCTTGAATTTA<br>AGACTACAGACTTTCA  |

## 5. Material

|            |   |
|------------|---|
| DPP4 fw    | TGCAGGCCCATGTAGTCAAATTC AAGAGATTTGACTACATGGG<br>CCTGCTTTTTTC      |
| DPP4 rev   | TCGAGAAAAAAGCAGGCCCATGTAGTCAAATCTCTTGAATTTG<br>ACTACATGGGCCTGCA   |
| LMAN2 fw   | TGTGACCGTTTGCTAAATAATTCAAGAGATTATTTAGCAAACG<br>GTCACTTTTTTC       |
| LMAN2 rev  | TCGAGAAAAAAGTGACCGTTTGCTAAATAATCTCTTGAATTAT<br>TTAGCAAACGGTCACA   |
| NT fw      | TGCGCGATAGCGCTAATAATTTTCAAGAGAAATTATTAGCGCT<br>ATCGCGCTTTTTTC     |
| NT rev     | TCGAGAAAAAAGCGCGATAGCGCTAATAATTTCTCTTGAAAAT<br>TATTAGCGCTATCGCGCA |
| PABPC1 fw  | TGAACGGCTGTTTCCTCTTATTCAAGAGATAAGAGGAAACAGC<br>CGTTCTTTTTTC       |
| PABPC1 rev | TCGAGAAAAAAGAACGGCTGTTTCCTCTTATCTCTTGAATAAG<br>AGGAAACAGCCGTTCA   |
| RAB32 fw   | TGTGCTGGGGTGGTAATAAATTCAAGAGATTTATTACCACCCC<br>AGCACTTTTTTC       |
| RAB32 rev  | TCGAGAAAAAAGTGCTGGGGTGGTAATAAATCTCTTGAATTTA<br>TTACCACCCCAGCAC    |

### Primer for cloning the sgRNA sequence into the Cas9 expression plasmid

| Name            | Sequence                  |
|-----------------|---------------------------|
| ANXA3 sgRNA fw  | CACCGGGGATATCATGGCATCTATC |
| ANXA3 sgRNA rev | AAACGATAGATGCCATGATATCCCC |

### Primer for ANXA3 knock out sequencing

| Name            | Sequence              |
|-----------------|-----------------------|
| ANXA3 sgRNA fw  | AGCAAATGGGATACCCAATGT |
| ANXA3 sgRNA rev | CCTTTCCGCCTTGGTGTCAT  |

### Primer for cloning additional restriction sites and sp/E1/Flag-E2 into LEGO iCer2 MCS

| Name              | Sequence                               |
|-------------------|--|
| LeGO MCS fw       | AATTCGACCTCGAGTCTAGAGC                 |
| LeGO-MCS rev      | GGCCGCTCTAGACTCGAGGTCG                 |
| sp/E1/Flag-E2 fw  | TAACTCGAGAATGGGTGCTCCTTTTCTATCTTCTTGCT |
| sp/E1/Flag-E2 rev | GCTTAGCGGCCGCTCATGCTTCGGCCTGGCCCAA     |

**Primer for miR122 elongation**

| Name   | Sequence  |
|--------|---|
| miR122 | GTCGTATCCAGTGCGGTGTCGTGGAGTCCGGCAATTGCACTGGA<br>TACGACCAAACAC |

**Primer to replace mCherry by a puromycin resistance gene in lentiviral shRNA construct**

| Name     | Sequence  |
|----------|---|
| Puro fw  | ATGCTAGCGCTACCGGTCCGCCACCATGACCGAGTACAAGCCC<br>ACGGTG |
| Puro rev | GAGAATTCTTAGGCACCGGGCTTG                              |

**Primer to generate Flag-E2 expressing Jc1 and JFH1 viral constructs**

| Name                            | Sequence   |
|---------------------------------|--|
| BsiWI_ J6 (A) fw                | GGACATGATGATGAACTGG                                  |
| E2-Flag (B) rev                 | CCCTTGTCATCGTCTGCTCCTTGTAGTCCGCGTCCACCCCG<br>GCGGCC  |
| Flag-E2 (C) fw                  | GGACGACGATGACAAGGGATCAGGAGCACGCACCCATAC<br>TGTTGGGGG |
| NS2_ JFH1 (D) NotI rev          | CCATCGCGGCCGCCGCGCAC                                 |
| BsiWI_ J6 (A) fw                | GGACATGATGATGAACTGG                                  |
| JFH1 <sup>E2-Flag</sup> (B) rev | CTTGTCATCGTCTGCTCCTTGTAACTGCAACAGCGCCTCC<br>AACGGTGG |
| JFH1 <sup>E2-Flag</sup> (C) fw  | AAGGATGACGATGACAAGGGAGGCGGTGGCGTGTTTCAG<br>CCATGGCCC |
| NS2_ JFH1 NotI (D) rev          | CCATCGCGGCCGCCGCGCAC                                 |

**Primer used for RT-qPCR**

| Name         | Sequence                |
|--------------|-------------------------|
| 18S rRNA fw  | GTAACCCGTTGAACCCATT     |
| 18S rRNA rev | CCATCCAATCGGTAGTAGCG    |
| ANXA2 fw     | TCTACTGTTTACGAAATCCTGTG |
| ANXA2 rev    | AGTATAGGCTTTGACAGACCCAT |
| ANXA3 fw     | GAGAGGTCAAATGCACAGCG    |
| ANXA3 rev    | CTGGTGGAGTCACTAGGGC     |
| ANXA4 fw     | GGAGGTACTGTCAAAGCTGCT   |
| ANXA4 rev    | GGCAAGGACGCTAATAATGGC   |

## 5. Material

---

|                    |                         |
|--------------------|-------------------------|
| ANXA5 fw           | GTTTGGCAGGGATCTTCTGGA   |
| ANXA5 rev          | TCATAAAGCCGAGAGGGTTTCA  |
| ARF4 fw            | CCCTCTTCTCCCGACTATTTGG  |
| ARF4 rev           | GCACAAGTGGCTTGAACATACC  |
| C14orf166 fw       | TTCCGACGCAAGTTGACGG     |
| C14orf166 rev      | CTGTCTTCAATCTTGTAGTGCCT |
| DDX1 fw            | TCTCCGAGATGGGTGTAATGC   |
| DDX1 rev           | ACCTCCTCCTAAGATCAATGGG  |
| DPP4 fw            | TACAAAAGTGACATGCCTCAGTT |
| DPP4 rev           | TGTGTAGAGTATAGAGGGGCAGA |
| GAPDH fw           | AAGGTGAAGGTCGGAGTCAAC   |
| GAPDH rev          | GGGGTCATTGATGGCAACAATA  |
| human ANXA3 fw     | CCTTTTGGACATTCGAACA     |
| human ANXA3 rev    | GATTTTAAAGAGTGTGATTTCA  |
| JFH1 fw            | CGGGAGAGCCATAGTGG       |
| JFH1 rev           | AGTACCACAAGGCCTTTTCG    |
| LMAN2 fw           | GTACGTCTGACCCCTGACGA    |
| LMAN2 rev          | CTGTGCCGTGGACTTTGAAG    |
| miR122 fw          | GGGGTGGAGTGTGACAATG     |
| miR122 rev         | CAGTGCGTGTTCGTGGAGT     |
| PABPC1 fw          | CAGGCTCACCTCACTAACCAG   |
| PABPC1 rev         | GGTAGGGGTTGATTACAGGGT   |
| RAB32 fw           | CTGCCCCGTTTCCTAGTGGA    |
| RAB32 rev          | GGGATTTGTTCTCTGCTCTCAAG |
| $\beta$ -actin fw  | CATGTACGTTGCTATCCAGGC   |
| $\beta$ -actin rev | CTCCTTAATGTCACGCACGAT   |

### 5.4.1. DNA / Protein ladder

| Name   | Company                            |
|--|------------------------------------|
| GeneRuler™ DNA Ladder Mix                          | Fermentas, Darmstadt               |
| PageRuler Prestained                               | ThermoFisher Bioscience, Darmstadt |
| PageRuler Prestained Protein Ladder, 10 to 180 kDa | ThermoFisher Bioscience, Darmstadt |

### 5.4.2. PCR nucleotides

dNTPs (ThermoFisher Bioscience, Darmstadt).

## 5.5. Plasmids

### 5.5.1. HCV plasmids

| Name   | Description   | Reference/Cloning   |
|--|---|---|
| Con1 subgenomic replicon                     | Con1 subgenomic replicon carrying a neomycin resistance gene.   | [Cho04]   |
| pBR322 Jc1                                   | WT HCV Jc1 chimera.   | [Pie06]   |
| pBR322 Jc1 $\Delta$ E1E2-NS5A-HA             | Replicon deleted in E1E2 (see below), carrying 3xHA and 6xHis tags in D3 of NS5A.   | [Vog13]   |
| pBR322 Jc1 <sup>Flag-E2</sup>                | HCV Jc1 carrying a Flag-E2 fusion protein   | Overlap extension PCR as described [Egg14].   |
| pBR322 Jc1 <sup>Flag-E2-NS5AB-eGFP-BSD</sup> | HCV Jc1 expressing Flag-tagged E2 and eGFP and BSD resistance gene between a duplicated NS5A-NS5B cleavage site.                | Overlap extension PCR as described.   |
| pBR322 Jc1 <sup>Flag-E2-NS5A-HA</sup>        | HCV Jc1 expressing Flag-tagged E2 and eGFP and 3xHA and 6xHis tags in D3 of NS5A.   | Constructed from pBR322 Jc1 $\Delta$ E1E2-NS5A-HA and pBR322 Jc1 <sup>Flag-E2</sup> |
| pBR322 Jc1 <sup>NS5AB-XFP</sup>              | HCV Jc1 and fluorescent proteins, selection markers, or the firefly luciferase in between a duplicated NS5A-NS5B cleavage site. | [Web13a]  |
| pBR322 Jc1 <sup>p7-GLuc-2A-NS2</sup>         | HCV Jc1 expressing Gaussia luciferase in between a duplicated 2A cleavage site.   | Overlap extension PCR as described [Mar08].   |
| pBR322 Jc $\Delta$ E1E2-NS5AB-FLuc           | Replicon, where a portion of the E1/E2 genes from amino acids 313-567 of the Jc1 polyprotein is deleted.                        | [Web13b]  |
| pBR322 JFH1 <sup>WT</sup>                    | WT isolate from patient with acute fulminante Hepatitis C infection.  | [Wak05]   |
| pBR322 JFH1 <sup>Flag-E2</sup>               | HCV JFH1 carrying a Flag-E2 fusion protein  | Overlap extension PCR as described [Egg14].   |



## 5.5.2. Expression plasmids

| Name                  | Description  | Reference/Cloning   |
|-----------------------|--|---|
| LeGO-iCer             | Lentiviral overexpression plasmid carrying cerulean.   | [Web08]   |
| LeGO-iCer2            | Lentiviral overexpression plasmid carrying cerulean and an IRES.   | [Web08]   |
| LeGO-iCer2 ANXA3-HA   | LeGO-iCer2 expressing HA tagged ANXA3.   | Subcloned from pEBB ANXA-HA and LeGo-iCer2 MCS.   |
| LeGO-iCer2 E1/Flag-E2 | E2 Flag-tagged E1/E2 expression construct containing the core signal peptide cloned into LeGO-iCer2 MSC.                                 | PCR-amplified sequence from amino acids 171-750 of Jc1 <sup>FLAG-E2-NS5AB-eGFP</sup> was used and cloned into the modified LeGO-iCer2 MCS |
| LeGO-iCer2 Flag-core  | LeGO-iCer2 expressing Flag tagged core (2a).   | Subcloned from pHR Flag-Core and LeGo-iCer2 MCS.  |
| LeGO-iCer2 MCS        | LeGO-iCer2 with additional XbaI/XhoI restriction sides.  | PCR amplified, cloned into LeGo-iCer2.  |
| LeGO-iCer2 NS5A-Flag  | LeGO-iCer2 expressing Flag tagged NS5A (2a).   | Subcloned from pHR HCV-Flag and LeGo-iCer2 MCS  |
| pCDNA HCV -Flag       | HCV proteins (2a) with a 3x Flag-tag at the C-terminal side.   | [Ram15]   |
| pCMV6 ANXA3 WT        | Untagged human ANXA3   | SC116952 (Origene)  |
| pCMV $\delta$ R8.91   | Lentiviral packaging construct   | [Nal96]   |
| pEBB                  | Expression plasmid   | [Tan95]   |
| pEBB ANXA3-HA         | Human ANXA3-HA fusion protein  | ANXA3 PCR amplified from SC116952 cloned into pEBB plasmid.   |
| pEBB ANXA3-HA mut.    | shRNA resistant ANXA3-HA fusion protein.   | Overlap extension PCR as described.   |
| pHR Flag-core         | HCV core (2a) with a 3x Flag-tag at the N-terminal side.   | [Ram15]   |
| pHR Core eGFP         | Lentiviral expression construct carrying HCV core (1b) under an EF1a promotor control, followed by an ECMV IRES driving eGFP expression. | [Her10]   |
| pMD.G                 | VSV-G glycoprotein construct   | [Nal96]   |
| pSicoR-MS1            | Lentiviral shRNA expression plasmid carrying mcherry.  | [Her10, Wis11]  |

|                      |  |                                     |
|----------------------|--|-------------------------------------|
| pSicoR-MS1 Puro      | Lentiviral shRNA expression plasmid carrying a puromycin resistance gene.                | Overlap extension PCR as described. |
| pSpCas9 (BB)-2A-Puro | Cas9 expression plasmid  | 48139 (Addgene)                     |
| Trip-RFP-NLS-IPS     | Reporter system to visualize an HCV infection, by translocation of RFP into the nucleus. | [Jon10a]                            |

## 5.6. Enzymes

### 5.6.1. Restriction endonucleases

All restriction endonucleases were purchased from New England Biolabs GmbH and used with buffers according to manufacturer's instructions.

### 5.6.2. Other enzymes

| Name  | Company                            |
|---|------------------------------------|
| Alkaline Phosphatase, Calf Intestinal (CIP) | New England Biolabs GmbH, Ipswich  |
| Maxima SYBR Green/Rox qPCR Master Mix       | Life Technologies, Darmstadt       |
| Phusion High-Fidelity DNA Polymerase        | ThermoFisher Bioscience, Darmstadt |
| Proteinase K                                | Life Technologies, Darmstadt       |
| Super Script II Reverse Transcriptase       | ThermoFisher Bioscience, Darmstadt |
| T4 DNA Ligase                               | ThermoFisher Bioscience, Darmstadt |
| T4 Polynucleotide Kinase                    | New England Biolabs GmbH, Ipswich  |
| Taq DNA Polymerase                          | ThermoFisher Bioscience, Darmstadt |
| Trypsin-EDTA (0.05%)                        | ThermoFisher Bioscience, Darmstadt |

## 5.7. Inhibitors

| Name                                 | Company                                |
|--------------------------------------|--|
| Antipain                             | Sigma-Aldrich Chemie GmbH, Taufkirchen |
| Leupeptin                            | Sigma-Aldrich Chemie GmbH, Taufkirchen |
| Pepstatin A                          | Biomol GmbH, Hamburg                   |
| Phenylmethylsulfonyl fluoride (PMSF) | Sigma-Aldrich Chemie GmbH, Taufkirchen |
| Protease Inhibitor Cocktail (PIC)    | Sigma-Aldrich Chemie GmbH, Taufkirchen |
| RNAse AWAY                           | Carl Roth GmbH, Karlsruhe              |
| RNAse Inhibitor                      | Life Technologies, Darmstadt           |

## 5.8. Antibodies

### Primary antibodies

| Antigen/Species/Clone | Application             | Sequence                               |
|-----------------------|-------------------------|--|
| ANXA3, rb             | WB: 1:1000              | Sigma-Aldrich Chemie GmbH, Taufkirchen |
| ANXA3, rb, T-18       | WB:1:1000               | Santa Cruz Biotechnology, Heidelberg   |
| ApoB, rb              | WB: 1:1000              | Abcam, Cambridge                       |
| ApoE, rb              | WB: 1:5000, IF: 1:100   | Abcam, Cambridge                       |
| Calnexin, goat        | WB: 1:1000              | Santa Cruz Biotechnology, Heidelberg   |
| Calreticulin, rb      | WB: 1:1000              | Enzo Life Science, Farmingdale         |
| CD81, ms, M38         | FC: 1:100               | Biozol GmbH, Eching                    |
| CLDN1, ms             | WB: 1:1000, FC: 1:100   | Abnova, Walnut                         |
| Core, ms, C7-50       | WB: 1:1000, IF: 1:100   | Santa Cruz Biotechnology, Heidelberg   |
| E2, ms, AP-33         | WB: 1:2000, IF: 1:100   | Genentech Inc., San Francisco          |
| Flag- agarose, ms     | IP: 20 $\mu$ l / sample | Sigma-Aldrich Chemie GmbH, Taufkirchen |
| Flag- agarose, rb     | IP: 20 $\mu$ l / sample | Sigma-Aldrich Chemie GmbH, Taufkirchen |
| Flag, ms              | WB: 1:1000, IF: 1:100   | Sigma-Aldrich Chemie GmbH, Taufkirchen |
| Flag, rb              | WB: 1:1000, IF: 1:100   | Sigma-Aldrich Chemie GmbH, Taufkirchen |
| GM130, goat           | IF: 1:100               | Santa Cruz Biotechnology, Heidelberg   |
| HA- agarose, goat     | IP: 25 $\mu$ l / sample | Sigma-Aldrich Chemie GmbH, Taufkirchen |
| HA, goat, Y-11        | WB: 1:1000, IF: 1:100   | Santa Cruz Biotechnology, Heidelberg   |
| IgG2a, ms, eBM2a      |                         | Sigma-Aldrich Chemie GmbH, Taufkirchen |
| MnSOD, rb             | WB: 1:1000              | Enzo Life Science, Farmingdale         |
| NS5A, ms, 2F6/G11     | WB: 1:1000, IF: 1:100   | IBT GmbH, Reutlingen                   |
| NS5A, ms, 388         | WB: 1:1000              | Santa Cruz Biotechnology, Heidelberg   |
| OCLD, ms              | WB: 1:1000              | Life Technologies, Darmstadt           |
| PLIN2/ADRP, rb        | WB: 1:1000, IF: 1:50    | Abcam, Cambridge                       |

|                               |            |   |
|-------------------------------|------------|---|
| PLIN3/TIP47, rb<br>Rabbit IgG | WB: 1:1000 | Abcam, Cambridge<br>Sigma-Aldrich Chemie GmbH,<br>Taufkirchen |
| SR-B1, rb                     | FC: 1:100  | Santa Cruz Biotechnology, Hei-<br>delberg                     |
| $\beta$ -Actin, ms, AC-15     | WB: 1:2000 | Sigma-Aldrich Chemie GmbH,<br>Taufkirchen                     |
| $\beta$ -Tubulin, ms, B-512   | WB: 1:2000 | Sigma-Aldrich Chemie GmbH,<br>Taufkirchen                     |

**Secondary antibodies**

| <b>Antigen</b>   | <b>Application</b> | <b>Sequence</b>                |
|--|--------------------|--------------------------------|
| Alexa Flour 488 donkey anti-goat IgG (H+L)                       | IF: 1:1000         | Life Technologies, Darmstadt   |
| Alexa Flour 488 donkey anti-rabbit IgG (H+L)                     | IF: 1:1500         | Life Technologies, Darmstadt   |
| Alexa Flour 488 goat anti-mouse IgG (H+L)                        | IF: 1:1500         | Life Technologies, Darmstadt   |
| Alexa Flour 555 goat anti-mouse IgG (H+L)                        | IF: 1:1500         | Life Technologies, Darmstadt   |
| Alexa Flour 594 donkey anti-rabbit IgG(H+L)                      | IF: 1:1500         | Life Technologies, Darmstadt   |
| Alexa Flour 594 goat anti-mouse IgG (H+L)                        | IF: 1:1500         | Life Technologies, Darmstadt   |
| Alexa Flour 647 donkey anti-rabbit IgG (H+L)                     | IF: 1:1500         | Life Technologies, Darmstadt   |
| Alexa Flour 647 goat anti-mouse IgG (H+L)                        | IF: 1:1500         | Life Technologies, Darmstadt   |
| Peroxidase AffiniPure donkey anti-goat IgG (H+L), HRP conjugated | WB: 1:10.000       | JacksonImmunoResearch, Suffolk |
| Peroxidase AffiniPure goat anti-mouse IgG (H+L), HRP conjugated  | WB: 1:10.000       | JacksonImmunoResearch, Suffolk |
| Peroxidase AffiniPure goat anti-rabbit IgG (H+L), HRP conjugated | WB: 1:10.000       | JacksonImmunoResearch, Suffolk |

## 5.9. Dyes

| Name                       | Application  | Company                                |
|----------------------------|--------------|--|
| BODIPY                     | IF: 1:1000   | Life Technologies GmbH, Darmstadt      |
| Coomassie Blue G           |              | Sigma-Aldrich Chemie GmbH, Taufkirchen |
| Crystal violet             |              | Geyer Th. GmbH & CO. KG, Renningen     |
| Hoechst                    | IF: 1:6.000  | Sigma-Aldrich Chemie GmbH, Taufkirchen |
| LD540                      | IF: 1:10.000 | [Spa09]                                |
| LipidTox Green             | IF: 1:1500   | Life Technologies GmbH, Darmstadt      |
| LipidTox Red               | IF: 1:1500   | Life Technologies GmbH, Darmstadt      |
| Ponceau S                  |              | AppliChem GmbH, Darmstadt              |
| RotiBlue 5× Coomassie Blue |              | Carl Roth GmbH, Karlsruhe              |

## 5.10. Chemicals

| Name                              | Company                                |
|-----------------------------------|--|
| 1,4-Dithiothreitol (DTT)          | Sigma-Aldrich Chemie GmbH, Taufkirchen |
| 2-Mercaptoethanol                 | Sigma-Aldrich Chemie GmbH, Taufkirchen |
| 2-Propanol                        | AppliChem GmbH, Darmstadt              |
| 4x Roti load loading dye          | Carl Roth GmbH, Karlsruhe              |
| 6-Aminocaproic acid               | Sigma-Aldrich Chemie GmbH, Taufkirchen |
| 6-Aminocaproic acid               | Sigma-Aldrich Chemie GmbH, Taufkirchen |
| Acetic acid                       | AppliChem GmbH, Darmstadt              |
| Acetonitrile                      | Sigma-Aldrich GmbH, Taufkirchen        |
| Acrylamide:bis-acrylamide, 37.5:1 | Merck, Darmstadt                       |
| Adenosine triphosphate (ATP)      | AppliChem GmbH, Darmstadt              |
| Agar                              | AppliChem GmbH, Darmstadt              |
| Agarose                           | AppliChem GmbH, Darmstadt              |
| Albumin                           | Sigma-Aldrich Chemie GmbH, Taufkirchen |
| Albumin from bovine serum (BSA)   | Sigma-Aldrich Chemie GmbH, Taufkirchen |
| Ampicillin                        | AppliChem GmbH, Darmstadt              |
| Bacto-trypton                     | AppliChem GmbH, Darmstadt              |
| Bis-Tris                          | Sigma-Aldrich Chemie GmbH, Taufkirchen |
| Blasticidin S                     | AppliChem GmbH, Darmstadt              |

|  |  |
|--|--|
| Bromophenol blue   | AppliChem GmbH, Darmstadt              |
| Calcium chloride (CaCl <sub>2</sub> )                    | AppliChem GmbH, Darmstadt              |
| Catalase   | Roche, Basel                           |
| Chloroform   | AppliChem GmbH, Darmstadt              |
| Dimethyl sulfoxide (DMSO)                                | AppliChem GmbH, Darmstadt              |
| Dipotassium phosphate (K <sub>2</sub> HPO <sub>4</sub> ) | AppliChem GmbH, Darmstadt              |
| Dodecyl sulfate sodium salt (SDS)                        | AppliChem GmbH, Darmstadt              |
| ECL lumi-light western blotting substrate                | Roche, Basel                           |
| EDTA   | AppliChem GmbH, Darmstadt              |
| EGTA   | AppliChem GmbH, Darmstadt              |
| Ethanol  | AppliChem GmbH, Darmstadt              |
| Ethanol  | Geyer Th. GmbH & Co.KG, Renningen      |
| Ethidiumbromide  | AppliChem GmbH, Darmstadt              |
| Femto ECL  | Perbio, Darmstadt                      |
| Formic acid  | Sigma-Aldrich Chemie GmbH, Taufkirchen |
| FuGENE   | Promega, Madison                       |
| Glucose  | AppliChem GmbH, Darmstadt              |
| Glucose oxidase  | Sigma-Aldrich Chemie GmbH, Taufkirchen |
| Glutathione  | AppliChem GmbH, Darmstadt              |
| Glycerol   | AppliChem GmbH, Darmstadt              |
| Glycin   | AppliChem GmbH, Darmstadt              |
| HEPES  | Sigma-Aldrich Chemie GmbH, Taufkirchen |
| HPLC water   | AppliChem GmbH, Darmstadt              |
| Hydrogen chloride (HCl)                                  | AppliChem GmbH, Darmstadt              |
| Magnesium acetat (Mg(CH <sub>3</sub> COO) <sub>2</sub> ) | Sigma-Aldrich Chemie GmbH, Taufkirchen |
| Magnesium chloride (MgCl <sub>2</sub> )                  | AppliChem GmbH, Darmstadt              |
| Magnesium sulfate (MgSO <sub>4</sub> )                   | AppliChem GmbH, Darmstadt              |
| Methanol   | AppliChem GmbH, Darmstadt              |
| Mowiol 4-88  | AppliChem GmbH, Darmstadt              |
| n-Dodecyl β-D-maltoside                                  | Sigma-Aldrich Chemie GmbH, Taufkirchen |
| Nonfat dried milk powder                                 | AppliChem GmbH, Darmstadt              |
| Nonident-P40   | AppliChem GmbH, Darmstadt              |
| OptiPREP (60% Iodixanol)                                 | Sigma-Aldrich Chemie GmbH, Taufkirchen |
| Paraformaldehyde (PFA)                                   | AppliChem GmbH, Darmstadt              |
| Phenole-Chloroform-Isoamyl<br>(25:24:1 vol/vol/vol)      | alcohol<br>AppliChem GmbH, Darmstadt   |
| Polybrene (Hexadimethrinbromid)                          | Sigma-Aldrich GmbH, Taufkirchen        |

## 5. Material

---

|   |  |
|---|--|
| Polyethylene glycol   | AppliChem GmbH, Darmstadt                |
| Ponceau S   | AppliChem GmbH, Darmstadt                |
| Potassium dihydrogen phosphate (KH <sub>2</sub> PO <sub>4</sub> ) | AppliChem GmbH, Darmstadt                |
| Potassium acetate (CH <sub>3</sub> CO <sub>2</sub> K)             | AppliChem GmbH, Darmstadt                |
| Potassium chloride (KCl)  | AppliChem GmbH, Darmstadt                |
| Potassium hydroxide (KOH)   | AppliChem GmbH, Darmstadt                |
| RNA Stat-60   | AMS Biotechnology (Europe) Ltd, Abington |
| RNase free water  | Life Technologies, Darmstadt             |
| Roti-blue   | Carl Roth GmbH, Karlsruhe                |
| Saponin   | Sigma-Aldrich Chemie GmbH, Taufkirchen   |
| Sodium acetate (C <sub>2</sub> H <sub>3</sub> NaO <sub>2</sub> )  | Life Technologies, Darmstadt             |
| Sodium chloride (NaCl)  | AppliChem GmbH, Darmstadt                |
| Sodium deoxycholate   | AppliChem GmbH, Darmstadt                |
| Sodium hypochlorite   | Merck, Darmstadt                         |
| $\beta$ -Mercaptoethanolamin                                      | Sigma-Aldrich Chemie GmbH, Taufkirchen   |
| Sucrose   | AppliChem GmbH, Darmstadt                |
| Tris  | AppliChem GmbH, Darmstadt                |
| Triton-X-100  | AppliChem GmbH, Darmstadt                |
| Trizol  | Life Technologies, Darmstadt             |
| Tween 20 molecular biology grade                                  | AppliChem GmbH, Darmstadt                |
| Tween20   | AppliChem GmbH, Darmstadt                |
| Yeast extract   | AppliChem GmbH, Darmstadt                |

### 5.11. Kits

| Name  | Company                        |
|---|--------------------------------|
| CellTiter 96 <sup>®</sup> Aqueous One Solution Cell Proliferation Assay | Promega GmbH, Mannheim         |
| cPLA2 Assay   | Biomol GmbH, Hamburg           |
| DC Protein Assay  | BioRad GmbH, München           |
| HCV Core ELISA  | BioCat GmbH, Heidelberg        |
| Human ApoE ELISA  | Mabtech, Naka Strand           |
| MTP Activity Assay  | Roar Biomedical Inc., New York |
| Nucleobon Xtra Maxi Prep  | Macherey-Nagel GmbH, Düren     |
| Nucleospin Mini Prep  | Macherey-Nagel GmbH, Düren     |
| Nucleospin PCR & Gel clean up   | Macherey-Nagel GmbH, Düren     |



|                                 |                              |
|---------------------------------|------------------------------|
| Nucleospin RNA Virus            | Macherey-Nagel GmbH, Düren   |
| Nucleospin Tissue               | Macherey-Nagel GmbH, Düren   |
| Renilla Luciferase Assay System | Promega GmbH, Mannheim       |
| SILAC Protein Quantitation Kit  | Life Technologies, Darmstadt |
| T7 Megascript                   | Life Technologies, Darmstadt |

## 5.12. Solvents and buffers

| Name                   | Components  |
|------------------------|---|
| 10% Iodixanol          | 8.3 ml of 60% Iodixanol, 1 ml 0.1 M EDTA, 1.6 ml of 0.15 M Tris-HCl pH 8.0, 39.6 ml 0.25 M sucrose  |
| 10× Blot buffer        | 30.3 g/l Tris base, 144 g/l glycine, add 20% methanol to 1× blot buffer   |
| 10× SDS running buffer | 30.2 g/l Tris base, 188 g/l glycine, 10 g/l SDS   |
| 1M potassium phosphate | 190 mM KH <sub>2</sub> PO <sub>4</sub> , 810 mM K <sub>2</sub> HPO <sub>4</sub> , pH 7.4  |
| 20× TBS-T              | 200 mM Tris-HCl pH 7.7, 3 M NaCl, 1% Tween20  |
| 2× HBS                 | 16.36 g/l NaCl, 11.88 g/l HEPES, 0.5 g/l Na <sub>2</sub> HPO <sub>4</sub> × 2H <sub>2</sub> O adjusted to pH 7.23   |
| 2× SDS sample buffer   | 150 mM Tris-HCl, pH 6.8, 1.2% SDS, 30% glycerol, 0.002% bromophenol blue, 15% β-mercaptoethanol   |
| 40% Iodixanol          | 33.3 ml of 60% Iodixanol, 1 ml 0.1 M EDTA, 1.6 ml of 0.15 M Tris-HCl pH 8.0, 14.1 ml 0.25 M sucrose   |
| 6× Laemmli buffer      | 375 mM Tris-HCl pH 6.8, 25.8% glycerol, 10% SDS, 0.012% bromophenol blue  |
| Annealing buffer       | 200 mM CH <sub>3</sub> CO <sub>2</sub> K, 60 mM HEPES pH 7.4, 4 mM Mg(CH <sub>3</sub> COO) <sub>2</sub>   |
| Blocking buffer        | 5% nonfat dried milk powder in 1× TBS-T   |
| Blocking solution      | 5% BSA, 1% fish skin gelatin, 50 mM Tris in PBS   |
| Cell fixation          | 4% PFA/ PBS   |
| Coomassie blue         | 0.1% Coomassie blue, 40% methanol, 10% acetic acid  |
| Crystal violet         | 0.5% (w/v) crystal violet, 20% methanol   |
| Cytomix                | 120 mM KCl, 0.15 mM CaCl <sub>2</sub> , 10 mM K <sub>2</sub> HPO <sub>4</sub> / KH <sub>2</sub> PO <sub>4</sub> (pH 7.6), 25 mM HEPES, 2 mM EGTA, 5 mM MgCl <sub>2</sub> . Sterile filtrated; add 2 mM ATP and 5 mM glutathione before electroporation. |
| dSTORM imaging buffer  | 50 mM Tris-HCl pH 8, 50 mM NaCl, 50 mg/ml glucose oxidase, 40 μg/ml catalase, 10% glucose, 100 mM β-mercaptoethanolamin   |
| Freezing media         | 90% FCS, 10% DMSO   |

## 5. Material

---

|                                      |  |
|--------------------------------------|--|
| LD hypotonic buffer                  | 50 mM HEPES, 1 mM EDTA, 2 mM MgCl <sub>2</sub> , pH 7.4, 1× PIC  |
| LD isolation buffer (used for SILAC) | 0.25 M sucrose, 1 mM EDTA, 1 mM DTT, supplemented with protease inhibitor cocktail                           |
| LD isotonic buffer                   | 1.05 M sucrose, 50 mM HEPES, 100 mM KCl, 2 mM MgCl <sub>2</sub>  |
| LD wash buffer (used for SILAC)      | 50 mM potassium phosphate buffer pH 7.4, 100 mM KCl, 1 mM EDTA, 1 mM Phenylmethanesulfonyl fluoride          |
| Low stringency lysis buffer          | 50 mM Tris-HCl pH 7.4, 150 mM NaCl, 0,1% Nonidet P40, 1x PIC   |
| Mowiol                               | 0.2 M Tris-HCl, pH 8.5, 12% (w/v) Mowiol 4-88, 30% glycerol  |
| MTP homogenization buffer            | 150 mM NaCl, 10 mM Tris-HCl pH 7.4, 1 mM EDTA, 10 µl/ml, 1× PIC  |
| Native lysis buffer                  | 0.75 M 6-aminocaproic acid, 50 mM Tris-Bis, pH 7.0 supplemented with 15 µl 10% n-dodecyl-β-D-maltopyranoside |
| NP40 lysis buffer                    | 50 mM Tris-HCl pH 7.4, 150 mM NaCl, 1% NP-40, 1× PIC   |
| Ponceau S                            | 0.1% (w/v) ponceau S, 5% acetic acid   |
| Proteinase K buffer                  | 50 mM Tris-HCl, pH 8, 10 mM CaCl <sub>2</sub> , 1 mM DTT   |
| RIPA lysis buffer                    | 150 mM NaCl, 50 mM Tris-HCl pH 7.6, 1% Nonidet P40, 0.5% sodium deoxycholate, 5 mM EDTA, 1× PIC              |

### 5.13. Consumables

| Name   | Company                           |
|--|-----------------------------------|
| 12% Mini-PROTEAN <sup>®</sup> TGX Stain-Free <sup>™</sup> protein gels   | Biorad, Munich                    |
| 4-20% Mini-PROTEAN <sup>®</sup> TGX Stain-Free <sup>™</sup> protein gels | Biorad, Munich                    |
| Adhesive PCR seal  | Sarstedt AG & Co KG, Nümbrecht    |
| Amersham Hyperfilm ECL   | Geyer Th. GmbH & Co.KG, Renningen |
| Blunt-end cannula  | Kleiser Medical GmbH, Messkirch   |
| Cannula  | Sarstedt AG & Co KG, Nümbrecht    |
| Cell scraper   | VWR International GmbH, Darmstadt |
| Centrifuge tube, thinwall ultraclear                                     | Beckman Coulter GmbH, Krefeld     |
| Combitips  | VWR International GmbH, Darmstadt |

|                                   |                                    |
|-----------------------------------|------------------------------------|
| Cover slips                       | VWR International GmbH, Darmstadt  |
| Cryo-Tubes                        | Sarstedt AG & Co KG, Nümbrecht     |
| Electroporation cuvette 0.2 mm    | VWR International GmbH, Darmstadt  |
| Electroporation cuvette 0.4 mm    | VWR International GmbH, Darmstadt  |
| Eppendorf tubes                   | VWR International GmbH, Darmstadt  |
| Glass slides                      | VWR International GmbH, Darmstadt  |
| LabTek II chamber slides          | ThermoFisher Bioscience, Darmstadt |
| Mini-PROTEAN TGX precast gels     | Biorad, Munich                     |
| Nitrocellulose membrane           | Geyer Th. GmbH & Co.KG, Renningen  |
| PCR plates                        | Sarstedt AG & Co KG, Nümbrecht     |
| PCR tubes                         | VWR International GmbH, Darmstadt  |
| Pipette tips                      | VWR International GmbH, Darmstadt  |
| Pipette tips RNase free           | VWR International GmbH, Darmstadt  |
| Pipettes                          | Sarstedt AG & Co KG, Nümbrecht     |
| RNase free microfuge tubes        | Life Technologies, Darmstadt       |
| Sterile filter 0.2 $\mu\text{m}$  | Fisher Scientific GmbH, Darmstadt  |
| Sterile filter 0.45 $\mu\text{m}$ | Fisher Scientific GmbH, Darmstadt  |
| Syringe                           | neoLab GmbH, Heidelberg            |
| Tissue culture dishes             | Sarstedt AG & Co KG, Nümbrecht     |
| Tissue culture flasks             | Sarstedt AG & Co KG, Nümbrecht     |
| Tissue culture plates             | Sarstedt AG & Co KG, Nümbrecht     |
| Tubes 15 ml, 50 ml                | Greiner GmbH, Frickenhausen        |
| Whatman paper                     | GE Healthcare, München             |

## 5.14. Equipment

| <b>Name</b>                            | <b>Company</b>                         |
|--|--|
| 405 nm diode laser 100 mW              | Coherent Inc., Santa Clara             |
| 642 nm diode laser 45 mW               | Melles Griot GmbH, Didam               |
| 7500 fast real time PCR system         | Applied Biosystems, Darmstadt          |
| Acclaim PepMap $\mu$ -precolumn        | ThermoFisher Bioscience, Darmstadt     |
| Agarose casting stand                  | Bio-Rad Laboratories GmbH, Munich      |
| Agarose gel chamber                    | Bio-Rad Laboratories GmbH, Munich      |
| Argon laser 35-IMA-840-01              | Melles Griot GmbH, Didam               |
| BD FACS Canto flow cytometer           | BD Bioscience, Heidelberg              |
| Beamsplitter zt405/488/561/640rpc TIRF | Chroma Technology Corporation, Olching |

## 5. Material

---

|  |                                     |
|--|-------------------------------------|
| Centrifuge 5424R                                 | Eppendorf, Hamburg                  |
| Centrifuge 5810R                                 | Eppendorf, Hamburg                  |
| Centrifuge Sorvall RC5C Plus                     | ThermoFisher Bioscience, Darmstadt  |
| Diode laser CUBE 405-100C                        | Coherent Inc., Santa Clara          |
| DPSS laser 10 mW                                 | Melles Griot GmbH, Didam            |
| EMCCD camera iXon+ DU-897                        | Andor Technology, Belfast           |
| Emission filter brightline HC 446, 523, 600, 677 | Semrock, Inc. Rochester             |
| Fused-silica emitter (I.D. 10 $\mu$ m)           | New Objective, Woburn               |
| Gene Pulser Xcell electroporation system         | Biorad GmbH, Munich                 |
| GeneAmp PCR system 9700                          | AB Applied Biosystems, Darmstadt    |
| HeNe laser 5 mW                                  | Melles Griot GmbH, Didam            |
| Hera freezer                                     | ThermoFisher Bioscience, Darmstadt  |
| HERAsafe inkubator                               | ThermoFisher Bioscience, Darmstadt  |
| Herasafe sterile bench                           | ThermoFisher Bioscience, Darmstadt  |
| Infinite M200 plate reader                       | Tecan Group Ltd, Männedorf          |
| Innova 43 inkubator                              | New Brunswick Scientific, Hamburg   |
| Laboratory freezer                               | ThermoFisher Bioscience, Darmstadt  |
| Leica DMIL microscope                            | Leica Camera AG, Wetzlar            |
| LSR Fortessa flow cytometer                      | BD Bioscience, Heidelberg           |
| Magnetic stirrer heating plate IKA RH basic      | IKA-Werke GmbH & CO. KG, Staufen    |
| Micro centrifuge                                 | Carl Roth GmbH, Karlsruhe           |
| Mini Protean Tetra system                        | Biorad GmbH, Munich                 |
| Multipipette plus                                | Eppendorf AG, Hamburg               |
| Nanodrop   | PEQLAB Biotechnology GmbH, Erlangen |
| nano-UPLC system                                 | ThermoFisher Bioscience, Darmstadt  |
| Neubauer counting chamber                        | Cellomics Technology, Halethopre    |
| Nikon C2plus                                     | Nikon, Düsseldorf                   |
| Optima L-90K ultracentrifuge                     | Beckman Coulter GmbH, Krefeld       |
| Orbitrap mass spectrometer (Orbitrap Fusion)     | ThermoFisher Bioscience, Darmstadt  |
| Pipette boy                                      | VWR International GmbH, Darmstadt   |
| Pipettes Research plus                           | Eppendorf AG, Hamburg               |
| Plan Apo VC 60x H objective                      | Nikon, Tokyo                        |
| Quadrupole-time-of-flight mass spectrometer      | Micromass/Waters, Hertfordshire     |
| Refractometer DR 201-95                          | Krüß GmbH, Hamburg                  |
| Semiconductor laser Sapphire 561 LP              | Coherent Inc., Santa Clara          |

|                                       |                                       |
|---------------------------------------|---------------------------------------|
| Thermomixer comfort                   | Eppendorf, Hamburg                    |
| UV Illuminator                        | VWR International GmbH, Darmstadt     |
| Visible fiber laser 2RU-VFL-P-300-647 | MPB Communications Inc, Pointe Claire |
| Water bath WBT-series                 | LTF Labortechnik, Wasserburg          |
| Wide Mini Sub Cell GT                 | Biorad GmbH, Munich                   |

## 5.15. Software

| Name   | Developer/Reference              |
|--|----------------------------------|
| 7500 Software v2.3                           | AB Applied Biosystems, Darmstadt |
| BD FACSDiva 5.0.3                            | BD Bioscience, Heidelberg        |
| cisPath                                      | [Wan15]                          |
| Fiji   | [Sch12]                          |
| FlowJo                                       | Treestar Inc. Ashland            |
| gdata, lattice, gplots, and ggplot2 packages | [Wt15a, Sar08, Wt15b, Wic09]     |
| GeneOverlap                                  | [She13]                          |
| GraphPad Prism (5.03)                        | Graphpad, La Jola                |
| Image J                                      | NIJ                              |
| Imaris 7.6.1                                 | Bitplane, Zürich                 |
| MaxQuant version 1.5.2.8.                    | [Cox08]                          |
| MyGene                                       | [Mar14]                          |
| NIS-Elements                                 | Laboratory Imaging, Prag         |
| OpenMS and the OpenMS Proteomic Pipeline     | [Stu08, Koh07]                   |
| R  | R Core Team                      |
| RISMed                                       | [Kov15]                          |
| SILACAnalyzer                                | [Nil10]                          |



# 6. Methods

## 6.1. Molecular Biological Methods

### 6.1.1. Cultivation of bacteria

DH5 $\alpha$  and Stbl2 bacteria were cultured in LB media or on LB agar plates at 37 °C or 30 °C, respectively. All plasmids carry an ampicillin or kanamycin resistance gene allowing selection of transformed bacteria with 100  $\mu\text{g}/\text{ml}$  ampicillin or 50  $\mu\text{g}/\text{ml}$  kanamycin. Stbl2 bacteria were preferably used for the production of lentiviral plasmids.

### 6.1.2. Isolation of plasmid DNA

Plasmid DNA was isolated using the Nucleospin Mini Prep kit or the Nucleobon Xtra Maxi Prep kit according to the manufacturer's instructions. Precipitated DNA was resolved in DNA-free water. The DNA concentration and purity was measured by NanoDrop. DNA fragment size was confirmed by DNA electrophoresis on a 1–2% agarose gel.

### 6.1.3. Cloning

#### PCR

PCR was used for amplification of specific DNA fragments *in vitro*. Therefore, specific primers are used, flanking the DNA fragment of interest. For standard amplification PCR, following conditions were used.

| Cycles | Time     | Temperature (°C) | Description          |
|--------|----------|------------------|----------------------|
| 1      | 2 min    | 98               | Initial denaturation |
| 35     | 10 s     | 98               | Denaturation         |
|        | 30 s     | 60               | Annealing            |
|        | 1 min/kb | 72               | Elongation           |
| 1      | 10 min   | 72               | Final elongation     |
|        | $\infty$ | 4                |                      |

The standard PCR reaction mix for one 20  $\mu\text{l}$  reaction was used as followed.



| Description                              | Volume/Concentration |
|--|----------------------|
| Template DNA                             | 50 ng                |
| dNTPs (10 mM)                            | 0.4 $\mu$ l          |
| Primer fw ( 100 $\mu$ M)                 | 1 $\mu$ l            |
| Primer rev (100 $\mu$ M)                 | 1 $\mu$ l            |
| Phusion DNA polymerase                   | 0.2 $\mu$ l          |
| 5 $\times$ Phusion DNA polymerase buffer | 4 $\mu$ l            |
| H <sub>2</sub> O                         | <i>x</i> $\mu$ l     |

PCR product size was controlled by DNA electrophoresis on a 1% - 2% agarose gel and purified by the Nucleospin PCR & Gel clean up kit according to the manufacturer's instructions.

### Restriction endonuclease digestion

Restriction endonucleases are a popular tool to specifically cut and paste DNA fragments. Depending on the enzyme, different conditions regarding temperature, incubation time and additives are needed. The standard protocol for a 20  $\mu$ l reaction was:

| Description                  | Volume/Concentration | Time & Temperature |
|------------------------------|----------------------|--------------------|
| DNA                          | 1 $\mu$ g            | 1-2 h, 37 °C       |
| Restriction endonucleases I  | 1 $\mu$ l            |                    |
| Restriction endonucleases II | 1 $\mu$ l            |                    |
| 10 $\times$ Buffer           | 2 $\mu$ l            |                    |
| H <sub>2</sub> O             | <i>x</i> $\mu$ l     |                    |

DNA fragment size was controlled by DNA electrophoresis on a 1% - 2% agarose gel and purified by the Nucleospin PCR & Gel clean up kit according to the manufacturer's instructions.

### DNA ligation

The T4 DNA ligase catalyses the formation of a phosphodiester bond between 5' phosphate ends and free 3' OH ends of dsDNA. For this reaction ATP is essential. T4 DNA ligase is able to link blunt and sticky ends. However, digestion with the same set of restriction endonucleases is needed, to ligate DNA fragments (inserts) into a vector (plasmid). De-phosphorylation of digested vector DNA is required to avoid re-ligation of vector DNA. The standard protocol for one 10  $\mu$ l de-phosphorylation approach was:

| Description                 | Volume/Concentration | Time & Temperature |
|-----------------------------|----------------------|--------------------|
| Vector                      | 1 $\mu$ g            | 30 min, 37 °C      |
| CIP                         | 1 $\mu$ l            |                    |
| 10 $\times$ CutSmart Buffer | 1 $\mu$ l            |                    |
| H <sub>2</sub> O            | <i>x</i> $\mu$ l     |                    |

The de-phosphorylated vector DNA was purified by the Nucleospin PCR & Gel clean up kit according to the manufacturer's instructions. Additionally, insert DNA (can be generated by primers or produced by cut and paste of plasmids) can be phosphorylated, to increase the ligation efficiency between vector DNA and insert DNA. The standard protocol for phosphorylation of DNA inserts from primers was as followed:

| Description              | Volume ( $\mu$ l) | Time & Temperature |
|--------------------------|-------------------|--------------------|
| Primer fw (100 mM)       | 2                 |                    |
| Primer rev (100mM)       | 2                 | 30 min, 37 °C      |
| T4 Polynucleotide Kinase | 0.4               | followed by        |
| 10× T4 Ligase buffer     | 2                 | 20 min, 65 °C      |
| H <sub>2</sub> O         | <i>x</i>          |                    |

Then, primers were annealed by mixing 5  $\mu$ l of each primer together with 25  $\mu$ l annealing buffer and 15  $\mu$ l H<sub>2</sub>O. This mixture was incubated at 95 °C for 5 min, followed by incubation for 88 min, where the temperature dropped every minute by 1 °C. Ligation reactions (10  $\mu$ l) were performed according to the standard protocol using a PCR cycler. Ligation reactions without insert DNA served as a negative control.

| Description              | Volume ( $\mu$ l) | Time & Temperature | Cycles |
|--------------------------|-------------------|--------------------|--------|
| Insert                   | 3                 |                    |        |
| Vector                   | 1                 | 20 s, 28 °C        |        |
| T4 DNA ligase            | 0.5               | followed by        | 49     |
| 10× T4 DNA ligase buffer | 1                 | 20 s, 4 °C         |        |
| H <sub>2</sub> O         | <i>x</i>          |                    |        |

Alternatively, ligation reactions were incubated for 2 h at RT or overnight at 4 °C.

### Overlap extension PCR

Overlap extension PCR was used to generate viral Jc1 and JFH1 strains carrying a Flag-tagged-E2 fusion protein. The overlap extension PCR consists of two PCRs. The first PCR is used to amplify a PCR product with flanking primers (A, D) complementary to the end of the target sequence and two internal primers (B, C) with complementary ends carrying the tag sequence. Primers are listed above (see 5.4). HCV WT constructs were used as template (see 5.5.1).

## 6. Methods

| Description                              | Volume/Concentration |
|--|----------------------|
| Template DNA                             | 100 ng               |
| dNTPs (10 mM)                            | 1 $\mu$ l            |
| Primer (A / C) fw ( 100 $\mu$ M)         | 2.5 $\mu$ l          |
| Primer (B / D) rev (100 $\mu$ M)         | 2.5 $\mu$ l          |
| Phusion DNA polymerase                   | 0.5 $\mu$ l          |
| 5 $\times$ Phusion DNA polymerase buffer | 10 $\mu$ l           |
| H <sub>2</sub> O                         | <i>x</i> $\mu$ l     |

Each PCR was performed in a volume of 50  $\mu$ l/reaction.

| Cycles | Time     | Temperature ( $^{\circ}$ C) |
|--------|----------|-----------------------------|
| 1      | 2 min    | 98                          |
| 25     | 10 s     | 98                          |
|        | 30 s     | 55                          |
|        | 45 s     | 72                          |
| 1      | 10 min   | 72                          |
|        | $\infty$ | 4                           |

During the first PCR the fragments AB and CD are generated. Fragments were cleaned by DNA electrophoresis on a 2% agarose gel and purified by the Nucleospin PCR & Gel clean up kit according to the manufacturer's instructions. During the second PCR, the primer products were mixed, to allow the complementary ends of the primer products to hybridize. Then, primers A/D were added, leading to the final PCR product.

| Description                              | Volume/Concentration |
|--|----------------------|
| dNTPs (10 mM)                            | 1 $\mu$ l            |
| Primer product AB                        | 850 ng               |
| Primer product CD                        | 850 ng               |
| Phusion DNA polymerase                   | 0.5 $\mu$ l          |
| 5 $\times$ Phusion DNA polymerase buffer | 10 $\mu$ l           |
| H <sub>2</sub> O                         | <i>x</i> $\mu$ l     |

Reaction volume: 45  $\mu$ l.

| Cycles | Time  | Temperature ( $^{\circ}$ C) |
|--------|-------|-----------------------------|
| 1      | 2 min | 98                          |
| 15     | 10 s  | 98                          |
|        | 30 s  | 60                          |
|        | 45 s  | 72                          |

Add 2.5  $\mu\text{l}$  of primer A and D, respectively.

| Cycles | Time     | Temperature ( $^{\circ}\text{C}$ ) |
|--------|----------|------------------------------------|
| 1      | 2 min    | 98                                 |
| 20     | 10 s     | 98                                 |
|        | 30 s     | 55                                 |
|        | 45 s     | 72                                 |
| 1      | 10 min   | 72                                 |
|        | $\infty$ | 4                                  |

Fragments were cleaned by DNA electrophoresis on a 1% agarose gel and purified by the Nucleospin PCR& Gel clean up kit according to the manufacturer's instructions. Insert and vector DNA was sequentially digested with the restriction endonucleases NotI and BsiWI. Additionally, vector DNA was dephosphorylated. Then, insert and vector were ligated and transformed into DH5 $\alpha$  bacteria.

#### 6.1.4. Bacteria transformation

20  $\mu\text{l}$  of competent bacteria were thawed on ice. Then, 5  $\mu\text{l}$  ligation product or 0.5  $\mu\text{l}$  plasmid DNA was added and incubated for 15 min on ice. Bacteria were heat shocked at 42  $^{\circ}\text{C}$  for 45 s and incubated on ice for 1 min. 150  $\mu\text{l}$  of SOC medium was added and further incubated at 37  $^{\circ}\text{C}$  for 30 min. Then, bacteria were plated on agar plates containing the corresponding antibiotics and incubated overnight at 37  $^{\circ}\text{C}$ . Afterwards, colonies were picked, DNA was isolated and analysed for the insertion of the right DNA fragment by restriction endonuclease digestion and sequencing.

#### 6.1.5. DNA sequencing

Sequencing of DNA constructs was done by the commercial DNA sequencing provider GATC Biotech, Konstanz.

#### 6.1.6. Glycerol stocks

Overnight cultures of transformed bacteria were mixed 3:1 with 80% glycerol and stored at -80 $^{\circ}\text{C}$ .

#### 6.1.7. *In vitro* transcription of HCV RNA

Plasmids encoding the different HCV strains were linearized with SspI, purified by phenol-chloroform extraction and *in vitro* transcribed using the MegaScript T7 kit according to the manufacturer's instructions. RNA quality was controlled by electrophoresis on a 1% agarose gel. RNA concentration was determined by NanoDrop. 10  $\mu\text{g}$  RNA aliquots were stored at -80  $^{\circ}\text{C}$ .

## 6.2. Cell Biological Methods

### 6.2.1. Freeze and thaw of eukaryotic cells

Cells were immediately thawed for 1–2 min in a 37 °C water bath and transferred into a 75 cm<sup>2</sup> cell culture flask and cultured in 10 ml DMEM media over night at 37 °C. The next day, media was exchanged to remove death cells. For freezing, confluent cell culture flasks were trypsinized, centrifuged and re-suspended in  $1 \times 10^6$  cells/ml pre-cooled freezing media. Cells were stored at -80 °C. For longer storage periods, cells were stored in liquid nitrogen.

### 6.2.2. Cultivation of eukaryotic cells

Culturing of cells was performed at 37 °C, 5% CO<sub>2</sub> in a humidified atmosphere (95% relative humidity). Cells were cultured in DMEM media, which was exchanged every 2–3 days. Confluent cell cultures flasks (80%) were washed with PBS, incubated with Trypsin-EDTA for 3–5 min at 37 °C to detach cells, re-suspended in DMEM and split in a 1:5 to 1:10 ratio in a new cell culture flask for further culturing. Cell numbers were counted using a Neubauer counting chamber.

### 6.2.3. Knockout of ANXA3 using the CRISPR/Cas9 system

Clonal ANXA3 knockout cell lines were created using the CRISPR/Cas9 system as described [Ran13]. To knockout ANXA3 using the CRIPR/Cas9 system the target sequence was selected using the online tool on <http://crispr.genome-engineering.org>. The DNA primer encoding the sgRNA sequence was cloned into pSpCas9 (BB)-2A-Puro (PX459). Then pSpCas9 (BB)-2A-Puro (PX459) expressing the sgRNA targeting the ANXA3 locus was transfected into Huh7.5 cells using FuGENE. Clonal cell lines were analyzed by amplification and sequencing of the genomic locus and by RT-qPCR and western blotting.

### 6.2.4. Transfection of eukaryotic cells

#### Transfection of HEK293T cells to produce lentiviral particles

Lentiviral particles were essentially produced as previously described [Nal96].  $6 \times 10^6$  HEK293T cells were seeded in a 150 cm<sup>2</sup> cell culture dish and cultured for 24 h. The next day, 20 µg transfer plasmid, 15 µg packaging plasmid and 6 µg envelop plasmid were mixed with 50 µl CaCl<sub>2</sub> (2.5 M) and  $x$  µl H<sub>2</sub>O to a final volume of 500 µl. The DNA/CaCl<sub>2</sub> suspension was mixed 1:1 with 2×HBS and incubated for 10 min at RT to generate DNA-phosphate complexes. In the meantime, the media from HEK293T cells was replaced by 11 ml DMEM plus chloroquine (25 µM). Then DNA/phosphate complexes were added and incubated for 8 h at 37 °C. Media was replaced by 30 ml fresh DMEM and incubated for 3 days at 37 °C. Media, containing lentiviral particles was harvested, centrifuged, filtered and concentrated using ultracentrifugation for 2 h at 100.000 g. Lentiviral concentrate was aliquoted and stored at -80 °C. Lentiviral transductions were carried out in the presence of 4 µg/ml polybrene for 4 h at 37 °C. Lentiviral transduction efficacies were determined by titration on naïve Huh7.5 cells and analysis by flow cytometry.

#### FuGENE transfection of Huh7-derived cell lines

FuGENE was used to transiently transfect Huh7-derived cell lines with plasmid DNA. FuGENE/DNA were used in a 3:1 ratio, according to the manufacturer's instructions.

## Transfection of Huh7-derived cell lines and production HCV virus stocks

HCV viral stocks were prepared as described [Her10]. Briefly, Huh7.5 cells were trypsinized, washed once in Opti-MEM and re-suspended in cytomix buffer at  $10^7$  cells per ml. 400  $\mu$ l of the cell suspension were mixed with 10  $\mu$ g HCV RNA and pulsed at 260 V and 950  $\mu$ F using the Gene Pulser II. Cells were seeded and incubated for 2–3 h at 37 °C. Then, media was replaced by fresh media and cells were transferred into the BSL-3\*\* lab. Culture supernatant of transfected cells was harvested, filtered, and concentrated by polyethylene glycol precipitation and stored at -80 °C. For infection experiments, naïve Huh7.5 cells were incubated with virus preparations for 4 h at 37 °C.

### 6.2.5. Determination of viral titers (TCID<sub>50</sub>)

Viral titers were calculated by determining the tissue culture infectious dose TCID<sub>50</sub> essentially as described [Lin05]. Huh7.5 cells stably expressing the HCV reporter RFP-NLS-IPS [Jon10a] were seeded in 96-well plates and infected with serial dilutions of culture supernatants or concentrated viral stocks. 3–4 days later, cells were fixed with 4% PFA for 1 h and infection was monitored by translocation of RFP-NLS into the nucleus. To analyze intracellular infectivity, HCV RNA-transfected cells were trypsinized and  $1 \times 10^5$  cells were re-suspended in 1 ml DMEM and lysed by multiple cycles of freeze and thaw. Cell debris was removed by centrifugation for 5 min at 1000 rpm and TCID<sub>50</sub> was determined as described above.

### 6.2.6. HCV infection and viral spreading

To measure HCV spreading  $2 \times 10^5$  naïve or lentiviral-transduced Huh7.5 cells were seeded in 6-well plates, incubated for 24 h at 37 °C, and infected with HCV Jc1 reporter strains. 24 h post infection cells were split 1:3 and seeded into new 6-well plates. At day 2, 4, and 6 post infection cells were harvested and fixed with 4% PFA. Viral spreading was measured by detecting the fluorescent marker proteins by flow cytometry using the LSR Fortessa flow cytometer and analyzed using FlowJo software.

### 6.2.7. Subgenomic HCV replicon assays

For subgenomic replicon assays, cells were electroporated with *in vitro* transcribed replicon RNA as described before. 24 h post transfection cells were seeded in 10 cm cell culture dishes and selected with 1 mg/ml G418. After 3 weeks of selection, cells were fixed with 4% PFA for 20 min and stained with crystal violet.

### 6.2.8. Luciferase HCV replicon assays

To quantify firefly luciferase activity the luciferase assay system was used according to the manufacturer's instructions. Briefly, Huh7.5 cells were electroporated with *in vitro* transcribed  $\Delta$ E1/E2 luciferase replicon RNA as described before. Cells were re-suspended in 13 ml DMEM and seeded in a 12-well plate with 1 ml/well. 4 h, 24 h, 48 h, and 72 h after transfection cells were washed with PBS and lysed with 150  $\mu$ l  $1 \times$  cell culture lysis buffer and stored at -20 °C until all samples were harvested. Afterwards samples were transferred into a 96-well plate and centrifuged for 5 min at 1000 rpm to remove cell debris. Supernatant was transferred into a new 96-well plate. 20  $\mu$ l of sample was mixed with 100  $\mu$ l of luciferase assay reagent and measured

using an Infinite M200 plate reader. In addition, the protein concentration was determined using the DC Protein Assay.

### 6.2.9. MTT viability assay

Cell viability was analysed by using the CellTiter 96<sup>®</sup> AQueous One Solution Cell Proliferation assay according to the manufacturer's instructions.

### 6.2.10. Flow cytometry

Cells were washed with PBS, detached by Trypsin/EDTA treatment and re-suspended in DMEM. Cells were pelleted by centrifugation for 5 min at 1000 rpm. Supernatant was discarded and cells were fixed using 4% PFA. Cells were measured on a LSR Fortessa flow cytometer and analyzed using FlowJo software.

### 6.2.11. Immunofluorescence staining and confocal microscopy

“Cells grown on coverslips were fixed in 4% PFA for 1 h at room temperature, washed with PBS, and permeabilized in 0.1% Triton X-100 or 0.5% saponin for 5 min. After incubation in blocking solution for 1 h, cells were incubated with primary antibodies in blocking solution for 1 h at RT or o/n at 4 °C, washed and incubated with secondary antibodies for 1 h. When cells were permeabilized with saponin, 0.1% saponin was added to the antibody staining solutions. For LD staining, fixed cells were stained for 20 min with BODIPY or LD540, diluted in PBS. Coverslips were embedded in Mowiol mounting medium [Lon93]. CLSM was performed on a Nikon C2+ confocal laser scanning. The Nikon C2+ microscope was equipped with four lasers: a 405 nm diode laser, a 488 nm DPSS laser, a 543 nm HeNe laser and a 642 nm diode laser. A 60× violet corrected oil objective with a NA of 1.4 for imaging (Plan Apo VC 60× H, Nikon) was used. For colocalization analysis coloc2 in Fiji [Sch12] or JACoP in ImageJ was used” [Egg14]. Individual cells of several independent experiments were analyzed and the degree of colocalization was calculated using the Manders' colocalization coefficient and Pearson's correlation coefficient.

### 6.2.12. dSTORM and image analysis

“Datasets for dSTORM were acquired on a custom modified Nikon N-STORM microscope equipped with an Apo TIRF 100× oil immersion objective with a numerical aperture of 1.49 (Nikon), an electron multiplying charge-coupled device (EMCCD) camera and a quadband filter composed of a quad line beamsplitter and a quad line emission filter. For excitation of the fluorophores the following lasers were used: for Alexa Fluor 647 a 647 nm continuous wave visible fiber laser, for LipidTox Red a 150 mW 561 nm optically pumped semiconductor laser, and for Alexa Fluor 488 the 488 nm line of an argon gas laser. A 405 nm diode laser was used for switching back the fluorophores from the dark to the fluorescent state. For multicolour imaging the lasers were switched on and off alternately controlled by an acoustooptic optical tunable filter. The integration time of the EMCCD camera was set to 50–70 ms per frame with an EM gain of 300. The TIRF angle was adjusted to oblique incidence excitation as described [Dem11]. This allowed super-resolution imaging 1–2 μm deep into the sample. The focus was kept stable during acquisition using Nikon's perfect focus system. Super-resolution images were reconstructed from a series of 10,000–15,000 images per channel using the N-STORM analysis module v. 2.0.0.76 of

NIS Elements AR v. 4.00.07 (Laboratory imaging s.r.o.). 3D super-resolution microscopy was performed using an astigmatism-based approach as described [Hua08]. For each color channel a separate 3D calibration curve was used. 3D super-resolution images were visualized using Bit-plane Imaris 7.6.1 software. The imaging was performed in LabTek II chamber slides using an imaging buffer [Dem11] to facilitate a sufficient blinking of the fluorophores.” [Egg14]

### 6.2.13. HCV neutralization assay

Antibody-mediated neutralization of HCV infectivity was determined by using an HCVcc reporter virus expressing secreted Gaussia luciferase (Jc1<sup>p7-GLuc-2A-NS2</sup>) and a Renilla luciferase assay system according to the manufacturer’s instructions. HCV particles were incubated with various antibody concentrations (0.5–50  $\mu\text{g}/\text{ml}$ ) for 1 h at 37 °C and then used to infect naïve Huh7.5 cells. 4 h hours later, cells were washed twice with DMEM and cultured with 100  $\mu\text{l}$  media for 48 h at 37 °C. Afterwards 50  $\mu\text{l}$  of supernatant was inactivated with 50  $\mu\text{l}$  of 2 $\times$  Renilla luciferase lysis buffer for 1h at RT. HCV infection was determined by measuring luciferase activity as described before.

### 6.2.14. LD isolation

LD were isolated as described [Miy07]. Briefly, cells were scraped in PBS, lysed in hypotonic buffer with 30 strokes in a tight-fitting Dounce homogenizer. After spinning for 5 min at 1500 rpm, post-nuclear fractions were mixed with equal volumes of 1.05 M sucrose in isotonic buffer and placed at the bottom of SW60 Ti centrifuge tubes, overlaid with isotonic buffer containing 1 mM PMSF and centrifuged for 2 h at 100,000 g, 4 °C. Proteins from the floating LD fraction were harvested using a bended blunt cannula. LDs were washed in isotonic buffer and centrifuged for 10 min at 21,000 g, 4 °C. The underlying buffer was removed and protein levels were determined by DC Protein assay. For western blot analysis, cells were lysed in RIPA buffer for 30 min on ice, followed by SDS-PAGE and western blotting.

### 6.2.15. SILAC-labeling, HCV-infection, and LD isolation for mass spectrometry

For isotope metabolic protein labeling the SILAC Protein Quantitation kit according to the manufacturer’s instructions was used. Briefly, Huh7.5 cells were cultured in heavy media supplemented with  $^{13}\text{C}_6$  L-lysine-2HCl and  $^{13}\text{C}_6$  L-arginine-HCl or in light media containing L-lysine-2HCl and L-arginine-HCl for at least six passages. Incorporation efficiency was determined by mass spectrometry, using cell lysate separated by SDS-PAGE. Gels were stained with Coomassie blue and analyzed by mass spectrometry. After the incorporation was confirmed, light or heavy Huh7.5 cells were infected with Jc1<sup>NS5AB-mKO2-BSD</sup> or Jc1<sup>NS5AB-eGFP</sup> reporter strains and cultured for two to three weeks. Infection rates were measured by flow cytometry. In one half of the experiments HCV-infected cells were selected with 10  $\mu\text{g}/\text{ml}$  blasticidin for two weeks. One day before LD isolation, equal cell numbers of HCV-infected and control cells were seeded in 150  $\text{cm}^2$  dishes. For LD isolation equal numbers of HCV-infected and control cells were mixed and lysed in sucrose LD-isolation buffer using a Dounce homogenizer. After centrifugation for 5 min at 1000 g, post-nuclear fractions were placed at the bottom of SW60 Ti centrifuge tubes and overlaid with LD wash buffer. After centrifugation for 2 h at 100.000 g, 4 °C, the floating LD fraction was harvested using a bended blunt cannula and again placed in centrifuge tubes,



overlaid with LD wash buffer and centrifuged for 2 h at 100.000 g, 4 °C followed by three washing steps in LD wash buffer to increase the purity. After removal of the washing buffer, LD fractions were mixed with 4× Roti load loading dye and incubated on ice for 1 h. Afterwards, the LD-associated proteins were separated by SDS-PAGE. Gels were stained with RotiBlue and analyzed by mass spectrometry.

### 6.3. Biochemical Methods

#### 6.3.1. Cell lysis

For analysis of whole cell lysates, cells were washed with PBS and lysed using RIPA- or NP40 lysis buffer (supplemented with protease inhibitors) on ice for at least 30 min. Afterwards, cell debris was removed by centrifugation for 10 min at 11.000 g, 4 °C. Protein concentration was determined by DC assay, according to the manufacturer's instructions.

#### 6.3.2. SDS-PAGE and western blotting

Protein samples were mixed with 6× Laemmli buffer, boiled at 95 °C for 5 min and loaded onto a SDS-Polyacrylamid gel. The separation of proteins was performed in SDS running buffer at 180 V for 1 h. Then proteins were transferred onto a nitrocellulose membrane by tank blotting at 80 V for 90 min. Protein transfer was confirmed by staining the membrane with Ponceau S. Unspecific antibody binding was circumvented by blocking the membrane in block buffer at RT for 1 h. Afterwards, the membrane was incubated with primary antibody for 1 h or overnight at 4 °C. The membrane was washed three times in TBS-T to remove non-bound antibody, followed by the incubation with secondary antibody for 1 h at RT. Again, the membrane was washed three times with TBS-T and proteins were detected by chemiluminescence using Lumi-Light or SuperSignal West Femto ECL substrates.

#### 6.3.3. Membrane floatation assay

Membrane floatation assays of subgenomic replicon cells were essentially performed as described [Vog13]. Briefly,  $6 \times 10^6$  of Huh7.5 or Huh7.5 Con1 replicon cells were scraped in PBS, resuspended in 750  $\mu$ l 0.25 M sucrose/PBS supplemented with protease inhibitors and lysed on ice with 50 strokes in a tight-fitting Dounce homogenizer. After spinning for 10 min at 1000 g, the supernatant was transferred into a new tube and protein levels were determined using a DC Protein Assay. 0.75 mg of protein was adjusted in volume to 500  $\mu$ l with 1.05 M sucrose and mixed with 500  $\mu$ l 60% Iodixanol. A discontinuous Iodixanol gradient (20%, 10%) was layered on top of the lysate fraction and centrifuged at 200,000 g for 16 h at 4 °C using a SW60 Ti rotor. From top to bottom eight 500  $\mu$ l fractions were harvested. 40  $\mu$ l of each fraction were analyzed by SDS-PAGE and western blotting. To analyze intracellular ApoE distribution, membrane floatation assays of HCV-infected cells were performed in larger scales. Briefly,  $2 \times 10^6$  of lentiviral transduced Huh7.5 cells were infected with Jc1<sup>Flag-E2-NS5AB-eGFP-BSD</sup> and cultured in media containing 10  $\mu$ g/ml blasticidin for 8 days. Cells were scraped in PBS, resuspended in 1.5 ml 0.25 M sucrose/PBS containing protease inhibitors and lysed on ice with 200 passages in a tight-fitting Dounce homogenizer. Lysates were cleared by centrifugation at 1000 g for 10 min at 4 °C. Supernatants were transferred into a new tube and protein levels were determined using a DC Protein Assay. 3 mg of protein was adjusted to a final volume of 2 ml with sucrose/PBS.

Samples were mixed 1:1 with 2 ml 60% Iodixanol and transferred into a centrifugation tube and overlaid with 4 ml 20% Iodixanol and 4 ml 10% Iodixanol. Gradients were centrifuged at 200,000 g for 16 h at 4 °C using a SW40 rotor. 25 fractions were collected from top to bottom and analyzed by SDS-PAGE and western blotting.

#### 6.3.4. Iodixanol gradient centrifugation

To determine HCV particle density Iodixanol gradient centrifugation was performed as described [Cat13b]. Briefly, Iodixanol gradients were prepared with 6.5 ml of 10% and 6.5 ml of 40% Iodixanol dilutions using a two chamber gradient maker. Supernatant of Jc1<sup>NS5AB-eGFP</sup> transfected cells was centrifuged at 1000 g for 5 min to remove cell debris. 1 ml of supernatant was loaded on top of a gradient and centrifuged at 34,500 rpm for 16 h at 4 °C. From top to bottom twenty 500  $\mu$ l fractions were harvested. The first eleven fractions were used to isolate viral RNA, determine the infectivity (TCID<sub>50</sub>), and the density using a refractometer.

#### 6.3.5. 2D blue native /SDS-PAGE

For 2D blue native SDS-PAGE Huh7.5 cells were transfected with *in vitro* transcribed Jc1<sup>Flag-E2-NS5AB-eGFP-BSD</sup> RNA. 6 days post transfection,  $1 \times 10^6$  cells were washed with PBS and lysed in 80  $\mu$ l lysis native buffer for 30 min on ice. Lysates were centrifuged for 10 min at 14,000 rpm, 4 °C. Supernatants were transferred into a new tube and 1  $\mu$ g/ml pepstatin, 2  $\mu$ g/ml antipain, 20  $\mu$ g/ml leupeptin were added. Samples were mixed with 10  $\mu$ l 5 $\times$  Coomassie blue dye and 40  $\mu$ l of sample was loaded onto a 4–20% polyacrylamide gradient gel and electrophoresis was performed at a constant voltage of 150 V for 2.5 h at 4 °C. For the second dimension, sample lanes from blue native page were cut out and incubated in 2 $\times$  SDS sample buffer for 30 min. After equilibration, blue native page gel stripes were placed horizontally onto a 15% polyacrylamide SDS gel and overlaid with SDS sample buffer. Electrophoresis was performed for 40 min at 200 V. Core complexes were analyzed by western blotting.

#### 6.3.6. Proteinase K digestion protection assay

Proteinase K digestion protection assay was performed as previously described [Gen13]. Briefly, Huh7.5 cells were transfected with *in vitro* transcribed HCV Jc1 RNA and seeded in 6-well plates. 48 h post transfection cells were re-suspended in 170  $\mu$ l proteinase K buffer and lysed by five repeats of freeze and thaw on dry ice. Afterwards the lysate was divided into three 50  $\mu$ l portions. One portion was treated with 100  $\mu$ g/ml proteinase K on ice for 30 min, the second portion was treated with 1% Triton X-100 for 5 min prior to proteinase K digestion, while 50  $\mu$ l was left untreated. Proteinase K digestion was blocked by 5 mM phenylmethanesulfonyl fluoride. Protease protection of core was analyzed by western blotting. Signal intensities reflecting the core levels were quantified using image J.

#### 6.3.7. MTP activity measurement

Total cellular MTP activity was quantified using an MTP activity assay kit according to manufacturer's instructions. Briefly, the cells were washed with PBS and scraped in homogenization buffer. Cells were lysed by sonication and protein levels were determined using a DC Protein assay. 75  $\mu$ g of protein was incubated with 1  $\mu$ l donor and 1  $\mu$ l acceptor particles in 200  $\mu$ l total

volume homogenization buffer for 3–6 h at 37 °C. MTP activity was determined using an Infinite M200 plate reader.

### 6.3.8. Measurement of ApoE/ApoB secretion

$1 \times 10^5$  lentiviral-transduced Huh7.5 cells were seeded in a 12-well plate. To exclude cross-reaction with serum proteins, cells were washed once with Opti-MEM and incubated with Opti-MEM for 18 h at 37 °C. 30  $\mu$ l of the cell culture supernatant was analyzed by SDS-PAGE and western blotting with ApoE and ApoB antibodies. Signal intensities reflecting the ApoE and ApoB levels were quantified using Image J.

### 6.3.9. Quantification of HCV core and ApoE protein by ELISA

The amount of HCV core or ApoE protein was quantified using the Hepatitis C Virus Core Antigen ELISA kit or the Human ApoE ELISA Pro kit, respectively, according to manufacturer's instructions.

### 6.3.10. Co-immunoprecipitation

For co-immunoprecipitation, shRNA-expressing Huh7.5 cells were transfected with HCV RNA. Equal transfection rates were confirmed by flow cytometry. Cells were washed with PBS and lysed with 1 ml NP-40 lysis buffer for 1 h on ice. Afterwards cell debris was removed by centrifugation for 10 min at 11.000 rpm, 4 °C. For capturing Flag-tagged proteins, 1 mg protein was incubated with 30  $\mu$ l of Flag M2 affinity gel for 3 h at 4°C. Beads were then washed five times with ice-cold NP-40 lysis buffer and analyzed by SDS-PAGE and western blotting. For NS5A immunoprecipitation shRNA-expressing Huh7.5 cells were transfected with HCV Jc1<sup>Flag-E2-NS5A-HA</sup> RNA. After washing with PBS cells were lysed with 1 ml low stringency 0.1% NP-40 lysis buffer for 1 h on ice. Cell debris was removed by centrifugation for 10 min at 11.000 rpm, 4 °C. For capturing HA-tagged NS5A, 1 mg protein was incubated with 30  $\mu$ l of HA affinity gel for 3 h at 4°C. Beads were then washed five times with ice-cold 0.1% NP-40 lysis buffer and analyzed by SDS-PAGE and western blotting.

### 6.3.11. Affinity purification of HCV particles

HCV particles were isolated as described previously [Mer11]. Briefly, supernatant of Huh7.5 cells infected with HCV Jc1<sup>Flag-E2-NS5AB-eGFP</sup> was harvested and concentrated by polyethylene glycol 8000 precipitation. Afterwards approx. 30 ml of the concentrate was loaded on top of an Optiprep gradient (60%, 10%, PBS) and centrifuged at 96,281 g for 20 h at 4 °C using an SW28 rotor. Following centrifugation, the 27 ml from top of the gradient were discarded and the remainder of the gradient was harvested in 1 ml fractions. To purify HCV particles, virus preparations obtained from fraction 7 and 8 were incubated with 0.5 ml of Flag M2 affinity gel according to manufacturer's instructions. Samples were analyzed by western blotting.

### 6.3.12. Quantification of cPLA2 activity

The cPLA2 activity was quantified using the cPLA2 Assay kit according to manufacturer's instructions.

### 6.3.13. RNA isolation and quantitative RT-qPCR

Total cellular RNA was isolated using RNA Stat-60 or Tri reagent and treated with the TURBO DNA-free DNase. Viral RNA from the culture supernatant was isolated with the Nucleo-Spin RNA Virus kit. RNA levels were adjusted to carrier RNA input that was added in excess prior to RNA isolation. cDNA was synthesized using Superscript III reverse transcriptase with random hexamer primers, followed by RNase H digestion. For quantitative PCR, the primers listed above from the PrimerBank were used [Wan12] and SYBR green mastermix on a 7900HT Fast Real-time PCR System.

### 6.3.14. Mass spectrometry

Tryptic in-gel digestion was performed as described [She06]. After digestion, samples were evaporated and dissolved in 0.1% formic acid (FA, dissolved in HPLC-H<sub>2</sub>O) for LC-MS/MS-analysis. LC-ESI-MS/MS analyses were performed on a quadrupole-time-of-flight mass spectrometer (Q-TOF Premier) or on a linear trap quadrupole (LTQ) orbitrap mass spectrometer (Orbitrap Fusion). Both instruments were coupled with an ESI-source to a nano-UPLC system (nanoAcquity, Waters; Dionex UltiMate 3000 RSLCnano). LC-ESI-MS/MS analysis on Q-TOF mass spectrometer was performed as described [Kwi15]. For LC-ESI-MS/MS analysis on orbitrap mass spectrometer samples were loaded (5  $\mu$ l/min) on a trapping column (Acclaim PepMap  $\mu$ -precolumn, C18, 300  $\mu$ m  $\times$  5 mm, 5  $\mu$ m, 100 Å; buffer A: 0.1% FA in HPLC-H<sub>2</sub>O; buffer B: 0.1% FA in acetonitrile (ACN)) with 2% buffer B. After sample loading, the trapping column was washed for 5 min with 2% buffer B (5  $\mu$ l/min). The peptides were eluted with a flow-rate of 200 nl/min onto the separation column (nanoAcquity UPLC column, BEH 130 C18, Waters; 75  $\mu$ m  $\times$  250 mm, 1.7  $\mu$ m, 100 Å, custom made, Waters; 200 nl/min, gradient: 2-30% B in 30 min). The spray was generated from a fused-silica emitter (I.D. 10  $\mu$ m) at a capillary voltage of 1700 V. MS/MS measurements were carried out in data dependent acquisition mode (DDA) using top speed mode and a HCD collision energy of 28%. Every second a MS scan was performed over an m/z range from 400-1300, with a resolution of 120000 FWHM at m/z 200 (maximum injection time = 50 ms, AGC target =  $2 \times 10^5$ ). MS/MS spectra were recorded in the ion trap (rapid mode, maximum injection time = 200 ms, AGC target =  $1 \times 10^4$ ).

### 6.3.15. Data analysis

Data from LC-ESI-Q-TOF-MS/MS analysis were analyzed using the open-source software framework OpenMS [Stu08] and the OpenMS Proteomic Pipeline (TOPPAS) [Koh07]. For peptide and protein identification LC-MS/MS raw data was processed as described previously [Kwi15] with the exception that the MS/MS data were searched against a human decoy-database (Swiss-Prot, www.uniprot.org, downloaded November 10, 2014, 20,161). For SILAC quantification the raw data files were converted to \*.mzXML in profile mode using massWolf file converter. Further data processing was carried out with TOPPAS. The \*.mzXML files were converted to \*.mzML. For subsequent data processing the mzML files were filtered (only MS1 level, rt-range (s): 1800-5000) and smoothed (savitsky golay algorithm, frame length: 13, polynomial order: 4). SILAC pairs were detected and quantified using SILACAnalyzer [Nil10] with the following parameters: one missed cleavage, retention time threshold 10 s, intensity cutoff 20 counts, intensity correlation 0.7 and a model deviation of 1.8. A peptide required at least three isotopic peaks and maximal seven isotopic peaks to be taken into account by the SILACAnalyzer. Detected SILAC pairs were exported as \*.consensusXML and matched with peptide identifications (\*idXML) using

IDMapper (retention time tolerance: 10 s, m/z-tolerance: 1 Da). Results were exported as \*.csv and further statistical processing was carried out using mathematica. Only unique peptides were taken into account for SILAC quantification.

The LC-MS/MS data from orbitrap analysis were processed with MaxQuant version 1.5.2.8 [Cox08]. Peptide and protein identification was carried out with Andromeda against a human (Swiss-Prot, [www.uniprot.org](http://www.uniprot.org), downloaded November 10, 2014, 20,161) and a contaminant database (cRAP-database, <http://www.thegpm.org/crap>, 298 entries). The search was performed with a tolerance of 6 ppm on MS- and 0.6 Da on MS/MS-level. Carbamidomethylation was considered as a static modification on cysteine residues. Oxidation on methionine as well as  $^{13}\text{C}_6$ -label on lysine and arginine were considered as variable modifications. The search was performed with a false discovery rate (FDR) of 0.01 on both peptide and protein level. SILAC quantification was carried out with MaxQuant [Cox09], wherein only unique peptides were taken into account for SILAC quantification. To correct for different cell numbers or numbers of LDs the detection ratios of light over heavy peptides (L/H) or vice versa in swapped labeling conditions (H/L) were centered by dividing through the median of the identified proteins as described [Tin09]. Of note, under the used cell culture conditions no significant LD accumulation upon infection with Jc1-based HCV constructs was detected. To rule out any bias the MS data were additionally normalized to PLIN2/ADRP levels and similar results were generated. Normalizing quantitative MS data to the median is however preferable [Tin09].

### 6.3.16. Bioinformatics and statistical analysis

For bioinformatics and statistical analysis R [Tea15a], RStudio [Tea15b], and GraphPadPrism (GraphPad Software, Inc) was used. Data was analyzed and plotted using gdata [Wt15a], lattice [Sar08], gplots [Wt15b], and ggplot2 [Wic09] packages. Statistical analysis of overlaps with other HCV screens was performed using GeneOverlap [She13]. For automated PubMed searches we used RISMED [Kov15], MyGene for ID conversion [Mar14], and cisPath for protein network analysis and visualization [Wan15]. The gProfileR package for gene ontology annotation analysis with a p-value cutoff of 0.05 and “strong” hierarchical filtering was used [Rei15]. Statistical analysis was performed using unpaired two-tailed student’s *t*-test and in case of normalized data one sample *t*-test.

# Bibliography

- [Ama11] Y. Amako, G. H. Syed, and A. Siddiqui. *Protein kinase d negatively regulates hepatitis c virus secretion through phosphorylation of oxysterol-binding protein and ceramide transfer protein*. J Biol Chem **286**, 11265–74 (2011).
- [Ari07] Y. Ariumi, M. Kuroki, K. Abe, H. Dansako, M. Ikeda, T. Wakita, and N. Kato. *Ddx3 dead-box rna helicase is required for hepatitis c virus rna replication*. J Virol **81**, 13922–6 (2007).
- [Aro16] S. Arora, W. Lim, P. Bist, R. Perumalsamy, H. M. Lukman, F. Li, L. B. Welker, B. Yan, G. Sethi, P. A. Tambyah, A. M. Fairhurst, S. Alonso, and L. H. Lim. *Influenza a virus enhances its propagation through the modulation of annexin-a1 dependent endosomal trafficking and apoptosis*. Cell Death Differ **23**, 1243–56 (2016).
- [Bac10] P. Backes, D. Quinkert, S. Reiss, M. Binder, M. Zayas, U. Rescher, V. Gerke, R. Bartenschlager, and V. Lohmann. *Role of annexin a2 in the production of infectious hepatitis c virus particles*. J Virol **84**, 5775–89 (2010).
- [Bar03] B. Bartosch, J. Dubuisson, and F. L. Cosset. *Infectious hepatitis c virus pseudo-particles containing functional e1-e2 envelope protein complexes*. Journal of Experimental Medicine **197**, 633–642 (2003).
- [Bar06] H. Barth, E. K. Schnober, F. Zhang, R. J. Linhardt, E. Depla, B. Boson, F. L. Cosset, A. H. Patel, H. E. Blum, and T. F. Baumert. *Viral and cellular determinants of the hepatitis c virus envelope-heparan sulfate interaction*. J Virol **80**, 10579–90 (2006).
- [Bar13] R. Bartenschlager, V. Lohmann, and F. Penin. *The molecular and structural basis of advanced antiviral therapy for hepatitis c virus infection*. Nat Rev Microbiol **11**, 482–96 (2013).
- [Bat07] M. Bates, B. Huang, G. T. Dempsey, and X. Zhuang. *Multicolor super-resolution imaging with photo-switchable fluorescent probes*. Science **317**, 1749–53 (2007).
- [Ben10] W. J. Benga, S. E. Krieger, M. Dimitrova, M. B. Zeisel, M. Parnot, J. Lupberger, E. Hildt, G. Luo, J. McLauchlan, T. F. Baumert, and C. Schuster. *Apolipoprotein e interacts with hepatitis c virus nonstructural protein 5a and determines assembly of infectious particles*. Hepatology **51**, 43–53 (2010).
- [Ber14] F. Berri, G. Haffar, V. B. Le, A. Sadewasser, K. Paki, B. Lina, T. Wolff, and B. Riteau. *Annexin v incorporated into influenza virus particles inhibits gamma interferon signaling and promotes viral replication*. J Virol **88**, 11215–28 (2014).
- [Bes07] O. Beske, M. Reichelt, M. P. Taylor, K. Kirkegaard, and R. Andino. *Poliovirus infection blocks ergic-to-golgi trafficking and induces microtubule-dependent disruption of the golgi complex*. J Cell Sci **120**, 3207–18 (2007).

- [BF05] N. L. Benali-Furet, M. Chami, L. Houel, F. De Giorgi, F. Vernejoul, D. Lagorce, L. Buscail, R. Bartenschlager, F. Ichas, R. Rizzuto, and P. Paterlini-Brechot. *Hepatitis c virus core triggers apoptosis in liver cells by inducing er stress and er calcium depletion*. *Oncogene* **24**, 4921–4933 (2005).
- [Bis12] B. Bishe, G. H. Syed, S. J. Field, and A. Siddiqui. *Role of phosphatidylinositol 4-phosphate (pi4p) and its binding protein golph3 in hepatitis c virus secretion*. *J Biol Chem* **287**, 27637–47 (2012).
- [Bli02] K. J. Blight, J. A. McKeating, and C. M. Rice. *Highly permissive cell lines for subgenomic and genomic hepatitis c virus rna replication*. *Journal of Virology* **76**, 13001–13014 (2002).
- [Bou05] S. Boulant, C. Vanbelle, C. Ebel, F. Penin, and J. P. Lavergne. *Hepatitis c virus core protein is a dimeric alpha-helical protein exhibiting membrane protein features*. *J Virol* **79**, 11353–65 (2005).
- [Bra00] D. L. Brasaemle, B. Rubin, I. A. Harten, J. Gruia-Gray, A. R. Kimmel, and C. Londos. *Perilipin a increases triacylglycerol storage by decreasing the rate of triacylglycerol hydrolysis*. *Journal of Biological Chemistry* **275**, 38486–93 (2000).
- [Bra04] M. Brajenovic, G. Joberty, B. Kuster, T. Bouwmeester, and G. Drewes. *Comprehensive proteomic analysis of human par protein complexes reveals an interconnected protein network*. *J Biol Chem* **279**, 12804–11 (2004).
- [Buh01] K. K. Buhman, H. C. Chen, and Jr. Farese, R. V. *The enzymes of neutral lipid synthesis*. *J Biol Chem* **276**, 40369–72 (2001).
- [Bul09] A. V. Bulankina, A. Deggerich, D. Wenzel, K. Mutenda, J. G. Wittmann, M. G. Rudolph, K. N. Burger, and S. Honing. *Tip47 functions in the biogenesis of lipid droplets*. *J Cell Biol* **185**, 641–55 (2009).
- [Cam13] G. Camus, E. Herker, A. A. Modi, J. T. Haas, H. R. Ramage, Jr. Farese, R. V., and M. Ott. *Diacylglycerol acyltransferase-1 localizes hepatitis c virus ns5a protein to lipid droplets and enhances ns5a interaction with the viral capsid core*. *J Biol Chem* **288**, 9915–23 (2013).
- [Cam14] G. Camus, M. Schweiger, E. Herker, C. Harris, A. S. Kondratowicz, C. L. Tsou, Jr. Farese, R. V., K. Herath, S. F. Previs, T. P. Roddy, S. Pinto, R. Zechner, and M. Ott. *The hepatitis c virus core protein inhibits adipose triglyceride lipase (atgl)-mediated lipid mobilization and enhances the atgl interaction with comparative gene identification 58 (cgi-58) and lipid droplets*. *J Biol Chem* **289**, 35770–80 (2014).
- [Car12] F. A. Carvalho, F. A. Carneiro, I. C. Martins, I. Assuncao-Miranda, A. F. Faustino, R. M. Pereira, P. T. Bozza, M. A. Castanho, R. Mohana-Borges, A. T. Da Poian, and N. C. Santos. *Dengue virus capsid protein binding to hepatic lipid droplets (ld) is potassium ion dependent and is mediated by ld surface proteins*. *J Virol* **86**, 2096–108 (2012).
- [Cat13a] M. T. Catanese, J. Loureiro, C. T. Jones, M. Dorner, T. von Hahn, and C. M. Rice. *Different requirements for scavenger receptor class b type i in hepatitis c virus cell-free versus cell-to-cell transmission*. *J Virol* **87**, 8282–93 (2013).

- [Cat13b] M. T. Catanese, K. Uryu, M. Kopp, T. J. Edwards, L. Andrus, W. J. Rice, M. Silvestry, R. J. Kuhn, and C. M. Rice. *Ultrastructural analysis of hepatitis c virus particles*. Proc Natl Acad Sci U S A **110**, 9505–10 (2013).
- [Cat15] M. T. Catanese and M. Dorner. *Advances in experimental systems to study hepatitis c virus in vitro and in vivo*. Virology **479-480**, 221–33 (2015).
- [Che10] W. Cheung, M. Gill, A. Esposito, C. F. Kaminski, N. Courousse, S. Chwetzoff, G. Trugnan, N. Keshavan, A. Lever, and U. Desselberger. *Rotaviruses associate with cellular lipid droplet components to replicate in viroplasm, and compounds disrupting or blocking lipid droplets inhibit viroplasm formation and viral replication*. Journal of Virology **84**, 6782–98 (2010).
- [Cho89] Q. L. Choo, G. Kuo, A. J. Weiner, L. R. Overby, D. W. Bradley, and M. Houghton. *Isolation of a cDNA clone derived from a blood-borne non-a, non-b viral hepatitis genome*. Science **244**, 359–62 (1989).
- [Cho00] G. J. Choukroun, V. Marshansky, C. E. Gustafson, M. McKee, R. J. Hajjar, A. Rosenzweig, D. Brown, and J. V. Bonventre. *Cytosolic phospholipase a(2) regulates golgi structure and modulates intracellular trafficking of membrane proteins*. J Clin Invest **106**, 983–93 (2000).
- [Cho04] J. Choi, K. J. Lee, Y. Zheng, A. K. Yamaga, M. M. Lai, and J. H. Ou. *Reactive oxygen species suppress hepatitis c virus rna replication in human hepatoma cells*. Hepatology **39**, 81–9 (2004).
- [Cho15] N. J. Cho, C. Lee, P. S. Pang, E. A. Pham, B. Fram, K. Nguyen, A. Xiong, E. H. Sklan, M. Elazar, E. S. Koytak, C. Kersten, K. K. Kanazawa, C. W. Frank, and J. S. Glenn. *Phosphatidylinositol 4,5-bisphosphate is an hcv ns5a ligand and mediates replication of the viral genome*. Gastroenterology **148**, 616–25 (2015).
- [Chu08] R. T. Chung, Jr. Gale, M., S. J. Polyak, S. M. Lemon, T. J. Liang, and J. H. Hoofnagle. *Mechanisms of action of interferon and ribavirin in chronic hepatitis c: Summary of a workshop*. Hepatology **47**, 306–20 (2008).
- [Cof06] C. M. Coffey, A. Sheh, I. S. Kim, K. Chandran, M. L. Nibert, and J. S. Parker. *Reovirus outer capsid protein micro1 induces apoptosis and associates with lipid droplets, endoplasmic reticulum, and mitochondria*. Journal of Virology **80**, 8422–38 (2006).
- [Col10] T. S. Collier, P. Sarkar, W. L. Franck, B. M. Rao, R. A. Dean, and D. C. Muddiman. *Direct comparison of stable isotope labeling by amino acids in cell culture and spectral counting for quantitative proteomics*. Anal Chem **82**, 8696–702 (2010).
- [Col12] K. E. Collier, N. S. Heaton, K. L. Berger, J. D. Cooper, J. L. Saunders, and G. Randall. *Molecular determinants and dynamics of hepatitis c virus secretion*. PLoS Pathogens **8**, e1002466 (2012).
- [Cou11] N. A. Counihan, S. M. Rawlinson, and B. D. Lindenbach. *Trafficking of hepatitis c virus core protein during virus particle assembly*. PLoS Pathogens **7**, e1002302 (2011).



- [Cox08] J. Cox and M. Mann. *Maxquant enables high peptide identification rates, individualized p.p.b.-range mass accuracies and proteome-wide protein quantification*. *Nat Biotechnol* **26**, 1367–72 (2008).
- [Cox09] J. Cox, I. Matic, M. Hilger, N. Nagaraj, M. Selbach, J. V. Olsen, and M. Mann. *A practical guide to the maxquant computational platform for silac-based quantitative proteomics*. *Nat Protoc* **4**, 698–705 (2009).
- [Cox15] A. L. Cox. *Medicine. global control of hepatitis c virus*. *Science* **349**, 790–1 (2015).
- [Cun10] W. Cun, J. Jiang, and G. Luo. *The c-terminal alpha-helix domain of apolipoprotein e is required for interaction with nonstructural protein 5a and assembly of hepatitis c virus*. *J Virol* **84**, 11532–41 (2010).
- [Dem11] G. T. Dempsey, J. C. Vaughan, K. H. Chen, M. Bates, and X. Zhuang. *Evaluation of fluorophores for optimal performance in localization-based super-resolution imaging*. *Nature Methods* **8**, 1027–36 (2011).
- [Dia10] D. L. Diamond, A. J. Syder, J. M. Jacobs, C. M. Sorensen, K. A. Walters, S. C. Proll, J. E. McDermott, M. A. Gritsenko, Q. Zhang, R. Zhao, T. O. Metz, 2nd Camp, D. G., K. M. Waters, R. D. Smith, C. M. Rice, and M. G. Katze. *Temporal proteome and lipidome profiles reveal hepatitis c virus-associated reprogramming of hepatocellular metabolism and bioenergetics*. *PLoS Pathog* **6**, e1000719 (2010).
- [Dor13] M. Dorner, J. A. Horwitz, B. M. Donovan, R. N. Labitt, W. C. Budell, T. Friling, A. Vogt, M. T. Catanese, T. Satoh, T. Kawai, S. Akira, M. Law, C. M. Rice, and A. Ploss. *Completion of the entire hepatitis c virus life cycle in genetically humanized mice*. *Nature* **501**, 237–41 (2013).
- [Dre09] M. Dreux and F. L. Cosset. *Detection of neutralizing antibodies with hcv pseudoparticles (hcvpp)*. *Methods Mol Biol* **510**, 427–38 (2009).
- [Dre12] M. Dreux, U. Garaigorta, B. Boyd, E. Decembre, J. Chung, C. Whitten-Bauer, S. Wieland, and F. V. Chisari. *Short-range exosomal transfer of viral rna from infected cells to plasmacytoid dendritic cells triggers innate immunity*. *Cell Host Microbe* **12**, 558–70 (2012).
- [DT12] V. L. Dao Thi, C. Granier, M. B. Zeisel, M. Guerin, J. Mancip, O. Granio, F. Penin, D. Lavillette, R. Bartenschlager, T. F. Baumert, F. L. Cosset, and M. Dreux. *Characterization of hepatitis c virus particle subpopulations reveals multiple usage of the scavenger receptor bi for entry steps*. *J Biol Chem* **287**, 31242–57 (2012).
- [Egg14] D. Eggert, K. Rösch, R. Reimer, and E. Herker. *Visualization and analysis of hepatitis c virus structural proteins at lipid droplets by super-resolution microscopy*. *PLoS One* **9**, e102511 (2014).
- [Eva07] M. J. Evans, T. von Hahn, D. M. Tscherne, A. J. Syder, M. Panis, B. Wolk, T. Hatziioannou, J. A. McKeating, P. D. Bieniasz, and C. M. Rice. *Claudin-1 is a hepatitis c virus co-receptor required for a late step in entry*. *Nature* **446**, 801–805 (2007).
- [Far09] Jr. Farese, R. V. and T. C. Walther. *Lipid droplets finally get a little r-e-s-p-e-c-t*. *Cell* **139**, 855–60 (2009).

- [Far12] M. J. Farquhar, K. Hu, H. J. Harris, C. Davis, C. L. Brimacombe, S. J. Fletcher, T. F. Baumert, J. Z. Rappoport, P. Balfe, and J. A. McKeating. *Hepatitis c virus induces cd81 and claudin-1 endocytosis*. *J Virol* **86**, 4305–16 (2012).
- [Flo13] B. Flottmann, M. Gunkel, T. Lisauskas, M. Heilemann, V. Starkuviene, J. Reymann, and H. Erfle. *Correlative light microscopy for high-content screening*. *BioTechniques* **55**, 243–52 (2013).
- [Fri01] P. Friebe, V. Lohmann, N. Krieger, and R. Bartenschlager. *Sequences in the 5' non-translated region of hepatitis c virus required for rna replication*. *J.Virol.* **75**, 12047–12057 (2001).
- [Fri05] P. Friebe, J. Boudet, J. P. Simorre, and R. Bartenschlager. *Kissing-loop interaction in the 3' end of the hepatitis c virus genome essential for rna replication*. *J.Virol.* **79**, 380–392 (2005).
- [Gas08] P. Gastaminza, G. Cheng, S. Wieland, J. Zhong, W. Liao, and F. V. Chisari. *Cellular determinants of hepatitis c virus assembly, maturation, degradation, and secretion*. *J Virol* **82**, 2120–9 (2008).
- [Gas10] P. Gastaminza, K. A. Dryden, B. Boyd, M. R. Wood, M. Law, M. Yeager, and F. V. Chisari. *Ultrastructural and biophysical characterization of hepatitis c virus particles produced in cell culture*. *J Virol* **84**, 10999–1009 (2010).
- [Ge09] D. Ge, J. Fellay, A. J. Thompson, J. S. Simon, K. V. Shianna, T. J. Urban, E. L. Heinzen, P. Qiu, A. H. Bertelsen, A. J. Muir, M. Sulkowski, J. G. McHutchison, and D. B. Goldstein. *Genetic variation in il28b predicts hepatitis c treatment-induced viral clearance*. *Nature* **461**, 399–401 (2009).
- [Gen13] J. Gentsch, C. Brohm, E. Steinmann, M. Friesland, N. Menzel, G. Vieyres, P. M. Perin, A. Frentzen, L. Kaderali, and T. Pietschmann. *hepatitis c virus p7 is critical for capsid assembly and envelopment*. *PLoS Pathog* **9**, e1003355 (2013).
- [Ger02] V. Gerke and S. E. Moss. *Annexins: from structure to function*. *Physiol Rev* **82**, 331–71 (2002).
- [Gon01] G. Gong, G. Waris, R. Tanveer, and A. Siddiqui. *Human hepatitis c virus ns5a protein alters intracellular calcium levels, induces oxidative stress, and activates stat-3 and nf-kappa b*. *Proc Natl Acad Sci U S A* **98**, 9599–604 (2001).
- [Gul03] D. Gully, D. Moinier, L. Loiseau, and E. Bouveret. *New partners of acyl carrier protein detected in escherichia coli by tandem affinity purification*. *FEBS Lett* **548**, 90–6 (2003).
- [Har08] M. Harashima, K. Harada, Y. Ito, M. Hyuga, T. Seki, T. Ariga, T. Yamaguchi, and S. Niimi. *Annexin a3 expression increases in hepatocytes and is regulated by hepatocyte growth factor in rat liver regeneration*. *J Biochem* **143**, 537–45 (2008).
- [Har10] H. J. Harris, C. Davis, J. G. Mullins, K. Hu, M. Goodall, M. J. Farquhar, C. J. Mee, K. McCaffrey, S. Young, H. Drummer, P. Balfe, and J. A. McKeating. *Claudin association with cd81 defines hepatitis c virus entry*. *J Biol Chem* **285**, 21092–102 (2010).

- [Har11] C. Harris, E. Herker, Jr. Farese, R. V., and M. Ott. *Hepatitis c virus core protein decreases lipid droplet turnover: a mechanism for core-induced steatosis*. *J Biol Chem* **286**, 42615–25 (2011).
- [Hei10] M. Heilemann. *Fluorescence microscopy beyond the diffraction limit*. *J Biotechnol* **149**, 243–51 (2010).
- [Hen08] J. I. Henke, D. Goergen, J. Zheng, Y. Song, C. G. Schuttler, C. Fehr, C. Junemann, and M. Niepmann. *microrna-122 stimulates translation of hepatitis c virus rna*. *EMBO J* **27**, 3300–10 (2008).
- [Her10] E. Herker, C. Harris, C. Hernandez, A. Carpentier, K. Kaehlcke, A. R. Rosenberg, Jr. Farese, R. V., and M. Ott. *Efficient hepatitis c virus particle formation requires diacylglycerol acyltransferase-1*. *Nat Med* **16**, 1295–8 (2010).
- [Hir15] H. Hiramoto, H. Dansako, M. Takeda, S. Satoh, T. Wakita, M. Ikeda, and N. Kato. *Annexin a1 negatively regulates viral rna replication of hepatitis c virus*. *Acta Med Okayama* **69**, 71–8 (2015).
- [Hsi12] K. Hsieh, Y. K. Lee, C. Londos, B. M. Raaka, K. T. Dalen, and A. R. Kimmel. *Perilipin family members preferentially sequester to either triacylglycerol-specific or cholesteryl-ester-specific intracellular lipid storage droplets*. *J Cell Sci* **125**, 4067–76 (2012).
- [Hsu03] M. Hsu, J. Zhang, M. Flint, C. Logvinoff, C. Cheng-Mayer, C. M. Rice, and J. A. McKeating. *Hepatitis c virus glycoproteins mediate ph-dependent cell entry of pseudotyped retroviral particles*. *Proceedings of the National Academy of Sciences of the United States of America* **100**, 7271–7276 (2003).
- [Hua07] H. Huang, F. Sun, D. M. Owen, W. P. Li, Y. Chen, M. Gale, and J. Ye. *Hepatitis c virus production by human hepatocytes dependent on assembly and secretion of very low-density lipoproteins*. *Proceedings of the National Academy of Sciences of the United States of America* **104**, 5848–5853 (2007).
- [Hua08] B. Huang, W. Wang, M. Bates, and X. Zhuang. *Three-dimensional super-resolution imaging by stochastic optical reconstruction microscopy*. *Science* **319**, 810–3 (2008).
- [Hus12] M. M. Hussain, P. Rava, M. Walsh, M. Rana, and J. Iqbal. *Multiple functions of microsomal triglyceride transfer protein*. *Nutr Metab (Lond)* **9**, 14 (2012).
- [Jia12] J. Jiang, W. Cun, X. Wu, Q. Shi, H. Tang, and G. Luo. *Hepatitis c virus attachment mediated by apolipoprotein e binding to cell surface heparan sulfate*. *J Virol* **86**, 7256–67 (2012).
- [Jir10] V. Jirasko, R. Montserret, J. Y. Lee, J. Gouttenoire, D. Moradpour, F. Penin, and R. Bartenschlager. *Structural and functional studies of nonstructural protein 2 of the hepatitis c virus reveal its key role as organizer of virion assembly*. *PLoS Pathogens* **6**, e1001233 (2010).
- [Jon10a] C. T. Jones, M. T. Catanese, L. M. Law, S. R. Khetani, A. J. Syder, A. Ploss, T. S. Oh, J. W. Schoggins, M. R. MacDonald, S. N. Bhatia, and C. M. Rice. *Real-time imaging of hepatitis c virus infection using a fluorescent cell-based reporter system*. *Nat Biotechnol* **28**, 167–71 (2010).

- [Jon10b] D. M. Jones and J. McLauchlan. *Hepatitis c virus: assembly and release of virus particles*. J Biol Chem **285**, 22733–9 (2010).
- [Jop05] C. L. Jopling, M. Yi, A. M. Lancaster, S. M. Lemon, and P. Sarnow. *Modulation of hepatitis c virus rna abundance by a liver-specific microRNA*. Science **309**, 1577–81 (2005).
- [Kao16] C. C. Kao, G. Yi, and H. C. Huang. *The core of hepatitis c virus pathogenesis*. Curr Opin Virol **17**, 66–73 (2016).
- [Kim01] S. Kim, J. Ko, J. H. Kim, E. C. Choi, and D. S. Na. *Differential effects of annexins i, ii, iii, and v on cytosolic phospholipase a2 activity: specific interaction model*. FEBS Lett **489**, 243–8 (2001).
- [Kim02] Y. K. Kim, C. S. Kim, S. H. Lee, and S. K. Jang. *Domains i and ii in the 5' nontranslated region of the hcv genome are required for rna replication*. Biochem Biophys Res Commun **290**, 105–12 (2002).
- [Kis13] J. J. Kiser and C. Flexner. *Direct-acting antiviral agents for hepatitis c virus infection*. Annu Rev Pharmacol Toxicol **53**, 427–49 (2013).
- [Klu11] J. Klumperman. *Architecture of the mammalian golgi*. Cold Spring Harb Perspect Biol **3** (2011).
- [Koh07] O. Kohlbacher, K. Reinert, C. Gropl, E. Lange, N. Pfeifer, O. Schulz-Trieglaff, and M. Sturm. *Topp—the openms proteomics pipeline*. Bioinformatics **23**, e191–7 (2007).
- [Koh14] A. Kohli, A. Shaffer, A. Sherman, and S. Kottlilil. *Treatment of hepatitis c: a systematic review*. JAMA **312**, 631–40 (2014).
- [Kov15] S. Kovalchik. *Rismed: Download content from ncbi databases*. (2015).
- [Kue08] L. Kuerschner, C. Moessinger, and C. Thiele. *Imaging of lipid biosynthesis: how a neutral lipid enters lipid droplets*. Traffic **9**, 338–52 (2008).
- [Kwi15] M. Kwiatkowski, M. Wurlitzer, M. Omid, L. Ren, S. Kruber, R. Nimer, W. D. Robertson, A. Horst, R. J. Miller, and H. Schluter. *Ultrafast extraction of proteins from tissues using desorption by impulsive vibrational excitation*. Angew Chem Int Ed Engl **54**, 285–8 (2015).
- [Lac15] D. H. Lackner, A. Carre, P. M. Guzzardo, C. Banning, R. Mangena, T. Henley, S. Oberndorfer, B. V. Gapp, S. M. Nijman, T. R. Brummelkamp, and T. Burckstummer. *A generic strategy for crispr-cas9-mediated gene tagging*. Nat Commun **6**, 10237 (2015).
- [Lai15] R. F. Laine, A. Albecka, S. van de Linde, E. J. Rees, C. M. Crump, and C. F. Kaminski. *Structural analysis of herpes simplex virus by optical super-resolution imaging*. Nat Commun **6**, 5980 (2015).
- [Lav11] D. Lavanchy. *Evolving epidemiology of hepatitis c virus*. Clin Microbiol Infect **17**, 107–15 (2011).

- [Laz07] C. A. Lazaro, M. Chang, W. Tang, J. Campbell, D. G. Sullivan, D. R. Gretch, L. Corey, R. W. Coombs, and N. Fausto. *Hepatitis c virus replication in transfected and serum-infected cultured human fetal hepatocytes*. *Am J Pathol* **170**, 478–89 (2007).
- [Lea06] G. Leandro, A. Mangia, J. Hui, P. Fabris, L. Rubbia-Brandt, G. Colloredo, L. E. Adinolfi, T. Asselah, J. R. Jonsson, A. Smedile, N. Terrault, V. Paziienza, M. T. Giordani, E. Giostra, A. Sonzogni, G. Ruggiero, P. Marcellin, E. E. Powell, J. George, F. Negro, and H. C. V. Meta-Analysis Individual Patients' Data Study Group. *Relationship between steatosis, inflammation, and fibrosis in chronic hepatitis c: a meta-analysis of individual patient data*. *Gastroenterology* **130**, 1636–42 (2006).
- [Leb85] J. S. Lebkowski, S. Clancy, and M. P. Calos. *Simian virus 40 replication in adenovirus-transformed human cells antagonizes gene expression*. *Nature* **317**, 169–71 (1985).
- [Lee14] J. Y. Lee, E. G. Acosta, I. K. Stoeck, G. Long, M. S. Hiet, B. Mueller, O. T. Fackler, S. Kallis, and R. Bartenschlager. *Apolipoprotein e likely contributes to a maturation step of infectious hepatitis c virus particles and interacts with viral envelope glycoproteins*. *J Virol* **88**, 12422–37 (2014).
- [Li09] Q. Li, A. L. Brass, A. Ng, Z. Hu, R. J. Xavier, T. J. Liang, and S. J. Elledge. *A genome-wide genetic screen for host factors required for hepatitis c virus propagation*. *Proc Natl Acad Sci U S A* **106**, 16410–5 (2009).
- [Li11] Y. Li. *The tandem affinity purification technology: an overview*. *Biotechnol Lett* **33**, 1487–99 (2011).
- [Li13] Q. Li, V. Pene, S. Krishnamurthy, H. Cha, and T. J. Liang. *Hepatitis c virus infection activates an innate pathway involving ikk-alpha in lipogenesis and viral assembly*. *Nature Medicine* **19**, 722–9 (2013).
- [Lia15] C. C. Liao, Y. L. Lin, and C. F. Kuo. *Effect of high-fat diet on hepatic proteomics of hamsters*. *J Agric Food Chem* **63**, 1869–81 (2015).
- [Lin05] B. D. Lindenbach and C. M. Rice. *Unravelling hepatitis c virus replication from genome to function*. *Nature* **436**, 933–938 (2005).
- [Lin06] B. D. Lindenbach, P. Meuleman, A. Ploss, T. Vanwolleghem, A. J. Syder, J. A. McKeating, R. E. Lanford, S. M. Feinstone, M. E. Major, G. Leroux-Roels, and C. M. Rice. *Cell culture-grown hepatitis c virus is infectious in vivo and can be recultured in vitro*. *Proceedings of the National Academy of Sciences of the United States of America* **103**, 3805–3809 (2006).
- [Lin13] B. D. Lindenbach and C. M. Rice. *The ins and outs of hepatitis c virus entry and assembly*. *Nat Rev Microbiol* **11**, 688–700 (2013).
- [Lis07] L. L. Listenberger, A. G. Ostermeyer-Fay, E. B. Goldberg, W. J. Brown, and D. A. Brown. *Adipocyte differentiation-related protein reduces the lipid droplet association of adipose triglyceride lipase and slows triacylglycerol turnover*. *Journal of Lipid Research* **48**, 2751–61 (2007).

- [Liu12] L. Liu, B. E. Fisher, D. L. Thomas, A. L. Cox, and S. C. Ray. *Spontaneous clearance of primary acute hepatitis c virus infection correlated with high initial viral rna level and rapid hvr1 evolution*. *Hepatology* **55**, 1684–91 (2012).
- [LM14] U. Loizides-Mangold, S. Clement, A. Alfonso-Garcia, E. Branche, S. Conzelmann, C. Parisot, E. O. Potma, H. Riezman, and F. Negro. *Hcv 3a core protein increases lipid droplet cholesteryl ester content via a mechanism dependent on sphingolipid biosynthesis*. *PLoS One* **9**, e115309 (2014).
- [Loh99] V. Lohmann, F. Korner, J. Koch, U. Herian, L. Theilmann, and R. Bartenschlager. *Replication of subgenomic hepatitis c virus rnas in a hepatoma cell line*. *Science* **285**, 110–113 (1999).
- [Loh14] V. Lohmann and R. Bartenschlager. *On the history of hepatitis c virus cell culture systems*. *J Med Chem* **57**, 1627–42 (2014).
- [Lon93] A. Longin, C. Souchier, M. Ffrench, and P. A. Bryon. *Comparison of anti-fading agents used in fluorescence microscopy: image analysis and laser confocal microscopy study*. *J Histochem Cytochem* **41**, 1833–40 (1993).
- [Loz03] P. Y. Lozach, H. Lortat-Jacob, A. de Lacroix de Lavalette, I. Staropoli, S. Foug, A. Amara, C. Houles, F. Fieschi, O. Schwartz, J. L. Virelizier, F. Arenzana-Seisdedos, and R. Altmeyer. *Dc-sign and l-sign are high affinity binding receptors for hepatitis c virus glycoprotein e2*. *J Biol Chem* **278**, 20358–66 (2003).
- [Lup11] J. Lupberger, M. B. Zeisel, F. Xiao, C. Thumann, I. Fofana, L. Zona, C. Davis, C. J. Mee, M. Turek, S. Gorke, C. Royer, B. Fischer, M. N. Zahid, D. Lavillette, J. Fresquet, F. L. Cosset, S. M. Rothenberg, T. Pietschmann, A. H. Patel, P. Pessaux, M. Doffoel, W. Raffelsberger, O. Poch, J. A. McKeating, L. Brino, and T. F. Baumert. *Egfr and epha2 are host factors for hepatitis c virus entry and possible targets for antiviral therapy*. *Nature Medicine* **17**, 589–95 (2011).
- [Lus16] M. Lussignol, M. Kopp, K. Molloy, G. Vizcay-Barrena, R. A. Fleck, M. Dorner, K. L. Bell, B. T. Chait, C. M. Rice, and M. T. Catanese. *Proteomics of hcv virions reveals an essential role for the nucleoporin nup98 in virus morphogenesis*. *Proc Natl Acad Sci U S A* **113**, 2484–9 (2016).
- [Lyn14] R. K. Lyn, R. Singaravelu, S. Kargman, S. O’Hara, H. Chan, R. Oballa, Z. Huang, D. M. Jones, A. Ridsdale, R. S. Russell, A. W. Partridge, and J. P. Pezacki. *Stearoyl-coa desaturase inhibition blocks formation of hepatitis c virus-induced specialized membranes*. *Sci Rep* **4**, 4549 (2014).
- [Mag13] M. Maglione and S. J. Sigrist. *Seeing the forest tree by tree: super-resolution light microscopy meets the neurosciences*. *Nat Neurosci* **16**, 790–7 (2013).
- [Man06] M. Mann. *Functional and quantitative proteomics using silac*. *Nat Rev Mol Cell Biol* **7**, 952–8 (2006).
- [Man13] M. P. Manns and T. von Hahn. *Novel therapies for hepatitis c - one pill fits all?* *Nat Rev Drug Discov* **12**, 595–610 (2013).

- [Mar06] S. Martin and R. G. Parton. *Lipid droplets: a unified view of a dynamic organelle*. Nat Rev Mol Cell Biol **7**, 373–8 (2006).
- [Mar08] S. Marukian, C. T. Jones, L. Andrus, M. J. Evans, K. D. Ritola, E. D. Charles, C. M. Rice, and L. B. Dustin. *Cell culture-produced hepatitis c virus does not infect peripheral blood mononuclear cells*. Hepatology **48**, 1843–50 (2008).
- [Mar13] D. N. Martin and S. L. Uprichard. *Identification of transferrin receptor 1 as a hepatitis c virus entry factor*. Proc Natl Acad Sci U S A **110**, 10777–82 (2013).
- [Mar14] A. Mark, R. Thompson, and C. Wu. *mygene: Access mygene.info\_services* (2014).
- [Mas08] T. Masaki, R. Suzuki, K. Murakami, H. Aizaki, K. Ishii, A. Murayama, T. Date, Y. Matsuura, T. Miyamura, T. Wakita, and T. Suzuki. *Interaction of hepatitis c virus nonstructural protein 5a with core protein is critical for the production of infectious virus particles*. J Virol **82**, 7964–76 (2008).
- [Mat11a] M. Matto, E. H. Sklan, N. David, N. Melamed-Book, J. E. Casanova, J. S. Glenn, and B. Aroeti. *Role for adp ribosylation factor 1 in the regulation of hepatitis c virus replication*. Journal of Virology **85**, 946–56 (2011).
- [Mat11b] K. A. Mattos, V. G. Oliveira, H. D’Avila, L. S. Rodrigues, R. O. Pinheiro, E. N. Sarno, M. C. Pessolani, and P. T. Bozza. *Tlr6-driven lipid droplets in mycobacterium leprae-infected schwann cells: Immunoinflammatory platforms associated with bacterial persistence*. Journal of Immunology **187**, 2548–58 (2011).
- [ME16] J. Modaresi Esfeh and K. Ansari-Gilani. *Steatosis and hepatitis c*. Gastroenterol Rep (Oxf) **4**, 24–9 (2016).
- [Men12] N. Menzel, W. Fischl, K. Hueging, D. Bankwitz, A. Frentzen, S. Haid, J. Gentzsch, L. Kaderali, R. Bartenschlager, and T. Pietschmann. *Map-kinase regulated cytosolic phospholipase a2 activity is essential for production of infectious hepatitis c virus particles*. PLoS Pathog **8**, e1002829 (2012).
- [Mer11] A. Merz, G. Long, M. S. Hiet, B. Brugger, P. Chlanda, P. Andre, F. Wieland, J. Krijnse-Locker, and R. Bartenschlager. *Biochemical and morphological properties of hepatitis c virus particles and determination of their lipidome*. J Biol Chem **286**, 3018–32 (2011).
- [Mer13] L. W. Meredith, H. J. Harris, G. K. Wilson, N. F. Fletcher, P. Balfe, and J. A. McKeating. *Early infection events highlight the limited transmissibility of hepatitis c virus in vitro*. J Hepatol **58**, 1074–80 (2013).
- [Mes15] J. P. Messina, I. Humphreys, A. Flaxman, A. Brown, G. S. Cooke, O. G. Pybus, and E. Barnes. *Global distribution and prevalence of hepatitis c virus genotypes*. Hepatology **61**, 77–87 (2015).
- [Meu05] P. Meuleman, L. Libbrecht, R. De Vos, B. de Hemptinne, K. Gevaert, J. Vandekerckhove, T. Roskams, and G. Leroux-Roels. *Morphological and biochemical characterization of a human liver in a upa-scid mouse chimera*. Hepatology **41**, 847–56 (2005).

- [Meu08] P. Meuleman and G. Leroux-Roels. *The human liver-upa-scid mouse: a model for the evaluation of antiviral compounds against hbv and hcv*. *Antiviral Res* **80**, 231–8 (2008).
- [Mir16] M. Mirsaeidi, S. Gidfar, A. Vu, and D. Schraufnagel. *Annexins family: insights into their functions and potential role in pathogenesis of sarcoidosis*. *J Transl Med* **14**, 89 (2016).
- [Miy07] Y. Miyanari, K. Atsuzawa, N. Usuda, K. Watashi, T. Hishiki, M. Zayas, R. Bartenschlager, T. Wakita, M. Hijikata, and K. Shimotohno. *The lipid droplet is an important organelle for hepatitis c virus production*. *Nat Cell Biol* **9**, 1089–97 (2007).
- [Mor97] K. Moriya, H. Yotsuyanagi, Y. Shintani, H. Fujie, K. Ishibashi, Y. Matsuura, T. Miyamura, and K. Koike. *Hepatitis c virus core protein induces hepatic steatosis in transgenic mice*. *Journal of General Virology* **78** ( Pt 7), 1527–1531 (1997).
- [Mou14] A. Mousnier, D. Swieboda, A. Pinto, A. Guedan, A. V. Rogers, R. Walton, S. L. Johnston, and R. Solari. *Human rhinovirus 16 causes golgi apparatus fragmentation without blocking protein secretion*. *J Virol* **88**, 11671–85 (2014).
- [Mur13] W. Muranyi, S. Malkusch, B. Muller, M. Heilemann, and H. G. Krausslich. *Super-resolution microscopy reveals specific recruitment of hiv-1 envelope proteins to viral assembly sites dependent on the envelope c-terminal tail*. *PLoS Pathog* **9**, e1003198 (2013).
- [Nak82] H. Nakabayashi, K. Taketa, K. Miyano, T. Yamane, and J. Sato. *Growth of human hepatoma cells lines with differentiated functions in chemically defined medium*. *Cancer Res* **42**, 3858–63 (1982).
- [Nal96] L. Naldini, U. Blomer, P. Gally, D. Ory, R. Mulligan, F. H. Gage, I. M. Verma, and D. Trono. *In vivo gene delivery and stable transduction of nondividing cells by a lentiviral vector*. *Science* **272**, 263–7 (1996).
- [Nas13] N. Naseri, M. Joyce, Y. Rouleau, P. Yang, S. Yao, D. L. Tyrrell, and J. P. Pezacki. *Modulation of fatty acid synthase enzyme activity and expression during hepatitis c virus replication*. *Chem Biol* **20**, 570–82 (2013).
- [Nev12] G. Neveu, R. Barouch-Bentov, A. Ziv-Av, D. Gerber, Y. Jacob, and S. Einav. *Identification and targeting of an interaction between a tyrosine motif within hepatitis c virus core protein and ap2m1 essential for viral assembly*. *PLoS Pathog* **8**, e1002845 (2012).
- [Nil10] Lars Nilse, Marc Sturm, David Trudgian, Mogjiborahman Salek, Paul F G. Sims, Kathleen M Carroll, and Simon J Hubbard. *SILAC Analyzer - A Tool for Differential Quantitation of Stable Isotope Derived Data*, Vol. 6160 of *Lecture Notes in Computer Science*, book section 4, S. 45–55. Springer Berlin Heidelberg, 2010.
- [Ohs05] Y. Ohsaki, Y. T. Maeda, and T. T. Fujimoto. *Fixation and permeabilization protocol is critical for the immunolabeling of lipid droplet proteins*. *Histochem. Cell Biol.* 445–452 (2005).
- [Ohs06] Y. Ohsaki, J. Cheng, A. Fujita, T. Tokumoto, and T. Fujimoto. *Cytoplasmic lipid droplets are sites of convergence of proteasomal and autophagic degradation of apolipoprotein b*. *Mol Biol Cell* **17**, 2674–83 (2006).



- [Pan15] Q. Z. Pan, K. Pan, Q. J. Wang, D. S. Weng, J. J. Zhao, H. X. Zheng, X. F. Zhang, S. S. Jiang, L. Lv, Y. Tang, Y. Q. Li, J. He, Q. Liu, C. L. Chen, H. X. Zhang, and J. C. Xia. *Annexin a3 as a potential target for immunotherapy of liver cancer stem-like cells*. *Stem Cells* **33**, 354–66 (2015).
- [Pau14] D. Paul, V. Madan, and R. Bartenschlager. *Hepatitis c virus rna replication and assembly: living on the fat of the land*. *Cell Host Microbe* **16**, 569–79 (2014).
- [Paw04] J. M. Pawlotsky. *Pathophysiology of hepatitis c virus infection and related liver disease*. *Trends Microbiol* **12**, 96–102 (2004).
- [Per02] G. Perlemuter, A. Sabile, P. Letteron, G. Vona, A. Topilco, Y. Chretien, K. Koike, D. Pessayre, J. Chapman, G. Barba, and C. Brechot. *Hepatitis c virus core protein inhibits microsomal triglyceride transfer protein activity and very low density lipoprotein secretion: a model of viral-related steatosis*. *FASEB Journal* **16**, 185–194 (2002).
- [Per12] C. F. Pereira, J. Rossy, D. M. Owen, J. Mak, and K. Gaus. *Hiv taken by storm: super-resolution fluorescence microscopy of a viral infection*. *Virology Journal* **9**, 84 (2012).
- [Pey08] P. Peyron, J. Vaubourgeix, Y. Poquet, F. Levillain, C. Botanch, F. Bardou, M. Daffe, J. F. Emile, B. Marchou, P. J. Cardona, C. de Chastellier, and F. Altare. *Foamy macrophages from tuberculous patients’ granulomas constitute a nutrient-rich reservoir for m. tuberculosis persistence*. *PLoS Pathog* **4**, e1000204 (2008).
- [Pfa14] S. Pfaender, R. J. Brown, T. Pietschmann, and E. Steinmann. *Natural reservoirs for homologs of hepatitis c virus*. *Emerg Microbes Infect* **3**, e21 (2014).
- [Pie06] T. Pietschmann, A. Kaul, G. Koutsoudakis, A. Shavinskaya, S. Kallis, E. Steinmann, K. Abid, F. Negro, M. Dreux, F. L. Cosset, and R. Bartenschlager. *Construction and characterization of infectious intragenotypic and intergenotypic hepatitis c virus chimeras*. *Proceedings of the National Academy of Sciences of the United States of America* **103**, 7408–13 (2006).
- [Plo10] A. Ploss, S. R. Khetani, C. T. Jones, A. J. Syder, K. Trehan, V. A. Gaysinskaya, K. Mu, K. Ritola, C. M. Rice, and S. N. Bhatia. *Persistent hepatitis c virus infection in microscale primary human hepatocyte cultures*. *Proc Natl Acad Sci U S A* **107**, 3141–5 (2010).
- [Poe15] M. Poenisch, P. Metz, H. Blankenburg, A. Ruggieri, J. Y. Lee, D. Rupp, I. Rebhan, K. Diederich, L. Kaderali, F. S. Domingues, M. Albrecht, V. Lohmann, H. Erfle, and R. Bartenschlager. *Identification of hnrnpk as regulator of hepatitis c virus particle production*. *PLoS Pathog* **11**, e1004573 (2015).
- [Poh03] S. Pohlmann, J. Zhang, F. Baribaud, Z. Chen, G. J. Leslie, G. Lin, A. Granelli-Piperno, R. W. Doms, C. M. Rice, and J. A. McKeating. *Hepatitis c virus glycoproteins interact with dc-sign and dc-signr*. *J Virol* **77**, 4070–80 (2003).
- [Pol04] R. S. Polishchuk and A. A. Mironov. *Structural aspects of golgi function*. *Cell Mol Life Sci* **61**, 146–58 (2004).

- [Pop11] C. I. Popescu, N. Callens, D. Trinel, P. Roingeard, D. Moradpour, V. Descamps, G. Duverlie, F. Penin, L. Heliot, Y. Rouille, and J. Dubuisson. *Ns2 protein of hepatitis c virus interacts with structural and non-structural proteins towards virus assembly*. PLoS Pathog **7**, e1001278 (2011).
- [Pow11] M. H. Powdrill, E. P. Tchesnokov, R. A. Kozak, R. S. Russell, R. Martin, E. S. Svarovskaia, H. Mo, R. D. Kouyos, and M. Gotte. *Contribution of a mutational bias in hepatitis c virus replication to the genetic barrier in the development of drug resistance*. Proc Natl Acad Sci U S A **108**, 20509–13 (2011).
- [Pre11] J. Prentoe and J. Bukh. *Hepatitis c virus expressing flag-tagged envelope protein 2 has unaltered infectivity and density, is specifically neutralized by flag antibodies and can be purified by affinity chromatography*. Virology **409**, 148–55 (2011).
- [Qui10] C. A. Quiner and W. T. Jackson. *Fragmentation of the golgi apparatus provides replication membranes for human rhinovirus 1a*. Virology **407**, 185–95 (2010).
- [Rab16] S. Rabhi, I. Rabhi, B. Trentin, D. Piquemal, B. Regnault, S. Goyard, T. Lang, A. Descoteaux, J. Enninga, and L. Guizani-Tabbane. *Lipid droplet formation, their localization and dynamics during leishmania major macrophage infection*. PLoS One **11**, e0148640 (2016).
- [Ram15] H. R. Ramage, G. R. Kumar, E. Verschueren, J. R. Johnson, J. Von Dollen, T. Johnson, B. Newton, P. Shah, J. Horner, N. J. Krogan, and M. Ott. *A combined proteomics/genomics approach links hepatitis c virus infection with nonsense-mediated mrna decay*. Mol Cell **57**, 329–40 (2015).
- [Ran13] F. A. Ran, P. D. Hsu, J. Wright, V. Agarwala, D. A. Scott, and F. Zhang. *Genome engineering using the crispr-cas9 system*. Nat Protoc **8**, 2281–308 (2013).
- [Ray04] P. S. Ray and S. Das. *Inhibition of hepatitis c virus ires-mediated translation by small rnas analogous to stem-loop structures of the 5'-untranslated region*. Nucleic Acids Res **32**, 1678–87 (2004).
- [Rei15] J. Reimand, R. Kolde, and T. Arak. *gprofiler: Interface to the 'g:profiler' toolkit*. (2015.).
- [Res04] U. Rescher and V. Gerke. *Annexins—unique membrane binding proteins with diverse functions*. J Cell Sci **117**, 2631–9 (2004).
- [Rig99] G. Rigaut, A. Shevchenko, B. Rutz, M. Wilm, M. Mann, and B. Seraphin. *A generic protein purification method for protein complex characterization and proteome exploration*. Nat Biotechnol **17**, 1030–2 (1999).
- [Ros03] A. Rosengarth and H. Luecke. *A calcium-driven conformational switch of the n-terminal and core domains of annexin a1*. J Mol Biol **326**, 1317–25 (2003).
- [Rou12] K. J. Roux, D. I. Kim, M. Raida, and B. Burke. *A promiscuous biotin ligase fusion protein identifies proximal and interacting proteins in mammalian cells*. J Cell Biol **196**, 801–10 (2012).

- [Sai12] Jr. Sainz, B., N. Barretto, D. N. Martin, N. Hiraga, M. Imamura, S. Hussain, K. A. Marsh, X. Yu, K. Chayama, W. A. Alrefai, and S. L. Uprichard. *Identification of the niemann-pick c1-like 1 cholesterol absorption receptor as a new hepatitis c virus entry factor*. *Nat Med* **18**, 281–5 (2012).
- [Sak05] H. Sakamoto, K. Okamoto, M. Aoki, H. Kato, A. Katsume, A. Ohta, T. Tsukuda, N. Shimma, Y. Aoki, M. Arisawa, M. Kohara, and M. Sudoh. *Host sphingolipid biosynthesis as a target for hepatitis c virus therapy*. *Nat Chem Biol* **1**, 333–7 (2005).
- [Sak15] H. A. Saka, J. W. Thompson, Y. S. Chen, L. G. Dubois, J. T. Haas, A. Moseley, and R. H. Valdivia. *Chlamydia trachomatis infection leads to defined alterations to the lipid droplet proteome in epithelial cells*. *PLoS One* **10**, e0124630 (2015).
- [Sam09] M. M. Samsa, J. A. Mondotte, N. G. Iglesias, I. Assuncao-Miranda, G. Barbosa-Lima, A. T. Da Poian, P. T. Bozza, and A. V. Gamarnik. *Dengue virus capsid protein usurps lipid droplets for viral particle formation*. *PLoS Pathogens* **5**, e1000632 (2009).
- [Sar08] D. Sarkar. *Lattice: Multivariate Data Visualization with R*. Springer, New York, 2008.
- [Sat06] S. Sato, M. Fukasawa, Y. Yamakawa, T. Natsume, T. Suzuki, I. Shoji, H. Aizaki, T. Miyamura, and M. Nishijima. *Proteomic profiling of lipid droplet proteins in hepatoma cell lines expressing hepatitis c virus core protein*. *J. Biochem.* **139**, 921–930 (2006).
- [Sax12] V. Saxena, C. K. Lai, T. C. Chao, K. S. Jeng, and M. M. Lai. *Annexin a2 is involved in the formation of hepatitis c virus replication complex on the lipid raft*. *J Virol* **86**, 4139–50 (2012).
- [Sch07] T. Schaller, N. Appel, G. Koutsoudakis, S. Kallis, V. Lohmann, T. Pietschmann, and R. Bartenschlager. *Analysis of hepatitis c virus superinfection exclusion by using novel fluorochrome gene-tagged viral genomes*. *J Virol* **81**, 4591–603 (2007).
- [Sch12] J. Schindelin, I. Arganda-Carreras, E. Frise, V. Kaynig, M. Longair, T. Pietzsch, S. Preibisch, C. Rueden, S. Saalfeld, B. Schmid, J. Y. Tinevez, D. J. White, V. Hartenstein, K. Eliceiri, P. Tomancak, and A. Cardona. *Fiji: an open-source platform for biological-image analysis*. *Nat Methods* **9**, 676–82 (2012).
- [Sha07] A. Shavinskaya, S. Boulant, F. Penin, J. McLauchlan, and R. Bartenschlager. *The lipid droplet binding domain of hepatitis c virus core protein is a major determinant for efficient virus assembly*. *J. Biol. Chem.* **282**, 37158–69 (2007).
- [Sha11] N. R. Sharma, G. Mateu, M. Dreux, A. Grakoui, F. L. Cosset, and G. B. Melikyan. *Hepatitis c virus is primed by cd81 protein for low ph-dependent fusion*. *J Biol Chem* **286**, 30361–76 (2011).
- [She06] A. Shevchenko, H. Tomas, J. Havlis, J. V. Olsen, and M. Mann. *In-gel digestion for mass spectrometric characterization of proteins and proteomes*. *Nat Protoc* **1**, 2856–60 (2006).
- [She13] L. Shen. *Geneoverlap: Test and visualize gene overlaps*. (2013).







- [Shi02] S. T. Shi, S. J. Polyak, H. Tu, D. R. Taylor, D. R. Gretch, and M. M. Lai. *Hepatitis c virus ns5a colocalizes with the core protein on lipid droplets and interacts with apolipoproteins*. *Virology* **292**, 198–210 (2002).
- [Shi12] T. Shimakami, D. Yamane, R. K. Jangra, B. J. Kempf, C. Spaniel, D. J. Barton, and S. M. Lemon. *Stabilization of hepatitis c virus rna by an ago2-mir-122 complex*. *Proc Natl Acad Sci U S A* **109**, 941–6 (2012).
- [Sim05] P. Simmonds, J. Bukh, C. Combet, G. Deleage, N. Enomoto, S. Feinstone, P. Halfon, G. Inchauspe, C. Kuiken, G. Maertens, M. Mizokami, D. G. Murphy, H. Okamoto, J. M. Pawlotsky, F. Penin, E. Sablon, I. T. Shin, L. J. Stuyver, H. J. Thiel, S. Viazov, A. J. Weiner, and A. Widell. *Consensus proposals for a unified system of nomenclature of hepatitis c virus genotypes*. *Hepatology* **42**, 962–73 (2005).
- [Sol94] E. Solito, S. Nuti, and L. Parente. *Dexamethasone-induced translocation of lipocortin (annexin) 1 to the cell membrane of u-937 cells*. *Br J Pharmacol* **112**, 347–8 (1994).
- [Spa09] J. Spandl, D. J. White, J. Peychl, and C. Thiele. *Live cell multicolor imaging of lipid droplets with a new dye, ld540*. *Traffic* **10**, 1579–84 (2009).
- [Stu08] M. Sturm, A. Bertsch, C. Gropl, A. Hildebrandt, R. Hussong, E. Lange, N. Pfeifer, O. Schulz-Trieglaff, A. Zerck, K. Reinert, and O. Kohlbacher. *Openms - an open-source software framework for mass spectrometry*. *BMC Bioinformatics* **9**, 163 (2008).
- [Sum05] Jr. Sumpster, R., Y. M. Loo, E. Foy, K. Li, M. Yoneyama, T. Fujita, S. M. Lemon, and Jr. Gale, M. *Regulating intracellular antiviral defense and permissiveness to hepatitis c virus rna replication through a cellular rna helicase, rig-i*. *Journal of Virology* **79**, 2689–99 (2005).
- [Sun15] V. Sundaramoorthy, J. M. Sultana, and J. D. Atkin. *Golgi fragmentation in amyotrophic lateral sclerosis, an overview of possible triggers and consequences*. *Front Neurosci* **9**, 400 (2015).
- [Swe02] D. A. Sweeney, A. Siddhanta, and D. Shields. *Fragmentation and re-assembly of the golgi apparatus in vitro. a requirement for phosphatidic acid and phosphatidylinositol 4,5-bisphosphate synthesis*. *J Biol Chem* **277**, 3030–9 (2002).
- [Sy06] T. Sy and M. M. Jamal. *Epidemiology of hepatitis c virus (hcv) infection*. *Int J Med Sci* **3**, 41–6 (2006).
- [Sye10] G. H. Syed, Y. Amako, and A. Siddiqui. *Hepatitis c virus hijacks host lipid metabolism*. *Trends in endocrinology and metabolism* **21**, 33–40 (2010).
- [Tai09] A. W. Tai, Y. Benita, L. F. Peng, S. S. Kim, N. Sakamoto, R. J. Xavier, and R. T. Chung. *A functional genomic screen identifies cellular cofactors of hepatitis c virus replication*. *Cell Host Microbe* **5**, 298–307 (2009).
- [Tan95] M. Tanaka, R. Gupta, and B. J. Mayer. *Differential inhibition of signaling pathways by dominant-negative sh2/sh3 adapter proteins*. *Mol Cell Biol* **15**, 6829–37 (1995).
- [Tea15a] R Core Team. *A language and environment for statistical computing*. (2015). R Foundation for Statistical Computing. <http://www.R-project.org>.

- [Tea15b] RStudio Team. *Rstudio: Integrated development environment for r*. (2015).
- [Tho13] E. Thomas, M. G. Ghany, and T. J. Liang. *The application and mechanism of action of ribavirin in therapy of hepatitis c*. *Antivir Chem Chemother* **23**, 1–12 (2013).
- [Tin06] P. Tingting, F. Caiyun, Y. Zhigang, Y. Pengyuan, and Y. Zhenghong. *Subproteomic analysis of the cellular proteins associated with the 3' untranslated region of the hepatitis c virus genome in human liver cells*. *Biochem Biophys Res Commun* **347**, 683–91 (2006).
- [Tin09] L. Ting, M. J. Cowley, S. L. Hoon, M. Guilhaus, M. J. Raftery, and R. Cavicchioli. *Normalization and statistical analysis of quantitative proteomics data generated by metabolic labeling*. *Mol Cell Proteomics* **8**, 2227–42 (2009).
- [Tol16] D. A. Toledo, H. D'Avila, and R. C. Melo. *Host lipid bodies as platforms for intracellular survival of protozoan parasites*. *Front Immunol* **7**, 174 (2016).
- [Ton15] M. Tong, T. M. Fung, S. T. Luk, K. Y. Ng, T. K. Lee, C. H. Lin, J. W. Yam, K. W. Chan, F. Ng, B. J. Zheng, Y. F. Yuan, D. Xie, C. M. Lo, K. Man, X. Y. Guan, and S. Ma. *Anxa3/jnk signaling promotes self-renewal and tumor growth, and its blockade provides a therapeutic target for hepatocellular carcinoma*. *Stem Cell Reports* **5**, 45–59 (2015).
- [vdL11] S. van de Linde, A. Loschberger, T. Klein, M. Heidbreder, S. Wolter, M. Heilemann, and M. Sauer. *Direct stochastic optical reconstruction microscopy with standard fluorescent probes*. *Nature Protocols* **6**, 991–1009 (2011).
- [Vel16] A. P. Velazquez, T. Tatsuta, R. Ghillebert, I. Drescher, and M. Graef. *Lipid droplet-mediated er homeostasis regulates autophagy and cell survival during starvation*. *J Cell Biol* **212**, 621–31 (2016).
- [Vie10] G. Vieyres, X. Thomas, V. Descamps, G. Duverlie, A. H. Patel, and J. Dubuisson. *Characterization of the envelope glycoproteins associated with infectious hepatitis c virus*. *J Virol* **84**, 10159–68 (2010).
- [Vil97] S. A. Villano, D. Vlahov, K. E. Nelson, C. M. Lyles, S. Cohn, and D. L. Thomas. *Incidence and risk factors for hepatitis c among injection drug users in baltimore, maryland*. *J Clin Microbiol* **35**, 3274–7 (1997).
- [Vog13] D. A. Vogt, G. Camus, E. Herker, B. R. Webster, C. L. Tsou, W. C. Greene, T. S. Yen, and M. Ott. *Lipid droplet-binding protein tip47 regulates hepatitis c virus rna replication through interaction with the viral ns5a protein*. *PLoS Pathog* **9**, e1003302 (2013).
- [Wak05] T. Wakita, T. Pietschmann, T. Kato, T. Date, M. Miyamoto, Z. J. Zhao, K. Murthy, A. Habermann, H. G. Krausslich, M. Mizokami, R. Bartenschlager, and T. J. Liang. *Production of infectious hepatitis c virus in tissue culture from a cloned viral genome*. *Nat. Med.* **11**, 791–796 (2005).
- [Wan12] X. Wang, A. Spandidos, H. Wang, and B. Seed. *Primerbank: a pcr primer database for quantitative gene expression analysis, 2012 update*. *Nucleic Acids Res* **40**, D1144–9 (2012).

- [Wan15] L. Wang. *cispath: Visualization and management of the protein-protein interaction networks*. (2015).
- [Wat12] T. Watanabe, Y. Ito, A. Sato, T. Hosono, S. Niimi, T. Ariga, and T. Seki. *Annexin a3 as a negative regulator of adipocyte differentiation*. *J Biochem* **152**, 355–63 (2012).
- [Web08] K. Weber, U. Bartsch, C. Stocking, and B. Fehse. *A multicolor panel of novel lentiviral "gene ontology" (lego) vectors for functional gene analysis*. *Mol Ther* **16**, 698–706 (2008).
- [Web13a] B. Webster, M. Ott, and W. C. Greene. *Evasion of superinfection exclusion and elimination of primary viral rna by an adapted strain of hepatitis c virus*. *J Virol* **87**, 13354–69 (2013).
- [Web13b] B. Webster, S. Wissing, E. Herker, M. Ott, and W. C. Greene. *Rapid intracellular competition between hepatitis c viral genomes as a result of mitosis*. *J Virol* **87**, 581–96 (2013).
- [Wed15] H. Wedemeyer, G. J. Dore, and J. W. Ward. *Estimates on hcv disease burden worldwide - filling the gaps*. *J Viral Hepat* **22 Suppl 1**, 1–5 (2015).
- [Wei09] S. Weinlich, S. Huttelmaier, A. Schierhorn, S. E. Behrens, A. Ostareck-Lederer, and D. H. Ostareck. *Igf2bp1 enhances hcv ires-mediated translation initiation via the 3'utr*. *RNA* **15**, 1528–42 (2009).
- [Wel15] M. A. Welte. *Expanding roles for lipid droplets*. *Curr Biol* **25**, R470–81 (2015).
- [Wic09] H. Wickham. *ggplot2: elegant graphics for data analysis*. Springer, New York, 2009.
- [Wil14a] F. Wilfling, J. T. Haas, T. C. Walther, and Jr. Farese, R. V. *Lipid droplet biogenesis*. *Curr Opin Cell Biol* **29**, 39–45 (2014).
- [Wil14b] F. Wilfling, A. R. Thiam, M. J. Olarte, J. Wang, R. Beck, T. J. Gould, E. S. Allgeyer, F. Pincet, J. Bewersdorf, Jr. Farese, R. V., and T. C. Walther. *Arf1/copi machinery acts directly on lipid droplets and enables their connection to the er for protein targeting*. *Elife* **3**, e01607 (2014).
- [Wis11] S. Wissing, M. Montano, J. L. Garcia-Perez, J. V. Moran, and W. C. Greene. *Endogenous apobec3b restricts line-1 retrotransposition in transformed cells and human embryonic stem cells*. *J Biol Chem* **286**, 36427–37 (2011).
- [Wt15a] G. R. Warnes et al. *gdata: Various r programming tools for data manipulation*. (2015).
- [Wt15b] G. R. Warnes et al. *gplots: Various r programming tools for plotting data* (2015).
- [Wu13] N. Wu, S. Liu, C. Guo, Z. Hou, and M. Z. Sun. *The role of annexin a3 playing in cancers*. *Clin Transl Oncol* **15**, 106–10 (2013).
- [Xia14] F. Xiao, I. Fofana, L. Heydmann, H. Barth, E. Soulier, F. Habersetzer, M. Doffoel, J. Bukh, A. H. Patel, M. B. Zeisel, and T. F. Baumert. *Hepatitis c virus cell-cell transmission and resistance to direct-acting antiviral agents*. *PLoS Pathog* **10**, e1004128 (2014).













- [Xu12] S. Xu, R. Pei, M. Guo, Q. Han, J. Lai, Y. Wang, C. Wu, Y. Zhou, M. Lu, and X. Chen. *Cytosolic phospholipase a2 gamma is involved in hepatitis c virus replication and assembly*. J Virol **86**, 13025–37 (2012).
- [Yan05] W. Yan and S. S. Chen. *Mass spectrometry-based quantitative proteomic profiling*. Brief Funct Genomic Proteomic **4**, 27–38 (2005).
- [Zay16] M. Zayas, G. Long, V. Madan, and R. Bartenschlager. *Coordination of hepatitis c virus assembly by distinct regulatory regions in nonstructural protein 5a*. PLoS Pathog **12**, e1005376 (2016).
- [Zha16] J. Zhang, D. Nguyen, and K. Q. Hu. *Chronic hepatitis c virus infection: A review of current direct-acting antiviral treatment strategies*. N Am J Med Sci (Boston) **9**, 47–54 (2016).
- [Zon13] L. Zona, J. Lupberger, N. Sidahmed-Adrar, C. Thumann, H. J. Harris, A. Barnes, J. Florentin, R. G. Tawar, F. Xiao, M. Turek, S. C. Durand, F. H. Duong, M. H. Heim, F. L. Cosset, I. Hirsch, D. Samuel, L. Brino, M. B. Zeisel, F. Le Naour, J. A. McKeating, and T. F. Baumert. *Hras signal transduction promotes hepatitis c virus cell entry by triggering assembly of the host tetraspanin receptor complex*. Cell Host Microbe **13**, 302–13 (2013).








# A. Toxicity of chemicals

| Chemical                  | GHS hazard pictograms   | GHS hazard statements                                       | GHS precautionary statements   |
|---------------------------|---|---|--|
| 1,4-Dithiothreitol        |    | H302<br>H315<br>H319<br>H412                                | P264<br>P270<br>P280<br>P302<br>P352<br>P305 + P351 + P338                             |
| 2-Mercaptoethanol         |   | H301 + H331<br>H310<br>H315<br>H317<br>H318<br>H373<br>H410 | P261<br>P280<br>P301 + P310 + P330<br>P302 + P352 + P310<br>P305 + P351 + P338<br>P310 |
| 2-Propanol                |  | H225<br>H319<br>H336  | P210<br>P305 + P351 + P338<br>P261   |
| Acetic acid               |  | H226<br>H314  | P280<br>P305 + P351 + P338<br>P310   |
| Acetonitrile              |  | H225<br>H332<br>H302<br>H312<br>H319                        | P210<br>P261<br>P280<br>P305 + P351 + P338<br>P370 + P378<br>P403 + P235               |
| Acrylamide:bis-acrylamide |  | H302<br>H312<br>H315<br>H319                                | P260<br>P280<br>P281<br>P305 + P351 + P338   |
















A. Toxicity of chemicals




|                             |  |   |  |
|-----------------------------|--|---|--|
|                             |  | H317<br>H340<br>H350<br>H361f<br>H372                         | P405<br>P501   |
| Blasticidin S               |   | H300  | P264<br>P301 + P310  |
| Calcium chloride            |   | H319  | P264<br>P280<br>P305 + P351 + P338<br>P337 + P313                                      |
| Chloroform                  |    | H302<br>H315<br>H319<br>H331<br>H336<br>H351<br>H361d<br>H372 | P201<br>P261<br>P304 + P340 + P311<br>P305 + P351 + P338<br>P308 + P313<br>P403 + P233 |
| Crystal violet              |   <br> | H351<br>H302<br>H318<br>H410                                  | P273<br>P280<br>P305 + P351 + P338<br>P501   |
| Dodecyl sulfate sodium salt |     | H228<br>H302 + H332<br>H315<br>H318<br>H335<br>H412           | P210<br>P261<br>P273<br>P305 + P351 + P338   |
| EDTA                        |   | H319  | P264<br>P280<br>P305 + P351 + P338<br>P337 + P313                                      |

|                   |   |                              |   |
|-------------------|---|------------------------------|---|
| Ethanol           |    | H225<br>H319<br>H302<br>H371 | P210<br>P260<br>P280<br>P308 + P311<br>P337 + P313<br>P403 + P235                             |
| Ethidiumbromide   |    | H302<br>H330<br>H341         | P281<br>P305 + P351 + P338<br>P309<br>P310<br>P302 + P352                                     |
| Formic acid       |    | H226<br>H302<br>H314<br>H331 | P210<br>P280<br>P303 + P361 + P353<br>P304 + P340 + P310<br>P305 + P351 + P338<br>P403 + P233 |
| G418              |  | H317<br>H334<br>H316         | P285<br>P304 + P341<br>P305 + P351 + P338<br>P332 + P313<br>P261<br>P280                      |
| Hoechst           |  | H302<br>H315<br>H319         | P305 + P351 + P338  |
| Hydrogen chloride |  | H315<br>H319<br>H335         | P305 + P351 + P338<br>P301 + P330 + P331<br>P314  |
| LipidTox Green    |  | H227<br>H316<br>H320<br>H335 | P312<br>P304 + P340<br>P261<br>P305 + P351 + P338<br>P337 + P313<br>P332 + P313               |

A. Toxicity of chemicals

|  |   |  |  |
|--|---|--|--|
|  |   |  | P264   |
| LipidTox Red                           |    | H227<br>H316<br>H320<br>H335                                 | P312<br>P304 + P340<br>P261<br>P305 + P351 + P338<br>P337 + P313<br>P332 + P313<br>P264                              |
| Methanol                               |    | H225<br>H331<br>H311<br>H301<br>H370                         | P210<br>P260<br>P280<br>P301 + P310<br>P311  |
| Nonident-P40                           |    | H318<br>H412   | P280<br>P273<br>P305 + P351 + P338   |
| Paraformaldehyde                       |   | H228<br>H302<br>H332<br>H315<br>H317<br>H318<br>H335<br>H351 | P281<br>P305 + P351 + P338<br>P304 + P340<br>P308 + P313<br>P302 + P352  |
| Phenole-Chloroform-<br>Isoamyl alcohol |  | H301<br>H311<br>H331<br>H314<br>H351<br>H373<br>H401<br>H341 | P301 + P310<br>P301 + P330 + P331<br>P303 + P361 + P353<br>P305 + P351 + P338<br>P304 + P340<br>P312<br>P280<br>P264 |

|                                 |   |  |  |
|---------------------------------|---|--|--|
| Phenylmethane-sulfonyl fluoride |    | H301<br>H314   | P303 + P361 + P353<br>P301 + P330 + P331<br>P305 + P351 + P338<br>P330<br>P310<br>P264 |
| Polybrene                       |    | H302   |  |
| Potassium hydroxide             |    | H290<br>H302<br>H314   | P280<br>P305 + P351 + P338<br>P313   |
| Proteinase K                    |    | H334   | P304 + P340<br>P342 + P311<br>P284   |
| RNase Away                      |   | H315<br>H319   | P280<br>P332 + P313<br>P305 + P351 + P338<br>P362<br>P264<br>P337 + P313               |
| RNA-Stat60/Trizol               |  | H301<br>H311<br>H331<br>H314<br>H335<br>H341<br>H373<br>H412 | P301 + P310<br>P280<br>P261<br>P304 + P340<br>P303 + P361 + P353<br>P305 + P351 + P338 |
| Saponin                         |  | H319<br>H335   | P261<br>P305 + P351 + P338   |
| Sodium deoxycholate             |  | H302   | P301 + P312 + P330   |

|                     |   |                       |  |
|---------------------|---|-----------------------|--|
| Sodium hydroxide    |  | H290<br>H314          | P260<br>P264<br>P280<br>P301 + P330<br>P303 + P361 + P353<br>P501              |
| Sodium hypochlorite |  | H314<br>H400          | P260<br>P280<br>P303 + P361 + P353<br>P304 + P340 + P310<br>P305 + P351 + P338 |
| Triton-X100         |  | H302 + H319<br>+ H411 | P280<br>P273<br>P305 + P351 + P338<br>P310                                     |

### GHS Pictogram Guide



**Acute Toxic;** Identifies chemicals with the following hazards:  
Irritant, Skin sensitizer, Acute toxicity (harmful), Narcotic effects, Respiratory tract infection, Hazardous ozone layer.



**Severe Toxic;** Identifies chemicals with the following hazards:  
Acute toxicity (fatal or toxic).



**Health Hazard;** Identifies chemicals with the following hazards:  
Carinogen, Mutagenicity, Reproductive toxicity, Respiratory sensitizer, Target organ toxicity, Aspiration toxicity.



**Environmental;** Identifies chemicals with the following hazards:  
Aquatic toxicity.



**Corrosive;** Identifies chemicals with the following hazards:  
Skin corrosion, Eye damage, Corrosive metals.



**Flame;** Identifies chemicals with the following hazards:  
Flammables, Pyrophorics, Self-heating, Emits flammable gas, Self-reactives, Organic peroxides.



**Gas cylinder**; Identifies chemicals with the following hazards:  
Gases under pressure.

## A.1. GHS Hazard statements

### A.1.1. Physical hazards:

H200: Unstable explosive  
H201: Explosive; mass explosion hazard  
H202: Explosive; severe projection hazard  
H203: Explosive; fire, blast or projection hazard  
H204: Fire or projection hazard  
H205: May mass explode in fire  
H206: Fire, blast or projection hazard; increased risk of explosion if desensitizing agent is reduced  
H207: Fire or projection hazard; increased risk of explosion if desensitizing agent is reduced  
H208: Fire hazard; increased risk of explosion if desensitizing agent is reduced  
H220: Extremely flammable gas  
H221: Flammable gas  
H222: Extremely flammable aerosol  
H223: Flammable aerosol  
H224: Extremely flammable liquid and vapour  
H225: Highly flammable liquid and vapour  
H226: Flammable liquid and vapour  
H227: Combustible liquid  
H228: Flammable solid  
H229: Pressurized container: may burst if heated  
H230: May react explosively even in the absence of air  
H231: May react explosively even in the absence of air at elevated pressure and/or temperature  
H232: May ignite spontaneously if exposed to air  
H240: Heating may cause an explosion  
H241: Heating may cause a fire or explosion  
H242: Heating may cause a fire  
H250: Catches fire spontaneously if exposed to air  
H251: Self-heating; may catch fire  
H252: Self-heating in large quantities; may catch fire  
H260: In contact with water releases flammable gases which may ignite spontaneously  
H261: In contact with water releases flammable gas  
H270: May cause or intensify fire; oxidizer  
H271: May cause fire or explosion; strong oxidizer  
H272: May intensify fire; oxidizer  
H280: Contains gas under pressure; may explode if heated  
H281: Contains refrigerated gas; may cause cryogenic burns or injury  
H290: May be corrosive to metals

### A.1.2. Health hazards:

H300: Fatal if swallowed  
H301: Toxic if swallowed  
H302: Harmful if swallowed  
H303: May be harmful if swallowed  
H304: May be fatal if swallowed and enters airways  
H305: May be harmful if swallowed and enters airways  
H310: Fatal in contact with skin  
H311: Toxic in contact with skin  
H312: Harmful in contact with skin  
H313: May be harmful in contact with skin  
H314: Causes severe skin burns and eye damage  
H315: Causes skin irritation  
H316: Causes mild skin irritation  
H317: May cause an allergic skin reaction  
H318: Causes serious eye damage  
H319: Causes serious eye irritation  
H320: Causes eye irritation  
H330: Fatal if inhaled  
H331: Toxic if inhaled  
H332: Harmful if inhaled  
H333: May be harmful if inhaled  
H334: May cause allergy or asthma symptoms or breathing difficulties if inhaled  
H335: May cause respiratory irritation  
H336: May cause drowsiness or dizziness  
H340: May cause genetic defects  
H341: Suspected of causing genetic defects  
H350: May cause cancer  
H351: Suspected of causing cancer  
H360: May damage fertility or the unborn child  
H361: Suspected of damaging fertility or the unborn child  
H361d: Suspected of damaging the unborn child  
H362: May cause harm to breast-fed children  
H370: Causes damage to organs  
H371: May cause damage to organs  
H372: Causes damage to organs through prolonged or repeated exposure  
H373: May cause damage to organs through prolonged or repeated exposure

### A.1.3. Environmental hazards:

H400: Very toxic to aquatic life  
H401: Toxic to aquatic life  
H402: Harmful to aquatic life  
H410: Very toxic to aquatic life with long-lasting effects  
H411: Toxic to aquatic life with long-lasting effects  
H412: Harmful to aquatic life with long-lasting effects  
H413: May cause long-lasting harmful effects to aquatic life

H420: Harms public health and the environment by destroying ozone in the upper atmosphere

## A.2. GHS precautionary statements

### A.2.1. Prevention precautionary statements:

- P101: If medical advice is needed, have product container or label at hand.
- P102: Keep out of reach of children.
- P103: Read label before use.
- P201: Obtain special instructions before use.
- P202: Do not handle until all safety precautions have been read and understood.
- P210: Keep away from heat/sparks/open flames/hot surfaces. - No smoking.
- P211: Do not spray on an open flame or other ignition source.
- P220: Keep/Store away from clothing/.../combustible materials.
- P221: Take any precaution to avoid mixing with combustibles...
- P222: Do not allow contact with air.
- P223: Keep away from any possible contact with water, because of violent reaction and possible flash fire.
- P230: Keep wetted with...
- P231: Handle under inert gas.
- P232: Protect from moisture.
- P233: Keep container tightly closed.
- P234: Keep only in original container.
- P235: Keep cool.
- P240: Ground/bond container and receiving equipment.
- P241: Use explosion-proof electrical/ventilating/lighting/.../ equipment.
- P242: Use only non-sparking tools.
- P243: Take precautionary measures against static discharge.
- P244: Keep reduction valves free from grease and oil.
- P250: Do not subject to grinding/shock/.../friction.
- P251: Pressurized container: Do not pierce or burn, even after use.
- P260: Do not breathe dust/fume/gas/mist/vapours/spray.
- P261: Avoid breathing dust/fume/gas/mist/vapours/spray.
- P262: Do not get in eyes, on skin, or on clothing.
- P263: Avoid contact during pregnancy/while nursing.
- P264: Wash thoroughly after handling.
- P270: Do not eat, drink or smoke when using this product.
- P271: Use only outdoors or in a well-ventilated area.
- P272: Contaminated work clothing should not be allowed out of the workplace.
- P273: Avoid release to the environment.
- P280: Wear protective gloves/protective clothing/eye protection/face protection.
- P281: Use personal protective equipment as required.
- P282: Wear cold insulating gloves/face shield/eye protection.
- P283: Wear fire/flame resistant/retardant clothing.
- P284: Wear respiratory protection.
- P285: In case of inadequate ventilation wear respiratory protection.
- P231 + P232: Handle under inert gas. Protect from moisture.



P235 + P410: Keep cool. Protect from sunlight.

### **A.2.2. Response precautionary statements:**

P301: IF SWALLOWED:

P302: IF ON SKIN:

P303: IF ON SKIN (or hair):

P304: IF INHALED:

P305: IF IN EYES:

P306: IF ON CLOTHING:

P307: IF exposed:

P308: IF exposed or concerned:

P309: IF exposed or if you feel unwell:

P310: Immediately call a POISON CENTER or doctor/physician.

P311: Call a POISON CENTER or doctor/physician.

P312: Call a POISON CENTER or doctor/physician if you feel unwell.

P313: Get medical advice/attention.

P314: Get medical advice/attention if you feel unwell.

P315: Get immediate medical advice/attention.

P320: Specific treatment is urgent (see ... on this label).

P321: Specific treatment (see ... on this label).

P322: Specific measures (see ... on this label).

P330: Rinse mouth.

P331: Do NOT induce vomiting.

P332: If skin irritation occurs:

P333: If skin irritation or rash occurs:

P334: Immerse in cool water/wrap in wet bandages.

P335: Brush off loose particles from skin.

P336: Thaw frosted parts with lukewarm water. Do no rub affected area.

P337: If eye irritation persists:

P338: Remove contact lenses, if present and easy to do. Continue rinsing.

P340: Remove victim to fresh air and keep at rest in a position comfortable for breathing.

P341: If breathing is difficult, remove victim to fresh air and keep at rest in a position comfortable for breathing.

P342: If experiencing respiratory symptoms:

P350: Gently wash with plenty of soap and water.

P351: Rinse cautiously with water for several minutes.

P352: Wash with plenty of soap and water.

P353: Rinse skin with water/shower.

P360: Rinse immediately contaminated clothing and skin with plenty of water before removing clothes.

P361: Remove/Take off immediately all contaminated clothing.

P362: Take off contaminated clothing and wash before reuse.

P363: Wash contaminated clothing before reuse.

P370: In case of fire:

P371: In case of major fire and large quantities:

P372: Explosion risk in case of fire.

- P373: DO NOT fight fire when fire reaches explosives.
- P374: Fight fire with normal precautions from a reasonable distance.
- P375: Fight fire remotely due to the risk of explosion.
- P376: Stop leak if safe to do so.
- P377: Leaking gas fire: Do not extinguish, unless leak can be stopped safely.
- P378: Use ... for extinction.
- P380: Evacuate area.
- P381: Eliminate all ignition sources if safe to do so.
- P390: Absorb spillage to prevent material damage.
- P391: Collect spillage.
- P301 + P310: IF SWALLOWED: Immediately call a POISON CENTER or doctor/physician.
- P301 + P312: IF SWALLOWED: Call a POISON CENTER or doctor/physician if you feel unwell.
- P301 + P330 + P331: IF SWALLOWED: rinse mouth. Do NOT induce vomiting.
- P302 + P334: IF ON SKIN: Immerse in cool water/wrap in wet bandages.
- P302 + P350: IF ON SKIN: Gently wash with plenty of soap and water.
- P302 + P352: IF ON SKIN: Wash with plenty of soap and water.
- P303 + P361 + P353: IF ON SKIN (or hair): Remove/Take off immediately all contaminated clothing. Rinse skin with water/shower.
- P304 + P340: IF INHALED: Remove victim to fresh air and keep at rest in a position comfortable for breathing.
- P304 + P341: IF INHALED: If breathing is difficult, remove victim to fresh air and keep at rest in a position comfortable for breathing.
- P305 + P351 + P338: IF IN EYES: Rinse cautiously with water for several minutes. Remove contact lenses, if present and easy to do. Continue rinsing.
- P306 + P360: IF ON CLOTHING: rinse immediately contaminated clothing and skin with plenty of water before removing clothes.
- P307 + P311: IF exposed: Call a POISON CENTER or doctor/physician.
- P308 + P313: IF exposed or concerned: Get medical advice/attention.
- P309 + P311: IF exposed or if you feel unwell: Call a POISON CENTER or doctor/physician.
- P332 + P313: If skin irritation occurs: Get medical advice/ attention.
- P333 + P313: If skin irritation or rash occurs: Get medical advice/ attention.
- P335 + P334: Brush off loose particles from skin. Immerse in cool water/wrap in wet bandages.
- P337 + P313: If eye irritation persists: Get medical advice/ attention.
- P342 + P311: If experiencing respiratory symptoms: Call a POISON CENTER or doctor/physician.
- P370 + P376: In case of fire: Stop leak if safe to do so.
- P370 + P378: In case of fire: Use ... for extinction.
- P370 + P380: In case of fire: Evacuate area.
- P370 + P380 + P375: In case of fire: Evacuate area. Fight fire remotely due to the risk of explosion.
- P371 + P380 + P375: In case of major fire and large quantities: Evacuate area. Fight fire remotely due to the risk of explosion.
- P401: Store ...
- P402: Store in a dry place.
- P403: Store in a well-ventilated place.
- P404: Store in a closed container.

- P405: Store locked up.
- P406: Store in corrosive resistant/... container with a resistant inner liner.
- P407: Maintain air gap between stacks/pallets.
- P410: Protect from sunlight.
- P411: Store at temperatures not exceeding ...°C/...°F.
- P412: Do not expose to temperatures exceeding 50 °C/122 °F.
- P413: Store bulk masses greater than ... kg/...lbs at temperatures not exceeding ...°C/...°F.
- P420: Store away from other materials.
- P422: Store contents under...
- P402 + P404: Store in a dry place. Store in a closed container.
- P403 + P233: Store in a well-ventilated place. Keep container tightly closed.
- P403 + P235: Store in a well-ventilated place. Keep cool.
- P410 + P403: Protect from sunlight. Store in a well-ventilated place.
- P410 + P412: Protect from sunlight. Do not expose to temperatures exceeding 50 celcius degrees.
- P411 + P235: Store at temperatures not exceeding ...Keep cool.
- P501: Dispose of contents/container to...

## B. Supplementary data

**Table S1, related to Figure 3.3: Summary of proteins identified in all SILAC experiments.** Shown is the Uniprot ID and the Gene Name of proteins identified in all four SILAC experiments (#1-#4) with the log<sub>2</sub> enrichment HCV-infected/control as well as the mean and p-value.

| ID     | #1       | #2       | #3      | #4       | Name      | Mean    | p-value |    |
|--------|----------|----------|---------|----------|-----------|---------|---------|----|
| O00571 | 1.32388  | 0.63600  | 6.55937 | 4.22554  | DDX3X     | 3.18620 | 0.10210 |    |
| Q9Y224 | 1.81456  | 2.33360  | 4.35531 | 3.33010  | C14orf166 | 2.95840 | 0.01335 | *  |
| Q92499 | 1.77599  | 2.30851  | 4.41773 | 3.31405  | DDX1      | 2.95407 | 0.01483 | *  |
| Q9NZI8 | 1.83309  | 3.12895  | 4.80768 | 1.43630  | IGF2BP1   | 2.80150 | 0.03462 | *  |
| Q9Y3I0 | 1.59536  | 2.12724  | 3.26686 | 2.75320  | RTCB      | 2.43567 | 0.00683 | ** |
| P11940 | 1.64123  | 1.92790  | 2.33740 | 1.31583  | PABPC1    | 1.80559 | 0.00363 | ** |
| O95340 | 1.60118  | 1.53122  | 1.15598 | 2.28542  | PAPSS2    | 1.64345 | 0.00602 | ** |
| P27487 | 0.67433  | 2.10144  | 1.31036 | 2.45103  | DPP4      | 1.63429 | 0.02634 | *  |
| P12429 | 1.66883  | 1.84247  | 0.91496 | 1.59566  | ANXA3     | 1.50548 | 0.00511 | ** |
| P50454 | 0.49490  | 2.00259  | 1.00911 | 1.86877  | SERPINH1  | 1.34384 | 0.03315 | *  |
| Q9NVJ2 | 0.10778  | 1.45296  | 1.86391 | 1.48391  | ARL8B     | 1.22714 | 0.04970 | *  |
| P08670 | 0.70209  | 1.12440  | 1.80065 | 1.10283  | VIM       | 1.18249 | 0.01388 | *  |
| P07339 | -0.04550 | 2.32990  | 1.46763 | 0.86039  | CTSD      | 1.15310 | 0.10462 |    |
| P45880 | 0.53004  | 0.82395  | 2.17999 | 0.64936  | VDAC2     | 1.04583 | 0.07183 |    |
| P10620 | 0.27532  | 1.29933  | 1.72902 | 0.30273  | MGST1     | 0.90160 | 0.08974 |    |
| P55157 | 0.24910  | 0.76107  | 1.21545 | 1.37958  | MTTP      | 0.90130 | 0.03803 | *  |
| Q92820 | -0.31239 | 1.06497  | 1.28730 | 1.33947  | GGH       | 0.84484 | 0.11907 |    |
| P05023 | 0.11197  | 1.21522  | 0.77869 | 1.24809  | ATP1A1    | 0.83849 | 0.05059 |    |
| P43307 | -0.00140 | 1.11810  | 2.18771 | -0.05856 | SSR1      | 0.81146 | 0.22509 |    |
| P23246 | -0.27926 | 0.06492  | 2.42359 | 0.93614  | SFPQ      | 0.78635 | 0.28306 |    |
| P21796 | 0.27098  | 0.60617  | 1.79538 | 0.41696  | VDAC1     | 0.77237 | 0.11299 |    |
| Q99536 | 0.43284  | 0.84141  | 1.42562 | 0.37794  | VAT1      | 0.76945 | 0.05007 |    |
| P07237 | 0.26416  | 0.94671  | 0.94726 | 0.88927  | P4HB      | 0.76185 | 0.01958 | *  |
| Q969H8 | 0.13498  | 0.74830  | 1.25197 | 0.90976  | MYDGF     | 0.76125 | 0.04721 | *  |
| P30040 | 0.22281  | 0.77891  | 1.02418 | 1.00858  | ERP29     | 0.75862 | 0.02707 | *  |
| P18085 | 0.90468  | 0.88830  | 0.37075 | 0.86416  | ARF4      | 0.75697 | 0.00987 | ** |
| P07099 | 0.05151  | 1.15880  | 1.68188 | 0.12741  | EPHX1     | 0.75490 | 0.15489 |    |
| P17844 | -0.13104 | -0.36127 | 2.14884 | 1.26489  | DDX5      | 0.73035 | 0.30638 |    |
| Q6DD88 | 0.40362  | 0.70900  | 1.48297 | 0.31409  | ATL3      | 0.72742 | 0.07145 |    |
| Q13637 | 0.47840  | 1.35384  | 0.95709 | 0.11657  | RAB32     | 0.72647 | 0.07491 |    |

B. Supplementary data

|        |          |          |         |          |         |         |         |   |
|--------|----------|----------|---------|----------|---------|---------|---------|---|
| Q9BRX8 | 0.18081  | 0.96434  | 1.71669 | 0.03768  | FAM213A | 0.72488 | 0.15875 |   |
| P62277 | 0.47534  | -0.11429 | 1.82375 | 0.68103  | RPS13   | 0.71646 | 0.17562 |   |
| P39656 | 0.16023  | 0.99832  | 1.70512 | -0.01292 | DDOST   | 0.71269 | 0.17106 |   |
| P04844 | 0.11094  | 1.05344  | 1.64885 | -0.00079 | RPN2    | 0.70311 | 0.17237 |   |
| Q14444 | 0.36551  | 0.06242  | 1.24681 | 1.11979  | CAPRIN1 | 0.69863 | 0.09350 |   |
| P25705 | 0.27447  | 1.00912  | 1.27919 | 0.21756  | ATP5A1  | 0.69509 | 0.07902 |   |
| Q9UHG3 | 0.01235  | 0.97878  | 1.47271 | 0.30923  | PCYOX1  | 0.69327 | 0.12583 |   |
| P04843 | 0.14913  | 1.03261  | 1.61971 | -0.06609 | RPN1    | 0.68384 | 0.17958 |   |
| P49755 | -0.00693 | 0.72277  | 1.98283 | -0.06745 | TMED10  | 0.65780 | 0.26153 |   |
| P06576 | 0.25234  | 1.04084  | 1.30498 | 0.03105  | ATP5B   | 0.65731 | 0.12084 |   |
| Q99623 | 0.35464  | 0.81660  | 1.45955 | -0.02977 | PHB2    | 0.65026 | 0.13547 |   |
| Q12907 | 1.01770  | 1.05491  | 0.85059 | -0.34153 | LMAN2   | 0.64542 | 0.14710 |   |
| P27824 | 0.39540  | 0.90038  | 1.52603 | -0.24747 | CANX    | 0.64359 | 0.18583 |   |
| Q9Y277 | 0.17929  | 0.37200  | 1.95870 | 0.06004  | VDAC3   | 0.64250 | 0.24319 |   |
| Q5T0D9 | 0.62020  | 0.13719  | 1.59510 | 0.21720  | TPRG1L  | 0.64242 | 0.15071 |   |
| P08134 | 0.65037  | 1.10057  | 0.65213 | 0.09514  | RHOC    | 0.62455 | 0.05611 |   |
| Q07955 | -0.34129 | -0.03878 | 1.24466 | 1.55126  | SRSF1   | 0.60396 | 0.28630 |   |
| P13804 | -0.25928 | 0.74856  | 0.59757 | 1.30554  | ETFA    | 0.59810 | 0.16189 |   |
| Q8TCT9 | 0.15843  | 0.82288  | 1.59871 | -0.21533 | HM13    | 0.59117 | 0.23467 |   |
| P62280 | 0.08677  | 0.03922  | 1.63327 | 0.59983  | RPS11   | 0.58977 | 0.20944 |   |
| P62701 | 0.21329  | -0.24974 | 1.83074 | 0.55738  | RPS4X   | 0.58792 | 0.27909 |   |
| P27797 | 0.07979  | 0.63403  | 1.00424 | 0.62287  | CALR    | 0.58523 | 0.05438 |   |
| Q04837 | 0.02141  | 0.64090  | 0.46581 | 1.20936  | SSBP1   | 0.58437 | 0.09781 |   |
| Q07065 | -0.11033 | 0.89338  | 1.78201 | -0.23030 | CKAP4   | 0.58369 | 0.30441 |   |
| P35232 | 0.22909  | 0.82144  | 1.40289 | -0.16970 | PHB     | 0.57093 | 0.19559 |   |
| P11233 | -0.51511 | 0.48601  | 1.59744 | 0.70992  | RALA    | 0.56957 | 0.28073 |   |
| O94905 | 0.09831  | 0.77308  | 1.42242 | -0.03574 | ERLIN2  | 0.56452 | 0.19182 |   |
| P09651 | -0.28097 | -0.20576 | 1.55718 | 1.17066  | HNRNPA1 | 0.56028 | 0.31970 |   |
| Q9H2U2 | -0.30064 | 0.87231  | 0.51413 | 1.14564  | PPA2    | 0.55786 | 0.17372 |   |
| P49411 | -0.17886 | 0.47877  | 0.42587 | 1.47749  | TUFM    | 0.55082 | 0.20667 |   |
| Q9BVK6 | -0.02445 | 0.66744  | 1.77353 | -0.22276 | TMED9   | 0.54844 | 0.31069 |   |
| P61247 | 0.30055  | -0.09777 | 1.11740 | 0.87071  | RPS3A   | 0.54772 | 0.14032 |   |
| P09543 | -0.10297 | 0.77934  | 1.58069 | -0.09394 | CNP     | 0.54078 | 0.27282 |   |
| P23284 | 0.20916  | 0.60539  | 0.69269 | 0.63450  | PPIB    | 0.53544 | 0.01667 | * |
| P15880 | 0.34477  | -0.04539 | 1.01036 | 0.80645  | RPS2    | 0.52905 | 0.11151 |   |
| P62249 | 0.46058  | -0.09578 | 0.75638 | 0.93793  | RPS16   | 0.51478 | 0.10720 |   |
| P30101 | -0.05371 | 0.38215  | 0.85692 | 0.77700  | PDIA3   | 0.49059 | 0.10057 |   |
| P40926 | -0.18847 | 0.41929  | 0.50388 | 1.21549  | MDH2    | 0.48755 | 0.18848 |   |
| P40616 | 0.38112  | 0.37384  | 1.08524 | 0.10226  | ARL1    | 0.48561 | 0.10395 |   |

|        |          |          |          |          |           |         |         |    |
|--------|----------|----------|----------|----------|-----------|---------|---------|----|
| Q9NQC3 | 0.33745  | 0.64106  | 1.04046  | -0.08241 | RTN4      | 0.48414 | 0.13419 |    |
| O60701 | 0.75096  | 0.01316  | -0.03723 | 1.15811  | UGDH      | 0.47125 | 0.20417 |    |
| Q9NYU2 | -0.21839 | 0.39552  | 0.84448  | 0.83411  | UGGT1     | 0.46393 | 0.16092 |    |
| P30048 | -0.38654 | 0.62195  | 0.38760  | 1.21912  | PRDX3     | 0.46053 | 0.25973 |    |
| P05091 | -0.03602 | 0.59953  | -0.07244 | 1.31812  | ALDH2     | 0.45230 | 0.26087 |    |
| Q9NR31 | 0.44555  | 0.12302  | 0.28097  | 0.92418  | SAR1A     | 0.44343 | 0.08325 |    |
| P48681 | 0.34721  | -0.19870 | 1.38007  | 0.23992  | NES       | 0.44213 | 0.27766 |    |
| P05141 | 0.03759  | 0.46286  | 1.06380  | 0.19879  | SLC25A5   | 0.44076 | 0.14552 |    |
| Q00839 | -0.09792 | -0.07630 | 0.90528  | 1.02900  | HNRNPU    | 0.44002 | 0.24531 |    |
| P22307 | -0.14861 | 0.47002  | 0.28845  | 1.13677  | SCP2      | 0.43666 | 0.20054 |    |
| P37802 | 0.78122  | 0.11651  | 0.31368  | 0.51307  | TAGLN2    | 0.43112 | 0.05607 |    |
| P22626 | -0.63662 | -0.01108 | 1.82214  | 0.54083  | HNRNPA2B1 | 0.42882 | 0.47235 |    |
| P35221 | -0.14057 | 0.42358  | 0.59193  | 0.82330  | CTNNA1    | 0.42456 | 0.13065 |    |
| Q9Y4L1 | -0.20220 | 0.38328  | 0.85244  | 0.62909  | HYOU1     | 0.41565 | 0.16468 |    |
| P63261 | 0.34258  | 0.42890  | 0.55218  | 0.31365  | ACTG1     | 0.40933 | 0.00465 | ** |
| O95292 | 0.08315  | 0.71800  | 0.95556  | -0.17643 | VAPB      | 0.39507 | 0.23272 |    |
| P42704 | -0.27215 | 0.20009  | 0.41061  | 1.22345  | LRPPRC    | 0.39050 | 0.29967 |    |
| P51659 | -0.15662 | 0.35514  | 0.98943  | 0.33627  | HSD17B4   | 0.38105 | 0.20315 |    |
| P30050 | 0.45108  | 0.37957  | 0.52496  | 0.16216  | RPL12     | 0.37945 | 0.01675 | *  |
| O00116 | 0.14713  | 0.82837  | 0.76610  | -0.24486 | AGPS      | 0.37418 | 0.24190 |    |
| P23396 | 0.48675  | -0.24048 | -0.33123 | 1.55871  | RPS3      | 0.36844 | 0.46103 |    |
| P62750 | 0.15788  | 0.18690  | 0.73522  | 0.36282  | RPL23A    | 0.36070 | 0.07278 |    |
| P25398 | 0.59860  | 0.01378  | -0.27296 | 1.07558  | RPS12     | 0.35375 | 0.32508 |    |
| P39019 | 0.36815  | -0.10930 | -0.16986 | 1.29786  | RPS19     | 0.34671 | 0.38184 |    |
| Q9H7Z7 | -0.13941 | 0.17763  | 1.36912  | -0.02628 | PTGES2    | 0.34527 | 0.39371 |    |
| O75369 | 0.09071  | 0.57006  | 0.06034  | 0.62923  | FLNB      | 0.33758 | 0.11280 |    |
| O43707 | -0.13178 | 0.57557  | 0.45088  | 0.44485  | ACTN4     | 0.33488 | 0.12494 |    |
| Q13011 | -0.35977 | -0.30586 | 0.52213  | 1.47727  | ECH1      | 0.33344 | 0.49587 |    |
| P05388 | 0.58925  | 0.13998  | 0.63779  | -0.06293 | RPLP0     | 0.32602 | 0.15325 |    |
| O43491 | 0.06253  | -0.16535 | 0.62720  | 0.77948  | EPB41L2   | 0.32596 | 0.24317 |    |
| Q14697 | -0.42202 | 0.15778  | 0.88467  | 0.67119  | GANAB     | 0.32290 | 0.34869 |    |
| P11021 | -0.17719 | 0.37621  | 0.71125  | 0.37414  | HSPA5     | 0.32110 | 0.17934 |    |
| Q01082 | -0.03923 | 0.75806  | 0.52513  | 0.01077  | SPTBN1    | 0.31368 | 0.20688 |    |
| P09327 | 0.60147  | 103.667  | -1.17555 | 0.76300  | VIL1      | 0.30640 | 0.58481 |    |
| Q92841 | -0.58119 | -0.48414 | 1.19632  | 1.09164  | DDX17     | 0.30566 | 0.57319 |    |
| P52597 | -0.01059 | 0.19898  | 0.07301  | 0.94931  | HNRNPF    | 0.30268 | 0.26227 |    |
| P09211 | 0.49750  | 0.46468  | -0.39787 | 0.61680  | GSTP1     | 0.29528 | 0.29508 |    |
| Q99714 | -0.52548 | 0.35898  | 0.25185  | 1.08990  | HSD17B10  | 0.29381 | 0.43953 |    |
| P61604 | -0.39635 | 0.18188  | 0.30615  | 1.03815  | HSPE1     | 0.28246 | 0.40861 |    |

B. Supplementary data

|        |          |          |          |          |          |         |         |  |
|--------|----------|----------|----------|----------|----------|---------|---------|--|
| P10809 | -0.25885 | 0.09010  | -0.01195 | 130.726  | HSPD1    | 0.28164 | 0.47945 |  |
| P62873 | -0.26911 | 0.38215  | 0.77310  | 0.21010  | GNB1     | 0.27406 | 0.29400 |  |
| P46782 | 0.40859  | -0.32521 | -0.10656 | 1.05380  | RPS5     | 0.25766 | 0.46257 |  |
| P07355 | -0.25044 | 1.05059  | -0.58155 | 0.81197  | ANXA2    | 0.25764 | 0.56330 |  |
| P14625 | -0.20848 | 0.12972  | 0.67808  | 0.42944  | HSP90B1  | 0.25719 | 0.27176 |  |
| Q8N128 | 0.60170  | 0.84615  | 0.22207  | -0.64456 | FAM177A1 | 0.25634 | 0.48979 |  |
| Q9UBM7 | -0.30467 | 0.57278  | 1.10208  | -0.40561 | DHCR7    | 0.24114 | 0.55236 |  |
| Q86UP2 | -0.27609 | 0.87678  | 1.07623  | -0.72688 | KTN1     | 0.23751 | 0.62560 |  |
| P62913 | 0.56503  | -0.04184 | 0.09367  | 0.31448  | RPL11    | 0.23283 | 0.17799 |  |
| P14314 | -0.46802 | -0.03130 | 0.85500  | 0.53194  | PRKCSH   | 0.22191 | 0.50519 |  |
| Q9Y5M8 | 0.14443  | 0.17636  | 1.12321  | -0.56639 | SRPRB    | 0.21941 | 0.57171 |  |
| P38646 | -0.46691 | 0.20096  | 0.19089  | 0.91987  | HSPA9    | 0.21121 | 0.50994 |  |
| Q04917 | 0.41692  | 0.19159  | 0.01428  | 0.17407  | YWHAH    | 0.19921 | 0.09538 |  |
| Q9BUF5 | 0.14642  | 0.05581  | 0.06582  | 0.50907  | TUBB6    | 0.19428 | 0.16667 |  |
| P00505 | -0.51547 | -0.12196 | 0.49686  | 0.90961  | GOT2     | 0.19226 | 0.58716 |  |
| P13667 | -0.16173 | -0.03967 | 0.72101  | 0.23876  | PDIA4    | 0.18959 | 0.40466 |  |
| Q14152 | 0.10677  | -0.13723 | -0.10085 | 0.88549  | EIF3A    | 0.18855 | 0.48685 |  |
| P63104 | 0.38865  | 0.21186  | 0.01683  | 0.12288  | YWHAZ    | 0.18506 | 0.10019 |  |
| Q96AG4 | -0.08080 | 0.45226  | 0.71962  | -0.35121 | LRRC59   | 0.18497 | 0.50380 |  |
| O60664 | 0.27660  | 1.05724  | 0.18468  | -0.78103 | PLIN3    | 0.18437 | 0.65804 |  |
| Q00610 | -0.07327 | 0.46728  | -0.07554 | 0.41042  | CLTC     | 0.18222 | 0.30763 |  |
| P29966 | 0.27170  | 0.41475  | 0.46180  | -0.42667 | MARCKS   | 0.18040 | 0.44635 |  |
| P37108 | 0.20124  | 0.22106  | 0.43952  | -0.17094 | SRP14    | 0.17272 | 0.26590 |  |
| Q8TC12 | -0.03251 | 0.12911  | 1.01385  | -0.43230 | RDH11    | 0.16954 | 0.61726 |  |
| P78417 | 0.45893  | 0.28015  | -0.08696 | 0.01647  | GSTO1    | 0.16715 | 0.27111 |  |
| Q15459 | 0.15686  | -0.13534 | -0.24271 | 0.85759  | SF3A1    | 0.15910 | 0.56633 |  |
| P60953 | -0.04580 | 0.22201  | 0.62894  | -0.20114 | CDC42    | 0.15100 | 0.46692 |  |
| Q9H2M9 | -0.04241 | 0.31390  | -0.08066 | 0.37647  | RAB3GAP2 | 0.14183 | 0.31684 |  |
| P16615 | 0.02341  | 0.23444  | 0.89702  | -0.58943 | ATP2A2   | 0.14136 | 0.67607 |  |
| O43747 | -0.04858 | -0.02232 | 0.23178  | 0.40296  | AP1G1    | 0.14096 | 0.28224 |  |
| Q8WVM8 | 0.09719  | 0.21057  | 0.61478  | -0.36360 | SCFD1    | 0.13973 | 0.53735 |  |
| O00299 | 0.38792  | 0.16550  | -0.03403 | 0.01607  | CLIC1    | 0.13387 | 0.25237 |  |
| P31943 | -0.30214 | -0.29688 | 0.13752  | 0.98548  | HNRNPH1  | 0.13100 | 0.69458 |  |
| O43684 | 0.34849  | -0.06441 | -0.12149 | 0.32158  | BUB3     | 0.12104 | 0.40170 |  |
| Q13813 | -0.23736 | 0.70147  | 0.11784  | -0.13667 | SPTAN1   | 0.11132 | 0.63345 |  |
| O60763 | -0.40829 | 0.42460  | 0.31090  | 0.08528  | USO1     | 0.10312 | 0.61517 |  |
| Q13636 | -0.11517 | 0.84953  | 0.42766  | -0.79465 | RAB31    | 0.09184 | 0.81279 |  |
| P00352 | 0.30788  | 0.15891  | -0.52386 | 0.40109  | ALDH1A1  | 0.08601 | 0.70874 |  |
| Q15393 | -0.01077 | 0.16887  | -0.44658 | 0.60331  | SF3B3    | 0.07871 | 0.74135 |  |

|        |          |          |          |          |         |          |         |  |
|--------|----------|----------|----------|----------|---------|----------|---------|--|
| P12956 | 0.29161  | -0.11034 | 0.43385  | -0.31602 | XRCC6   | 0.07477  | 0.69624 |  |
| P02786 | -0.31431 | -0.36916 | 1.08921  | -0.11407 | TFRC    | 0.07292  | 0.84535 |  |
| P37837 | 0.46577  | -0.11611 | -0.04460 | -0.03504 | TALDO1  | 0.06750  | 0.64905 |  |
| P52272 | -0.53226 | -0.11700 | 0.51128  | 0.40499  | HNRNPM  | 0.06675  | 0.80084 |  |
| P46459 | -0.29204 | 0.13423  | 0.55142  | -0.17287 | NSF     | 0.05519  | 0.78847 |  |
| Q15366 | 0.39739  | -0.39573 | 0.37904  | -0.17125 | PCBP2   | 0.05236  | 0.80974 |  |
| P22059 | -0.09060 | 0.19799  | 0.03153  | 0.05905  | OSBP    | 0.04949  | 0.46469 |  |
| P61978 | -0.11267 | -0.18300 | -0.14591 | 0.60264  | HNRNPK  | 0.04026  | 0.84415 |  |
| Q01105 | 0.44824  | -0.41711 | 0.06157  | 0.06817  | SET     | 0.04022  | 0.83505 |  |
| Q9BUP3 | -0.12855 | 0.02966  | 0.84179  | -0.61537 | HTATIP2 | 0.03188  | 0.92280 |  |
| P63244 | 0.33786  | -0.38655 | -1.07627 | 1.24277  | GNB2L1  | 0.02945  | 0.95646 |  |
| P23528 | 0.19419  | 0.09584  | -0.16949 | -0.00519 | CFL1    | 0.02884  | 0.73496 |  |
| P17931 | 0.39998  | 0.31314  | -0.97378 | 0.37498  | LGALS3  | 0.02858  | 0.93731 |  |
| P51148 | -0.20661 | 0.67715  | 0.18403  | -0.55384 | RAB5C   | 0.02518  | 0.93014 |  |
| Q12931 | -0.17388 | -0.68966 | 0.21794  | 0.73952  | TRAP1   | 0.02348  | 0.94302 |  |
| O43264 | 0.10055  | 0.27928  | 0.05587  | -0.38155 | ZW10    | 0.01354  | 0.92919 |  |
| Q13765 | 0.61117  | -0.64519 | -0.32035 | 0.39281  | NACA    | 0.00961  | 0.97608 |  |
| O94979 | 0.19627  | -0.19808 | -0.07226 | 0.11111  | SEC31A  | 0.00926  | 0.92368 |  |
| Q12905 | -0.09463 | -0.24969 | 0.54458  | -0.16947 | ILF2    | 0.00770  | 0.96887 |  |
| Q9BZZ5 | -0.07964 | -0.22357 | -0.15112 | 0.44721  | API5    | -0.00178 | 0.99142 |  |
| P08758 | 0.37531  | 0.17993  | -0.73892 | 0.15331  | ANXA5   | -0.00760 | 0.97755 |  |
| Q9H0N0 | -0.36097 | 0.60385  | 0.33271  | -0.62592 | RAB6C   | -0.01258 | 0.96792 |  |
| P29401 | 0.24890  | -0.16159 | -0.23415 | 0.08645  | TKT     | -0.01510 | 0.90095 |  |
| Q7KZF4 | 0.14366  | -0.13210 | -0.19634 | 0.11441  | SND1    | -0.01759 | 0.85080 |  |
| P20340 | -0.37376 | 0.42883  | 0.55322  | -0.69332 | RAB6A   | -0.02126 | 0.94865 |  |
| P04075 | 0.45044  | -0.09815 | -0.25827 | -0.20391 | ALDOA   | -0.02747 | 0.87668 |  |
| P53621 | 0.12775  | 0.17981  | -0.00026 | -0.43889 | COPA    | -0.03290 | 0.82996 |  |
| P05455 | 0.35011  | -0.46289 | -0.08045 | 0.05694  | SSB     | -0.03407 | 0.85295 |  |
| P35579 | 0.12348  | -0.01365 | -0.69294 | 0.43326  | MYH9    | -0.03746 | 0.88476 |  |
| P60900 | 0.45242  | 0.00046  | -0.96914 | 0.34899  | PSMA6   | -0.04182 | 0.90543 |  |
| P14324 | -0.02462 | 0.00066  | 0.02338  | -0.17457 | FDPS    | -0.04379 | 0.39936 |  |
| P08865 | 0.35057  | -0.47210 | -1.08724 | 1.01827  | RPSA    | -0.04763 | 0.92432 |  |
| P07910 | -0.37052 | 0.03085  | 0.17375  | -0.02600 | HNRNPC  | -0.04798 | 0.70560 |  |
| Q01581 | 0.46594  | -0.32480 | -0.34904 | -0.03230 | HMGCS1  | -0.06005 | 0.77213 |  |
| Q04637 | 0.24952  | -0.31830 | -0.17805 | 0.00079  | EIF4G1  | -0.06151 | 0.65019 |  |
| P40925 | 0.23927  | -0.13242 | -0.25207 | -0.10474 | MDH1    | -0.06249 | 0.59546 |  |
| P09525 | 0.41321  | 0.38985  | -1.36937 | 0.29358  | ANXA4   | -0.06818 | 0.88528 |  |
| P46777 | 0.19064  | -0.23984 | -0.81166 | 0.58317  | RPL5    | -0.06942 | 0.83138 |  |
| P68371 | -0.12293 | -0.13635 | -0.33750 | 0.28966  | TUBB4B  | -0.07678 | 0.60065 |  |



B. Supplementary data

|        |          |          |          |          |          |          |         |  |
|--------|----------|----------|----------|----------|----------|----------|---------|--|
| Q9Y678 | 0.20275  | 0.23779  | -0.37015 | -0.38244 | COPG1    | -0.07801 | 0.68159 |  |
| P53618 | 0.29057  | 0.17229  | -0.23587 | -0.54061 | COPB1    | -0.07840 | 0.70889 |  |
| P51149 | -0.11482 | 0.54762  | 0.16021  | -0.92667 | RAB7A    | -0.08342 | 0.80664 |  |
| P52565 | 0.39201  | -0.04322 | -0.10620 | -0.58871 | ARHGDI1A | -0.08653 | 0.69549 |  |
| P07148 | -0.22677 | -0.11302 | -0.42607 | 0.41942  | FABP1    | -0.08661 | 0.66442 |  |
| P31939 | 0.17840  | -0.10189 | -0.26822 | -0.16170 | ATIC     | -0.08835 | 0.42242 |  |
| P30153 | 0.18687  | -0.09948 | -0.27852 | -0.18717 | PPP2R1A  | -0.09457 | 0.41687 |  |
| P14618 | 0.21224  | -0.43978 | -0.20434 | 0.03835  | PKM      | -0.09838 | 0.53900 |  |
| P34932 | -0.22973 | -0.14772 | -0.22439 | 0.19819  | HSPA4    | -0.10091 | 0.39318 |  |
| P35606 | 0.02002  | 0.11915  | -0.19212 | -0.37557 | COPB2    | -0.10713 | 0.40399 |  |
| P45974 | 0.04347  | -0.00046 | -0.12036 | -0.35375 | USP5     | -0.10777 | 0.31262 |  |
| Q709C8 | -0.30850 | 0.04828  | 0.57888  | -0.75220 | VPS13C   | -0.10839 | 0.72596 |  |
| P13639 | 0.34087  | -0.46060 | -0.39761 | 0.03929  | EEF2     | -0.11951 | 0.57300 |  |
| P60842 | 0.29782  | -0.69873 | -0.07074 | -0.01750 | EIF4A1   | -0.12229 | 0.59899 |  |
| Q15365 | -0.00002 | -0.02267 | -0.22382 | -0.25736 | PCBP1    | -0.12597 | 0.15533 |  |
| Q9NY33 | 0.22723  | -0.08834 | -0.29164 | -0.36599 | DPP3     | -0.12969 | 0.40036 |  |
| P30041 | 0.24337  | -0.05866 | -0.38890 | -0.31790 | PRDX6    | -0.13052 | 0.42988 |  |
| P27348 | 0.25456  | -0.15417 | -0.19728 | -0.42713 | YWHAQ    | -0.13101 | 0.42368 |  |
| P22314 | -0.14559 | -0.19932 | -0.23430 | 0.00428  | UBA1     | -0.14373 | 0.07179 |  |
| P10599 | 0.44424  | -0.11429 | -0.37535 | -0.54271 | TXN      | -0.14702 | 0.54474 |  |
| Q9UL25 | -0.36734 | 0.36113  | 0.33148  | -0.92029 | RAB21    | -0.14876 | 0.66153 |  |
| P62258 | 0.00002  | -0.26423 | -0.26178 | -0.07603 | YWHAE    | -0.15050 | 0.10957 |  |
| P17987 | -0.19767 | -0.34952 | -0.72230 | 0.66740  | TCP1     | -0.15052 | 0.64405 |  |
| P19338 | -0.15126 | -0.43577 | -0.63669 | 0.61675  | NCL      | -0.15174 | 0.61934 |  |
| P28074 | 0.23285  | -0.23445 | -1.09151 | 0.47147  | PSMB5    | -0.15541 | 0.68273 |  |
| Q13435 | -0.00559 | -0.93336 | -0.60971 | 0.91493  | SF3B2    | -0.15843 | 0.72253 |  |
| Q8TAT6 | 0.16961  | 0.02613  | -0.06364 | -0.77632 | NPLOC4   | -0.16105 | 0.50015 |  |
| Q15149 | -0.09282 | 0.67837  | -0.73246 | -0.50619 | PLEC     | -0.16328 | 0.63510 |  |
| P61006 | -0.39323 | 0.63995  | 0.28089  | -1.21393 | RAB8A    | -0.17158 | 0.70249 |  |
| P02771 | -0.64031 | 0.06348  | -0.04098 | -0.09892 | AFP      | -0.17918 | 0.33748 |  |
| Q99873 | 0.33300  | -0.68392 | -0.45139 | 0.08438  | PRMT1    | -0.17948 | 0.49998 |  |
| P47897 | 0.22790  | -0.23661 | -0.97823 | 0.24717  | QARS     | -0.18494 | 0.56533 |  |
| P40227 | -0.12480 | -0.45383 | -0.69096 | 0.52642  | CCT6A    | -0.18579 | 0.53266 |  |
| Q15907 | -0.08022 | 0.37509  | 0.20384  | -1.24465 | RAB11B   | -0.18649 | 0.64463 |  |
| P49588 | -0.08089 | -0.52480 | -0.24527 | 0.10385  | AARS     | -0.18678 | 0.25581 |  |
| Q06323 | -0.18220 | -0.46543 | -0.17664 | 0.07620  | PSME1    | -0.18701 | 0.18959 |  |
| P50991 | -0.10892 | -0.51680 | -0.52818 | 0.37578  | CCT4     | -0.19453 | 0.42968 |  |
| P28066 | 0.12385  | -0.27807 | -0.87367 | 0.21968  | PSMA5    | -0.20205 | 0.47567 |  |
| Q86VP6 | 0.10822  | -0.36813 | -0.25559 | -0.31842 | CAND1    | -0.20848 | 0.14924 |  |

|        |          |          |          |          |          |          |         |    |
|--------|----------|----------|----------|----------|----------|----------|---------|----|
| Q13263 | 0.32777  | -0.65767 | -0.32989 | -0.19972 | TRIM28   | -0.21488 | 0.37143 |    |
| Q9Y265 | 0.09639  | -0.59126 | -0.26150 | -0.12024 | RUVBL1   | -0.21915 | 0.22595 |    |
| P62937 | 0.28397  | -0.38016 | -0.50026 | -0.28576 | PPIA     | -0.22055 | 0.29397 |    |
| P00558 | 0.27763  | -0.30224 | -0.57184 | -0.32528 | PGK1     | -0.23043 | 0.29052 |    |
| P11142 | 0.09362  | -0.40680 | -0.33577 | -0.28025 | HSPA8    | -0.23230 | 0.12901 |    |
| Q9Y230 | -0.03601 | -0.64246 | -0.17454 | -0.07632 | RUVBL2   | -0.23233 | 0.19505 |    |
| P25205 | 0.32483  | -0.92338 | -0.70051 | 0.32722  | MCM3     | -0.24296 | 0.51685 |    |
| Q9BRQ8 | -0.19069 | -0.02182 | 0.20888  | -0.97130 | AIFM2    | -0.24373 | 0.41126 |    |
| P07437 | -0.11038 | -0.76406 | -0.12743 | -0.00802 | TUBB     | -0.25247 | 0.23962 |    |
| Q92890 | 0.46800  | -0.24070 | -0.35009 | -1.00464 | UFD1L    | -0.28186 | 0.41887 |    |
| Q9Y2Z0 | 0.04633  | -0.37817 | 0.04977  | -0.85890 | SUGT1    | -0.28524 | 0.27836 |    |
| P49748 | -109.611 | -0.08882 | 0.62406  | -0.58089 | ACADVL   | -0.28544 | 0.49268 |    |
| Q99497 | 0.19396  | -0.45023 | -0.33230 | -0.55697 | PARK7    | -0.28638 | 0.18403 |    |
| P50990 | -0.16800 | -0.48072 | -0.94785 | 0.43767  | CCT8     | -0.28972 | 0.39228 |    |
| P52209 | 0.18903  | -0.47977 | -0.44324 | -0.45554 | PGD      | -0.29738 | 0.16432 |    |
| Q92616 | -0.14912 | -0.32853 | -0.47482 | -0.25318 | GCN1     | -0.30141 | 0.02177 | *  |
| P61106 | -0.39465 | 0.43699  | -0.04302 | -1.20682 | RAB14    | -0.30187 | 0.44771 |    |
| Q14974 | -0.12528 | -0.53079 | -0.21709 | -0.33702 | KPNB1    | -0.30254 | 0.04078 | *  |
| P78371 | -0.07081 | -0.67402 | -0.48664 | 0.01335  | CCT2     | -0.30453 | 0.16152 |    |
| Q16850 | -0.47859 | -0.45971 | 0.80273  | -1.08791 | CYP51A1  | -0.30587 | 0.49743 |    |
| Q15185 | -0.03908 | -0.65328 | -0.28682 | -0.24576 | PTGES3   | -0.30624 | 0.09612 |    |
| Q9NP72 | -0.22840 | 0.25151  | -0.66753 | -0.58634 | RAB18    | -0.30769 | 0.23804 |    |
| P62826 | 0.02251  | -0.52155 | -0.37664 | -0.35542 | RAN      | -0.30777 | 0.07696 |    |
| O75643 | -0.27917 | -0.53605 | -0.56833 | 0.15152  | SNRNP200 | -0.30801 | 0.16104 |    |
| P61019 | -0.63693 | 0.18257  | 0.31881  | -1.09945 | RAB2A    | -0.30875 | 0.42794 |    |
| Q14204 | -0.34796 | -0.34581 | -0.38903 | -0.16916 | DYNC1H1  | -0.31299 | 0.00775 | ** |
| P06733 | 0.16739  | -0.68906 | -0.34996 | -0.38611 | ENO1     | -0.31444 | 0.17495 |    |
| P33991 | 0.18530  | -1.09806 | -0.78242 | 0.42465  | MCM4     | -0.31763 | 0.45204 |    |
| Q9H0U4 | -0.45869 | 0.24061  | 0.00026  | -1.05849 | RAB1B    | -0.31908 | 0.34587 |    |
| P49736 | 0.32308  | -1.12513 | -0.78896 | 0.22303  | MCM2     | -0.34199 | 0.41477 |    |
| P30086 | 0.11793  | -0.27194 | -0.51505 | -0.72155 | PEBP1    | -0.34766 | 0.14951 |    |
| Q8NBQ5 | -0.27103 | 0.24446  | -0.59453 | -0.79287 | HSD17B11 | -0.35349 | 0.21648 |    |
| P07737 | 0.11028  | -0.41021 | -0.57986 | -0.53563 | PFN1     | -0.35385 | 0.11222 |    |
| P07900 | -0.12184 | -0.55826 | -0.38014 | -0.36519 | HSP90AA1 | -0.35636 | 0.02846 | *  |
| P04406 | 0.15118  | -0.65076 | -0.45348 | -0.48386 | GAPDH    | -0.35923 | 0.13328 |    |
| Q9UL46 | -0.33646 | -0.57417 | -0.20890 | -0.34257 | PSME2    | -0.36553 | 0.01716 | *  |
| Q99541 | -0.48294 | 0.07061  | -0.35154 | -0.70189 | PLIN2    | -0.36644 | 0.10959 |    |
| P55072 | 0.00165  | -0.09487 | -0.46108 | -0.91523 | VCP      | -0.36738 | 0.17558 |    |
| Q14566 | 0.11558  | -1.17179 | -0.73610 | 0.28516  | MCM6     | -0.37679 | 0.35656 |    |

B. Supplementary data

|        |          |          |          |          |          |          |         |     |
|--------|----------|----------|----------|----------|----------|----------|---------|-----|
| P53396 | 0.09531  | -0.24349 | -1.08201 | -0.27834 | ACLY     | -0.37713 | 0.22799 |     |
| Q8WUM4 | 0.01561  | -0.11241 | -0.37132 | -1.04881 | PDCD6IP  | -0.37923 | 0.20825 |     |
| O14980 | -0.05417 | -0.43051 | 0.10618  | -1.14106 | XPO1     | -0.37989 | 0.26455 |     |
| P60174 | -0.03920 | -0.54520 | -0.44757 | -0.49735 | TPI1     | -0.38233 | 0.04597 | *   |
| P12004 | 0.16366  | -1.09016 | -0.40220 | -0.23296 | PCNA     | -0.39041 | 0.23249 |     |
| O75874 | -0.26057 | -0.38250 | -0.79003 | -0.14059 | IDH1     | -0.39342 | 0.06854 |     |
| Q9P2E9 | -0.66306 | -0.31115 | 0.31782  | -0.98319 | RRBP1    | -0.40989 | 0.23773 |     |
| O95716 | -0.53129 | 0.23486  | -0.27686 | -1.14235 | RAB3D    | -0.42891 | 0.23096 |     |
| Q16531 | -0.28041 | -0.65847 | -0.67302 | -0.13410 | DDB1     | -0.43650 | 0.04872 | *   |
| Q9Y490 | -0.28308 | -0.41001 | -0.42782 | -0.67667 | TLN1     | -0.44940 | 0.01208 | *   |
| P09936 | 0.23629  | -1.12915 | -0.36140 | -0.59678 | UCHL1    | -0.46276 | 0.20051 |     |
| P00387 | -0.74081 | 0.18448  | -0.12006 | -135.760 | CYB5R3   | -0.50850 | 0.23409 |     |
| Q06830 | -0.29566 | -0.35004 | -0.91181 | -0.49948 | PRDX1    | -0.51425 | 0.03451 | *   |
| O75911 | -0.48423 | 0.11145  | -0.68542 | -1.00533 | DHRS3    | -0.51588 | 0.11571 |     |
| O60610 | -0.76280 | -0.12504 | -0.27352 | -0.94095 | DIAPH1   | -0.52558 | 0.07343 |     |
| P55060 | 0.01901  | -0.70513 | -0.08995 | -1.41515 | CSE1L    | -0.54781 | 0.19564 |     |
| Q6UX53 | -0.43755 | 0.63411  | -0.99419 | -1.40698 | METTL7B  | -0.55115 | 0.30108 |     |
| P32119 | -0.13143 | -0.80902 | -0.82083 | -0.47945 | PRDX2    | -0.56018 | 0.04156 | *   |
| P22234 | -0.18683 | -0.95182 | -0.95359 | -0.15305 | PAICS    | -0.56132 | 0.08904 |     |
| O43175 | -0.18570 | -1.28821 | -0.58008 | -0.31722 | PHGDH    | -0.59280 | 0.09493 |     |
| P08238 | -0.32392 | -1.12375 | -0.55740 | -0.39375 | HSP90AB1 | -0.59971 | 0.04553 | *   |
| Q8N5I4 | -0.20230 | -0.56277 | -0.86353 | -0.82751 | DHRSX    | -0.61403 | 0.02765 | *   |
| Q15738 | -0.36924 | 0.07799  | -0.54638 | -1.66348 | NSDHL    | -0.62528 | 0.18976 |     |
| P23526 | -0.05807 | -102.457 | -0.72403 | -0.69721 | AHCY     | -0.62597 | 0.05419 |     |
| Q8IZ81 | -0.63832 | -0.28246 | -0.16768 | -1.44488 | ELMOD2   | -0.63333 | 0.11566 |     |
| Q9H6V9 | -0.44224 | -0.15645 | -0.82559 | -1.18698 | LDAH     | -0.65282 | 0.06224 |     |
| Q14534 | -0.58479 | -0.32945 | -0.65977 | -1.05764 | SQLE     | -0.65791 | 0.02228 | *   |
| P00338 | -0.47704 | -0.74480 | -0.81845 | -0.62899 | LDHA     | -0.66732 | 0.00293 | **  |
| P04792 | -0.62647 | -1.58605 | 0.02830  | -0.52769 | HSPB1    | -0.67798 | 0.13635 |     |
| Q8NBX0 | -0.65804 | -0.27987 | -0.77870 | -1.08962 | SCCPDH   | -0.70156 | 0.02477 | *   |
| Q92538 | -0.06262 | -0.46939 | -0.66009 | -1.69319 | GBF1     | -0.72132 | 0.12922 |     |
| P78527 | -0.73028 | -0.63633 | -0.39685 | -1.23035 | PRKDC    | -0.74845 | 0.02358 | *   |
| O00410 | -0.20800 | -1.32964 | -0.28406 | -1.25431 | IPO5     | -0.76900 | 0.08466 |     |
| Q01469 | -0.14839 | -1.06715 | -0.85593 | -1.09181 | FABP5    | -0.79082 | 0.03715 | *   |
| P16949 | -0.29307 | -1.21316 | -0.82112 | -0.94927 | STMN1    | -0.81916 | 0.02410 | *   |
| Q99653 | -0.95268 | -0.78935 | -0.71329 | -0.96178 | CHP1     | -0.85427 | 0.00081 | *** |
| Q96LJ7 | -0.77498 | -0.79834 | -1.03187 | -0.88034 | DHRS1    | -0.87138 | 0.00064 | *** |
| Q9Y617 | -0.13982 | -1.64718 | -0.82710 | -1.01514 | PSAT1    | -0.90731 | 0.06124 |     |
| O95573 | -0.72040 | -0.50879 | -0.82748 | -1.73305 | ACSL3    | -0.94743 | 0.03927 | *   |

|        |          |          |          |          |         |          |         |     |
|--------|----------|----------|----------|----------|---------|----------|---------|-----|
| P56937 | -1.18350 | -0.68151 | -0.62779 | -1.55189 | HSD17B7 | -1.01117 | 0.01922 | *   |
| Q96AD5 | -0.65654 | -0.64320 | -1.28779 | -1.54497 | PNPLA2  | -1.03312 | 0.01998 | *   |
| Q96E22 | -0.43463 | -0.91416 | -0.74717 | -2.09110 | NUS1    | -1.04676 | 0.06294 |     |
| P20700 | -0.99479 | -0.86382 | -0.88026 | -1.48100 | LMNB1   | -1.05497 | 0.00536 | **  |
| Q8WTS1 | -0.98729 | -0.96946 | -0.91931 | -1.39798 | ABHD5   | -1.06851 | 0.00236 | **  |
| P48449 | -0.75353 | -0.67409 | -0.87779 | -2.05578 | LSS     | -1.09030 | 0.04375 | *   |
| P49327 | -0.57158 | -1.02407 | -1.53074 | -1.35767 | FASN    | -1.12102 | 0.01305 | *   |
| Q96RL7 | -0.96540 | -0.62958 | -0.57806 | -2.62380 | VPS13A  | -1.19921 | 0.08887 |     |
| P04114 | -3.47622 | -0.59634 | -0.24513 | -0.59948 | APOB    | -1.22929 | 0.20133 |     |
| Q9NST1 | -1.47374 | -1.56903 | -1.54770 | -2.19229 | PNPLA3  | -1.69569 | 0.00203 | **  |
| O60488 | -1.45985 | -1.52584 | -0.88665 | -3.02767 | ACSL4   | -1.72500 | 0.03262 | *   |
| Q13085 | -1.14609 | -1.90005 | -1.86358 | -2.58949 | ACACA   | -1.87480 | 0.00786 | **  |
| Q9H8H3 | -2.30816 | -1.89596 | -1.80180 | -2.42221 | METTL7A | -2.10704 | 0.00081 | *** |



# List of Figures

|   |    |
|---|----|
| 1.1. Global prevalence of HCV genotypes. . . . .  | 12 |
| 1.2. The HCV entry process. . . . .   | 14 |
| 1.3. HCV genome organization and polyprotein processing. . . . .  | 16 |
| 1.4. HCV assembly. . . . .  | 20 |
| 1.5. HCV; a lipovirion. . . . .   | 21 |
| 1.6. HCV cell culture systems. . . . .  | 23 |
| 1.7. Cells used as HCV culture systems <i>in vitro</i> . . . . .  | 24 |
| 1.8. Morphology of LDs. . . . .   | 25 |
| 1.9. Formation of LDs. . . . .  | 26 |
| 1.10. Spatial resolution of several microscopy techniques. . . . .  | 28 |
| 1.11. Co-localization of the COPI machinery at LDs analyzed by STED. . . . .                                  | 29 |
| 1.12. Principle of dSTORM. . . . .  | 29 |
| 1.13. Crystal structure of ANXA1. . . . .   | 30 |
|   |    |
| 3.1. Precursor ion and fragment ion mass spectrum of the SILAC labeled peptide DLT <sup>1</sup> YLMK. . . . . | 36 |
| 3.2. Experimental outline of quantitative LD proteome analysis. . . . .                                       | 37 |
| 3.3. Quantitative analysis of identified LD-associated proteins. . . . .                                      | 38 |
| 3.4. Characterization of LD proteome of HCV-infected cells. . . . .   | 39 |
| 3.5. Gene ontology enrichment analysis and protein interaction network of dysregulated proteins. . . . .      | 40 |
| 3.6. mRNA knockdown of candidate LDs-associated host factors. . . . .   | 41 |
| 3.7. Depletion of ANXA3 and ARF4 inhibits HCV spreading infection. . . . .                                    | 42 |
| 3.8. RNAi validation of Annexin A2–A5. . . . .  | 43 |
| 3.9. HCV spreading infection in Annexin A2–A5 knockdown cells. . . . .  | 44 |
| 3.10. CRISPR/Cas9 mediated ANXA3 knockout. . . . .  | 45 |
| 3.11. Viability of ANXA3-knockdown and -knockout cell lines and ANXA3 protein expression. . . . .             | 45 |
| 3.12. Knockout of ANXA3 severely reduces viral spreading. . . . .   | 47 |
| 3.13. Overexpression of ANXA3 decreases cell viability and consequently HCV replication. . . . .              | 48 |
| 3.14. ANXA3 is recruited to LDs in Con1 SGR- or HCV-infected cells. . . . .                                   | 50 |
| 3.15. ANXA3 expression is not influenced by HCV infection. . . . .  | 51 |
| 3.16. ANXA3 co-localizes with NS5A in LD-associated membranes. . . . .  | 52 |
| 3.17. Co-localization of Flag-tagged HCV proteins and HA-tagged ANXA3. . . . .                                | 53 |
| 3.18. ANXA3 does not show a direct interaction with Flag-tagged HCV proteins. . . . .                         | 54 |
| 3.19. ANXA3 co-localizes with core or NS5A at LDs. . . . .  | 55 |
| 3.20. Expression of core or NS5A is sufficient to re-localize ANXA3 to LDs. . . . .                           | 56 |
| 3.21. HCV RNA replication and viral protein expression is not affected by ANXA3. . . . .                      | 57 |

|  |    |
|--|----|
| 3.22. Knockdown of ANXA3 expression significantly reduced secretion of HCV RNA genomes. . . . .  | 58 |
| 3.23. ANXA3 regulates HCV progeny virion production. . . . .   | 59 |
| 3.24. Trafficking of core and NS5A to LDs works independently of ANXA3. . . . .  | 60 |
| 3.25. ANXA3 is not involved in the formation of HMM core complexes and core envelopment. . . . .   | 61 |
| 3.26. cPLA2 activity is not affected by ANXA3-knockdown. . . . .   | 62 |
| 3.27. ANXA3 influences the specific infectivity and the density of HCV virions. . . . .  | 63 |
| 3.28. ANXA3 contributes to ApoE and ApoB secretion in HCV replicating cells. . . . .   | 64 |
| 3.29. ANXA3 is not a component of the HCV virion. . . . .  | 66 |
| 3.30. Neutralization assay of HCV particles. . . . .   | 67 |
| 3.31. ANXA3 facilitates the interaction of ApoE with E2. . . . .   | 68 |
| 3.32. ANXA3 acts on the luminal side of the ER and doesn't interact directly with NS5A. . . . .  | 69 |
| 3.33. Silencing of ANXA3 affects the co-localization of core and Flag-E2. . . . .  | 70 |
| 3.34. Silencing of ANXA3 reduces the co-localization of Flag-E2 and ApoE. . . . .  | 71 |
| 3.35. ANXA3-HA does not interact with core, E2 or ApoE in HCV-infected cells. . . . .  | 72 |
| 3.36. No differences in membrane- association of ApoE, core and Flag-E2 in shANXA3 cells. . . . .  | 73 |
| 3.37. HCV-induced morphological changes of the Golgi compartment are less pronounced in shANXA3 cells. . . . .                             | 74 |
| 3.38. ANXA3 affects Golgi scattering in HCV-infected cells. . . . .  | 75 |
| 3.39. Characterization of Jc1 <sup>Flag-E2</sup> and JFH1 <sup>Flag-E2</sup> HCVcc constructs. . . . .                                     | 76 |
| 3.40. Subcellular localization of Flag and E2. . . . .   | 77 |
| 3.41. Subcellular localization of core and Flag-E2 in Jc1 <sup>Flag-E2</sup> - and JFH1 <sup>Flag-E2</sup> -infected cells. . . . .        | 78 |
| 3.42. Subcellular localization of NS5A and Flag-E2 in Jc1 <sup>Flag-E2</sup> - and JFH1 <sup>Flag-E2</sup> -infected cells. . . . .        | 80 |
| 3.43. Visualization of LDs in dSTORM. . . . .  | 81 |
| 3.44. dSTORM images of core overlapping with Flag-E2 and LipidTox Red. . . . .   | 83 |
| 3.45. dSTORM images of NS5A overlapping with Flag-E2 and LipidTox Red. . . . .   | 84 |
| 3.46. Analysis of co-localization according to Manders of core/NS5A with Flag-E2 at LDs visualized by super resolution microscopy. . . . . | 85 |
| 3.47. 2D and 3D dSTORM images of Jc1 <sup>Flag-E2</sup> - and JFH1 <sup>Flag-E2</sup> -infected cells. . . . .                             | 86 |
| 3.48. 3D distribution and co-localization analysis of viral proteins at LDs. . . . .   | 87 |
| 3.49. 3D reconstruction of core, Flag-E2, and LDs in Jc1 <sup>Flag-E2</sup> -infected cells. . . . .                                       | 89 |
| 3.50. 3D reconstruction of core, Flag-E2, and LDs in JFH1 <sup>Flag-E2</sup> -infected cells. . . . .                                      | 90 |
| 3.51. 3D reconstruction of NS5A, Flag-E2, and LDs in Jc1 <sup>Flag-E2</sup> -infected cells. . . . .                                       | 91 |
| 3.52. 3D reconstruction of NS5A, Flag-E2, and LDs in JFH1 <sup>Flag-E2</sup> -infected cells. . . . .                                      | 92 |
| 4.1. ANXA3 impacts maturation of nascent viral particles. . . . .  | 96 |







# Danksagung

Zuallererst möchte ich mich herzlich bei Frau Dr. Eva Herker bedanken. Dafür, dass Sie mir die Arbeit an einem hochspannenden Thema ermöglicht hat. Ich möchte mich auch für den Freiraum, selbständig zu arbeiten und eigene Ideen in das Projekt einfließen zu lassen, bedanken. Auch stand Sie mir immer mit Rat und Tat zu Seite. Vielen Dank für die hilfreiche Unterstützung und die anregenden Diskussionen, die maßgeblich zum Gelingen dieser Arbeit beigetragen haben. Ich möchte mich auch für das Vertrauen zur Präsentation vieler gemeinsamer Forschungsergebnisse bedanken.

Ebenso möchte ich mich bei Herrn PD Dr. Markus Perbandt für die Zweitbetreuung meiner Dissertation danken. Bei Herrn Prof. Dr. Wolfgang Maison und Herrn Prof. Dr. Wolfram Brune möchte ich mich für die Begutachtung meiner Disputation bedanken.

Der gesamten Arbeitsgruppe „HCV Replikation“ möchte ich ganz herzlich für die tolle Zeit danken. Danke, dass Ihr mich in allen Lebenslagen unterstützt habt und immer ein offenes Ohr für mich hattet. Ihr habt wesentlich dazu beigetragen, dass ich immer Spaß an meinem Projekt hatte. Danke für die tolle Atmosphäre!

Ich möchte mich auch bei Dr. Marcel Kwiatkowski und Prof. Dr. Hartmut Schlüter für die tolle Zusammenarbeit bedanken. Ohne Ihre Unterstützung wäre ein großer Teil dieser Arbeit nicht möglich gewesen.



# Eidesstattliche Versicherung

Hiermit versichere ich an Eides statt, die vorliegende Dissertation selbst verfasst und keine anderen als die angegebenen Hilfsmittel benutzt zu haben. Die eingereichte schriftliche Fassung entspricht der auf dem elektronischen Speichermedium. Ich versichere, dass diese Dissertation nicht in einem früheren Promotionsverfahren eingereicht wurde.

Hamburg, den